

ISSN 2667-4211

ESKİŞEHİR TECHNICAL UNIVERSITY
JOURNAL OF SCIENCE AND TECHNOLOGY
A – Applied Sciences and Engineering

8th International Fiber and Polymer Research Symposium

Volume **22** 8th ULPAS - Special Issue 2021

**Volume: 22 / 8th ULPAS - Special Issue 2021**

Eskiőehir Technical University Journal of Science and Technology A - Applied Sciences and Engineering (formerly Anadolu University Journal of Science and Technology A - Applied Sciences and Engineering) is an **peer-reviewed** and **refereed international journal** by Eskiőehir Technical University. Since 2000, it has been regularly published and distributed biannually and it has been published quarterly and **electronically only since 2016**.

Manuscripts submitted for publication are analyzed in terms of scientific quality, ethics and research methods in terms of its compliance by the Editorial Board representatives of the relevant areas. Then, the abstracts of the appropriate articles are sent to two different referees with a well-known in scientific area. If the referees agree to review the article, full text in the framework of the privacy protocol is sent. In accordance with the decisions of referees, either directly or corrected article is published or rejected. Confidential reports of the referees in the journal archive will be retained for ten years. All post evaluation process is done electronically on the internet. Detailed instructions to authors are available in each issue of the journal.

Eskiőehir Technical University holds the copyright of all published material that appear in Eskiőehir Technical University Journal of Science and Technology A - Applied Sciences and Engineering.

"Anadolu Üniversitesi Bilim ve Teknoloji Dergisi A - Uygulamalı Bilimler ve Mühendislik (Anadolu University Journal of Science and Technology A - Applied Sciences and Engineering)" published within Anadolu University started to be published within Eskiőehir Technical University which was established due to statute law 7141, in 2018. Hence, the name of the journal is changed to " Eskiőehir Technical University Journal of Science and Technology A - Applied Sciences and Engineering (Eskiőehir Teknik Üniversitesi Bilim ve Teknoloji Dergisi A - Uygulamalı Bilimler ve Mühendislik)".

Indexed by **DOAJ** - Directory of Open Access Journals, **EBSCO** and **ULAKBİM**



Volume: 22 / 8th ULPAS - Special Issue 2021

Owner / Publisher: Prof. Dr. Tuncay DÖĐEROĐLU for Eskiőehir Technical University

EDITOR-IN-CHIEF

Prof. Dr. Murat TANIŐLI

Eskiőehir Technical University, Institute of Graduate Programs, 26470 Eskiőehir, TURKEY

Phone: +90-222-321 35 50 /**ext.:** 1755

Fax: +90-222 335 41 22

e-mail: mtanisli@eskisehir.edu.tr

CONTACT INFORMATION

Eskiőehir Technical University Journal of Science and Technology

Eskiőehir Technical University, Institute of Graduate Programs, 26470 Eskiőehir, TURKEY

Phone: +90-222-321 35 50 /**ext.:** 1767

Fax: +90-222 335 41 22

e-mail : btda@eskisehir.edu.tr



Volume: 22 / 8th ULPAS - Special Issue 2021

OWNER

Tuncay DÖĐEROĐLU, The Rector of Eskiőehir Technical University

EDITORIAL BOARD

Murat TANIŐLI, Editor in Chief

ULPAS SPECIAL ISSUE EDITOR'S

Prof. Dr. Ali DEMİR

İstanbul Technical University; Textile Engineering

Prof. Dr. Yusuf ULCAY

Bursa Uludağ University, Textile Engineering

Assoc. Prof. Hüseyin AVCI

Eskiőehir Osmangazi University, Metallurgical and Materials Engineering

Assoc. Prof. Ali KILIÇ

İstanbul Technical University; Textile Engineering

Secretary/Typset

Handan YİĐİT

8th ULPAS 2021 Special Issue

International Fiber and Polymer Research Symposium (ULPAS) is held at different universities twice a year since 2016. The 8th ULPAS was organized by Eskişehir Osmangazi University on June 18-19, 2021. The symposium is principally devoted to enhance the development and use of the polymers and fibrous materials in different end-uses besides their usage in pure textiles and clothing. It has been enabling to build up a scientific and productive dialogue between members, academicians and industry people from different countries.

The 8th ULPAS symposium was focused on “**Fiber and Polymer Research in Defense Industry**” with associated **bio-defense** topics. Furthermore, the following subjects were discussed during the symposium:

1. Fibers, composites and textile structures in defense and space industry.
2. Medical textiles and composites for defense priorities.
3. Technical fibers (high temperature resistant silica, carbon, glass, basalt and similar fibers).
4. Textile and composite structures for transport and civil aviation.
5. Fibers and textile applications for home security and criminology.
6. Innovative fibers, energy applications and wearable technologies.
7. Fiber and polymer research in bio-security.

Following on from our very successful and enjoyable online 8. International Fiber and Polymer Research Symposium, we have requested to extend an invitation for selected papers by the scientific committee at the conference to submit their full-papers to *Eskişehir Technical University Journal of Science and Technology A - Applied Sciences and Engineering*. Each paper was evaluated by anonymous reviewers then as the field editors, we have made decision on it. We strongly believe that these symposium series can reach to many different research areas, whether they work mainly as researchers or students, hence they can see new pathways to integrate for innovation and cutting-edge research.

We take this opportunity to thank the organizing committee and the Rector of Eskişehir Osmangazi University for organizing the symposium and for providing the facilities. Our special and sincere thanks go to the supporting defense industry institutions, Presidency of The Republic of Turkey, Presidency of Defense Industries (SSB), Turkish Aerospace Industries (TAI/TUSAŞ), Aselsan, TEI, Havelsan, Roketsan, Boren, Mechanical and Chemical Industry Corporation (MKE). This symposium has been a real R&D meeting point for the Turkish Industrial Research and Development Centers. We are extremely grateful for this and we extend our warm thanks to all participating R&D Centers. We would also like to express our gratitude to the Fiber and Polymer Research Institute Secretariat for their diligence.

EDITORS

Prof. Dr. Yusuf Ulcay

Prof. Dr. Ali Demir

Assoc. Prof. Ali Kılıç

Assoc. Prof. Hüseyin Avcı



ABOUT

Eskişehir Technical University Journal of Science and Technology A - Applied Sciences and Engineering (formerly Anadolu University Journal of Science and Technology A - Applied Sciences and Engineering) is an peer-reviewed and refereed international journal by Eskişehir Technical University. Since 2000, it has been regularly published and distributed biannually and it has been published quarterly and electronically only since 2016.

- **The journal accepts only ENGLISH language manuscripts.**
- **The journal is indexed by EBSCO, DOAJ and ULAKBIM.**

AIM AND SCOPE

The journal publishes high quality original research papers in the field of engineering and applied science. Special Issues devoted to important topics in science and technology will occasionally be published. The journal publishes research papers in the fields of applied science and technology such as Physics, Biology, Mathematics, Statistics, Chemistry and Chemical Engineering, Environmental Sciences and Engineering, Civil Engineering, Earth and Atmospheric Sciences, Electrical and Electronical Engineering, Computer Science and Informatics, Materials Sciences and Engineering, Mechanical Engineering, Mining Engineering, Industrial Engineering, Aeronautics and Astronautics, Health Sciences, Pharmaceutical Sciences, and so on.

PEER REVIEW PROCESS

Manuscripts are first reviewed by the editorial board in terms of its its journal's style rules scientific content, ethics and methodological approach. If found appropriate, the manuscript is then send to at least two renown referees by editor. The decision in line with the referees may be an acceptance, a rejection or an invitation to revise and resubmit. Confidential review reports from the referees will be kept in archive. All submission process manage through the online submission systems.

OPEN ACCESS POLICY

This journal provides immediate open access to its content on the principle that making research freely available to the public supports a greater global exchange of knowledge.

Copyright notice and type of licence : **CC BY-NC-ND.**

The journal doesn't have Article Processing Charge (APC) or any submission charges.

ETHICAL RULES

You can reach the Ethical Rules in our journal in full detail from the link below:

<https://dergipark.org.tr/tr/pub/estubtda/page/10202>

AUTHOR GUIDELINES

All manuscripts must be submitted electronically.

You will be guided stepwise through the creation and uploading of the various files. There are no page charges. Papers are accepted for publication on the understanding that they have not been published and are not going to be considered for publication elsewhere. Authors should certify that neither the manuscript nor its main contents have already been published or submitted for publication in another journal. We ask a signed **Copyright Form** to start the evaluation process. After a manuscript has been submitted, it is not possible for authors to be added or removed or for the order of authors to be changed. If authors do so, their submission will be cancelled.

Manuscripts may be rejected without peer review by the editor-in-chief if they do not comply with the instructions to authors or if they are beyond the scope of the journal. After a manuscript has been accepted for publication, i.e. after referee-recommended revisions are complete, the author will not be permitted to make any changes that constitute departures from the manuscript that was accepted by the editor. Before publication, the galley proofs are always sent to the authors for corrections. Mistakes or omissions that occur due to some negligence on our part during final printing will be rectified in an errata section in a later issue.

This does not include those errors left uncorrected by the author in the galley proof. The use of someone else's ideas or words in their original form or slightly changed without a proper citation is considered plagiarism and will not be tolerated. Even if a citation is given, if quotation marks are not placed around words taken directly from another author's work, the author is still guilty of plagiarism. All manuscripts received are submitted to iThenticateR, a plagiarism checking system, which compares the content of the manuscript with a vast database of web pages and academic publications. Manuscripts judged to be plagiarised or self-plagiarised, based on the iThenticateR report or any other source of information, will not be considered for publication.

CONFLICT OF INTEREST STATEMENT

The authors are obliged to present the conflict of interest statement at the end of the article.

Preparation of Manuscript

Style and Format: Manuscripts should be **single column** by giving one-spaced with 2.5-cm margins on all sides of the page, in Times New Roman font (font size 11). Every page of the manuscript, including the title page, references, tables, etc., should be numbered. All copies of the manuscript should also have line numbers starting with 1 on each consecutive page.

Manuscripts must be upload as word document (*.doc, *.docx vb.). Please avoid uploading texts in *.pdf format.

Manuscripts should be written in English.

Symbols, Units and Abbreviations: Standard abbreviations and units should be used; SI units are recommended. Abbreviations should be defined at first appearance, and their use in the title and abstract should be avoided. Generic names of chemicals should be used. Genus and species names should be typed in italic or, if this is not available, underlined.

Please refer to equations with capitalisation and unabbreviated (e.g., as given in Equation (1)).

Manuscript Content: Articles should be divided into logically ordered and numbered sections. Principal sections should be numbered consecutively with Arabic numerals (1. Introduction, 2. Formulation of problem, etc.) and subsections should be numbered 1.1., 1.2., etc. Do not number the Acknowledgements or References sections. The text of articles should be, if possible, divided into the following sections: Introduction, Materials and Methods (or Experimental), Results, Discussion, and Conclusion.

Title and contact information

The first page should contain the full title in sentence case (e.g., Hybrid feature selection for text classification), the full names (last names fully capitalised) and affiliations (in English) of all authors (Department, Faculty, University, City, Country, E-mail), and the contact e-mail address for the clearly identified corresponding author.

Abstract

The abstract should provide clear information about the research and the results obtained, and should not exceed 300 words. The abstract should not contain citations and must be written in Times New Roman font with font size 9.

Keywords

Please provide 3 to 5 keywords which can be used for indexing purposes.

Introduction

The motivation or purpose of your research should appear in the “Introduction”, where you state the questions you sought to answer, and then provide some of the historical basis for those questions.

Methods

Provide sufficient information to allow someone to repeat your work. A clear description of your experimental design, sampling procedures, and statistical procedures is especially important in papers describing field studies, simulations, or experiments. If you list a product (e.g., animal food, analytical device), supply the name and location of the manufacturer. Give the model number for equipment used.

Results

Results should be stated concisely and without interpretation.

Discussion

Focus on the rigorously supported aspects of your study. Carefully differentiate the results of your study from data obtained from other sources. Interpret your results, relate them to the results of previous research, and discuss the implications of your results or interpretations.

Conclusion

This should state clearly the main conclusions of the research and give a clear explanation of their importance and relevance. Summary illustrations may be included.

Acknowledgments

Acknowledgments of people, grants, funds, etc. should be placed in a separate section before the reference list. The names of funding organizations should be written in full.

Conflict of Interest Statement

The authors are obliged to present the conflict of interest statement at the end of the article after the acknowledgments section.

References

Citations in the text should be identified by numbers in square brackets. The list of references at the end of the paper should be given in order of their first appearance in the text or in alphabetical order according to the surname of the first author. All authors should be included in reference lists unless there are 10 or more, in which case only the first 10 should be given, followed by ‘et al.’. Do not use individual sets of square brackets for citation numbers that appear together, e.g., [2, 3, 5–9], not [2], [3], [5]–[9]. Do not include personal communications, unpublished data, websites, or other unpublished materials as references, although such material may be inserted (in parentheses) in the text. In the case of publications in languages other than English, the published English title should be provided if one exists, with an annotation such as “(article in Turkish with an abstract in English)”. If the publication was not published with an English title, cite the original title only; do not provide a self-translation. References should be formatted as follows (please note the punctuation and capitalisation):

Journal articles

Journal titles should be abbreviated according to ISI Web of Science abbreviations.

Guyon I and Elisseeff A. An introduction to variable and feature selection. *J. Mach. Learn. Res.* 2003; 3: 1157-1182.

Izadpanahi S, Ozcinar C, Anbarjafari G and Demirel H. Resolution enhancement of video sequences by using discrete wavelet transform and illumination compensation. *Turk J. Elec. Eng. & Comp. Sci.* 2012; 20: 1268-1276.

Books

Haupt RL and Haupt SE. *Practical Genetic Algorithms*. 2nd ed. New York, NY, USA: Wiley, 2004.

Kennedy J and Eberhart R. *Swarm Intelligence*. San Diego, CA, USA: Academic Press, 2001.

Chapters in books

Poore JH, Lin L, Eschbach R and Bauer T. Automated statistical testing for embedded systems. In: Zander J, Schieferdecker I, Mosterman PJ, editors. *Model-Based Testing for Embedded Systems*. Boca Raton, FL, USA: CRC Press, 2012. pp. 111-146.

Conference proceedings

Li RTH and Chung SH. Digital boundary controller for single-phase grid-connected CSI. In: *IEEE 2008 Power Electronics Specialists Conference*; 15–19 June 2008; Rhodes, Greece. New York, NY, USA: IEEE. pp. 4562-4568.

Theses

Boynukalin Z. Emotion analysis of Turkish texts by using machine learning methods. MSc, Middle East Technical University, Ankara, Turkey, 2012.

Tables and Figures

All illustrations (photographs, drawings, graphs, etc.), not including tables, must be labelled “Figure.” Figures must be submitted in the manuscript.

All tables and figures must have a caption and/or legend and be numbered (e.g., Table 1, Figure 2), unless there is only one table or figure, in which case it should be labelled “Table” or “Figure” with no numbering. Captions must be written in sentence case (e.g., Macroscopic appearance of the samples.). The font used in the figures should be Times New Roman with 9 pt. If symbols such as \times , μ , η , or ν are used, they should be added using the Symbols menu of Word.

All tables and figures must be numbered consecutively as they are referred to in the text. Please refer to tables and figures with capitalisation and unabbreviated (e.g., “As shown in Figure 2...”, and not “Fig. 2” or “figure 2”).

The resolution of images should not be less than 118 pixels/cm when width is set to 16 cm. Images must be scanned at 1200 dpi resolution and submitted in jpeg or tiff format. Graphs and diagrams must be drawn with a line weight between 0.5 and 1 point. Graphs and diagrams with a line weight of less than 0.5 point or more than 1 point are not accepted. Scanned or photocopied graphs and diagrams are not accepted.

Figures that are charts, diagrams, or drawings must be submitted in a modifiable format, i.e. our graphics personnel should be able to modify them. Therefore, if the program with which the figure is drawn has a “save as” option, it must be saved as *.ai or *.pdf. If the “save as” option does not include these extensions, the figure must be copied and pasted into a blank Microsoft Word document as an editable object. It must not be pasted as an image file (tiff, jpeg, or eps) unless it is a photograph.

Tables and figures, including caption, title, column heads, and footnotes, must not exceed 16 × 20 cm and should be no smaller than 8 cm in width. For all tables, please use Word’s “Create Table” feature, with no tabbed text or tables created with spaces and drawn lines. Please do not duplicate information that is already presented in the figures.

ESKİŞEHİR TECHNICAL UNIVERSITY JOURNAL OF SCIENCE AND TECHNOLOGY
A – Applied Sciences and Engineering
Volume: 22 / 8th ULPAS - Special Issue 2021
CONTENTS

RESEARCH ARTICLE

COMPRESSION AND INTERLAMINAR SHEAR PROPERTIES OF NANOPARTICLE DOPED HYBRID NANOFIBER INTERLEAVED GLASS/EPOXY COMPOSITES <i>F. Metin, A. Avcı</i>	1
REUSABLE FABRIC MASKS AGAINST COVID-19 <i>M. E. Üreyen, N. Zarif, E. Kaynak Uraz</i>	10
MECHANICAL PERFORMANCE OF CARBON - ARAMID FIBER-REINFORCED LAMINATED COMPOSITES UNDER IMPACT AND SHEAR LOADING <i>B. N. Atmaca, R. Oruç, G. Aşçı, K. Yiğit, S. Yüzer, Y. Polat, B. Ekici</i>	19
STRETCHABLE PIEZORESISTIVE SENSORS WITH GRAPHENE AND POLYANILINE COATED WOVEN POLYESTER FABRICS <i>M. Çetinoğlu, G. Fındık, Ö. F. Ünsal, A. Bedeloğlu</i>	28
ENHANCING UV PROTECTION AND HYDROPHOBIC ABILITIES OF POLYESTER TEXTILES BY NOVEL SURFACE MODIFICATION TECHNIQUES <i>A. Akpek</i>	39
THERMOFORMING PROCESS PARAMETER OPTIMIZATION OF THERMOPLASTIC PEKK/CF and PPS <i>M. Çobanoğlu, R. E. Ece, F. Öztürk</i>	51
WEARABLE TEXTILE-BASED PIEZOELECTRIC NANOGENERATORS WITH GRAPHENE/ZNO/AgNW <i>E. Demir, Ö. F. Ünsal, F. Emiroğlu, A. Bedeloğlu</i>	59
DEVELOPMENT AND CHARACTERIZATION OF VITAMIN B9 - ELECTROSPRAYED NON-WOVEN SURFACES FOR WOUND HEALING APPLICATIONS <i>F. N. Parn, K. Yıldırım, G. Taner, E. Kıldalı</i>	70
INVESTIGATION OF 3D CULTURE OF HUMAN ADIPOSE TISSUE-DERIVED MESENCHYMAL STEM CELLS IN A MICROFLUIDIC PLATFORM <i>C. Özel, Y. Koç, A. Topal, A. Ebrahimi, T. Şengel, H. Ghorbanpoor, F. Doğan Guzel, O. Uysal, A. Eker Sarıboyacı, H. Avcı</i>	85
DESIGN ALGINATE BASED BLENDS FOR LIVING COMPOSITE FIBERS TO PROMOTE WOUND HEALING <i>C. Özel, T. Şengel, A. Ebrahimi, E. Apaydın, H. Ghorbanpoor, A. Eker Sarıboyacı, O. Uysal, M. Ozkurt, H. Avcı</i>	98
INVESTIGATION OF MECHANICAL AND PHYSICAL PROPERTIES OF GRAPHENE WITH EPOXY MATRIX <i>M. B. Öztürkmen, M. Özkutlu Demirel, Y. Öz</i>	112
SiO₂ PARTICLE EMBEDDED SILICA AEROGELS: ENVIRONMENTAL AND ENERGY APPLICATIONS <i>S. Bütün Şengel, Ş. Somaklı, V. Bütün</i>	120
SYNTHESIS AND CHARACTERIZATION OF POLY[(2-DIMETHYLAMINO)ETHYL METHACRYLATE]-PAN/TiO₂ COMPOSITE CRYOGELS AND THEIR USE IN SEPARATION STUDY <i>S. Bütün Şengel, Ş. Somaklı, V. Bütün</i>	129



COMPRESSION AND INTERLAMINAR SHEAR PROPERTIES OF NANOPARTICLE DOPED HYBRID NANOFIBER INTERLEAVED GLASS/EPOXY COMPOSITES

Fatih METİN^{1,*} , Ahmet AVCI² 

¹ Department of Metallurgical and Materials Engineering, Konya Technical University, 42075, Konya, Turkey

² Department of Biomedical Engineering, Necmettin Erbakan University, 42140, Konya, Turkey

ABSTRACT

The effects of SiC-Fe₃O₄ nanoparticles doped electrospun Polysulfone (PSF) nanofibers on compressive and interlaminar shear strength of glass/epoxy composite laminates were investigated in this study. Pure PSF and hybrid PSF nanofibers were produced by the electrospinning process. Nanofiber interleaved glass/epoxy composite laminates were manufactured by using a vacuum-assisted hand-lay-up method. The addition of SiC-Fe₃O₄ nanoparticles into PSF nanofibers improved the tensile properties of nanofiber mats. The results revealed that PSF hybrid nanofiber interleaving increased the compressive and interlaminar shear strengths of composite laminates up to 26% and 12.4%, respectively.

Keywords: Electrospinning, Nanofiber interleaving, Mechanical testing, Composite laminates

1. INTRODUCTION

Fiber-reinforced polymer composites have superior material properties like strength-to-weight ratio, stiffness-to-weight ratio, and low density compared to traditional metallic materials. Therefore, they are used widely in aircraft, automotive, marine, and many other industrial applications to reduce weight and improve structural performance [1, 2]. However, the coexistence of brittle epoxy matrix and the anisotropic nature of fiber-reinforced composites can lead to unexpected damages growing with intra-ply cracks, delamination, and fiber failure, respectively. Delamination occurring in the resin-rich interlaminar region is one of the most common damages in fiber-reinforced polymer composites [3, 4].

In recent years, thermoplastic nanofiber interleaving, first introduced by Dzenis and Reneker [5], has become an attractive technique to enhance the toughness of weak interlaminar regions in fiber-reinforced composites. Thermoplastic nanofibers are produced by the electrospinning method and accumulated on a separate surface or directly fabric layer. Having diameters in nanoscales, tiny thickness with a porous structure, and a very high area to volume ratio are the superior properties of electrospun nanofibers [6, 7]. Many studies have been reported that PA6.6 [3, 8], PAN [6, 9], PVDF [10], PVA [11], PSF [12-15] nanofibers interleaving improved the mechanical properties of fiber-reinforced composites. These entangled nanofibers act like the hoops and loops in Velcro to enhance interlaminar toughness and take an active role in interlaminar toughening mechanisms like crack bridging, crack deflection, plastic deformation, and nanofiber pull-out [16]. Beylergil, et al. [8] carried out three-point bending, tensile, compression, Charpy impact, interlaminar shear strength, and DCB (Double cantilever beam) tests on reference and nanofiber reinforced carbon/epoxy composites to examine the effects of PA 6.6 nanofibers on mechanical properties. They revealed that PA 6.6 nanofibers improved flexural modulus by 16%, flexural strength by 13%, compression strength by 15%, and Charpy impact strength by 18%, while a 10% decrease in the tensile strength. Li, et al. [13] used PSF films and nanofibers for increasing Mode I fracture toughness of carbon /epoxy composites. The results showed that PSF nanofiber interleaving improved the Mode I fracture toughness by 140%

*Corresponding Author: fatihmetin64@gmail.com

Received: 03.08.2021

Published: 30.11.2021

and 280% compared to film interleaved and untoughened composite laminates. Anand, et al. [17] showed that interleaved Nylon 6/6 nanofibers with an areal density of 0.4 gsm could increase compressive and interlaminar shear strengths by 30% and 17%, respectively, in glass/epoxy composites.

The addition of nanoparticles into electrospun nanofibers can further increase the mechanical strengths of nanofiber mats and nanofiber interleaved polymer matrix composites. Liu, et al. [18] observed no significant change in diameter and morphological properties of PLGA/MWCNT composite nanofibers with 1 wt% MWCNT compared to pure PLGA nanofibers. Moreover, the addition of 1 wt% MWCNT improved the tensile strength and Young's modulus of nanofibers by 49% and 88%, respectively. Li, et al. [14] studied the effects of 5 wt%, 10 wt%, 15 wt%, and 20 wt% MWCNT-EP/PSF hybrid nanofibers on flexural, interlaminar shear strength (ILSS), and Mode II fracture toughness on carbon/epoxy composite laminates. They observed that 20 wt% MWCNT-EP/PSF hybrid nanofibers increased the flexural strength and modulus by 13.3% and 22.8%, respectively, compared to PSF toughened laminates. The results showed that the ILSS of 20 wt% MWCNT-EP/PSF hybrid nanofiber toughened laminates was 11.9% higher than the reference laminates. The best improvement of Mode II fracture toughness was achieved in 10 wt% MWCNT-EP/PSF hybrid nanofiber toughened laminates, compared to PSF toughened laminates.

In the literature, no study has been found examining the effects of SiC-Fe₃O₄ nanoparticle doped PSF hybrid nanofiber interleaving on the mechanical performance of glass/epoxy composites. This study aims to improve the compressive strength and interlaminar shear strength of glass/epoxy composites by incorporating pure PSF nanofibers, 1 wt%, and 2 wt% SiC-Fe₃O₄/PSF hybrid nanofibers between plies.

2. EXPERIMENTAL

2.1. Material

Polysulfone (PSF) pellets were purchased from Sigma-Aldrich. Acetone (AC) and Dimethylacetamide (DMAC) were used as solvents of PSF pellets. SiC and Fe₃O₄ nanoparticles were supplied from Nanografi. 2/2 twill weave E-glass woven fabrics having 390 g/m² areal weight were provided from Hexcel. Epoxy resin (MGS L 160) and curing agent (MGS H 160) were obtained from Hexion.

2.2. Method

Three different polymeric solutions were prepared for the electrospinning process. For the first solution, 20 wt% PSF pellets were dissolved in a mixture of DMAC/AC (9:1 w/w) on a magnetic stirrer at 70 ° C for 5 hours for pure PSF solution. For the second and third solutions, 1 wt% and 2 wt% SiC-Fe₃O₄ nanoparticles by PSF weight were separately dispersed in the mixture of DMAC/AC (9:1 w/w) using an ultrasonic sonicator for 10 minutes. Then, 20 wt% PSF pellets were dissolved in each mixture using the magnetic stirrer at 70 ° C for 5 hours. At the last step, SiC-Fe₃O₄ nanoparticles doped solutions were sonicated for 10 minutes at room temperature. Each PSF solution was withdrawn into four syringes and positioned on the syringe pump for electrospinning. The main parts of a typical electrospinning setup are shown in

Figure 1. The electrospinning process was performed at 26-32 kV applied voltage, 13 cm tip to collector distance, 1.5 ml/h feeding rate, and 600 rpm collector speed.

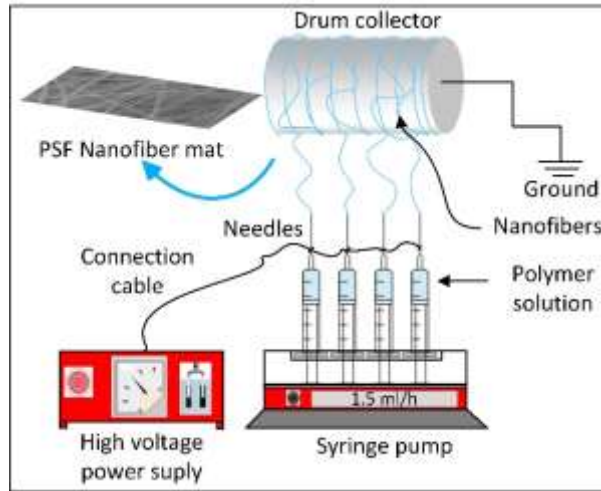


Figure 1. Schematic illustration of the electrospinning setup

Reference (non-interleaved), pure PSF interleaved, 1 wt% and 2 wt% SiC-Fe₃O₄/PSF interleaved composite laminates having eight plies of E-glass fabrics were manufactured using the vacuum-assisted hand lay-up method. Nanofiber mats with 160 mm x 300 mm in size were incorporated into each successive ply. After completing the hand lay-up process, the whole system sealed by a vacuum bag was vacuumed under 0.85 bar pressure for 1.5 hours to remove the excess epoxy resin and air bubbles, and then cured at 45 °C for 6 hours followed by 80 °C for 8 hours.

Tensile tests of pure PSF, 1 wt% and 2 wt% SiC-Fe₃O₄/PSF nanofiber mats were conducted with a Shimadzu AGS-X table-top universal testing machine having a 10 N load cell at the cross-head speed of 12 mm/min.

Figure 2 shows the preparation of tensile test strips of nanofiber mats and tensile test setup. Nanofiber mats were cut into strips 10 mm x 50 mm in size. Tensile test strips were glued to a paper square frame with double-sided tapes to protect the nanofibers from damage while mounting in the tensile grips. The paper frames were cut with scissors just before starting the test.

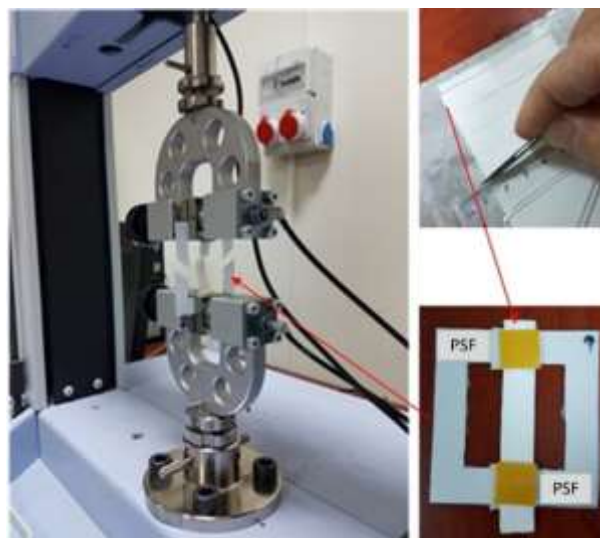


Figure 2. Preparation of tensile test strips of nanofiber mats and tensile testing

Compression and interlaminar shear tests of composite laminates were conducted with Shimadzu AGS-X Universal testing machine with a 100 kN load cell at the cross-head speed of 1.3 mm/min. Reference and nanofiber interleaved composite laminates were cut into specimens' dimensions to determine compressive and interlaminar shear strengths according to ASTM D695 and ASTM D3846. Figure 3 shows the specimen dimensions with double notches according to ASTM D3846 and the anti-buckling fixture used in compression and interlaminar shear strength tests. Interlaminar shear strength was calculated by dividing the maximum compression load by the interlaminar surface area (specimen width x the length between notches).

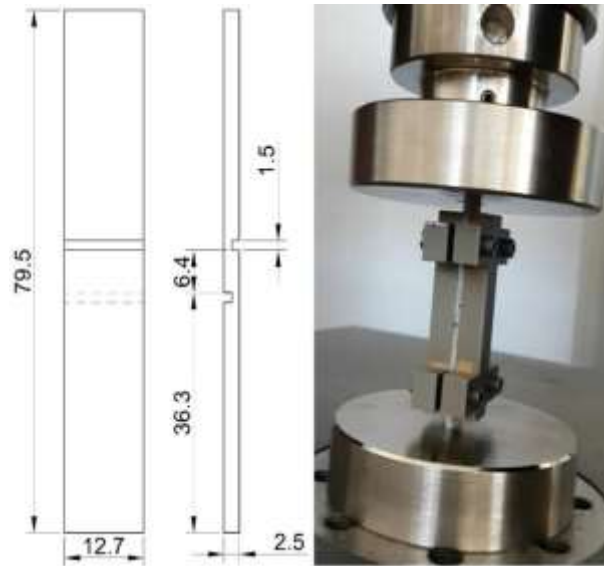


Figure 3. Interlaminar shear test specimen dimensions and anti-buckling fixture

3. RESULTS AND DISCUSSIONS

3.1. Sem Analysis of PSF Nanofibers

SEM images of pure PSF and 2 wt% SiC-Fe₃O₄/PSF hybrid PSF electrospun nanofibers are shown in Figure 4a and

Figure 4b. Nanofiber networks with a continuous and homogeneous form were obtained by the electrospinning process. The diameters of pure and hybrid nanofibers are between 300 and 500 nm. It is seen that there is no significant change in diameters and morphological properties of PSF nanofibers with 2 wt% SiC-Fe₃O₄ nanoparticles addition.

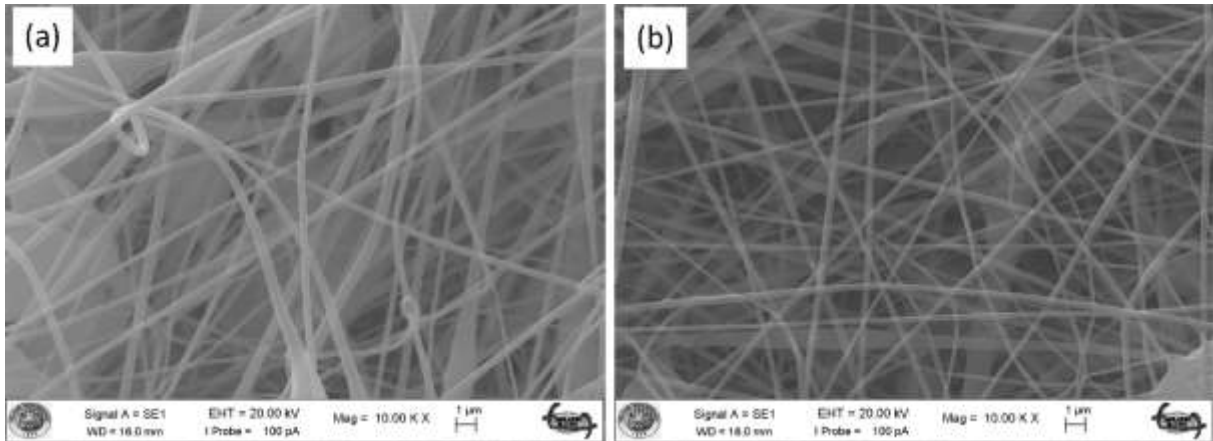


Figure 4. SEM images of (a) Pure PSF, (b) 2 wt% SiC/Fe₃O₄/PSF electrospun nanofibers.

3.2. Mechanical Tests

Effects of SiC-Fe₃O₄ nanoparticles addition to PSF solution in different concentrations on the tensile properties of electrospun PSF nanofibers are shown in Figure 5 and Table 1. In the stress-strain curves of the nanofiber mats in Figure 5, it is clearly seen that the nanoparticle doped hybrid nanofibers are positively separated from the pure PSF nanofibers until the breaking point. Compared to pure PSF nanofiber mats, no significant decrease in ductility was observed in 1% SiC-Fe₃O₄/PSF hybrid nanofiber mats. However, the elongation at break in 2% SiC Fe₃O₄/PSF hybrid nanofiber mats decreased by 13%, resulting in a significant loss in ductile deformation behavior.

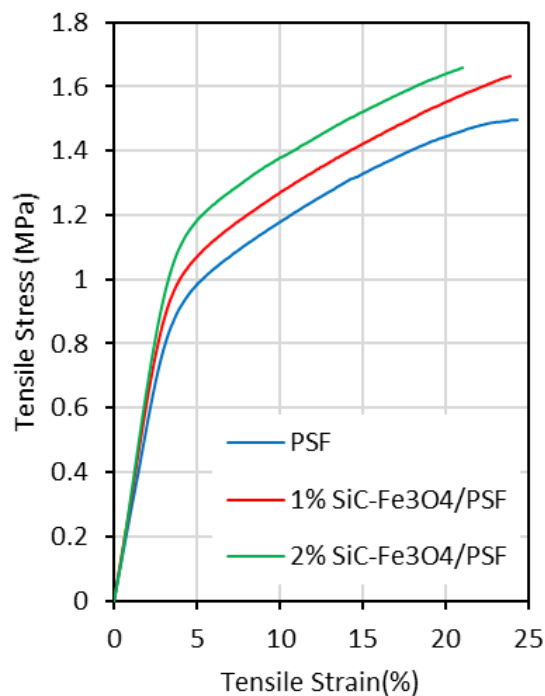


Figure 5. Tensile stress-strain curves of nanofiber mats

Considering the tensile strengths and Young's modulus values presented in Table 1, adding 1 wt% SiC-Fe₃O₄ nanoparticles into PSF nanofibers enhanced the tensile strength by 5% and Young's modulus by 27%. Moreover, 2 wt% SiC-Fe₃O₄/PSF hybrid nanofiber mats reached the highest tensile strength and Young's modulus values with an increase of 7.9% and 28.7%, respectively.

Table 1. Tensile properties of nanofiber mats

	Tensile Strength (Mpa)	Young's Modulus (Mpa)
PSF	1.54 ± 0.03	26.21 ± 0.26
1 wt% SiC-Fe ₃ O ₄ /PSF	1.62 ± 0.08	33.27 ± 1.89
2 wt% SiC-Fe ₃ O ₄ /PSF	1.66 ± 0.09	33.75 ± 2.32

Figure 6 shows the compressive stress-strain curves of reference and nanofiber interleaved composite laminates. The non-linear regions formed at the beginning of loading in the stress-strain curves of composites are toe regions caused by loosening, alignment, or seating of the specimens until the specimen is fully positioned between steel plates. The incorporation of PSF nanofiber mats between plies improved the compressive strength of glass/epoxy composite laminates. The reference composite laminate had a compressive strength of 210 MPa. Pure PSF, 1 wt% SiC-Fe₃O₄/PSF nanofiber interleaved laminates reached the compressive strength values of 264 MPa and 265 MPa, respectively, increasing by approximately 26%. 2 wt% SiC-Fe₃O₄/PSF nanofibers slightly decreased the compressive strength by 2% compared to pure PSF nanofibers. Relatively ductile PSF nanofibers made the interlaminar resin-rich regions tougher. Thus, nanofiber interleaving increased the ultimate compressive strain by up to 23% compared to the reference laminate. There was no considerable effect of 1 wt% and 2 wt% SiC-Fe₃O₄ nanoparticles addition into PSF nanofibers on the compressive strength of nanofiber interleaved laminates.

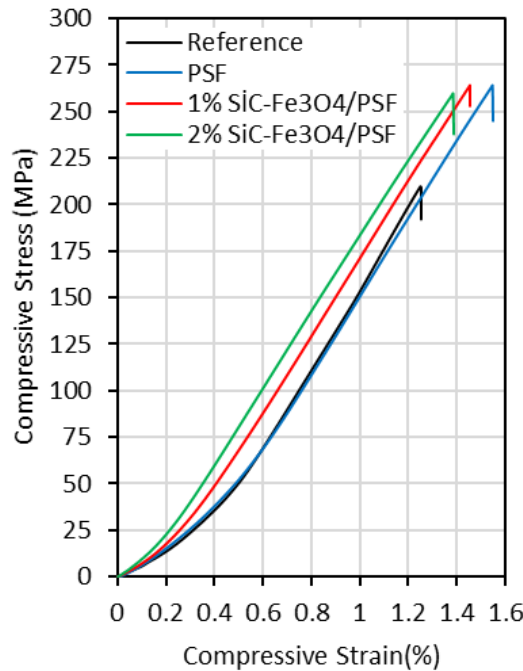


Figure 6. Compressive stress-strain curves of reference and nanofiber interleaved composite laminates

The influence of nanofiber interleaving on interlaminar shear strengths of glass/epoxy composite laminates is shown in Figure 7. The interlaminar shear strength of reference glass/epoxy composite laminates was 41.7 MPa. Pure PSF, 1 wt%, and 2 wt% SiC-Fe₃O₄/PSF nanofibers enhanced the interlaminar shear strength by 6.9%, 10%, and 12.4%, respectively. SiC-Fe₃O₄ nanoparticles doped PSF nanofibers provided further improvement in interlaminar shear resistance than that of the PSF nanofibers. 1 wt% and 2 wt% SiC-Fe₃O₄/PSF hybrid nanofibers increased the interlaminar shear strength by 3% and 5%, respectively, compared to pure PSF nanofibers.

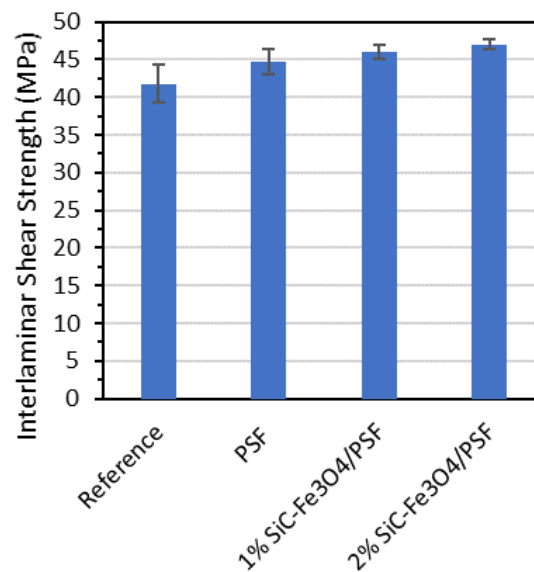


Figure 7. Interlaminar shear strength of reference and nanofiber interleaved composite laminates

4. CONCLUSIONS

In this study, pure and SiC-Fe₃O₄ nanoparticles doped PSF nanofibers were produced by the electrospinning method. Electrospun nanofibers were interleaved in glass/epoxy composites laminates to determine their effects on the compressive and interlaminar shear properties of the laminates. In summary,

The addition of SiC-Fe₃O₄ nanoparticles into PSF nanofibers improved tensile properties of nanofiber mats. 2 wt% SiC-Fe₃O₄ loading into PSF nanofibers provided the highest increase in the tensile strength and Young modulus by 7.9% and 28.7%, respectively.

1 wt% SiC-Fe₃O₄/PSF hybrid nanofibers increased the compressive strength by up to about 26% compared to reference laminates. However, it was observed that there was no significant difference in compressive strengths between hybrid and pure PSF nanofiber interleaved laminates.

The maximum improvement in the interlaminar shear strength was achieved by 2 wt% SiC-Fe₃O₄/PSF hybrid nanofibers with an increase of 12.4%.

Incorporation of pure PSF nanofibers and SiC-Fe₃O₄/PSF hybrid nanofibers between plies considerably enhanced compressive and interlaminar shear strength of glass/epoxy composites.

CONFLICT OF INTEREST

The authors stated that there are no conflicts of interest regarding the publication of this article.

REFERENCES

- [1] Wang RM, Zheng SR, Zheng YG. *Polymer Matrix Composites and Technology*: Elsevier Science, 2011.
- [2] Mallick PK. *Fiber-reinforced composites: materials, manufacturing, and design*: CRC press, 2007.
- [3] De Schoenmaker B, Van der Heijden S, De Baere I, Van Paepegem W, De Clerck K. Effect of electrospun polyamide 6 nanofibres on the mechanical properties of a glass fibre/epoxy composite. *Polymer Testing* 2013; 32: 1495-1501.
- [4] Palazzetti R, Zucchelli A. Electrospun nanofibers as reinforcement for composite laminates materials – A review. *Composite Structures* 2017; 182: 711-727.
- [5] Dzenis Y, Reneker D. Delamination resistant composites prepared by small fibre reinforcement at ply interfaces. Patent US6265333 B 2001; 1.
- [6] Molnár K, Mészáros L, Košťáková E. The effect of needleless electrospun nanofibrous interleaves on mechanical properties of carbon fabrics/epoxy laminates. *Express Polymer Letters* 2014; 8: 62-72.
- [7] Daelemans L, van der Heijden S, De Baere I, Rahier H, Van Paepegem W, De Clerck K. Using aligned nanofibres for identifying the toughening micromechanisms in nanofibre interleaved laminates. *Composites Science and Technology* 2016; 124: 17-26.
- [8] Beylergil B, Tanoğlu M, Aktaş E. Enhancement of interlaminar fracture toughness of carbon fiber-epoxy composites using polyamide-6,6 electrospun nanofibers. *Journal of Applied Polymer Science* 2017; 134.
- [9] Eskizeybek V, Yar A, Avcı A. CNT-PAN hybrid nanofibrous mat interleaved carbon/epoxy laminates with improved Mode I interlaminar fracture toughness. *Composites Science and Technology* 2018; 157: 30-39.
- [10] Saghafi H, Brugo T, Minak G, Zucchelli A. The effect of PVDF nanofibers on mode-I fracture toughness of composite materials. *Composites Part B: Engineering* 2015; 72: 213-216.
- [11] Beylergil B, Tanoğlu M, Aktaş E. Modification of Carbon Fibre/Epoxy Composites by Polyvinyl Alcohol (PVA) Based Electrospun Nanofibres. *Advanced Composites Letters* 2016; 25: 69-76.
- [12] Li G, Li P, Zhang C, Yu Y, Liu H, Zhang S, et al. Inhomogeneous toughening of carbon fiber/epoxy composite using electrospun polysulfone nanofibrous membranes by in situ phase separation. *Composites Science and Technology* 2008; 68: 987-994.
- [13] Li G, Li P, Yu Y, Jia X, Zhang S, Yang X, et al. Novel carbon fiber/epoxy composite toughened by electrospun polysulfone nanofibers. *Materials Letters* 2008; 62: 511-514.

- [14] Li P, Liu D, Zhu B, Li B, Jia X, Wang L, et al. Synchronous effects of multiscale reinforced and toughened CFRP composites by MWNTs-EP/PSF hybrid nanofibers with preferred orientation. *Composites Part A: Applied Science and Manufacturing* 2015; 68: 72-80.
- [15] Metin F, Avcı A. In-plane quasi-static and out-of-plane dynamic behavior of nanofiber interleaved glass/epoxy composites and finite element simulation. *Composite Structures* 2021; 270: 114085.
- [16] Dzenis Y. *Structural Nanocomposites*. Science 2008; 319: 419-420.
- [17] Anand A, Kumar N, Harshe R, Joshi M. Glass/epoxy structural composites with interleaved nylon 6/6 nanofibers. *Journal of Composite Materials* 2016; 51: 3291-3298.
- [18] Liu F, Guo R, Shen M, Wang S, Shi X. Effect of Processing Variables on the Morphology of Electrospun Poly[(lactic acid)-co-(glycolic acid)] Nanofibers. *Macromolecular Materials and Engineering* 2009; 294: 666-672.



REUSABLE FABRIC MASKS AGAINST COVID-19

Mustafa Erdem ÜREYEN^{1,2} , Nuran ZARİF³ , Elif KAYNAK^{2,4*} 

¹ Textile and Fashion Design Dept., Faculty of Architecture and Design, Eskisehir Technical University, Eskisehir, Turkey

² Advanced Technologies Research Center, Eskisehir Technical University, Eskisehir, Turkey

³ Grad. School of Sciences, Eskisehir Technical University, Eskisehir, Turkey

⁴ Chemical Engineering Dept., Faculty of Engineering, Eskisehir Technical University, Eskisehir, Turkey

ABSTRACT

Upon the outbreak of the COVID-19, community wide mask wearing has become an important tool to prevent the spread of the virus. The use of disposable masks -that are generally produced of three or more layers of synthetic nonwovens- by the general public is being questioned from an environmental and waste perspective. Conventional textile fabrics, on the other hand, may not provide the desired level of protection against the virus. In this study three layer fabric mask structures having a middle layer of nonwoven (100 g/m² or 120 g/m²) sandwiched between knitted polyester fabrics were prepared. The particle filtration and breathability properties of the fabric assemblies were investigated. In order to prevent bacterial growth and enable safer use, the outer layer was antibacterial and water repellent functionalized. The middle layer was also antibacterial treated. The air permeability of the three layer fabric structure with an antibacterial nonwoven (100 g/m²) middle layer and an antibacterial and water repellent outer layer was ≥ 96 l/m²/s. The particle filtration efficiency was 23% when tested for 0.3 μ m NaCl aerosol particles. The particle filtration efficiency was not reduced after washing up to 20 cycles.

Keywords: Face mask, Fabric, Antibacterial, Air permeability

1. INTRODUCTION

Before the global pandemic of Coronavirus Disease 2019 (COVID-19), the use of masks and respirators had been mostly limited to the industrial and healthcare settings where the protection of wearers from exposure to dangerous substances (chemical or biological) is required. There are well established national and international standards on the requirements of medical/surgical masks and respirators. For instance, the Turkish Standard TS EN 149 + A1 defines the requirements for respiratory protective devices and presents a classification (FFP1, FFP2 and FFP3) based on the performance criteria [1]. The classification of medical face masks (Type I, Type II, Type IIR) are defined in TS EN 14683+AC:2019-09 based on the assessment of bacterial filtration efficiency (%), differential pressure (Pa/cm²), microbial cleanliness (cfu/g) and splash resistance (kPa, only for Type IIR) [2].

Upon the outbreak of COVID-19, community-wide mask wearing was recommended by the authorities as the new coronavirus (SARS-CoV-2) mainly spreads in the form of liquid particles (liquid droplets, aerosols) from the mouth and nose, and mask wearing could reduce the risk of transmission of the virus [3, 4]. This has triggered the demand for face masks and eventually led to a shortage in the supply of face masks that are compliant with the previously established standards [5]. The use of fabric masks (barrier masks, community masks, DIY masks) by the general public has been debated not only due to the shortage of medical masks and respirators, but also because the fabric masks pose lower risk of adverse health effects [6, 7]. Surgical masks and N95 masks were found to cause discomfort as they prevent normal transpiration and increase perspiration [8]. The reports on the adverse skin reactions and sensation of dry nose due to the prolonged use of medical/surgical masks and respirators are not rarely found [9-11]. Several organizations, both regional and international, have issued guides and standards on the minimum requirements of the fabric masks [12-15]. Although the testing methods and/or

*Corresponding Author: elifkaynak@eskisehir.edu.tr

Received: 02.08.2021

Published: 30.11.2021

classifications vary, the published documents address three essential parameters: filtration, breathability and fit. In the absence of systematically reported data on the filtration performance of various textile fabrics/structures, most of the studies conducted so far have focused on the filtration performance of the masks [16, 17]. On the other hand, breathability is just as important due to the concerns associated to difficulty in breathing [6]. There are a few works concerned with both filtration and breathability performance of the fabric masks [18].

The increased use of disposable medical masks/respirators that are produced of several layers of nonwoven fabrics has also been raising concerns from an environmental and waste perspective [19]. The re-use or extended use of masks has also been questioned. The risk of bacterial growth on the mask due to successive use may also lead to serious health problems. The antimicrobial treatment of fabrics can provide efficient protection against microorganisms and address some of the problems related to the extended use of fabric masks [20]. Among other antibacterial agents, silver doped calcium phosphate based inorganic powders were successfully used for the antibacterial treatment of textiles [21]. Such inorganic structures are expected to pose lower toxicity as they tend to release silver ions at a relatively slow rate [22].

In this study the potential of the knitted polyester fabrics for the production of face masks has been investigated. Three layer fabric structures were designed to provide efficient filtration performance without compromising breathability. In order to reduce the risk of bacterial growth upon use, the middle and outer layers were antibacterial (A) treated. A water repellent (S) finish was applied on the outer layer to reduce the hydrophilicity of the polyester fabric. The performance of the fabric structure after washing has also been assessed to put forth the potential of mask for re-use after washing.

2. MATERIALS AND METHODS

Polyester (PET) knitted fabrics and 70% polyester (PET)-30% polyamide (PA) nonwoven fabrics were supplied by Meyteks Textile, Turkey and Mogul Co. Ltd, Turkey. Fabric properties are included in Table 1. For antibacterial treatment, an aqueous solution of silver doped calcium phosphate based antibacterial agent (PAG-C-75, Nanotech, Turkey) and an acrylic resin (ORGAL NA 430, Organik Kimya, Turkey) was prepared at pH=5-5.5. The fabrics were passed through this solution and squeezed with a laboratory padder (ATC-F350, Ataç, Turkey) to achieve 85% pick-up. After drying at 110°C for three minutes, the knitted fabrics were treated by a fluorocarbon based water repellent agent (Nuva 2110, Clariant, Turkey) to achieve 90% pick-up. Curing was performed at 160°C for three minutes.

Table 1. Fabric properties

Code	Type	Composition	Areal Density (g/m ²)	Thickness (µm)	Bulk Density (g/cm ³)
N1	Nonwoven	70% PET-30% PA	100	260	0.4
N2	Nonwoven	70% PET-30% PA	120	330	0.4
N3	Nonwoven	70% PET-30% PA	80	250	0.3
M1	Knitted	100% PET	128	430	0.3
M2	Knitted	100% PET	114	400	0.3
M3	Knitted	92% PET-8% EL	237	580	0.4

The fabric surfaces were analyzed by a light microscope (Discovery V20, Zeiss, Germany) equipped with a digital camera (Axiocam ERc 5s, Zeiss, Germany). Fabrics were tested for antimicrobial activity (ASTM E2149:2020) using *Escherichia coli* (ATCC 25922) as the test organism. The initial bacteria concentration was 1.5×10^5 cfu/ml. The % reduction (R) was calculated according to Equation 1 where A and C are the number of colony-forming units in the test specimen and control (untreated) specimen in cfu/ml, respectively, after the contact time (24 hours).

$$R\% = \frac{C - A}{C} \times 100 \quad (1)$$

In order to resemble mask assemblies, three types of fabric structures (I, II, III) each having three layers of fabric were prepared as shown in Figure 1. For each assembly the inner layer fabric that would be in contact with the mouth, nose and skin was of 100% polyester (M1) and used without any further treatment. Structure Type I is composed of untreated fabric layers. Structure Type II represents the samples which consist of a middle layer of PET/PA blend nonwoven (N1 or N2) and an outer layer of a knitted polyester fabric, both treated with the antibacterial agent. Structure Type III represents the samples which consists of a middle layer of antibacterial treated PET/PA blend nonwoven (N1 or N2) and an outer layer of antibacterial and water repellent treated polyester. Fabrics and fabric structures were tested for breathability according to TS 391 ISO 9237 using an air permeability tester (Proser, Turkey) at a pressure drop of 100 Pa. Three measurements were collected from different parts of each sample and the average results were reported.

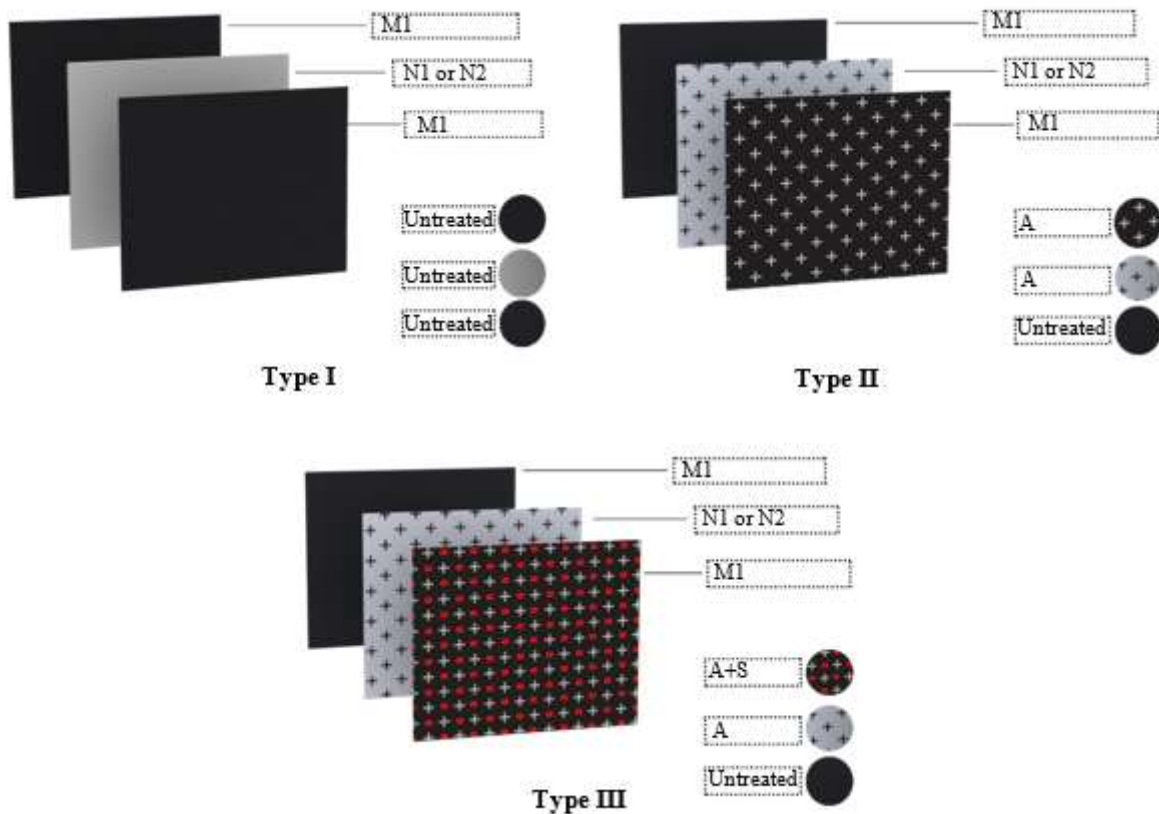


Figure 1. Three layer fabric structures (A: Antibacterial S: Water Repellent)

The particle filtration efficiency (η) of three layer structures was tested with an automated filter tester (8130a, TSI, USA) using NaCl aerosol particles of $0.3 \mu\text{m}$ at a flow rate of 95 L/min (face velocity of

15.8 cm/sec). The filtration efficiency was calculated using Equation 2 where C_u and C_d are the aerosol concentrations at the upstream and downstream, respectively.

$$\eta\% = \frac{C_u - C_d}{C_u} \times 100 \quad (2)$$

Washing was performed according to ISO 6330-2002 5A program in a wascator (FOM 71 CLS, Electrolux, Sweden) and the durability was tested after 20 washing cycles.

3. RESULTS AND DISCUSSION

3.1. Breathability

Air permeability is often used to evaluate the breathability of textile fabrics [23]. The air permeability values of different fabrics, measured as received, are given in Figure 2.

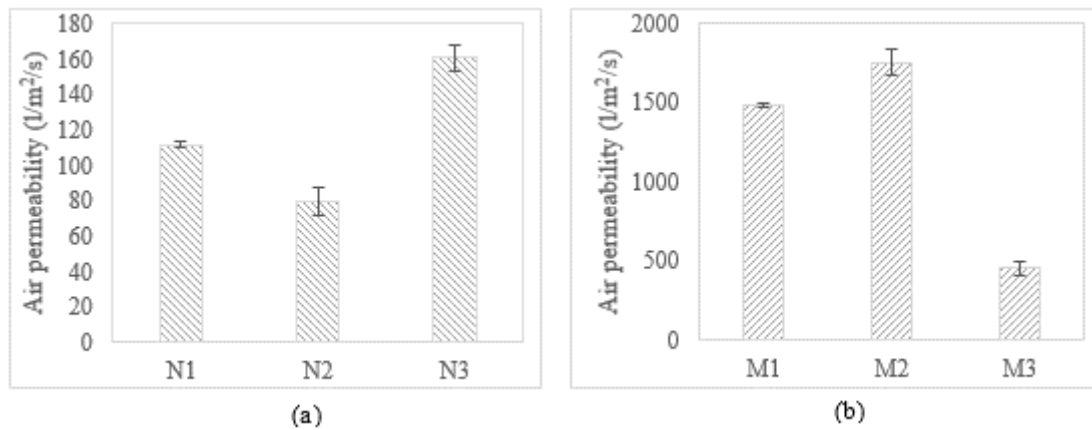


Figure 2. Air permeability of fabrics

Among the most important factors that control the air permeability of a fabric are, areal density, thickness and bulk density [24, 25]. As can be seen in Figure 2 (a), for the PET/PA blended nonwoven fabrics (N1, N2 and N3), as the areal density, bulk density and thickness increases the air permeability decreases. When compared to M1, sample M2 has a lower areal density and thickness and thus higher air permeability (Figure 2(b)). As can be seen in Figure 3 (c), the sample M3 which has the highest areal density, bulk density and thickness, also has a less porous structure which resulted in a lower air permeability. The air permeability measurement results of three layer fabric structures are given in Table 2. Each sample code begins with the outer layer fabric type, the middle and inner layer fabrics were mentioned consecutively. The letters “A” and/or “S” following the fabric type denote the treatment applied to that fabric. The air permeability of the fabric structure decreased when the areal density of the middle (nonwoven) layer was increased. The air permeability of structures having antibacterial treated layers were higher than those having only untreated layers. This may be due to the heat applied during drying/fixation which damage the nonwoven fabric structure and loosen the pores (Figure 3 (e)). The air permeability of N1 after antibacterial treatment was increased by 37%, whereas, such an increase was not observed for M1. Nevertheless, the air permeability of Type II and Type III samples (M1AN1AM1, M1ASN1AM1, M1AN2AM1, M1ASN2AM1) were ≥ 96 l/m²/s which is the minimum value of air permeability specified in CWA 17553:2020 [15]. The air permeability values of fabric structures, whether treated or untreated, were reduced gradually upon washing possibly due to fabric shrinkage and felting (Figure 3 (f)).

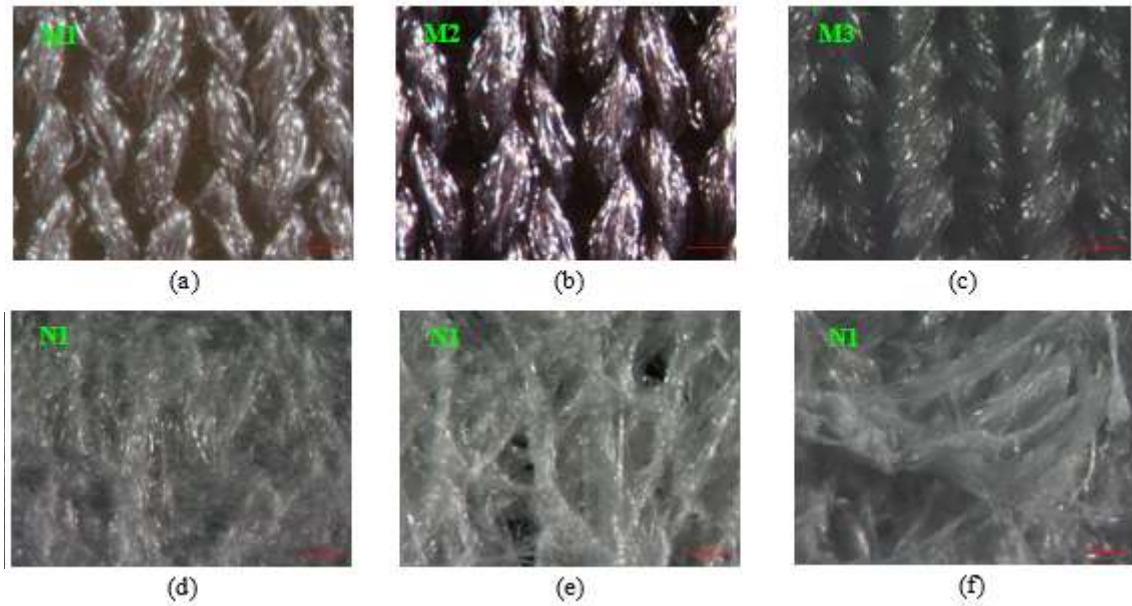


Figure 3. Microscopy images of untreated a) M1, b) M2, c) M3, d)N1, e) AB treated N1, f) AB treated N1 after 20 washing cycles at 50X magnification.

Table 2. Air permeability of three layer fabric structures (W:Washing cycle, SD:standard deviation)

Sample Code	Middle Layer Fabric	Structure Type	Air permeability (before washing) \pm SD l/m ² /s	Air permeability (after 5 W) \pm SD l/m ² /s	Air permeability (after 20 W) \pm SD l/m ² /s
M1N1M1	N1	I	91.7 \pm 5.7	77.1 \pm 5.8	75.4 \pm 3.3
M1AN1AM1	N1	II	134.5 \pm 9.1	101.7 \pm 8.1	82.5 \pm 4.3
M1ASN1AM1	N1	III	145.8 \pm 5.6	107.1 \pm 4.2	83.5 \pm 1.8
M1N2M1	N2	I	72.3 \pm 6.5	69.5 \pm 6.3	67.7 \pm 0.9
M1AN2AM1	N2	II	96.8 \pm 9.0	88.2 \pm 7.1	69.1 \pm 6.1
M1ASN2AM1	N2	III	96.8 \pm 10.2	70.8 \pm 4.9	65.6 \pm 3.2

3.2. Particle Filtration

The particle filtration efficiencies were calculated using Equation 1, for two different fabric structures (Type I and Type III in Figure 1) having N1 or N2 fabric as their middle layers. The calculated values are presented in Figure 4. The particle filtration efficiency of sample M1N2M1 (36.2%) was higher than that of M1N1M1 (32.2%). In comparison to M1N1M1, the better filtration performance of M1N2M1 may be attributed to the higher grammage and thickness of the middle layer nonwoven (N2) used in the structure [26]. The filtration efficiencies of both samples were reduced after treatment. After 20 washing cycles, the filtration efficiency of treated samples (M1ASN1AM1, M1ASN2AM1) were enhanced. These results are in good agreement with the decreasing tendency of air permeability after washing. In this study the tests were carried out using NaCl aerosol particles of 0.3 μ m. Although the current European standards for fabric masks specify the minimum filtration efficiency (90%) to particles of 3 μ m [15], aerosol particles of smaller size were specified in some other standards for respirators and face

masks [27]. Previous studies have shown that the filtration efficiency increases significantly with the increasing particle size of the aerosol used for testing [28, 29].

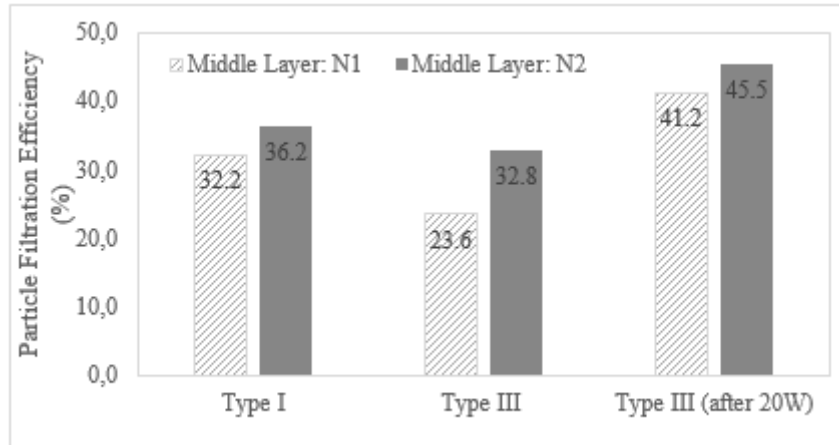


Figure 4. Particle filtration efficiency of three layer structures (W: Washing cycle)

3.3. Antimicrobial Activity

The fabrics N1, N2 and M1 were tested for antimicrobial activity after being treated with antibacterial and water repellent agents. The treated samples were washed according to the standard washing procedure and the washed samples were also tested to evaluate the effect of washing on antimicrobial activity. The antimicrobial activity test results are presented in Table 3. The PET/PA blended nonwoven samples exhibited higher antimicrobial activity than polyester knitted fabric. This may be due to larger surface areas of nonwoven fabrics which enable them to accommodate higher amounts of antibacterial agent [30]. The reduction in antimicrobial activity also occurred at a greater extent in polyester knitted fabric after washing when compared to the samples PET/PA blended nonwoven samples.

Table 3. Antimicrobial test results

Code	Treatment	Reduction (%) Before Washing	Reduction (%) After 20 Washing Cycles
N1	A	99.99	99.64
N2	A	99.99	98.85
M1	A+S	97.73	95.91

4. CONCLUSION

Antibacterial and/or water repellent finishes may be useful in reducing the health risks associated with the extended use of masks during the pandemic. However, these treatments may lead to significant changes in the fabric structure and porosity and thus, breathability and filtration properties. It was shown that for the three layer fabric assemblies, the filtration efficiency to 0.3 μm particles was reduced after functional treatments but increased after washing. The increase in filtration performance after washing might be promising in terms of reuse. The number of uses on the other hand is limited by the reduction in air permeability. Type II and Type III fabric structures using 100 g/m^2 nonwoven could comply with the current air permeability requirement ($\geq 96 \text{ l}/\text{m}^2/\text{s}$) up to 5 washing cycles.

ACKNOWLEDGEMENTS

This work was supported by the Eskişehir Technical University Scientific Research Projects Commission [grant number 20GAP073] and Scientific and Technological Research Council of Turkey (TÜBİTAK) 2247-C STAR program.

CONFLICT OF INTEREST

The authors stated that there are no conflicts of interest regarding the publication of this article.

REFERENCES

- [1] TSE. Solunumla İlgili Koruyucu Cihazlar -Parçacıklara Karşı Koruma Amaçlı Filtreli Yarım Maskeler - Özellikler, Deneyler ve İşaretleme TSE EN 149 + A1: 2010.
- [2] TSE. Tıbbi yüz maskeleri – Gereklilikler ve deney yöntemleri TS EN 14683+AC: 2019.
- [3] Cheng VC, Wong SC, Chuang VW, So SY, Chen JH, Sridhar S, To KK, Chan JF, Hung IF, Ho PL, et al. The role of community-wide wearing of face mask for control of coronavirus disease 2019 (COVID-19) epidemic due to SARS-CoV-2. *J Infect*, 2020;81:107-14.
- [4] WHO. Mask use in the context of COVID-19: interim guidance. 2020.
- [5] OECD. The Face Mask Global Value Chain in the COVID-19 Outbreak: Evidence and Policy Lessons, 2020.
- [6] ECDC. Using face masks in the community: first update effectiveness in reducing transmission of COVID-19. Stockholm2021.
- [7] Techasatian L, Lebsing S, Uppala R, Thaowandee W, Chaiyarit J, Supakunpinyo C, Panombualert S, Mairiang D, Saengnipanthkul S, Wichajarn K, et al. The Effects of the Face Mask on the Skin Underneath: A Prospective Survey During the COVID-19 Pandemic. *J Prim Care Community Health*, 2020;11:2150132720966167.
- [8] Purushothaman PK, Priyanga E, Vaidhyswaran R. Effects of Prolonged Use of Facemask on Healthcare Workers in Tertiary Care Hospital During COVID-19 Pandemic. *Indian J Otolaryngol Head Neck Surg*,2020:1-7.
- [9] Hu K, Fan J, Li X, Gou X, Li X, Zhou X. The adverse skin reactions of health care workers using personal protective equipment for COVID-19. *Medicine (Baltimore)*, 2020;99:e20603.
- [10] Xie Z, Yang YX, Zhang H. Mask-induced contact dermatitis in handling COVID-19 outbreak. *Contact Dermatitis*, 2020;83:166-7.
- [11] Yu J, Chen JK, Mowad CM, Reeder M, Hylwa S, Chisolm S, Dunnick CA, Goldminz AM, Jacob SE, Wu PA, et al. Occupational dermatitis to facial personal protective equipment in health care workers: A systematic review. *J Am Acad Dermatol*, 2021;84:486-94.
- [12] TSE. Solunumla İlgili Koruyucu Cihazlar -Parçacıklara Karşı Koruma Amaçlı Filtreli Yarım Maskeler - Özellikler, Deneyler Ve İşaretleme TSE K 599: 2002.

- [13] AFNOR. Barrier Masks: Guide to minimum requirements, methods of testing, making and use S76-001: 2020.
- [14] IPQ. Reusable community mask DNP TS C0042020007: 2020.
- [15] CEN. Community face coverings - Guide to minimum requirements, methods of testing and use CWA 17553: 2020.
- [16] Konda A, Prakash A, Moss GA, Schmoltdt M, Grant GD, Guha S. Aerosol Filtration Efficiency of Common Fabrics Used in Respiratory Cloth Masks. *ACS Nano*, 2020;14:6339-47.
- [17] Tcharkhtchi A, Abbasnezhad N, Zarbini Seydani M, Zirak N, Farzaneh S, Shirinbayan M. An overview of filtration efficiency through the masks: Mechanisms of the aerosols penetration. *Bioact Mater*, 2021;6:106-22.
- [18] Park S, Jayaraman S. From containment to harm reduction from SARS-CoV-2: a fabric mask for enhanced effectiveness, comfort, and compliance. *The Journal of The Textile Institute*, 2020;1-15.
- [19] Vanapalli KR, Sharma HB, Ranjan VP, Samal B, Bhattacharya J, Dubey BK, Goel S. Challenges and strategies for effective plastic waste management during and post COVID-19 pandemic. *Sci Total Environ*, 2021;750:141514.
- [20] Pullangott G, Kannan U, S G, Kiran DV, Maliyekkal SM. A comprehensive review on antimicrobial face masks: an emerging weapon in fighting pandemics. *RSC Advances*, 2021;11:6544-76.
- [21] Üreyen ME, Doğan A, Koparal AS. Antibacterial functionalization of cotton and polyester fabrics with a finishing agent based on silver-doped calcium phosphate powders. *Textile Research Journal*, 2012;82:1731-42.
- [22] Üreyen ME, Aslan C. Determination of silver release from antibacterial finished cotton and polyester fabrics into water. *The Journal of The Textile Institute*, 2016;1-8.
- [23] Hu JY, Li YI, Yeung KW. Air permeability. *Clothing Biosensory Engineering* 2006. p. 252-60.
- [24] Cook J, Kritzer P. Secondary Batteries – Nickel Systems | Alkaline Battery Separators. In: Garche J, editor. *Encyclopedia of Electrochemical Power Sources*: Elsevier; 2009; p. 424-51.
- [25] Çinçik E, Koç E. An analysis on air permeability of polyester/viscose blended needle-punched nonwovens. *Textile Research Journal*, 2011;82:430-42.
- [26] Cheng S, Muhaiminul ASM, Yue Z, Wang Y, Xiao Y, Militky J, Prasad M, Zhu G. Effect of Temperature on the Structure and Filtration Performance of Polypropylene Melt-Blown Nonwovens. *Autex Research Journal*, 2020;0.
- [27] Jones RM, Rempel D. Standards for Surgical Respirators and Masks: Relevance for Protecting Healthcare Workers and the Public During Pandemics. *Ann Work Expo Health*, 2021;65:495-504.

- [28] Sousa-Pinto B, Fonte AP, Lopes AA, Oliveira B, Fonseca JA, Costa-Pereira A, Correia O. Face masks for community use: An awareness call to the differences in materials. *Respirology*. 2020;25:894-5.
- [29] Nallathambi G, Evangelin S, Kasthuri R, Nivetha D. Multilayer nonwoven fabrics for filtration of micron and submicron particles. *Journal of Textile Engineering & Fashion Technology*, 2019;5.
- [30] Erdem R, Rajendran S. Influence of Silver Loaded Antibacterial Agent on Knitted and Nonwoven Fabrics and Some Fabric Properties. *Journal of Engineered Fibers and Fabrics*, 2016;11:38-46.



MECHANICAL PERFORMANCE OF CARBON - ARAMID FIBER-REINFORCED LAMINATED COMPOSITES UNDER IMPACT AND SHEAR LOADING

Beyza Nur ATMACA¹ , Ramazan ORUC^{1,2} , Gorkem ASCI^{1,2} , Kadir YIGIT¹ ,
Serkan YUZER^{1,2} , Yusuf POLAT^{2,3} , Bulent EKICI¹ 

¹Department of Mechanical Eng., Eng. Faculty, Marmara Uni., Istanbul, Turkey

²TEMAG Labs, Textile Tech. and Design Faculty, Istanbul Tech. Uni., Istanbul, Turkey

³Department of Mechanical Eng., Eng. and Arch. Faculty, Erzurum Tech. Uni., Erzurum, Turkey

ABSTRACT

In this study, the drop weight impact response and the interlaminar shear strength of hybrid carbon/aramid fiber-reinforced laminated composites with different stacking sequences were investigated. Seven different laminates including two types of sandwich-like interply hybrid, three types of interply hybrid, and two types of non-hybrid named carbon and aramid were produced using the vacuum-assisted resin transfer molding method. Drop weight impact and short-beam shear tests were applied to the laminates to calculate the low-velocity impact response and the interlaminar shear strength, respectively. It is observed that while the outer layer of the hybrid structure is carbon, the structure can carry less load but absorb more energy. Pure carbon and pure aramid composites cannot carry loads but can absorb energy as much as their hybrid versions can. Sandwich-like interply hybrid with central carbon showed the best results when load and energy values were compared. Also, sandwich-like interply hybrid with central carbon has higher ILSS among hybrid structures because its center region consists of carbon layers.

Keywords: Carbon fiber, Aramid fiber, Hybrid composites, Low-velocity impact response, Interlaminar shear strength (ILSS)

1. INTRODUCTION

Composite materials are widely used in many areas especially in aviation due to their mechanical and light-weight properties [1]. Increasing demand for composite materials led to the combination of different composite materials called hybrid structures [2]. These hybrid composites are used for increasing the effectiveness of non-hybrid structures. Carbon-aramid composites are one of the most known hybrid structures used in different areas [3].

The DWI test is generally applied to structures to determine the resistance of the material to a sudden impact force. A typical example of sudden impact is hail rain on aircraft wings. For each sequence, three samples were tested to include deviation of results from each other. The impact material effect on the peak load and energy absorption was discussed. Yang et al. [4] studied the low-velocity impact response of plain-woven glass and carbon fiber fabrics. Experimental results show that the energy absorption capacity of hybrid composites can be higher than non-hybrid composites in the impact event. In the study of Sun Ying et al. [5], it is observed that hybridization of carbon and aramid improves the impact properties of carbon/epoxy composites by softening the sharp drop after peak load.

The interlaminar shear strength (ILSS) parameter which can be determined by the short beam shear (SBS) test method, indicates the strength of composite material against delamination type damage. Previous studies on the carbon/glass fiber hybrid composites [6] and carbon/aramid fiber hybrid composites [7] showed the effects of the hybridization process, ply angle, and stacking sequence on the ILSS parameter.

*Corresponding Author: yfpolat1@gmail.com

Received: 02.08.2021 Published: 30.11.2021

Since the hybrid composites consist of different plies, there might be different problematic cases. There might be problems such as stress concentrations due to transverse multifilament failure [8], compatibility of different polymer phases [9], delamination of different layers [10]. These problems might cause catastrophic failures at the earlier stage of the composite. Therefore, necessary precautions should be taken by using standard test methods.

This study aims to examine and compare the low-velocity impact response and the interlaminar shear strength (ILSS) of carbon/aramid hybrid composites by drop weight impact (DWI) and short beam shear (SBS) tests.

2. EXPERIMENTAL

2.1 Material

A 200 g/m² plain woven carbon fiber fabric (DOWAKSA, Turkey) and TWARON CT709 aramid fiber fabric (Teijin, Holland) were used as reinforcement materials for the composites. The DTE1200 series of Duratek epoxy resin was used with the DTS2110 hardener.

2.2 Method

Carbon-aramid reinforced epoxy composite structures were produced with vacuum-assisted resin transfer molding (VARTM) technique as shown in Figure 1. In this system, 12 layers of reinforcing fabrics were stacked over a flat surface. A release film was laid under fabrics to remove the sample after production. Then, a flow mesh is used to make the resin flow fast, and a peel ply is used to separate the composite sample from the flow mesh. Two spiral tubes were placed to opposing edges. Furthermore, a vacuum bag was used to create a vacuum ambient to the system. The resin was fed from one spiral tube towards the other with the help of a vacuum pump. Hence, resin impregnation was completed after nearly 10 minutes. After resin impregnation, the system kept 36 hours under vacuum ambient to complete the curing process of the resin.

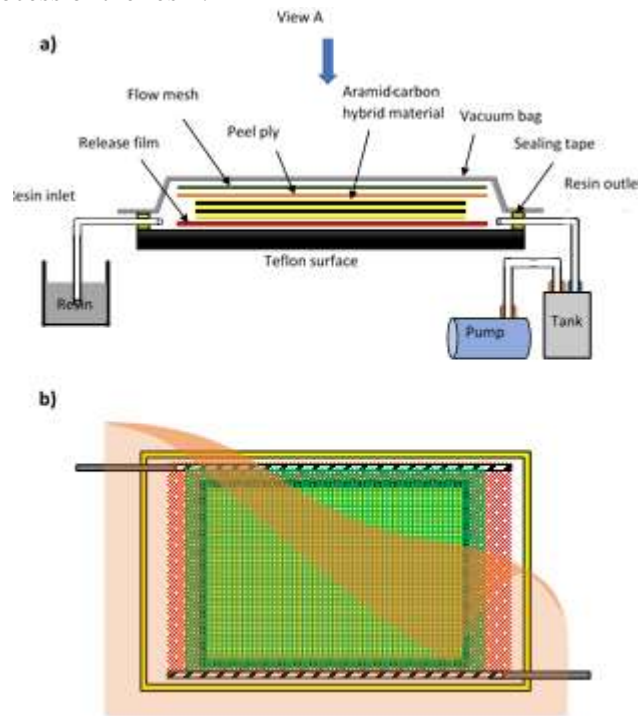


Figure 1. VARTM method demonstration (a) side view; (b) top view (view A)

Two types of sandwich-like interply hybrid ($[C_3A_3]_s$, $[A_3C_3]_s$), three types of interply hybrid ($[C_3A_3]_2$, $[A_3C_3]_2$ and $[CA]_6$) and two types of non-hybrid carbon ($[A_{12}]$) and aramid laminates ($[C_{12}]$) were tested for the comparative study. The stacking sequences of the laminates are given in Table 1. It has been seen that different stacking sequence of hybrid structures has shown different results under DWI and SBS tests [4], [5].

Table 1. Different stacking sequences of carbon/aramid hybrid laminates

Stacking Sequence	Ply number											
	1	2	3	4	5	6	7	8	9	10	11	12
$[C_{12}]$	Black	Black	Black	Black	Black	Black	Black	Black	Black	Black	Black	Black
$[A_{12}]$	Yellow	Yellow	Yellow	Yellow	Yellow	Yellow	Yellow	Yellow	Yellow	Yellow	Yellow	Yellow
$[C_3A_3]_s$	Black	Black	Black	Black	Black	Black	Black	Black	Black	Black	Black	Black
$[A_3C_3]_s$	Yellow	Yellow	Yellow	Yellow	Yellow	Yellow	Yellow	Yellow	Yellow	Yellow	Yellow	Yellow
$[C_3A_3]_2$	Black	Black	Black	Black	Black	Black	Black	Black	Black	Black	Black	Black
$[A_3C_3]_2$	Yellow	Yellow	Yellow	Yellow	Yellow	Yellow	Yellow	Yellow	Yellow	Yellow	Yellow	Yellow
$[CA]_6$	Black	Yellow	Black	Yellow	Black	Yellow	Black	Yellow	Black	Yellow	Black	Yellow

Low-velocity impact tests were carried out using the BESMAK BMT-DW series drop weight impact material testing machine according to the ASTM D7136 [6]. The demonstration of the DWI test is shown in Figure 2. The dimension of the DWI sample was 80 mm x 50 mm. At least five samples were tested and the average value was calculated. As a result of the literature review, the impactor energy required for the test was selected as 30 J. If a larger amount of energy were used, it would pierce the samples. Therefore, the damages in all samples would be the same. In this study, how much energy it absorbs at a given joule value and how it causes damage was analyzed.

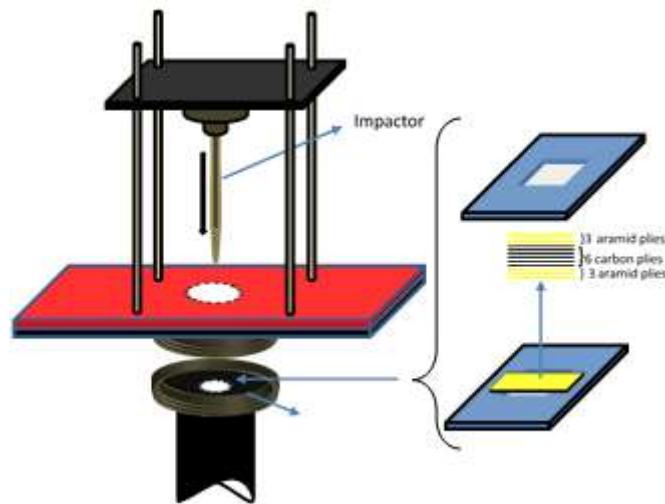


Figure 2. A closer demonstration of the DWI test setup.

ASTM D2344 [7] standard was used for the SBS test. The rectangular samples with dimensions of 24 mm x 8 mm were used. For each sequence, five samples were tested. The test was conducted using the AG-100kNXplus model of SHIMADZU. The demonstration of the SBS test is shown in Figure 3.

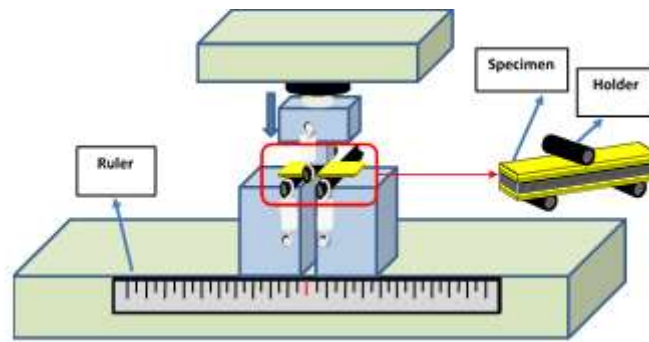


Figure 3. A closer demonstration of the SBS test setup

3. RESULTS AND DISCUSSIONS

After the laminates were produced, the thickness of each laminate was measured to use for the ILSS calculations. The thickness values are shown in Table 2.

Table 2. The thicknesses of the laminates

Sample	Thickness (mm)
[A ₁₂]	3.15
[C ₁₂]	3.20
[C ₃ A ₃] _s	3.15
[A ₃ C ₃] _s	2.95
[C ₃ A ₃] ₂	3.25
[A ₃ C ₃] ₂	3.05
[CA] ₆	3.10

3.1. Low-Velocity Impact Test

Damage to the specimens reveals information about the characteristic behavior of materials. When Figure 4 is examined, different forms of damage are observed. Aramid fiber absorbs the load in a ductile manner. On the contrary, carbon shows brittle behavior under the test. Damage types in the hybrid samples were different from those in the non-hybrid samples. Since one side of the laminate [CA]₆ is carbon fiber and one side is aramid fiber, the force was applied to the carbon fiber side in half of the samples and to the aramid fiber side in the other half, and damage behaviors were observed.

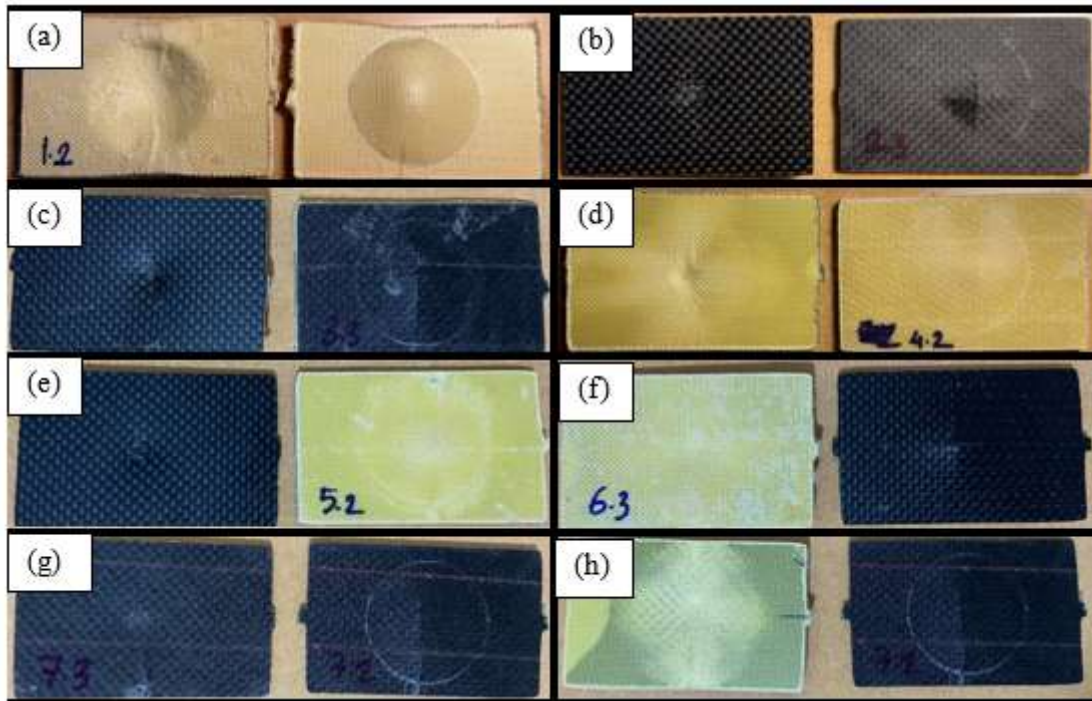


Figure 1. The damages in the specimens of the laminates (a)[A₁₂], (b) [C₁₂], (c) [C₃A₃]_s, (d) [A₃C₃]_s, (e) [C₃A₃]₂, (f) [A₃C₃]₂, (g) [CA]₆ from front and (h) [CA]₆ from back, respectively

When Figure 5 is investigated, it can be observed that the maximum load that the pure carbon and pure aramid composites can carry is less than hybrid composites.

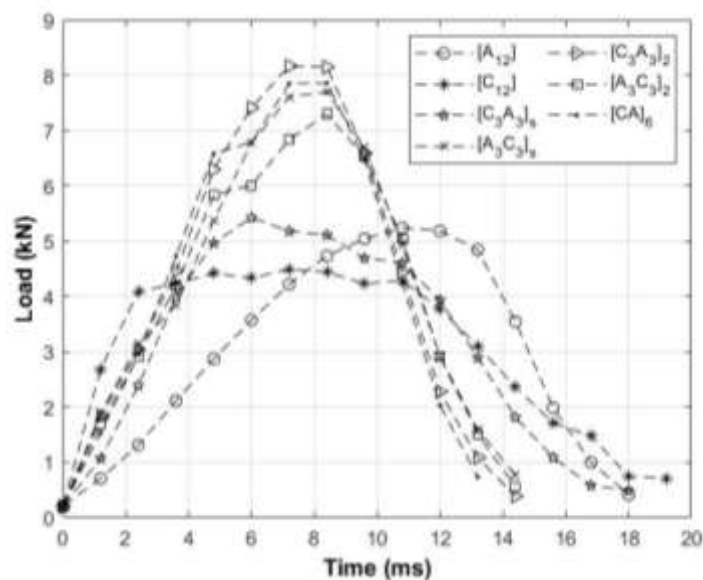


Figure 5. Load-time curves of hybrid composites

When Figure 6 is investigated, it is noticed that while non-hybrid carbon sample peak moment point energies shifts to the left, non-hybrid aramid sample peak moment point energy shifts to right, and remaining hybrid structures lie in between.

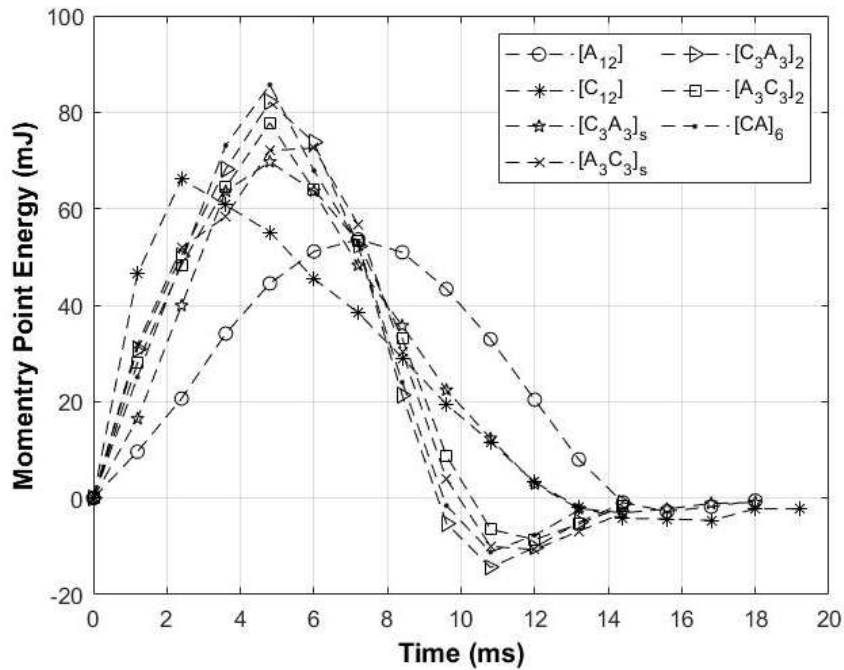


Figure 6. Momentary point energy-time curves of hybrid composites

The initial energy was set to 30 J for the DWI test. According to data in Table 3, as $[A_3C_3]_s$ carried the maximum load, in contrast, it showed the poorest energy absorption. When the data of the seven samples are compared, it is seen that $[A_3C_3]_s$ has the most proper maximum load, absorbed energy, and fiber weight fraction values.

Table 3. The average loads, absorbed energies, and fiber weight fraction values of the samples.

Sample	Max. Load (kN)	Absorbed Energy (J)	Fiber Weight Fraction (%)
$[A_{12}]$	5.139 ± 0.102	27.193 ± 0.035	54.962 ± 0.149
$[C_{12}]$	4.599 ± 0.126	26.700 ± 0.132	63.862 ± 0.528
$[C_3A_3]_s$	6.075 ± 0.557	27.091 ± 0.298	59.632 ± 0.527
$[A_3C_3]_s$	8.141 ± 0.314	25.463 ± 0.429	60.379 ± 0.310
$[C_3A_3]_2$	8.103 ± 0.320	26.023 ± 0.504	54.969 ± 0.649
$[A_3C_3]_2$	7.777 ± 0.650	26.767 ± 0.204	58.068 ± 0.437
$[CA]_6$	7.743 ± 0.436	26.715 ± 0.330	57.143 ± 0.000

3.2 Short Beam Shear Test

As shown in Figure 7, the weakest configurations have higher displacement, and the strongest configuration has low displacement [11].

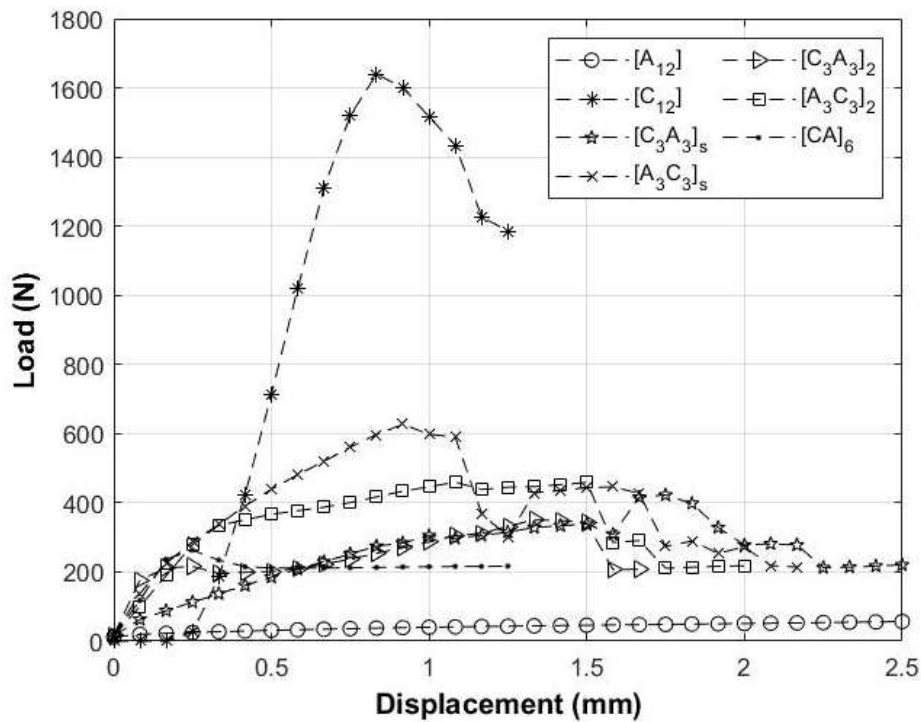


Figure 7. Load - displacement curves of hybrid composites

As seen in Table 4, $[A_{12}]$ full aramid composite configuration has the lowest ILSS due to its nature while the opposite situation is valid for $[C_{12}]$ full carbon composite configuration. The other five configurations contain the same amount of carbon and aramid. However, the ILSS of $[CA]_6$ is the weakest configuration because it has the greatest number of faces which is between different materials and this situation decreases its shear strength. In the SBS test, maximum normal stresses occur upper and lower surfaces of a specimen and maximum shear stress occurs at the middle plane of the specimen. $[A_3C_3]_s$ the configuration has higher ILSS among hybrid structures because its center region consists of carbon layers.

Table 4. Overall results for the SBS test

Sample	Max. Load (kN)	ILSS (MPa)
$[A_{12}]$	62.39 ± 9.03	1.86 ± 0.27
$[C_{12}]$	1604.98 ± 127.25	47.02 ± 3.73
$[C_3A_3]_s$	293.16 ± 41.28	8.72 ± 1.23
$[A_3C_3]_s$	590.82 ± 54.16	18.78 ± 1.72
$[C_3A_3]_2$	445.10 ± 39.41	13.68 ± 1.21
$[A_3C_3]_2$	352.53 ± 59.40	10.17 ± 1.71
$[CA]_6$	244.43 ± 28.90	7.39 ± 0.87

4. CONCLUSION

In this study, the effect of carbon aramid hybrid structures on the low-velocity impact response and ILSS was investigated experimentally. The following conclusions are obtained:

- It is observed that while the outer layer of the hybrid structure is carbon, such as $[C_{12}]$, $[C_3A_3]_s$, $[C_3A_3]_2$, $[CA]_6$, the structure can carry less load but absorb more energy.
- Pure carbon, and pure aramid, composites cannot carry loads but can absorb energy as much as their hybrid versions can.
- The sequence of $[A_3C_3]_s$ showed the best result when load and energy values were compared.
- It was observed that the DWI tests results were close and not affected by the stacking sequences of $[C_3A_3]_2$, $[A_3C_3]_2$, and $[CA]_6$.
- $[A_3C_3]_s$ the configuration has higher ILSS among hybrid structures because its center region consists of carbon layers.

5. FURTHER WORK

The further aim of the research will be conducting the other tests such as tensile, flexural, and dynamic mechanical analysis (DMA).

ACKNOWLEDGMENTS

The authors gratefully acknowledge AREKA Filtration Technologies Ltd. and Bulut Makina for providing financial support.

CONFLICT OF INTEREST

The authors stated that there are no conflicts of interest regarding the publication of this article.

REFERENCES

- [1] Abrate S. Impact on Composite Structures. Cambridge: Cambridge University Press, 1998. doi: 10.1017/CBO9780511574504.
- [2] Mallick PK. Fiber-reinforced composites: materials, manufacturing, and design, 3rd ed., [Expanded and rev. Ed.]. Boca Raton, FL: CRC Press, 2008.
- [3] Song JH. Pairing effect and tensile properties of laminated high-performance hybrid composites prepared using carbon/glass and carbon/aramid fibers. *Compos. Part B Eng*, Sep. 2015, vol. 79, pp. 61–66, doi: 10.1016/j.compositesb.2015.04.015.
- [4] Ying S, Mengyun T, Zhijun R, Baohui S and Li C. An experimental investigation on the low-velocity impact response of carbon–aramid/epoxy hybrid composite laminates. *J Reinf Plast Compos*, Dec. 2016, vol. 36, p. 073168441668089, doi: 10.1177/0731684416680893.
- [5] Krishnan P and Kishore, Interlaminar shear of woven fabric Kevlar-epoxy composites in three-point loading. *Mater. Sci. Eng. -Struct. Mater. Prop. Microstruct. Process. - Mater Sci Eng -Struct Mater*, Jun. 1995, vol. 197, pp. 113–118, doi: 10.1016/0921-5093(94)09742-9.

- [6] Turla P, Surae S, Reddy P and Shekar K. Interlaminar Shear Strength of Carbon Fiber and Glass Fiber Reinforced Epoxy Matrix Hybrid Composite, May, 2014.
- [7] Guled F and Chittappa H. Influence of interply arrangement on inter-laminar shear strength of carbon-Kevlar/epoxy hybrid composites, 2019; c. 2057, s. 020045. doi: 10.1063/1.5085616.
- [8] Kobelev VV. Explicit crack problem solutions of hybrid composites. *International Journal of Solids and Structures*, 1993; 30(3), 413–426. doi:10.1016/0020-7683(93)90176-8.
- [9] Artemenko SE, Kadykova YA. Hybrid composite materials. *Fibre Chemistry*, 2008; 40(6), 490–492. doi:10.1007/s10692-009-9091-4.
- [10] Herakovich CT. On the Relationship between Engineering Properties and Delamination of Composite Materials. *Journal of Composite Materials*, 1981; 15(4), 336–348. doi:10.1177/002199838101500404
- [11] D30 Committee, Test Method for Measuring the Damage Resistance of a Fiber-Reinforced Polymer Matrix Composite to a Drop-Weight Impact Event. ASTM International. doi: 10.1520/D7136_D7136M-15.
- [12] D30 Committee, Test Method for Short-Beam Strength of Polymer Matrix Composite Materials and Their Laminates. ASTM International, doi: 10.1520/D2344_D2344M-16.
- [13] I. Ary Subagia DG, Kim Y, Tijing L, Pant H and Shon HK. Effect of stacking sequence on the flexural properties of hybrid composites reinforced with carbon and basalt fibers. *Compos Part B Eng*, Mar, 2014; vol. 58, pp. 251–258, doi: 10.1016/j.compositesb.2013.10.027.



STRETCHABLE PIEZORESISTIVE SENSORS WITH GRAPHENE AND POLYANILINE COATED WOVEN POLYESTER FABRICS

Meryem ÇETİNOĞLU¹ , Gizem FINDIK¹ ,
Ömer Faruk ÜNSAL¹ , Ayşe ÇELİK BEDELOĞLU^{1*} 

¹ Polymer Materials Engineering Department, Faculty of Engineering and Natural Sciences, Bursa Technical University, Bursa, Turkey

ABSTRACT

Wearable electronics, which include wearable sensors, energy generating textiles, textile based energy storage devices, etc. is a rising trend on materials science and textile researches for last a few decades. Textile based flexible capacitors, nanogenerators, motion sensors, photovoltaic cells have been studied greatly and these devices getting commercial for last a few years. Strain is the concept that expresses mechanical deformation rate for a material. Strain sensors are smart materials, which works according to piezoelectric and piezoresistive mechanism to determine the mechanical deformation rate of materials, that can be used in mechanical characterization, structural quality control and, more recently, wearable electronics. Piezoresistive effect defines the electrical conductivity (or resistivity) changes of a material under mechanical stress. Especially on nanocomposite based strain sensors, contact between conductive nanoparticles is interrupted and this dissociation causes the resistivity change under mechanical effect. We have used a commercial, highly flexible woven fabric as base material and its flexibility provided the stretchable character for developed sensor fabric. Combining its flexibility with conductivity of graphene and/or polyaniline, promising resistivity values were observed. Furthermore, flexible nature of graphene and brittle behavior of polyaniline clearly seen in electro-mechanical characterization. The developed fabric strain sensor can be used in smart textiles and future applications for wearable electronics.

Keywords: Strain sensor, Graphene, Conductive polymer, Smart textiles, Electronic fabrics

1. INTRODUCTION

With the improvement of wearable technology flexible smart wearable devices have been significant in the daily life. One of these devices, flexible strain sensors have been attracted a lot of interest due to their highly flexibility on surface coating and with the purpose of observing structural stability of wearable electronics, smart devices, smart fabrics, soft robotic and materials lately [1]. Fabrics are useful for different implementations by the developing technology and taking the human body shape for smart textile applications [2–4]. In this qualifications some of the applications are based on elastic deformation ability. Strain sensors are the devices which have signal generation ability under mechanical forces [5].

Generally, various fibers, yarns and fabrics can be used to develop wearable devices. Lately, researches on flexible sensors based on successfully-produced fabrics for wearable devices are becoming more important [6]. For that reason, flexible fabrics with lycra is eligible for obtaining wearable flexible sensors that have high performance and easy production processes. Graphene and its derivatives are commonly used for flexible sensors in literature [7, 8], due to their remarkable electrical and mechanical properties [9]. Graphene is a material one-carbon-atom-thick, structure of hexagonally arranged, sp²-hybridized carbon atoms. In addition to its remarkable 2-dimensional structure, graphene also stands out with its low electrical resistance and thermal conductivity (31Ω/m² resistivity, 5300 W/m.K), and high mechanical properties compared to its thickness at the atomic level[10–12]. On the other hand, polyaniline is a conducting polymer that has a wide range of usage area, affordable, easily-producible and multi conductive [13, 14]. It can be synthesized with oxidative chemical or electrochemical

*Corresponding Author: ayse.bedeloglu@btu.edu.tr

Received: 03.08.2021 Published: 30.11.2021

oxidations by polymerization of aniline monomer, in acidic aqueous medium [15, 16]. PANI coating of textile materials is a low cost and efficient method by oxidative polymerization and PANI coated textiles have many usage areas such as; sensors electromagnetic protection, static charge distribution [17]. PANI can be implemented in coating the surface of polyester, nylon, wool, acrylic, cotton, silica and glass. It is a widely used polymer among conductive materials in addition to its unique properties such as high thermal, electrical and environmental/chemical stability as well as its reasonable cost. PANI is widely used with different materials such as graphene and its derivatives to gain synergistic mechanical or electrical effect due to its poor performance in energy storage, contra ion addition/discharge and charge/discharge cycle life and weak mechanical properties [13, 14, 18].

Thanks to easy applicable to textiles, low cost, unique electrical and mechanical properties, and synergistic effect of PANI and graphene (or derivatives), there too many researches on PANI/graphene based electronic textiles. Fabric electrodes, textile based supercapacitors, solar cells, sensors, and energy generators [19–23].

In this study, conductive fabrics were obtained by dip-coating and in-situ oxidative polymerization processes on elastic polyester fabric. Reduced graphene oxide (rGO), PANI or both are successfully coated onto the textile surface. The electrical resistances of the obtained conductive fabrics were measured simultaneously under tensile stress, and the feasibility of different coatings in sensor applications was evaluated by revealing the change in their electrical resistance with elongation. The fabrics also characterized by differential scanning calorimetry (DSC), Fourier-transform infrared spectrophotometry (FT-IR), UV-VIS spectrophotometry and scanning electron microscopy (SEM).

2. MATERIALS AND METHODS

2.1. Materials

For graphene oxide (GO) production, graphite (Merck), phosphoric acid (85% Sigma-Aldrich), sulfuric acid (98% Merck), hydrogen peroxide (35%, Sigma-Aldrich), hydrochloric acid (37%, Fischer Chemicals), ethyl alcohol (ISOLAB); for reduction process, hydrazine hydrate (55%, Sigma) and for polyaniline synthesis aniline (99,9%, Sigma-Aldrich), hydrochloric acid (37%, WVR Chemicals) and ammonium persulfate (APS) (98%, Sigma) were purchased.

2.2. Methods

Polyester fabric was washed at 30°C in a home-type washing machine then dried. In order to purify the dried fabric from the ions in the detergent or mains water, it was kept in distilled water for 30 minutes and dried again. Then it was cut into 6 cm × 20 cm dimensions.

2.2.1. rGO coating of fabrics

In this study, graphene oxide is used as graphene precursor material thanks to its highly homogenous dispersion ability in water. Graphene oxide (GO) was produced by wet chemical process, according to Improved Hummers' Method [24]. GO particles are purified by distilled water and centrifuged repeatedly in order to removal of residual ions and acid molecules which come from synthesis step. Purified GO was dried in fume hood in room conditions. GO dispersion was prepared at a concentration of 1 mg/mL by homogenizing solid GO in distilled water with an ultrasonic homogenizer. 6 cm × 20 cm fabrics are immersed in GO/water dispersion and kept in dispersion for 10 minutes for each coating and then dried at 50°C for 30 minutes. Fabrics were stored by coating once, twice and three times. Once,

twice or three times GO coated fabrics were reduced in 0.3 M hydrazine hydrate solution at 95°C for 3 hours [25].

2.2.2. PANI coating of fabrics

rGO coated or neat polyester fabrics were coated with polyaniline by in situ polymerization method. PANI synthesis was carried out in accordance with the method in the literature with presence of rGO coated or neat polyester fabric [26]. Firstly, aniline was dissolved in 1 M HCl solution. The reaction flask was cooled between 0-5 °C and the fabrics were immersed in the reaction flask by wrapping it around a cylinder like shaped apparatus to keep it stable and coat homogeneously. Ammonium persulfate used as initiator was also dissolved in 1 M HCl and added dropwise to the reaction flask. APS:aniline molar ratio was determined as 1:4. The reaction was continued for 3 hours from the start of addition of the initiator. Since the rGO coated fabrics shrink due to the heat during GO reduction process, the neat fabric was also boiled at the same temperature. All of samples were named in Table 1.

Table 1. Sample names of fabrics with different coatings

Sample Name	Coatings
rGP1	Once rGO + PANI
rGP2	Twice rGO + PANI
rGP3	3 times rGO + PANI
P	PANI
rG2	Twice rGO
rG3	3 times rGO
GO1	Once GO
GO2	Twice GO
GO3	3 times GO

2.2.3. Characterization

In order for determining the elastic region of the fabric, a tensile test was applied to fabric (SHIMADZU - AGS-X). It was then subjected to tensile test to examine its electro-mechanical sensing features. The fabric sensor was held for 5 seconds at every 5% elongation. Electrodes were mounted onto fabrics and connected a multimeter (KEITHLEY 2400) and resistance values were recorded at this time. The test speed was determined as 5 mm/s. The effect of the coating was observed by subjecting the raw fabric and rGO and/or PANI coated fabrics to FT-IR spectrophotometry (Nicolet- IS50), UV-VIS spectrophotometry, DSC methods. Fiber morphology and coated areas of fabrics also examined by SEM (Carl Zeiss / Gemini 300) device with different magnifications.

3. RESULTS

FT-IR analysis were performed between 400 cm⁻¹ and 4000 cm⁻¹ with Attenuated Total Reflectance (ATR) unit. As the result of FT-IR analyzes it was observed that the characteristic polyester peaks between 1750 cm⁻¹ and 400 cm⁻¹ were visible after coating, although their intensity decreased (Figure 1). It was determined that the C-H peaks at approximately 2900 cm⁻¹ disappeared with the coating process. The peaks at 1711 cm⁻¹ represents from stretch of carbonyl groups, at 1409 cm⁻¹ comes from aromatic groups on backbone, 1235 cm⁻¹ is C-O stretching, and 720 cm⁻¹ is C-H bending vibrations, respectively (Figure 1) [27–29].

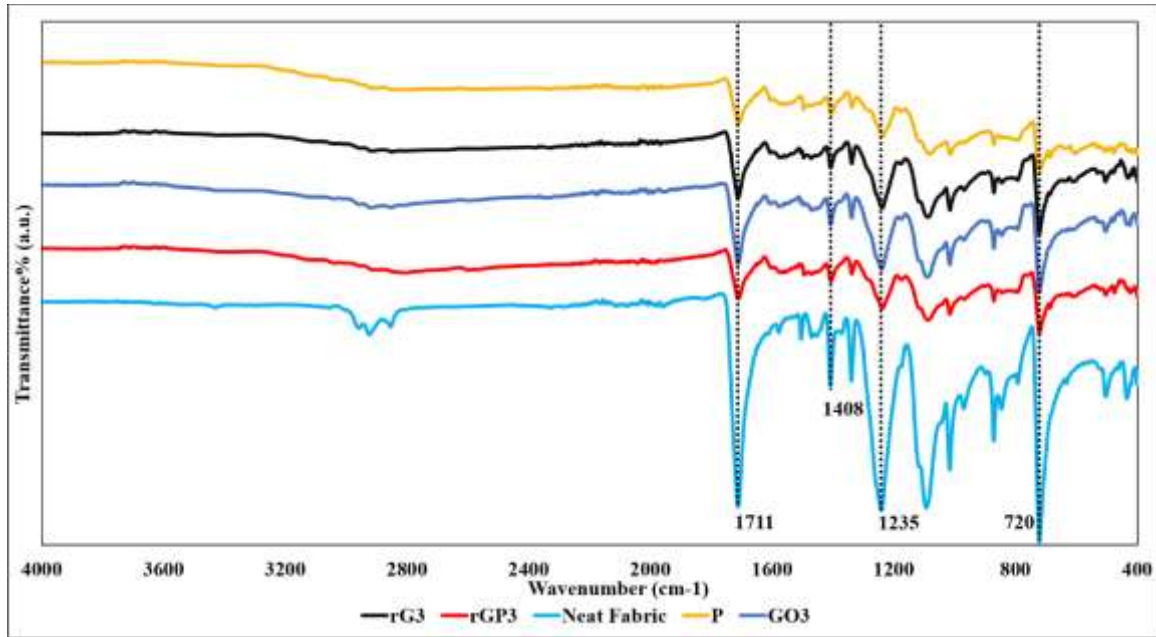


Figure 1. FT-IR spectra of neat and coated polyester fabrics

Light absorption characteristics of raw and coated fabrics were characterized with spectrophotometer between 350 nm-750 nm wavelength (Figure 2). UV-VIS absorbance spectra of neat polyester fabric showed regular absorbance curve with absorbance increase under 400 nm wavelength. However, graphene and/or PANI coated fabrics showed serrated and regular horizontal lines through the visible spectrum. Heterogeneity of graphene or PANI at nano or sub-micro scale caused this irregularity. The rG1 sample showed only different UV-VIS absorbance curve with lower light absorbance. Furthermore, PANI coated fabric showed a peak at 520 nm. This peak is the characteristic peak of polyaniline, according to literature [30].

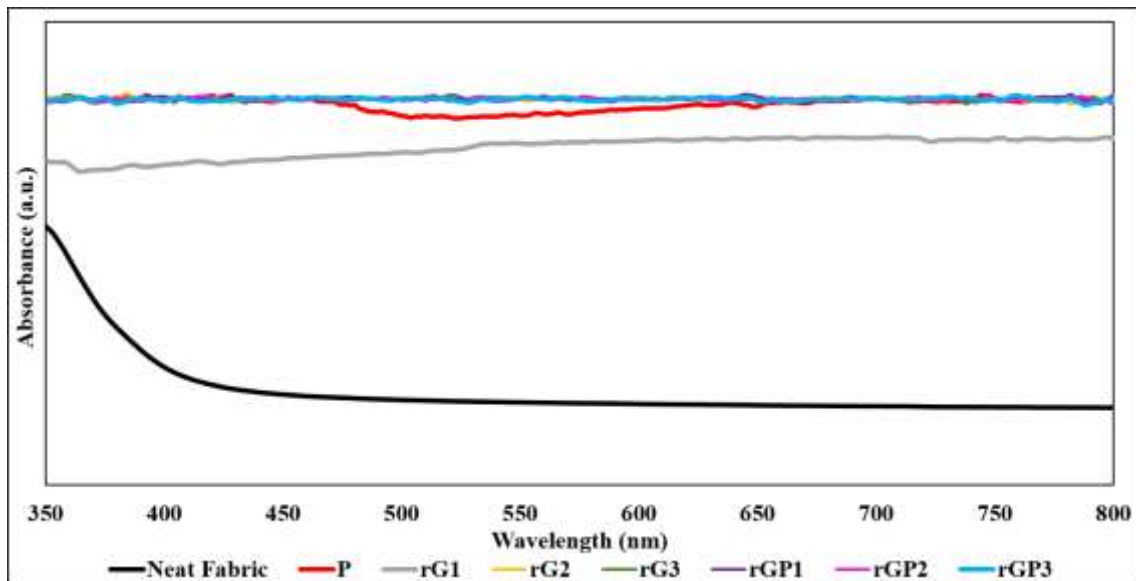


Figure 2. UV-VIS absorption curve of neat and coated fabrics

DSC analysis were performed in order to investigate the rGO and/or PANI effect on thermal properties of fabrics. DSC experiments were performed with 3 °C/min heating rate under nitrogen atmosphere. All samples gave a melting dip at 250 °C independently from coating amount and material (Figure 3). Additionally, PANI and rGO/PANI coated fabrics showed two dips at 139 °C and 210 °C which are caused by glass transition and melting of PANI, respectively [31].

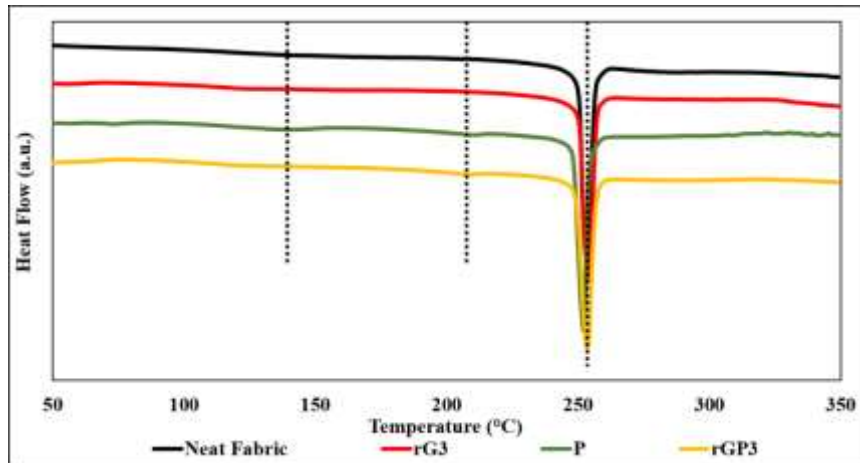


Figure 3. DSC curves of neat and coated fabrics

The woven fabrics were investigated by SEM technique to show fiber morphology, fabric surface and coating morphology. According to SEM images (Figure 3) of neat elastic polyester fabric, fabric surface was relatively rough, and diameter fibers were about 10 µm. Because of that, graphene sheets cannot completely wrap the fibers due to its a few micrometers of planar sizes. Graphene coating was consisting of partially wrapping of fibers, as shown in SEM images of rGO coated polyester fabric (Figure 4). Graphene sheets although could not wrap the woven fiber bundles, it could wrap the single fibers and wrapped fiber structure provided the electrical pathway formation. Moreover, graphene sheets could infuse the woven structure as an advantage of dip-coating method. SEM images also showed that the aniline successfully synthesized onto the fiber or rGO coated fiber surface (Figure 5).

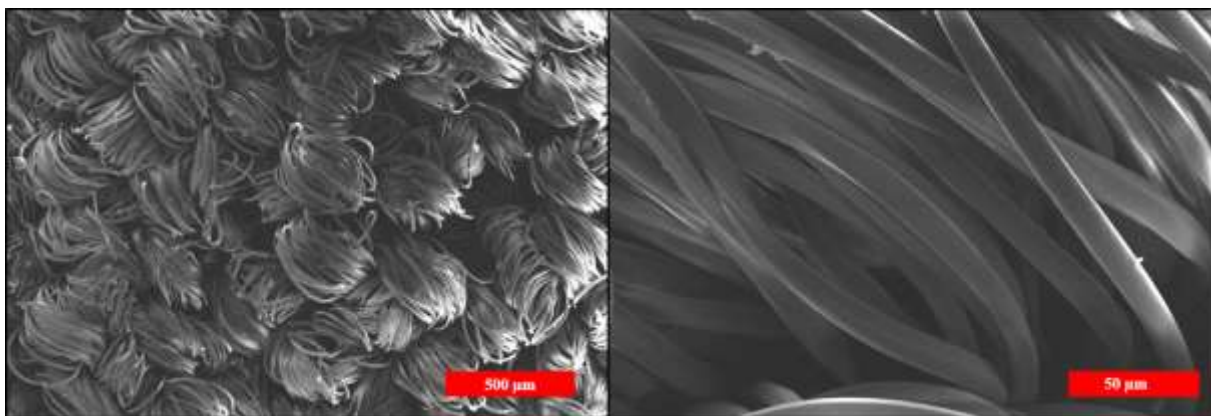


Figure 4. SEM images of neat polyester fabric

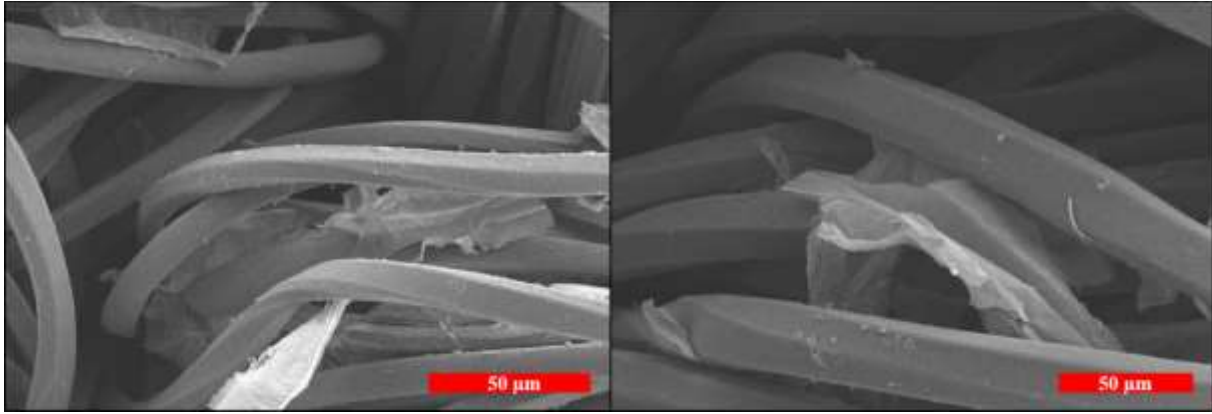


Figure 5. SEM images of rGO coated polyester fabrics

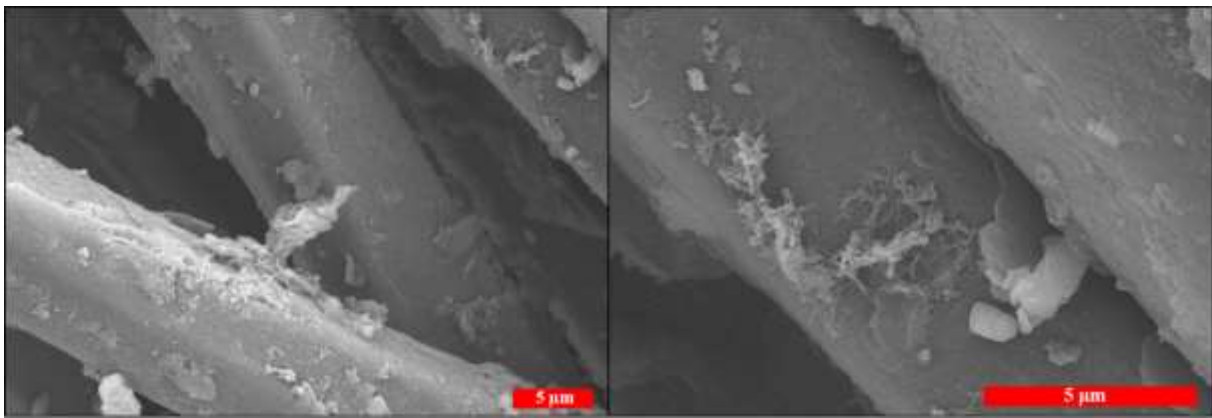


Figure 6. SEM images of PANI+rGO coated polyester fabrics

Neat fabric was an elastic and woven structure. Although elastic materials have regaining the original shape ability, because of high mechanical force and nature of polyester fibers, plastic deformation is possible for elastic polyester fabric. Because of that, a tensile test was performed on neat fabric in order to determine the elastic region. The fabric with 6 cm×15 cm sizes is used for tensile test and test speed was 5mm/s. Fabric sample also boiled at 95 °C to achieve structural equality with coated samples since the coated fabrics were exposed to heat in GO reduction process. As the result of the tensile tests, it was determined that the uncoated fabrics were in the elastic region up to 100% elongation and were exposed to plastic deformation at elongations above 100% (Figure 7). Since the range in which the fabric sensor can be used will be until the end of the elastic region, electromechanical tests were continued until the fabric reached 100% elongation value.

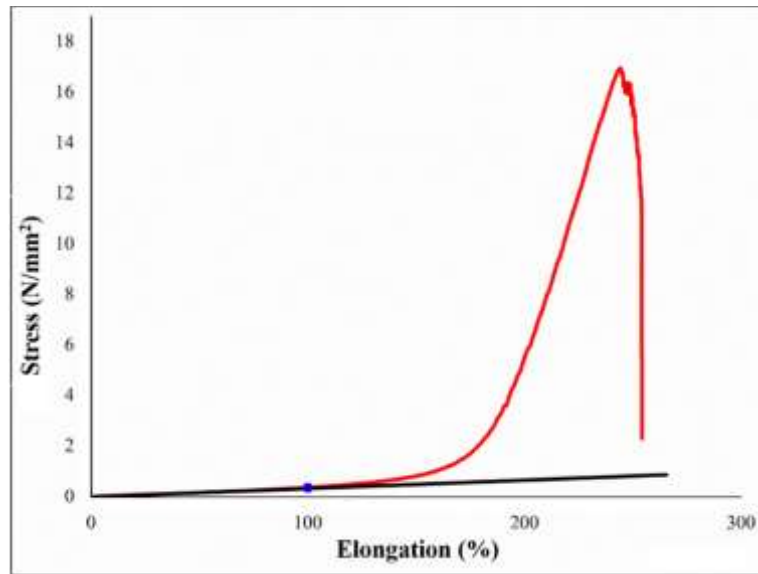


Figure 7. Stress-strain curve of neat fabric sample

In electromechanical tests, distance between shoulders were 10 cm. Copper tapes were mounted at the two ends of sample as top and bottom electrodes and electrical contacts connected to KEITHLEY 2400 multimeter. As mentioned in characterization topic, sample was elongated 5% and it stopped for 5 seconds. Resistivity value on multimeter's screen was manually recorded. This cycle was maintained until the total elongation reaches to 100%.

Firstly, PANI coated sample were electromechanically tested. It was observed that the resistance increased abruptly and the resistance value could not be read after 40% elongation, which also means that the resistance increased above 1 G Ω (Figure 8). The resistance changes up to this level was determined as 2488%. The maximum resistance value was measured as 68 M Ω . It was predicted that the reason for this abrupt increase and the loss of conductivity of the fabric at 40% elongation was due to the hard and fragile behavior of PANI [32].

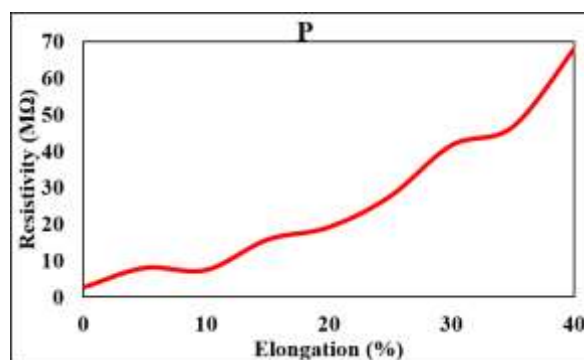


Figure 8. Elongation-electrical resistivity curve of PANI coated fabric

In rGO coated fabrics, it was determined that rG1 sample was quite insulating structure that it did not show any resistance value. It was observed that fabrics with initial resistances directly proportional to the amount of coating were produced in 2-layer and 3-layer rGO coated fabrics. It was determined that the electrical resistance of rG2 and rG3 fabrics increased by 12.5% and 30.4%, respectively, at the end of 100% elongation (Figure 9). Maximum electrical resistance of the rGO coated fabrics was measured

to be approximately 32MΩ. In the rGO-coated samples, a slower increase in resistance was observed with elongation movement, unlike the PANI-coated sample. The fact that the rGO particles were up to a few microns in width and length ensured that the fibers were tightly wrapped, the conductivity was higher than PANI, and the interface between fiber and conductive material was more stable [33].

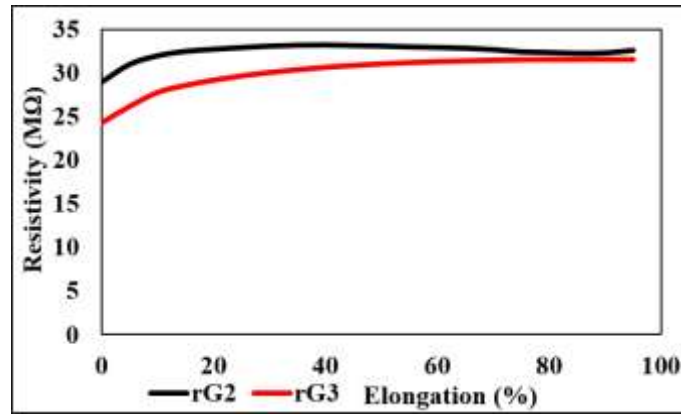


Figure 9. Elongation-electrical resistivity curve of rGO coated fabric

In electromechanical tests for 1 layer, 2 layer, and 3 layer rGO and fabric sensors coated with PANI on top of it, a more conductive structure was obtained compared to those coated with PANI or rGO. Under mechanical deformation, rG2 and rG3 samples and rGP2 and rGP3 samples showed similar curves, while rGP1 sample showed a non-linear curve. For rGP1, rGP2 and rGP3, the changes in resistance at the end of 100% elongation were measured as 191%, 87% and 97%, respectively (Figure 10). The synergistic effect of PANI and graphene derivatives in PANI/rGO samples was confirmed [34].

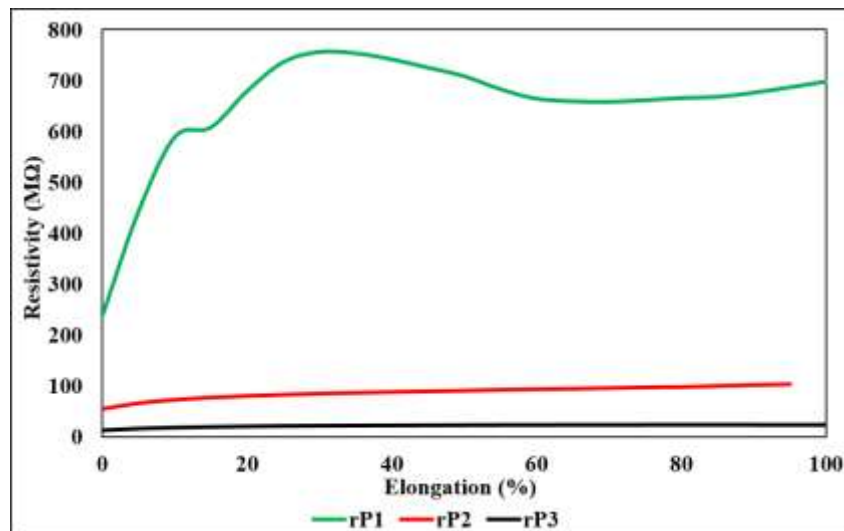


Figure 10. Elongation-electrical resistivity curve of rGO coated fabric

4. CONCLUSIONS

In electro-mechanical tests on conductive coated elastic fabrics, it was observed that the type and configuration of the coating material gave different responses in the detection of transformation. While a striking change in resistance to unit strain was observed in the PANI coated fabric, it was observed

that the intensity of this reaction decreased with the inclusion of rGO in the structure. On the other hand, it was determined that a signal can be received from the PANI coated sensor fabric up to a limited amount of elongation, and it can be used in a wider strain area in rGO and PANI/rGO coated structures despite the lower signal strength. The reason for this situation is the flexibility and particle sizes of graphene and its derivatives, and the hard and brittle structure of PANI. In the light of this study the reduction of fabric sensors with different reduction methods of GO in the following studies, coating with different methods and the application of different conductive polymer coatings on rGO to wearable electronics by comparing them among themselves are planned in future studies.

CONFLICT OF INTEREST

The authors stated that there are no conflicts of interest regarding the publication of this article.

REFERENCES

- [1] Hu J, Meng H, Li G and Ibekwe SI. A review of stimuli-responsive polymers for smart textile applications. *Smart Materials and Structures*, 2012; 21(5): 053001.
- [2] Jin LN, Shao F, Jin C, Zhang JN, Liu P, Guo MX and Bian SW. High-performance textile supercapacitor electrode materials enhanced with three-dimensional carbon nanotubes/graphene conductive network and in situ polymerized polyaniline. *Electrochimica Acta*, 2017; 249: 387–394.
- [3] Altin Y and Çelik Bedeloğlu A. Energy storage textile. *Advances in Functional and Protective Textiles*, 2020; 493–529.
- [4] Ünsal ÖF, Sezer Hiçyılmaz A, Yüksel Yılmaz AN, Altin Y, Borazan İ and Çelik Bedeloğlu A. 2020; Energy-generating textiles.
- [5] Yu P, Li Y, Zhao X, Wu L and Zhang Q. Graphene-wrapped polyaniline nanowire arrays on nitrogen-doped carbon fabric as novel flexible hybrid electrode materials for high-performance supercapacitor. *Langmuir*, 2014; 30(18): 5306–5313.
- [6] Yue B, Wang C, Ding X and Wallace GG. Polypyrrole coated nylon lycra fabric as stretchable electrode for supercapacitor applications. *Electrochimica Acta*, 2012;68: 18–24.
- [7] Yang Z, Pang Y, Han XL, Yang Y, Yang Y, Ling J, Jian M, Zhang Y and Ren TL. Graphene Textile Strain Sensor with Negative Resistance Variation for Human Motion Detection. *ACS Nano*, 2018; 12(9): 9134–9141.
- [8] Yang T, Jiang X, Zhong Y, Zhao X, Lin S, Li J, Li X, Xu J, Li Z and Zhu H. A wearable and highly sensitive graphene strain sensor for precise home-based pulse wave monitoring. *ACS Sensors*, 2017;2(7): 967–974.
- [9] Hill EW, Vijayaraghavan A and Novoselov K. Graphene sensors. *IEEE Sensors Journal*, 2011; 11(12): 3161–3170.
- [10] Bedeloğlu A and Taş M. Graphene and Its Production Methods. *Afyon Kocatepe University Journal of Sciences and Engineering*, 2016;16(3): 544–554.
- [11] Sadak O, Wang W, Guan J, Sundramoorthy A K, and Gunasekaran S. MnO₂ Nanoflowers

- Deposited on Graphene Paper as Electrode Materials for Supercapacitors. ACS Applied Nano Materials, (2019);2(12): 4386–4394
- [12] Sadak O, Sundramoorthy A K, and Gunasekaran S. Facile and green synthesis of highly conductive graphene paper. Carbon, (2018);138: 108–117
- [13] Ünsal OF, Altın Y and BEDELOĞLU A. Dielectric properties of polyaniline-functionalized carbon nanotube/pdms anocomposites. Uludağ University Journal of the Faculty of Engineering, 2020; 25(2): 861–874.
- [14] Altın Y, Unsal OF. and Celik Bedeloglu A. Fabrication and characterization of polyaniline functionalized graphene nanosheets (GNSs)/polydimethylsiloxane (PDMS) nanocomposite films, 2021; <https://doi.org/10.1177/09673911211023941>.
- [15] Sadak O, Prathap M U A, and Gunasekaran S. Facile fabrication of highly ordered polyaniline–exfoliated graphite composite for enhanced charge storage. Carbon, (2019);144: 756–763
- [16] Molina J, Esteves MF, Fernández J, Bonastre J and Cases F. Polyaniline coated conducting fabrics. Chemical and electrochemical characterization. European Polymer Journal, 2011; 47(10): 2003–2015.
- [17] Molina J, del Río, AI, Bonastre J and Cases F. Electrochemical polymerisation of aniline on conducting textiles of polyester covered with polypyrrole/AQSA. European Polymer Journal, 2009; 45(4): 1302–1315.
- [18] Saeb MR and Zarrintaj P. Polyaniline/graphene-based nanocomposites, In Fundamentals and Emerging Applications of Polyaniline, Elsevier, 2019; pp: 165–175.
- [19] Akter Shathi M, Minzhi C, Khoso NA, Deb H, Ahmed A and Sai Sai W. All organic graphene oxide and Poly (3, 4-ethylene dioxythiophene) - Poly (styrene sulfonate) coated knitted textile fabrics for wearable electrocardiography (ECG) monitoring. Synthetic Metals, 2020; 263: 116329.
- [20] Ünsal ÖF. Altın Y and Çelik Bedeloğlu A. Poly(vinylidene fluoride) nanofiber- based piezoelectric nanogenerators using reduced graphene oxide/polyaniline. Journal of Applied Polymer Science, 2020; 137(13): 48517.
- [21] Shao F, Bian SW, Zhu Q, Guo MX, Liu S and Peng YH. Fabrication of Polyaniline/Graphene/Polyester Textile Electrode Materials for Flexible Supercapacitors with High Capacitance and Cycling Stability. Chemistry – An Asian Journal, 2016; 11(13): 1906–1912.
- [22] Saberi Motlagh M and Mottaghitalab V. The charge transport characterization of the polyaniline coated carbon fabric as a novel textile based counter electrode for flexible dye-sensitized solar cell. Electrochimica Acta, 2017; 249: 308–317.
- [23] Song P, He X, Xie M, Tao J, Shen X., Ji Z, Yan Z, Zhai L and Yuan A. Polyaniline wrapped graphene functionalized textile with ultrahigh areal capacitance and energy density for high-performance all-solid-state supercapacitors for wearable electronics. Composites Science and Technology, 2020;198: 108305.

- [24] Marcano DC, Kosynkin DV, Berlin JM, Sinitskii A, Sun Z, Slesarev A, Alemany LB, Lu W and Tour JM. Improved synthesis of graphene oxide. *ACS Nano*, 2010; 4(8): 4806–4814.
- [25] Stankovich S, Dikin DA, Piner RD, Kohlhaas KA, Kleinhammes A, Jia Y, Wu Y, Nguyen SBT and Ruoff RS. Synthesis of graphene-based nanosheets via chemical reduction of exfoliated graphite oxide. *Carbon*, 2007; 45(7): 1558–1565.
- [26] Li M, Huang X, Wu C, Xu H, Jiang P and Tanaka T. Fabrication of two-dimensional hybrid sheets by decorating insulating PANI on reduced graphene oxide for polymer nanocomposites with low dielectric loss and high dielectric constant. *Journal of Materials Chemistry*, 2012; 22(44): 23477–23484.
- [27] Zhang C, He S, Wang D, Xu F, Zhang F and Zhang G. Facile fabricate a bioinspired Janus membrane with heterogeneous wettability for unidirectional water transfer and controllable oil–water separation. *Journal of Materials Science*, 2018;53(20): 14398–14411.
- [28] Bhattacharya SS and Chaudhari SB. Study on Structural, Mechanical and Functional Properties of Polyester Silica Nanocomposite Fabric. *International Journal of Pure and Applied Sciences and Technology*, 2014; 21(1): 43–52.
- [29] Hoghoghifard S, Mokhtari H and Dehghani S. Improving the conductivity of polyaniline-coated polyester textile by optimizing the synthesis conditions. *Journal of Industrial Textiles*, 2016; 46(2): 611–623.
- [30] Ünsal ÖF. İletken polimer ve grafen oksitle fonksiyonelleştirilmiş nanolif tabanlı piezoelektrik nanojeneratörler, 2018.
- [31] Sampreeth T, Al-Maghrabi MA, Bahuleyan BK and Ramesan MT. Synthesis, characterization, thermal properties, conductivity and sensor application study of polyaniline/cerium-doped titanium dioxide nanocomposites. *Journal of Materials Science*, 2018;53(1): 591–603.
- [32] Tian M, Wang Y, Qu L, Zhu S, Han G, Zhang X, Zhou Q, M. Du and S. Chi, Electromechanical deformation sensors based on polyurethane/polyaniline electrospinning nanofibrous mats. *Synthetic Metals*, 2016; 219: 11–19.
- [33] Ali MA, Umer R, Khan KA, Samad YA, Liao K and Cantwell W. Graphene coated piezo-resistive fabrics for liquid composite molding process monitoring. *Composites Science and Technology*, 2017;148: 106–114.
- [34] Cheng X, Kumar V, Yokozeki T, Goto T, Takahashi T, Koyanagi J, Wu L and Wang R. Highly conductive graphene oxide/polyaniline hybrid polymer nanocomposites with simultaneously improved mechanical properties. *Composites Part A: Applied Science and Manufacturing*, 2016; 82: 100–107.



ENHANCING UV PROTECTION AND HYDROPHOBIC ABILITIES OF POLYESTER TEXTILES BY NOVEL SURFACE MODIFICATION TECHNIQUES

Ali AKPEK^{1,*} 

¹Department of Biomedical Engineering, Faculty of Electric and Electronic, Yildiz Technical University, Istanbul, Turkey

ABSTRACT

In this study, water vapour permeability, wrinkle recovery, UV protection and contact angle properties of ion implanted Polyester (PES) fabrics were investigated. In order to achieve this goal; a Metal Vapor Vacuum Arc (MEVVA) source implanted Pb, Ag, Ag+N, Ti+O and Cr+O to the PES fabrics with 5×10^{16} ion/cm² and 30 kV acceleration voltage. The test results were compared with unimplanted PES fabric. The results indicated that UV Protection and contact angle values increased significantly and also almost no change observed at water vapour permeability and wrinkle recovery. These results also varied on severely with different ion species.

Keywords: Ion implantation, Wrinkle recovery, UV Protection, Hydrophobia, Contact angle

1. INTRODUCTION

The textile industry is on crisis. Continuous seek for a lower cost and environmentally friendly manufacturing methods are still not satisfactory enough. There are several promising techniques are being utilized to create products with higher quality, higher performance, special abilities and longer life span. Surface modification of textiles appears to be a good solution for all these problems. The surface treatments that alters any desired specifications of the textile surfaces without harming them will provide great benefits for all humankind [1].

For this reason, new methodologies are investigated to modify textiles with special abilities. It is obviously understood that one of these methodologies is one step ahead then all other techniques. This technique is called ion beam implantation technology.

Metal Vapour Vacuum Arc (MEVVA) appears to be one of the most effective surface modification technology available nowadays [1]. In this study, MEVVA was used for surface enhancement.

Ion implantation is a novel technique that enhances the surface properties of any selected materials. Ion implantation can especially be useful for the surfaces of the materials which can also have capability to upgrade the textile products from conventional textiles to smart textiles [2].

Ion implantation has been evaluated for several materials [3-12]. However, the textile applications are still very limited. In this study, MEVVA ion implantation technique was applied to textile surfaces in order to provide them UV resistance, hydrophobia, water vapour permeability and wrinkle recovery abilities.

2. EXPERIMENTAL

2.1. Ion implantation of polyester fabrics

A Metal Vapour Vacuum Arc (MEVVA) type of ion implantation system was used for Polyester (PES) fabrics [1]. In this study, MEVVA ion source implanted Pb, Ag, Ag+N, Ti+O or Cr+O to the polyester fabrics with 5×10^{16} ion/cm² and 30 kV acceleration voltage. Each ion species was implanted to a different 10x10 cm² sized 100% polyester fabric. From now on, the word polyester will refer 100% polyester fabric.

The ions penetration depth depends on several factors such as the energy level of the ions, ion doses, ion species, ion flux and the atom density in the substrate [13].

2.2. Water Vapor Permeability Test

The analysis of water vapor transport properties of textile materials are important in this study. Water vapor permeability tests provide measurable informations about the comfort properties of textiles. In this test ASTM F2298-03(2009)e1 Standard Test Methods for Water Vapor Diffusion Resistance and Air Flow Resistance of Clothing Materials Using the Dynamic Moisture Permeation Cell test methodology was used to determine water vapor permeability. [14]

2.3. Wrinkle Recovery Angle Test

Analysis of wrinkle recovery is also a very important parameter in this study since it provides information about either MEVVA harms the textiles or not. Wrinkle recovery tester is used to investigate the wrinkle structures of polyester fabrics. Tests were done according to the AATCC 128 Wrinkle Recovery of Fabrics: Appearance Method test methodology [15].

2.4. UV Protection Factor Test

UPF Protection factor test will provide the information of either MEVVA has capability to provide special abilities to textile materials or not. This test measured the amount of blocked and transmitted ultraviolet radiation on textile materials. The blocked percentage of UVA and UVB radiation is calculated according to AATCC Test Method 183-2004 Transmittance or Blocking of Erythemally Weighted Ultraviolet Radiation through Fabrics [16]. In order to achieve that a spectrophotometer is utilized. Spectrophotometer analyzed the transmittance of UV radiation in this study.

Table 1. UV Protection Factor(UPF) Categories.

UPF Categories	(%) UV Permeability
15-24 Protection	6.7-4.2
25-39 very well protection	4.1-2.6
40-50, 50+ perfect protection	<2.5



Figure 1. MEVVA Ion implantation Unit, (1) Control Panel, (2) Faraday Cage, (3) MEVVA Ion source, (4) Electrical supply circuit, (5) Charge control unit, (7), (8) Power supply, (9) Vacuum chamber

2.5. Contact Angle Test

This test was used to evaluate the fabric's capability of wetting by a standardized solutions with different surface tensions. In this work, standard drops of test liquids applied to polyester surfaces and observed for contact angle. The test methodology used in this test was AATCC 193-2004 Aqueous Liquid Repellency: Water/Alcohol Solution Resistance Test [17].

To compare success of each ion species at each test more efficiently, a success rate system was developed. This success rates were calculated with following formula

$$SR = [(100 \times B)/A]; \quad (1)$$

SR=Success rate,
 B= Test result of selected ion species,
 A=Test result of unimplanted polyester fabric.

For contact angle success rate; A=35, for UPF success rate; A=3,87 and for WRA success rate; A=296. These results are presented at Table 2. Detailed results were investigated in the following figures.

3. RESULTS AND DISCUSSION

After executing all the tests, the following table was resulted. All tests were achieved three times in order to obtain statistically meaningful results. The results presented below are arithmetic means of the experiments.

Table 2. All results obtained from the tests

No	Water Vapor Permeability (WVP)	Water Vapor Permeability Index (L)%	Wrinkle recovery angle (WRA°(W+F))	UV Protection Factor (UPF)	Contact Angle (°)
Unimplanted	546,6	109%	296°	3,87	35
Pb	394	95%	307 °	15	111,68
Ag	434,9	87,3%	281 °	30	113,32
Ag+N	524,3	105%	303 °	10	123,87
Ti+O	524	105%	284 °	10	125,05
Cr+0	451	90,7%	285 °	20	100,69

Two tests were realized in order to understand ion implanted polyester fabric's UV Protection and hydrophobia abilities. One was UPF test and the other was contact angle test. On the other hand, two tests were also realized to understand if there had been any degradation formed after the ion implantation, One was water vapor permeability test and the other was wrinkle recovery angle test. The reason for performing these tests to fabrics was if there had been any degradation on fabrics, the results of WVP and WRA tests would have been changed significantly when compared with unimplanted polyester fabric. However no significant change observed at any implanted polyester fabrics. This may prove that MEVVA ion implantation causes no deformation on the surfaces of polyester fabrics. Further experiments are necessary to prove this claim.

UPF and contact angle test results are very promising. At UPF test, when compared with unimplanted polyester, especially Ag and Cr+O implanted polyesters resulted with high efficiencies. Also, at contact angle test, all implanted polyesters presented at least 3 times higher efficiencies when compared with untreated polyester fabric.

3.1. SUCCESS RATES OF THE TESTS

When contact angle test was analysed, it is obviously understood that ion implanted fabrics has shown distinctive success. This means polyester fabrics had become more hydrophobic after implantation. The highest success was seen at Ti+O implantation, it has presented 3.57 times higher hydrophobia after implantation. The least success was shown at Cr+O ion implantation and even at that situation, it has presented 2,87 times higher hydrophobia when compared with unimplanted polyester fabric.

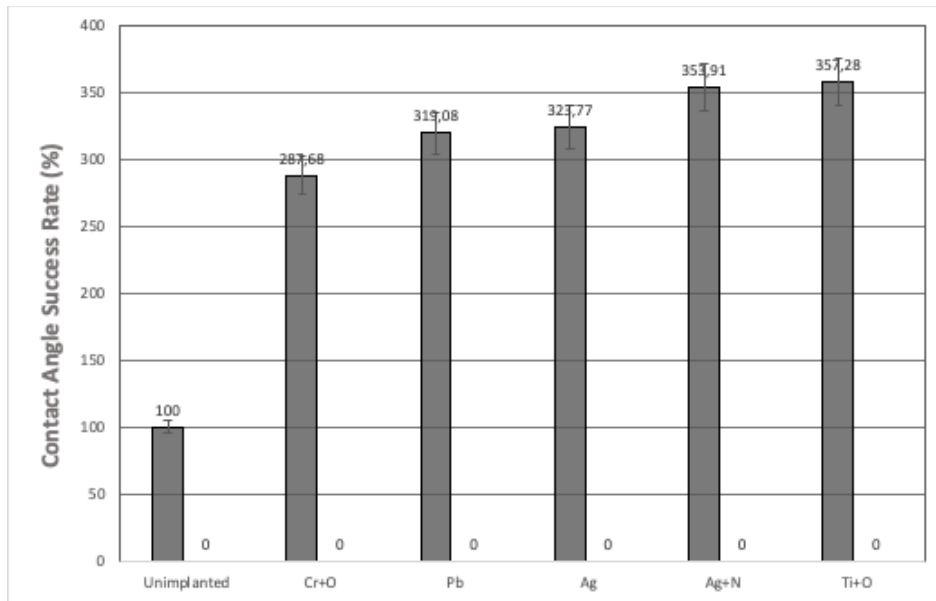


Figure 2. Contact angle success rate results of the ion implanted and unimplanted polyester fabrics

In this test, more contact angle success rate means more hydrophobia and more hydrophobia means more liquid repellent. Finally this means; less stains on textiles, less laundry, less electricity consumption, less detergent consumption, improved life-time for textiles, less textile production and a result with a more cleaner world. Original test results can be seen at Table 1.

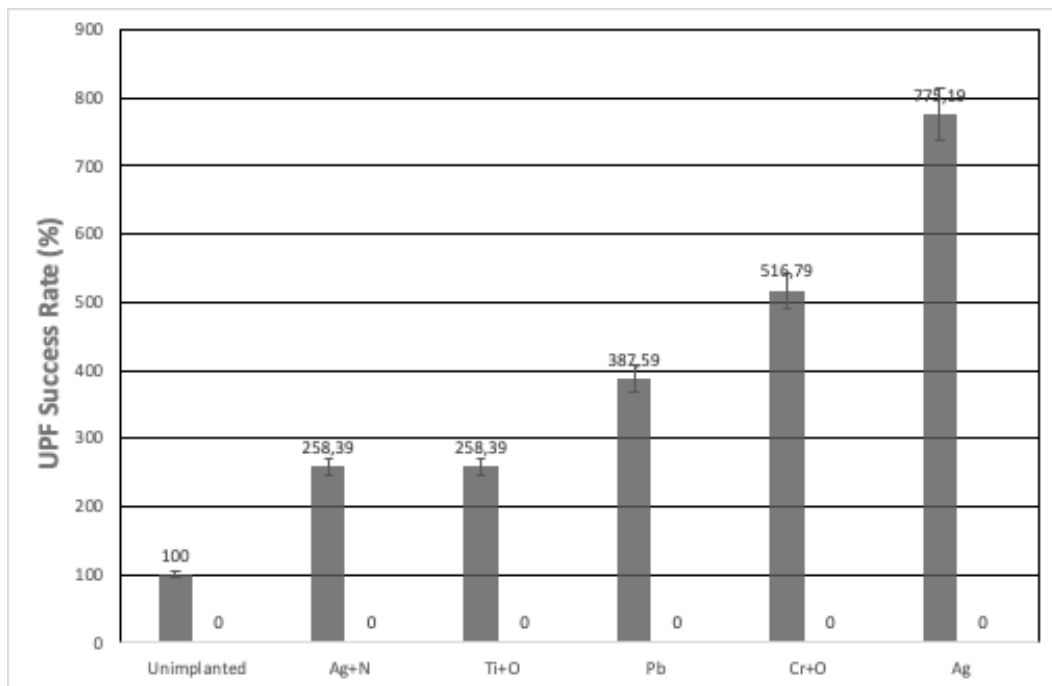


Figure 3. UV Protection Factor success rate results of ion implanted and unimplanted polyester fabrics

When UPF test analysed, it has been seen that ion implanted fabrics has presented the best results of the study. Especially Ag ion implanted polyester fabric has increased it's UPF value 775,19% higher when compared with unimplanted polyester fabric. Even the least successful Ag+N implantation has presented

258,39% increase it's UPF value. These results has proved us great benefits of MEVVA ion implantation for textile industry. Original test results can be seen at Table 2.

3.2. SUCCESS RATE OF CONTROL TESTS

Table 3: Water Vapor Permeability Test results.

No	Water Vapor Permeability (WVP)	Water Vapor Permeability Index (L)%
Unimplanted	546,6	109%
Pb	394	95%
Ag	434,9	87,3%
Ag+N	524,3	105%
Ti+O	524	105%
Cr+O	451	90,7%

When WVP tests resulted, it has been observed that only a slight difference occurred at ion implanted fabrics. The reason of this is implanted ion species do not cover and thicken the fibers. So, only a slight difference at WVP values may or may not perform on polyester fabrics. This results means, even after the implantation, polyester fabrics can still breath and will not disturb the user. This test proved us, MEVVA ion implantation has no harm for polyester fabrics. No success rate needed for water vapor permeability results due to WVP test has got it's own WVP Index.

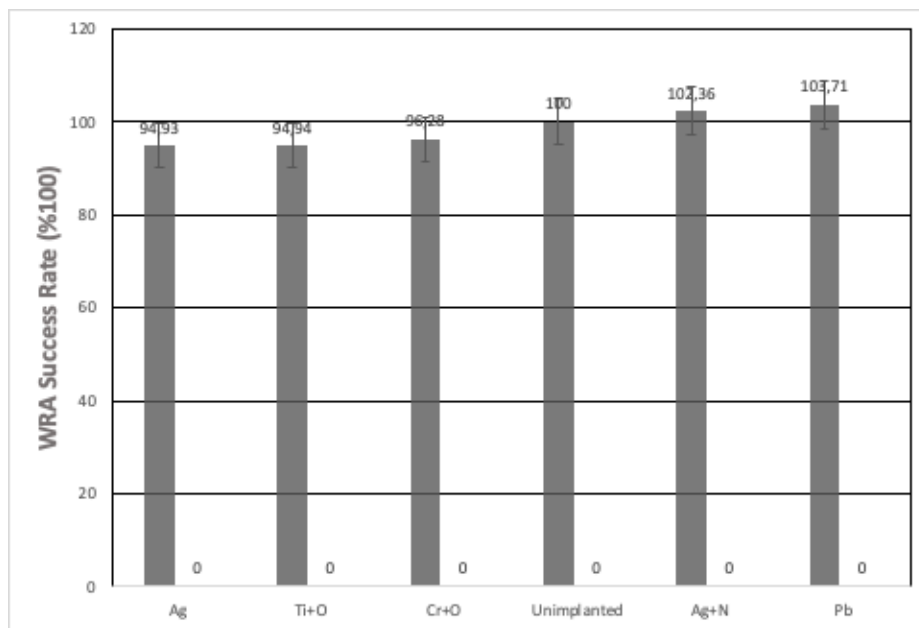


Figure 4. Wrinkle Recovery Angle (WRA) success rate results of ion implanted and unimplanted polyester fabrics.

When WRA tests resulted, it was noticed that all ion implanted polyester fabrics have almost same score with unimplanted one. Almost no difference seen in this test. This test proved that MEVVA ion implantation did not harden or loosen textile fibers. Because of this reason, all ion implanted polyesters could be able to present same wrinkle recovery angle performance with unimplanted polyester.

3.3. SUCCESS RATE OF ION SPECIES

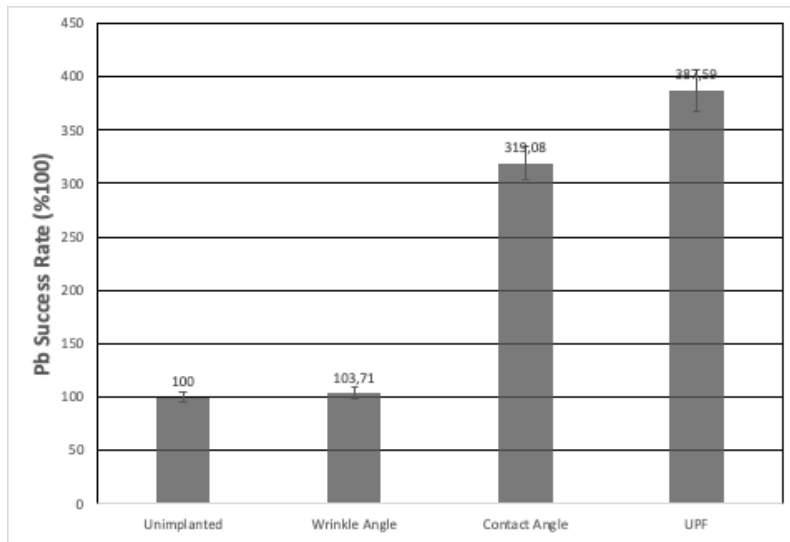


Figure 5. Pb success rate results at wrinkle recovery angle, contact angle and UPF tests. Water vapor permeability index result is 95%.

While determining success rate of each ion species, just like the figures shown before, unimplanted polyester fabric had taken as a reference point and success of ion species were analysed according to that reference point.

In Figure 5, it can be seen that Pb succeeded at much at UPF test. Also with same ion dose, Pb has presented very effective hydrophobia success rate which can be understood from contact angle test results. Finally it is seen that Pb has no harm for polyester fibers that can be analysed from wrinkle recovery angle and water vapor permeability index since if Pb implantation disordered the fibers of the fabric, wrinkle recovery angle would have been decreased or increased significantly. However, almost no change at wrinkle recovery angle was observed. This analyse can also rely on water vapor permeability index. No significant change was seen at that result too.

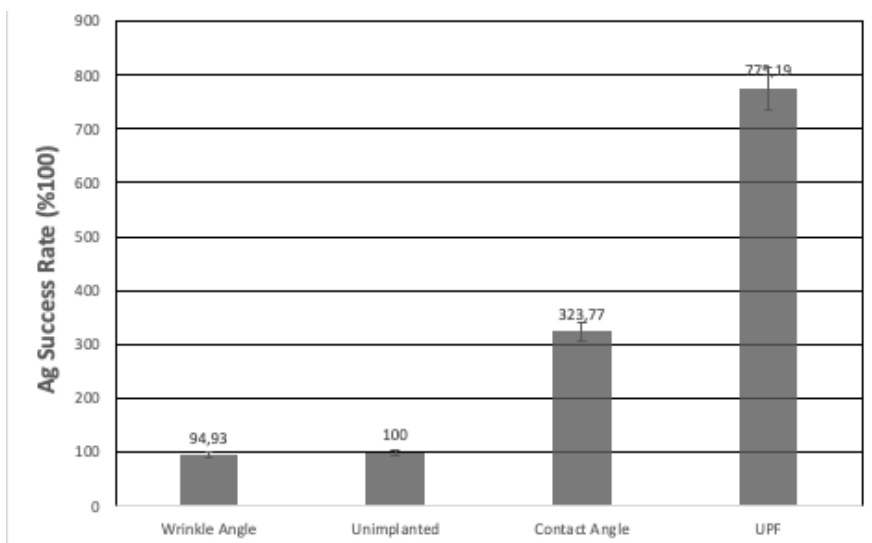


Figure 6. Ag success rate results at wrinkle recovery angle, contact angle and UPF tests. Water vapor permeability index result is 87,3%

In Figure 6, it has been seen that, Ag has the most successful result of the study at UPF test. The UPF result of Ag implanted polyester was increased 775,19% when compared with unimplanted polyester. Also with same ion dose, contact angle results increased significantly. As a similar result to Pb, no degradation at fibers was observed at polyester fabric. This can be analysed from both wrinkle recovery angle result and water vapor permeability index result. Almost no change was seen at both results. Further investigations will strengthen the results of this claim.

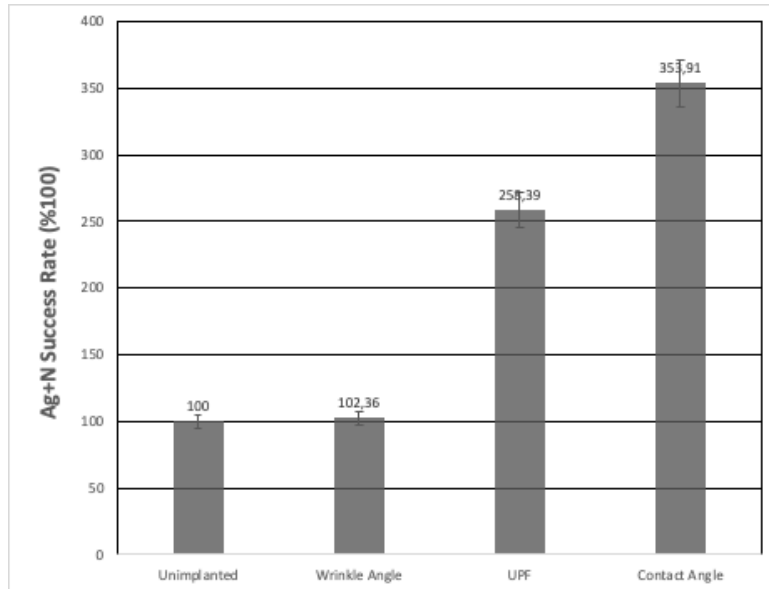


Figure 7. Ag+N success rate results at wrinkle recovery angle, contact angle and UPF tests. Water vapor permeability index result is 105%

In Figure 7, Ag+N implantation was succeeded at contact angle test at much and also it showed high success at UPF test. No significance increase or decrease determined at both wrinkle recovery angle test and water vapor permeability test.

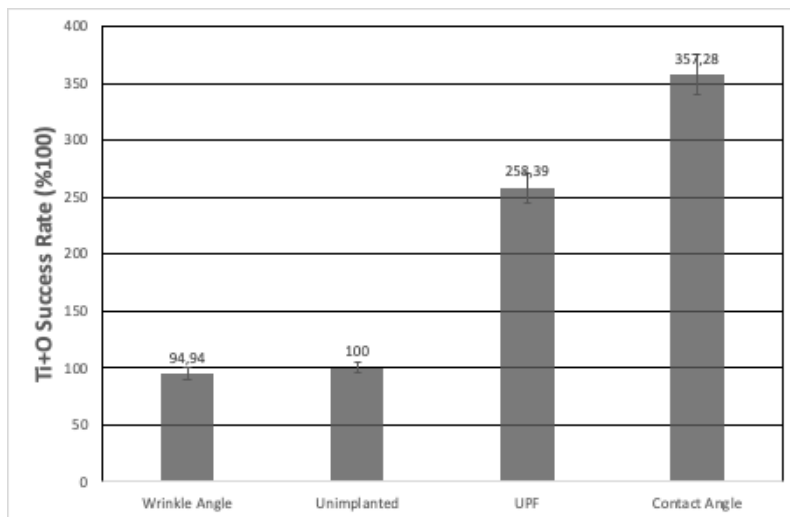


Figure 8. Ti+O success rate results at wrinkle recovery angle, contact angle and UPF tests. Water vapor permeability index result is 105%.

At Figure 8, Ti+O implantation presented its most successful result at contact angle test. Also UPF test resulted with success. Just like Pb, Ag, Ag+N; Ti+O did not result any degradation at polyester fabrics. This can be understood from wrinkle recovery angle and water vapor permeability index results.

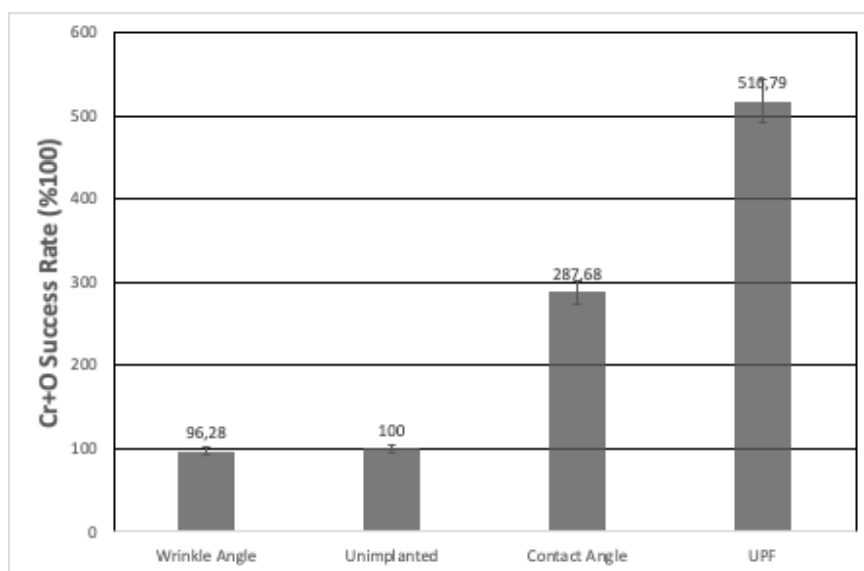


Figure 9. Cr+O success rate results at wrinkle recovery angle, contact angle and UPF tests. Water vapor permeability index result is 90,7%.

In Figure 9, Cr+O implantation presented one of the highest result of the study at UPF Test. Also contact angle test resulted with success. No disorder was presented at polyester fabrics.

4. CONCLUSION

Polyester (PES) textiles are at a leading position in their share at textile industry therefore polyester fabrics was used at this study. In the first part of this study, UV Protection Factors and contact angle test results of implanted PES fabrics were investigated. In order to achieve this goal; Pb, Ag, Ag+N, Ti+O and Cr+O implanted to the PES fabrics with 5×10^{16} ion/cm² and their test results were compared with unimplanted PES fabric. The results of tests are promising. It has been seen that at both Contact angle test and UPF test, all ion implanted polyester fabrics presented distinctive success.

In the second part of the study, wrinkle recovery angle and water vapor permeability tests were done at PES fabrics to understand if there are any degradation formed on polyester fabrics after the ion implantation. Just like the first two tests; Pb, Ag, Ag+N, Ti+O and Cr+O implanted to the PES fabrics with 5×10^{16} ion/cm² and their WVP and WRA test results were compared with unimplanted PES fabric. At the end of these tests, It has been understood that almost no significant disorder formed at polyester fabrics after ion implantation.

There might be several questions asked about why some elements and compounds behave much different than the others. There are several theories about how these ions effect the chemical structures of the materials however the exact answers of the chemical pathways of surface modification are still unknown up to date. Those answers can be research subjects of multiple other investigations.

This study proved us great benefits of MEVVA ion implantation on polyester textile surfaces. In additionally, as a more important result, this study has presented that MEVVA ion implantation technique is not harmful for polyester textiles fibers.

The results of this study were partially published at some conferences [18-19] and based on several prior studies achieved by same group [20-21]. The results shared at this paper are much more extended version of those studies.

Similarly, several investigations based on the antibacterial efficiencies of Ag and TiO₂ implantations by MEVVA are investigated deeply in another publication of the same group [22]. Therefore, those results are not included in this publication.

In addition, hopefully this study is aimed to strengthen the biomedical research achievements of the same group [23-28] and also be an important step at smart textile researches.

ACKNOWLEDGMENT

I would like to thank Mustafa Ahmet ÖZTARHAN for all the effort, supervision, equipment, and support he has provided for this research. Unfortunately, during the preparations of the manuscript, he passed away. May he rest in peace forever.

CONFLICT OF INTEREST

The author stated that there are no conflicts of interest regarding the publication of this article.

REFERENCES

- [1] Öktem T, Tarakcıoğlu I, Özdoğan E, Öztarhan A, Namlıgöz ES, Karaaslan A, Tek Z. Modification of friction and wear properties of PET Membrane fabrics by MEVVA ion implantation. *Materials Chemistry and Physics*, 2008; 108: 208-213.
- [2] Öktem T, Özdoğan E, Namlıgöz S.E, Öztarhan A, Tek Z, Tarakcıoğlu I, Karaaslan A. TUBITAK Textile Research Center, Izmir, Investigating the Applicability of Metal Ion Implantation Technique (MEVVA) to Textile Surfaces, *Textile Research Journal*, 2006; 76: 32.
- [3] Colwell JM, Wentrup-Byrne E, Bell JM, Wielunski LS. A study of the chemical and physical effects of ion implantation of micro-porous and nonporous PTFE. *Surface and Coatings Technology*, 2003; 168(2-3), 216-222.
- [4] Cottin P, Lessard RA, Knystautas EJ, Roorda S. Polymer waveguides under ion implantation: optical and chemical aspects. *Nuclear Instruments and Methods in Physics Research Section B: Beam Interactions with Materials and Atoms*, 1999; 151(1-4), 97-100.
- [5] Ge S, Wang Q, Zhang D, Zhu H, Xiong D, Huang C, Huang X, Friction and wear behavior of nitrogen ion implanted UHMWPE against ZrO₂ ceramic. *Wear*, 2003; 255(7-12), 1069-1075.
- [6] Huang N, Yang P, Leng YX, Wang J, Sun H, Chen JY, Wan GJ. Surface modification of biomaterials by plasma immersion ion implantation. *Surface and Coatings Technology*, 2004; 186(1-2), 218-226.

- [7] Karimi MV, Sinha SK., Kothari, D. C., Khanna, A. K., Tyagi, A. K. Effect of ion implantation on corrosion resistance and high temperature oxidation resistance of Ti deposited 316 stainless steel. *Surface and Coatings Technology*, 2002; 158, 609-614.
- [8] Nakamura N, Hirao K, Yamauchi, Y. Tribological properties of silicon nitride ceramics modified by ion implantation. *Journal of the European Ceramic Society*, 2004; 24(2), 219-224.
- [9] Sharkeev YP, Gritsenko BP, Fortuna SV, Perry AJ. Modification of metallic materials and hard coatings using metal ion implantation. *Vacuum*, 1999; 52(3), 247-254.
- [10] Youssef AA, Budzynski P, Filiks J, Kobzev AP, Sielanko J. Improvement of wear and hardness of steel by nitrogen implantation. *Vacuum*, 2004; 77(1), 37-45.
- [11] Yuguang W, Tonghe Z, Huixing Z, Xiaoji Z, Zhiwei D. Polymer modification by MEVVA source deposited and ion implantation. *Surface and Coatings Technology*, 2000; 131(1-3), 520-524.
- [12] Zhang J, Wu Q, Yu X, Zha P, Li H. Effect of aging on the morphology and wettability of polytetrafluoroethylene. *Materials Letters*, 2001; 48(6), 362-368.
- [13] Tonghe Z, Huixing Z, Changzhou J, Xiaoji Z, Yuguang W, Furong M, Jianzhong S. Industrialization of MEVVA source ion implantation. *Surface and Coatings Technology*, 2000; 128, 1-8.
- [14] ASTM F2298 - 03(2009)e1 Standard Test Methods for Water Vapor Diffusion Resistance and Air Flow Resistance of Clothing Materials Using the Dynamic Moisture Permeation Cell.
- [15] AATCC 128 Wrinkle Recovery of Fabrics: Appearance Method test methodology. American Association of Textile Chemists and Colorists technical manual.
- [16] AATCC Test Method 183-2004 Transmittance or Blocking of Erythemally Weighted Ultraviolet Radiation through Fabrics. American Association of Textile Chemists and Colorists technical manual.
- [17] AATCC 193-2004 Aqueous Liquid Repellency: Water/Alcohol Solution Resistance Test. American Association of Textile Chemists and Colorists, 01-Jan-2004.
- [18] Öztarhan A, Akpek A, Oks E, Nikolaev A. Modifying textiles with antibacterial effect, friction resistance, UV protection and electrostatic charge decay abilities by an alternative nanotextile technology called MEVVA ion implantation technique. In *Proceedings of the VIth Nanoscience and Nanotechnology Conference (NANOTR)*, 2010; 15-18.
- [19] Akpek A. Surface modification of textiles by MEVVA Ion Implantation and providing UV protection and hydrophobia abilities. In *Proceedings of the VIIIth International Fiber and Polymer Research Symposium, Eskişehir Osmangazi University, Turkey*. 2021: 270.
- [20] Öztarhan A, Akpek A, Oks E, Nikolaev A. Modifying medical textiles with antibacterial and friction resistance abilities by an alternative nanotextile technology called ion implantation technique. In *2010 15th National Biomedical Engineering Meeting IEEE*, 2010: 1-4.
- [21] Nikolaev AG, Savkin KP, Yushkov GY, Oks EM, Oztarhan A, Akpek A, Cireli I. Modification of the textile materials by vacuum arc ion source implantation. In *Proceedings of the 10th*

International Conference on Modification of Materials with Particle Beams and Plasma Flows (10th CMM), Tomsk, Rusya, 2010: 19-24.

- [22] Kızılkurtlu AA, Polat T, Aydın GB, Akpek A. Lung on a chip for drug screening and design. *Current pharmaceutical design*, 2018; 24: 5386-5396.
- [23] Akpek A. Analysis of Surface Properties of Ag and Ti Ion-Treated Medical Textiles by Metal Vapor Vacuum Arc Ion Implantation. *Coatings*, 2021; 11(1), 102.
- [24] Bulut S, Özçınar A, Çiftçioğlu Ç, Akpek A. A new algorithm for segmentation and fracture detection in X-ray images. In 2015 Medical Technologies National Conference (TIPTEKNO), IEEE. 2015:1-4.
- [25] Akpek A, Youn C, Kagawa T. Temperature measurement control problem of vibrational viscometers considering heat generation and heat transfer effect of oscillators. In 2013 9th Asian Control Conference (ASCC), IEEE. 2013: 1-6.
- [26] Çiftçioğlu Ç, Koçak O, Akpek A. Remote control of centrifuge and injection systems via MATLAB and ARDUINO. In 2015 Medical Technologies National Conference (TIPTEKNO), IEEE. 2015: 1-4.
- [27] Ugar T, Kogak O, Akpek A. New concept design of an insulin pen for visually impaired or blind diabetus mellitus patients. In 2016 Medical Technologies National Congress (TIPTEKNO), IEEE. 2016: 1-4.
- [28] Altinsu B, Koçak O, Akpek A. Design and analysis of an autoclave simulation using MATLAB/Simulink. In 2016 Medical Technologies National Congress (TIPTEKNO), IEEE. 2016: 1-4.



THERMOFORMING PROCESS PARAMETER OPTIMIZATION of THERMOPLASTIC PEKK/CF and PPS

Merve COBANOGLU ^{1*} , Remzi Ecmel ECE ² , Fahrettin OZTURK ³ 

^{1,2}Türk Havacılık ve Uzay Sanayii A.Ş., Ankara

³Türk Havacılık ve Uzay Sanayii A.Ş., Ankara Yıldırım Beyazıt Üniversitesi, Ankara

ABSTRACT

Thermoplastic composite parts in the aerospace industry have recently increased due to the reshaping and reusing potentials of thermoplastic composite materials. The thermoforming process is one of the effective manufacturing methods to form thermoplastic composite materials. The main benefits of the process are low cost and short process time. Optimization of the process parameters is essential to produce accurate parts. In this present study, effects of plate geometry and connection technique, preheating, and pressing parameters are investigated experimentally for the thermoforming of Poly Ether Ketone / Carbon Fiber (PEKK / CF) and Polyphenylene Sulfide (PPS) sheets. Results reveal that wrinkle and warping problems of the formed sheets are minimized by optimization of these parameters.

Keywords: Thermoplastic, Thermoforming, PEKK, PSS

1. INTRODUCTION

Composite materials are significant and attractive for many industries, especially for the aerospace industry. The superior mechanical properties and the substantial weight reduction in systems are the main reasons for their attractiveness [1]. Moreover, composites can provide comparable performance to conventional metallic materials while decreasing the weight from 10 to 50% [2]. Not only weight but also cost reduction is possible from 10 to 20% using composite instead of metallic materials [3]. Thermoset materials are widely used in the aerospace industry. However, the production of thermoset composites consists of many stages, which are obstacles to rapid production. Thermoplastics have got significant attention in primary aircraft parts due to their fast production advantage [4].

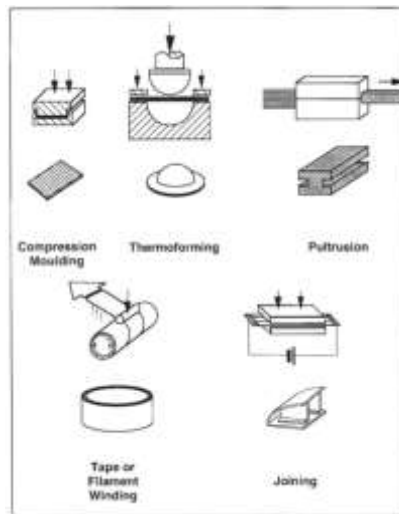


Figure 1. Processing methods for thermoplastic composites [6]

*Corresponding Author: merve.cobanoglu@tai.com.tr

Received: 12.08.2021 Published: 30.11.2021

There are many manufacturing methods developed for thermoplastic composites [5]. Some of these processes are generally used for thermosetting composites and sheet metal forming, but these fabrication techniques such as compression molding, tape winding, thermoforming, joining, and pultrusion have become for the thermoplastic composites (Figure 1) [6].

The aerospace industry is particularly interested in the press forming (thermoforming) of thermoplastic materials for rapid production [7]. Press forming is a type of ‘thermoforming,’ a set of processes for shaping a blank that has been melted by an oven and consists of three main steps: preheating, forming, and cooling.

Preheating is categorized as infrared (radiation) heating, contact or conduction heating, or convection heating, depending on how heat is applied to the blank. While contact heating is the most effective form of heating, and convection heating allows for the most uniform temperature distribution, contact heating fails in practical use due to bonding between tool and blank. Convection heating is slow and inefficient, lagging behind infrared heating. In the scope of rapid manufacturing, the most crucial parameter is the overall process time. [8,9] Infrared heating allows for a quick preheating process, reducing overall process time while providing great convenience and flexibility.

Blanks are heated over the melting temperature and transferred from the oven to the hot press system to form the pre-consolidated blanks into a 3-D shape. However, forming for thermoplastic composites have also some issues. It can be a restrictive aspect of whether the defects like warping and wrinkle can occur while processing. Wrinkles and warpage can cause damages that make the produced part a scrap. Moreover, the material defects which may not be noticed could cause catastrophic failure. Production parameters and processes must be examined precisely without errors since aircraft components have to comply with aviation regulations completely.

In the presented study, blank geometry, connection technique (blank to frame), heating, and pressing parameters are optimized to resolve the problems.

2. EXPERIMENTAL PROCEDURE

In this study, PPS and PEKK thermoplastic blanks were used. The aerospace-grade materials were supplied from TenCate and ATC companies. Sheets were formed at the Turkish Aerospace Thermoplastic Research Laboratory.

As mentioned earlier that preheating before shaping is essential for thermoplastics. Therefore, experiments were carried out in an IR oven. It is closed on four sides and has two tip-up gates, upper and lower heater sections. Each of these sections consists of 120-mm by 120-mm 25 ceramic heaters. Upper and lower sections can be controlled to set distances between surfaces of plate and heaters by servo motors, as seen in Figure 2 (a). Heaters in each section are divided into two groups to heat different controlled zones utilizing an embedded PID (Proportional integral derivative) control unit

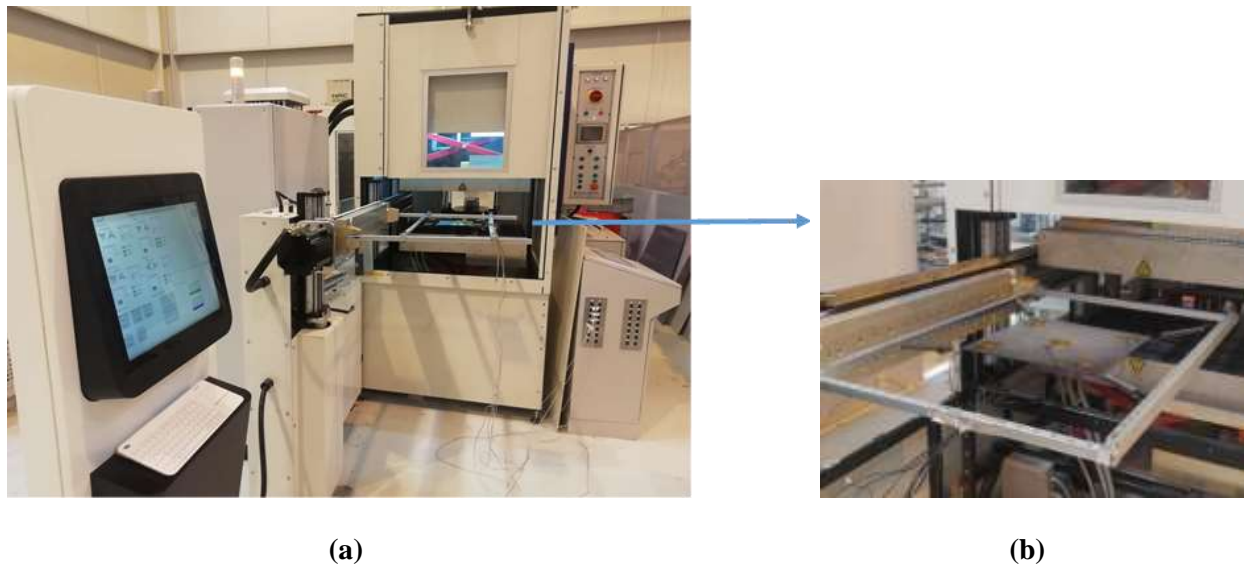


Figure 2. (a) Control and heating unit; (b) Experimental setup and the thermoplastic sheet attached to the frame

In PLC controlled PC, desired temperature, blank distance, heating ramp-up values were set. The temperature was checked by the system using Type-K thermocouples, which are placed inside of the heaters. When heaters reached that value, the blank was sent to the oven. The blank is held by springs from the corners to prevent materials from necking because of softening during heating. Holes were drilled in the four corners of the blank and connected to the frame with springs, as shown in Figure 2(b).

When the oven reached the desired temperature, the frame was sent, and the gates were closed. After a few minutes, the thermoplastic blank reaches the process temperature above the melting point. The molten blank was ready to be shaped. Therefore, it was left in the oven and moved under the press. When the frame located under the upper press side of the tool moved down, and the blank was stamped a few minutes between the press tool after the required time passed, the shaped blank was removed from the frame, and the thermoforming process thermoplastic composites was completed.

3. RESULTS AND DISCUSSION

In this paper, PPS and PEKK thermoplastic composites were used for the aircraft rib production process. It is necessary to fulfill the required mechanical properties. Therefore, it is required to find optimum parameters to get desired properties. The part should pass all required tests.

In Table 1, IR was preheating, and IR instant heating was compared. In IR preheating, the PPS plate has 51.9% faster heating to reach the steady-state temperature (t_{ss}), 8.63% higher plate temperature at steady state ($T_{ss,plate}$), 56.4% smaller temperature difference (ΔT_{ss}) and 82.9% lower power consumption (q_{avg}). These results were expected because IR heaters consume massive power to heat themselves first in IR instant heating, and the heated air contributes to heat the PPS plate faster. The critical issue is heating time for the part productions. As a result, IR preheating is more efficient for mass production and reduction of cycle time

Table 1. Results of Exp.1, Variable parameter: Heating method

	t_{ss} (sec)	$T_{ss,plate}$ (°C)	ΔT_{ss}	q_{ava} (watt)
IR preheating	380	200	300	500
IR instant heating	430	260	200	500

The part was successfully processed, as seen in Figure 3.



Figure 3. Produced aircraft rib

Based on experimental results, essential parameters were determined and optimized, i.e., heating temperature, heating time, and tooling temperature (Table 2). Degree of crystallinity tests was performed for thermoformed ribs, and results are shown in Figure 5. The expected percent of crystallinity values between 23 - 27% were achieved, and these values are sufficient to enable required mechanical properties. A summary of the degree of crystallinity is given in Table 3.

Table 2. Summary of optimum process parameters

Material	Oven Set Temperature (°C)	Tool Set Temperature (°C)	Preheating time (s)	Pressure (psi)	Time (tool) (s)
PPS	380	200	300	500	150
PEKK	430	260	200	500	130

Table 3. Summary of the degree of crystallinity

Sample Name	Sample Weight (mg)	Resin Content (%)	Percent Crystallinity (%)	Melting Temperature Peak (°C)
Blank Panel (BT) Run1	17.80	43	23.66	284.32
Blank Panel (BT) Run2	17.70	43	23.88	283.92
Blank Panel (BT) Run3	18.90	43	26.21	283.46
Rib Trial-2 (T2) Run1	17.50	43	24.07	281.78
Rib Trial-2 (T2) Run2	16.50	43	24.80	282.61

Rib Trial-2 (T2) Run3	17.30	43	23.72	281.41
--------------------------	-------	----	-------	--------

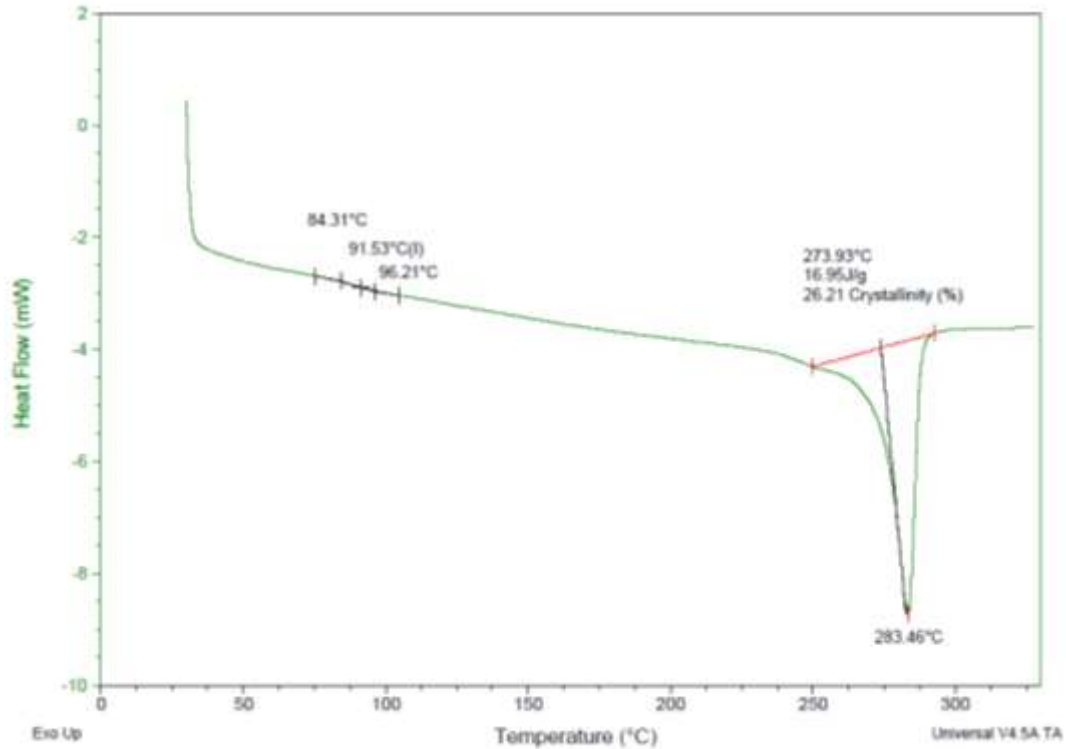


Figure 4. Degree of crystallinity graph

Micro-cut measurements (thickness measurements) of the surface profile were performed at different points from the web and both flanges of the part with a ball-ball micrometer (Figure 5.). It was observed that the thickness difference is within the acceptable tolerances. All the measurement data were tabulated in Table 4.

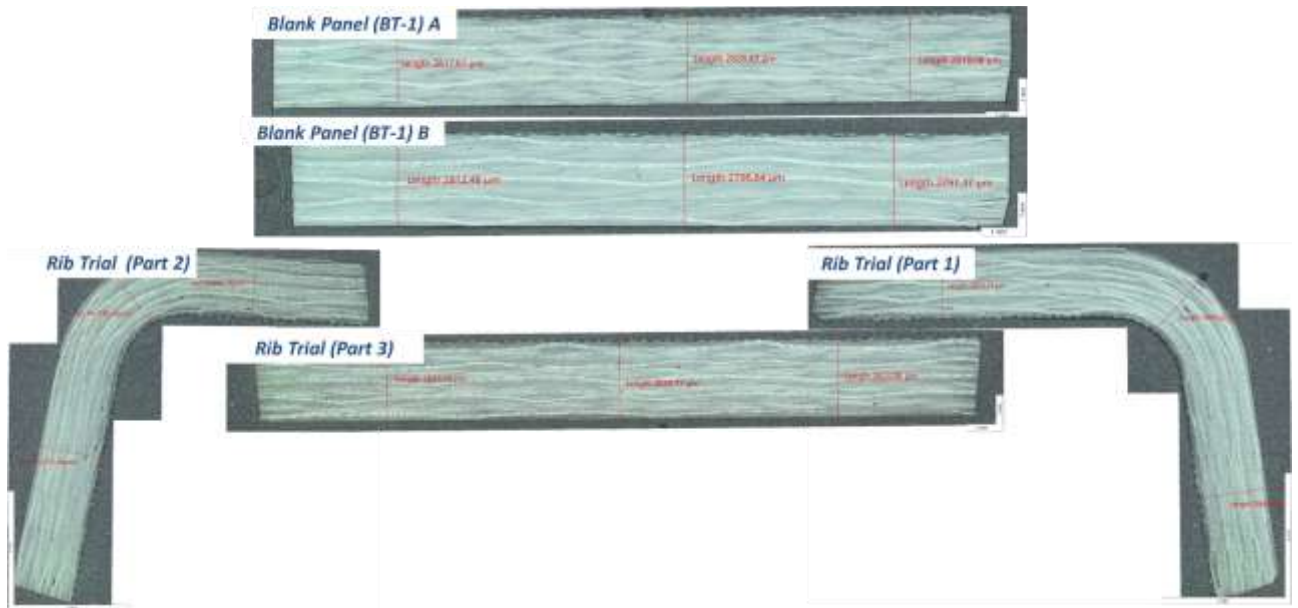


Figure 5. Micro-cut measurements of the PPS RIB

Table 4. Thickness measurements

	Zone 1 (µm)	Zone 2 (µm)	Zone 3 (µm)	Deviation Zone 1 (%)	Deviation Zone 2 (%)	Deviation Zone 3 (%)
Blank Panel A	2817	2828	2818	-0.46	-0.07	-0.42
Blank Panel B	2812	2796	2791	-0.64	-1.20	-1.38
Rib Trial (Part 1)	2853	2809	2809	0.81	-0.74	-0.74
Rib Trial (Part 2)	2840	2831	2776	0.35	0.04	-1.91
Rib Trial (Part 3)	2837	2826	2823	0.25	-0.14	-0.25

In addition to DSC and micro-cut analysis, tensile tests were also applied to PEKK and PPS samples to investigate their mechanical performance. Tensile tests were performed at the INSTRON testing machine. There were five samples prepared for each composite (PEKK and PPS) according to the ASTM D3171 - 99. Tensile tests were performed at room temperature and 5mm/min deformation speed. Results of these tensile tests are given in Figure 6 and Table 5. These results were average values of 5 samples.

Table 5. Tensile test results of the PEKK and PPS rib parts

	Ave. Tensile Strength (MPa)	Ave. Elastic Modulus (GPa)
PEKK	823.7 ± 63.2	24.3 ± 0.3
PPS	607.7 ± 17.3	23.1 ± 0.8

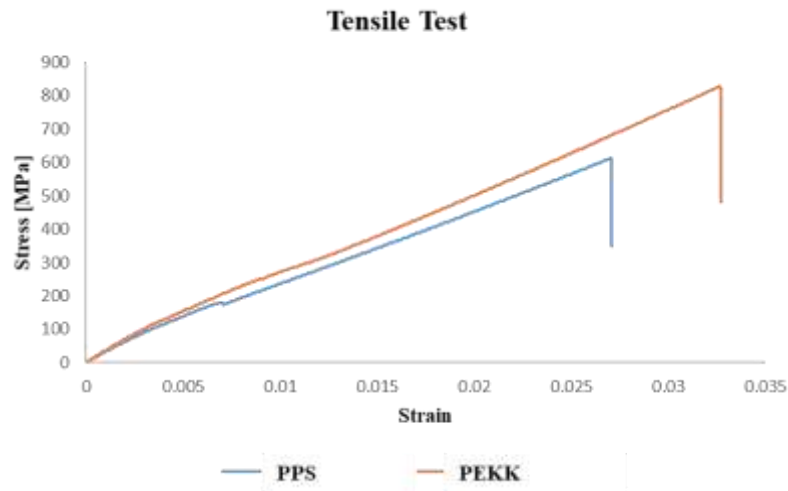


Figure 6. Tensile test results of PEKK and PPS thermoplastics

As seen from the results, the tensile strength of the PEKK is greater than PPS. Average tensile strength (608 MPa) and elastic modulus (23 GPa) of the PPS were observed. These results have complied with the literature [10]; therefore, it can be concluded that thermoforming process of PPS does not affect the mechanical properties. Moreover, tensile strength and elastic modulus results of the PEKK composite (824 MPa; 24 GPa) were also similar to the literature [11]. It shows that during thermoforming, the mechanical properties of the PEKK thermoplastic composite were also conserved. No significant change was recorded. As a result, selected thermoforming parameters for PEKK and PPS were accepted as optimum since their thermal and mechanical properties are not changed after they are shaped.

4. CONCLUSIONS

Thermoplastic composite materials are quite important for the aerospace industry, because of their superior advantages compared to metals and thermoset composites. Thermoforming is a standard method used for the shaping of thermoplastics. However, the thermoforming process has many parameters, and optimizing these parameters is critical for each material and part of the aircraft. This paper studied the thermoforming process of two different thermoplastic composites, e.g. PEKK and PPS. These two were selected since they are widely used in aircraft structures. After studying several parameters, the optimum of thermoforming parameters (temperature, pressure, time, etc.).

Results indicated that wrinkle and warping problems of the thermoformed sheets are minimized by parameter optimization. The most optimum parameters were determined.

FUTURE WORKS

This study was completed using consolidated blanks. In the future, the primary goal is to study consolidation, i.e., producing blanks from semi-crystalline pre-preg under high temperature and pressure conditions.

ACKNOWLEDGEMENT

This study is supported by Turkish Aerospace Industries Inc.'s 1515 - The Scientific and Technological Research Council of Turkey (TÜBİTAK) Frontier R&D Laboratory Support Programme, Project# 5189901.

CONFLICT OF INTEREST

The author stated that there are no conflicts of interest regarding the publication of this article.

REFERENCES

- [1] Cunningham JE, Monaghan PF, Brogan MT, and Cassidy SF. Modeling of preheating of flat panels prior to press forming, *Compos. Part A Appl. Sci. Manuf.*, 1997; vol. 28, no. 1, pp. 17–24.
- [2] Suong DG, Stephen VH, Tsai W. *Composite Materials Design and Applications*. CRC PRESS, 2003.
- [3] Abbasi F, Elfaleh I, Mistou S, Zghal A, Fazzini M, & Djilali T. Experimental and numerical investigations of a thermoplastic composite (carbon/PPS) thermoforming. *Structural Control and Health Monitoring*, 18, May 2011; 769–780. <https://doi.org/10.1002/stc>
- [4] Muzzy JD, Kays AO. Thermoplastic vs. thermosetting structural composites, *Polymer Composites*, 1984; vol. 5, no. 1, pp. 69–172.
- [5] Cogswell FN, *Thermoplastic Aromatic Polymers*; Butterworth-Heinemann Ltd., Oxford, 1992; 124-139.
- [6] Friedrich K, Hou M, & Krebs J. Chapter 4 Thermoforming of continuous fibre/thermoplastic composite sheets. *Composite Materials Series*, 1997; 11(C), 91–162. [https://doi.org/10.1016/S0927-0108\(97\)80006-9](https://doi.org/10.1016/S0927-0108(97)80006-9)
- [7] Offringa AR. Thermoplastic applications composites-rapid processing applications, *Compos. Part A*, 1996; vol. 27(A), pp.329–336,
- [8] Dutch Thermoplastic Composites “Aerospace Structures,” <http://www.composites.nl/products/aerospace-structures/>.
- [9] Saraiva F. Development of press forming techniques for thermoplastic composites Investigation of a multiple step forming approach, MSc Thesis in Aerospace Engineering Structural Integrity & Composites, TU Delft, 2017.
- [10] Chukov D, Nematulloev S., Zadorozhnyy M, Tcherdyntsev V, Stepashkin A & Zherebtsov D. Structure, mechanical and thermal properties of polyphenylene sulfide and polysulfone impregnated carbon fiber composites. *Polymers*, 2019; 11(4), 684.
- [11] Salek MH. Effect of processing parameters on the mechanical properties of carbon/PEKK thermoplastic composite materials (Doctoral dissertation, Concordia University), 2005.



WEARABLE TEXTILE-BASED PIEZOELECTRIC NANOGENERATORS WITH GRAPHENE/ZnO/AgNW

Emre DEMİR¹ , Ömer Faruk ÜNSAL¹ , Filiz EMİROĞLU² , Ayşe ÇELİK BEDELOĞLU^{1,*} 

¹ Polymer Materials Engineering Department, Faculty of Engineering and Natural Sciences, Bursa Technical University, Bursa, Turkey

² Almaxtex (Yeşim) Tekstil San Tic A.Ş., Bursa Turkey

ABSTRACT

In recent years, while people are dealing with problems such as global warming caused by environmental pollution caused by the use of traditional fossil energy sources, they have also faced the dilemma of energy crisis in the search for alternative renewable energy sources. The development of renewable and clean energy sources such as wind, solar and tidal energy has become increasingly important. In addition, nanogenerators, which convert waste mechanical energy into electrical energy through physical interaction, have attracted great interest among innovative studies in recent years. There is a need for maintenance-free and flexible wearable nanogenerators that can provide a sustainable power source for wearable/portable electronics. In this study, thermoplastic polyurethane (TPU) coated nanogenerator fabrics containing graphene / Zinc Oxide (ZnO) / Silver nanowires (AgNW) were developed for use in wearable electronics and the effect of zinc oxide concentration on the output power of textile-based nanogenerators was investigated. As a result, the nanogenerator fabricated using 7% by weight of ZnO produced 10 mW of power, indicating that ZnO-based materials can assist in the development of flexible TPU-based piezoelectric nanogenerators and advance to a new stage.

Keywords: Piezoelectric nanogenerator, Nanocomposite, Wearable electronic, Graphene, Textile electrode

1. INTRODUCTION

The use of fossil fuels for years along with the increasing energy demand has brought environmental problems, and the depletion of fossil fuels and their environmental damage has led to the concern of energy resources for the future. Driven by the latest technological advances and growing concerns about the environmental impact of the sustainability of traditional fuel usage, the possibility of generating significant amounts of clean, sustainable energy from renewable energy sources is of great interest worldwide for last a few decades. Solar, wind, biomass, and geothermal based energy sources are most known renewable energy sources [1]. It is stated that the global consumption of renewable energy sources will be reached a level equivalent to 318 exajoules (1 exajoule: 1 quintillion joules) of fossil fuels per year by 2050. This production rate also means that less than 0.01% of the 3.8 million exajoule solar energy reaching the earth's surface is used each year [2]. Moreover, there are studies that used two different energy conversion mechanisms in order to increase the energy conversion efficiency [3]. The conversion of small amounts of mechanical energy takes place between the vibrational and electrical forms of the material. The devices that convert small amounts of mechanical energy (or thermal) to electrical energy are named as nanogenerators [4]. The nanogenerators are divided into three main classes as pyroelectric nanogenerators that convert thermal energy into electrical energy, triboelectric nanogenerators and piezoelectric nanogenerators that convert mechanical energy into electrical energy [5]. Pyroelectric nanogenerators consist of thermally polarizable active layer and electrodes; thermally polarized active material generates the potential difference by a thermal gradient effect [6]. Triboelectric nanogenerators, based on static electrification between at least two different dielectric materials [7]. Finally, piezoelectric nanogenerators are devices that generate electrical energy under pressure or

*Corresponding Author: ayse.bedeloglu@btu.edu.tr

Received: 12.08.2021 Published: 30.11.2021

bending forces [8]. The nanogenerators convert human motion, water flow, rain droplets, wind, or vibration based mechanical energy into the electrical energy [9]. Wearable nanogenerators took remarkable attention for last five years in order to harvest human motion with textile comfort and low maintenance [10]. Wearable nanogenerators can be used for different purposes like health care sensors [11], energy harvesting [12], motion monitoring [13], human-machine interaction [14], and electronics [15]. Especially for wearable technologies, flexibility is one of the most studied points in engineering fields [16]. These devices can also be used as a power source for self-powered systems and reduce battery usage, which contributes to a reduction in environmental pollution in the long run.

ZnO, the well-known and cheapest piezoelectric material, is also a brittle, acid-soluble and white wurtzite crystal. ZnO nanowires was first time used as energy harvester in 2006 by Wang and then, nanogenerator concept was emerged. Wang produced vertically aligned ZnO nanowires on a polymeric substrate by chemical vapor deposition (CVD) method and The ZnO nano-forest produced electrical energy under the action of mechanical forces [9]. ZnO is also used by hybridizing with carbon-based materials for nanocomposite-based nanogenerator applications [17–20]. Chung et. al. used a thermoset polyurethane (PU) foam as substrate. PU foam was first coated with graphene oxide (GO) as bottom electrode and GO was reduced with ascorbic acid. Then, vertically aligned ZnO nanowires were grown by hydrothermal method. Finally thin Au film was coated onto nanogenerator as top electrode and nanogenerator generated 0.5 V voltage and 0.2 $\mu\text{A}/\text{cm}^2$ current density [21]. In another work, ZnO nano-forest was grown on graphene-coated PET foil. ZnO-graphene layer was detached from PET substrate and other side of graphene was also coated with ZnO nanowires by hydrothermal method and ZnO/graphene/ZnO structure is obtained. Indium tin oxide (ITO) coated PET foils were used as top and bottom electrodes of the nanogenerator. Obtained piezoelectric nanogenerator generated 0.17 V voltage and 27.5 nA current [17]. Zhou group developed a highly stretchable energy generator based on thermoplastic polyurethane (TPU), silver nanowires (AgNW), reduced graphene oxide (rGO) and ZnO nanowires. This study demonstrated that AgNW and rGO has a synergistic effect to form electrically conductive pathway [10]. Besides, the ZnO nanomaterials, perovskite nanomaterials [22], polyvinylidene fluoride (PVDF) films [23], or nanofibers [24] can also be used as piezoelectric nanogenerators, while ZnO is more preferred due to its low cost and easy synthesis advantages.

In this study, the effect of ZnO nanowire concentration on the output voltage and current of textile-based nanogenerator devices was investigated. AgNW and rGO were used to form conductive pathways and transmit the generated electrical charge from the ZnO nanowires to the upper and lower electrodes. However, since the concentrations of AgNW and rGO in the nanocomposite will affect the output signals, the conductive filler concentrations were kept constant for each sample to clearly observe the effect of ZnO on the output signals. The prepared nanocomposite solutions were coated on a polyaniline-coated cotton fabric as the bottom electrode and coagulated on the fabric. The nanogenerators were fabricated by mounting the upper and lower electrodes on fabric samples. The nanogenerators were subjected to the bending test to simulate human elbow movement and output signals were recorded simultaneously.

2. MATERIALS AND METHODS

2.1. Materials

Dimethyl formamide (DMF) (Merck) is used as solvent. Ether-based TPU was used as matrix polymer. Graphite powder(Merck), phosphoric acid (85% Sigma-Aldrich), sulfuric acid (98% Merck), hydrazine hydrate (55%, Sigma), hydrogen peroxide (35%, Sigma-Aldrich), hydrochloric acid (37%, Fischer Chemicals), and ethanol (ISOLAB) were used for rGO synthesis. Silver nitrate (99.5%, Sigma-Aldrich), polyvinylpyrrolidone (PVP), ethylene glycol (EG) (99.9% Sigma-Aldrich), and sodium chloride (NaCl) (99.9%, Sigma-Aldrich) were used for AgNW synthesis. Zinc nitrate hexahydrate, hexamethylene tetramine (HMTA) and ethanol were used for ZnO nanowire synthesis. Aniline (99.9%, Sigma-Aldrich),

hydrochloric acid (37%, WVR Chemicals) and ammonium persulfate (APS) (98%, Sigma) were used for polyaniline synthesis on fabric surface.

2.2. Methods

2.2.1. GO synthesis and chemical reduction

GO was synthesized according to Improved Hummers' Method [25]. 2 g of graphite powder was added into sulfuric acid-phosphoric acid mixture (9:1 by volume) and stirred for 30 minutes. After 30 minutes, 12 g of KMnO₄ was added into flask and reaction was maintained overnight at 50 °C. Obtained brown mixture was poured onto 300 mL of deionized (DI) water ice in order to prevent sudden temperature rise. Then, 2 mL of H₂O₂ (30%) added in reaction mixture to neutralize the excess amount of KMnO₄. Reaction mixture was centrifuged and brown GO powder was separated from liquid phase. GO flakes was washed with ethanol and HCl for once and washed with DI water for 20 times to removal of impurities. After washing step, GO was dried in fume hood for one week. GO powder was homogenized with ultrasonic homogenizator in DI water and reduced in 0.3 M hydrazine hydrate at 95 °C for 12 hours. Black rGO powder was washed with DMF for a few times to remove residual DI water and stored in DMF.

2.2.2. AgNW synthesis

AgNWs were synthesized with a modified method of literature [26]. Firstly, 0.007 g of NaCl was dissolved in 10 mL of EG. Separately, 0.204 g of AgNO₃ was dissolved in 10 mL EG. 1 g of PVP was also separately dissolved in 20 mL of EG at 80 °C. NaCl solution was added slowly into the PVP solution. AgNO₃ solution was also added dropwise to the reaction mixture. Heater was set to 180 °C and color change observed with increasing temperature (Figure 1). The color change is due to AgNO₃-Ag transformation and Ag nanocube-Ag nanowire transformation [27]. The reaction mixture was cooled at room conditions. The AgNW dispersion was washed several times with acetone and DI water to remove PVP and ionic impurities. The final product was washed several times with DMF and stored in DMF.



Figure 1. Color change with increasing temperature in AgNW synthesis

2.2.3. ZnO nanowire synthesis

0.1 M of Zn(NO₃)₂·6H₂O and 0,1 M HMTA solutions were mixed in equal volume [28]. Mixed solution was transferred in a PTFE lined hydrothermal reactor and heated to 180 °C for 8 hours. The reactor was cooled and white ZnO powder was washed with DI water and ethanol, respectively. Final powder was stored in DMF.

2.2.4. Polyaniline (PANI) coating of cotton fabric

PANI was synthesized by in-situ polymerization method [29]. with presence of woven cotton fabric. Molar ratio of aniline monomer and ammonium persulfate (initiator) was 4:1 and polymerization was performed in 1 M HCl solution. Firstly, Aniline-HCl solution was cooled in ice bath between 0-5 °C and cotton fabric was soaked in the solution. APS was dissolved in 1 M HCl solution and APS-HCl solution was added into monomer solution dropwise. Polymerization was maintained for 12 hours and PANI coated fabric was dried in an oven. Dried fabrics were doped with HCl fume.

2.2.5. Preparation of nanocomposite solutions

Each nanomaterial was stored in DMF, after synthesis steps and concentrations of each nanomaterial solution were determined by solvent removing method: Known volume of nanomaterial solution was heated up to 150 °C and residual solid was weighed with precision. All nanocomposite solutions contain 14% solid (polymer and additive) by weight. The concentration of conductive additives (rGO and AgNW) was 0.25% by weight in TPU. Nanomaterial concentrations were given in Table 1.

Table 1. Sample names and nanocomposite solution compounds

Sample Name	ZnO (%)	AgNW (%)	rGO (%)
PNG1	1	0.25	0.25
PNG2	3	0.25	0.25
PNG3	5	0.25	0.25
PNG4	7	0.25	0.25
PNG5	9	0.25	0.25

2.2.6. Device fabrication

PANI coated fabrics were used as substrate of nanogenerators. Nanocomposite solutions were firstly poured onto fabrics and nanocomposite films were coated with a film applicator with thickness of 200 µm. The fabrics were immediately immersed in 1M HCl solution to coagulate the PU. HCl solution in coagulation bath prevented the dedoping of PANI in coagulation step due to ion impurity in water. The nanocomposite film-coated fabrics were sandwiched between two aluminum tapes, as the top and bottom electrodes. Sandwiched structure encapsulated with polydimethylsiloxane (PDMS) to mechanical stability and electrical insulation [30].

2.2.7.Characterization

The morphological analysis of AgNW and ZnO nanowires was performed by scanning electron microscopy (LEO GEMINI 1530, Carl Zeiss SEM) under 5 kV voltage with the distance between 8-9 mm. The electromechanical characterization was performed with a periodic bending apparatus designed

in our previous study [30]. The electrical contacts of nanogenerators were connected to an oscilloscope (GW INSTEK 1102-B) and output signals were recorded. A current clamp (FLUKE i30s) was also used for output current measurements. Output power values are calculated with Ohm's Law [31]:

$$P = V \times I \quad (1)$$

where P is power, V is open circuit voltage and I is short circuit current.

3. RESULTS AND DISCUSSION

3.1. SEM Results

SEM images of ZnO nanowires were given in Figure 2. ZnO nanowires have a diameter of about 130 nm and a length of 570 nm. As seen in the SEM images, several ZnO nanowires were grown on a nucleus [32]. SEM images also showed successful synthesis of AgNWs (Figure 3). The diameter distribution of AgNWs was very homogeneous and very thin (mean 23.6 nm) at 700 nm in length.

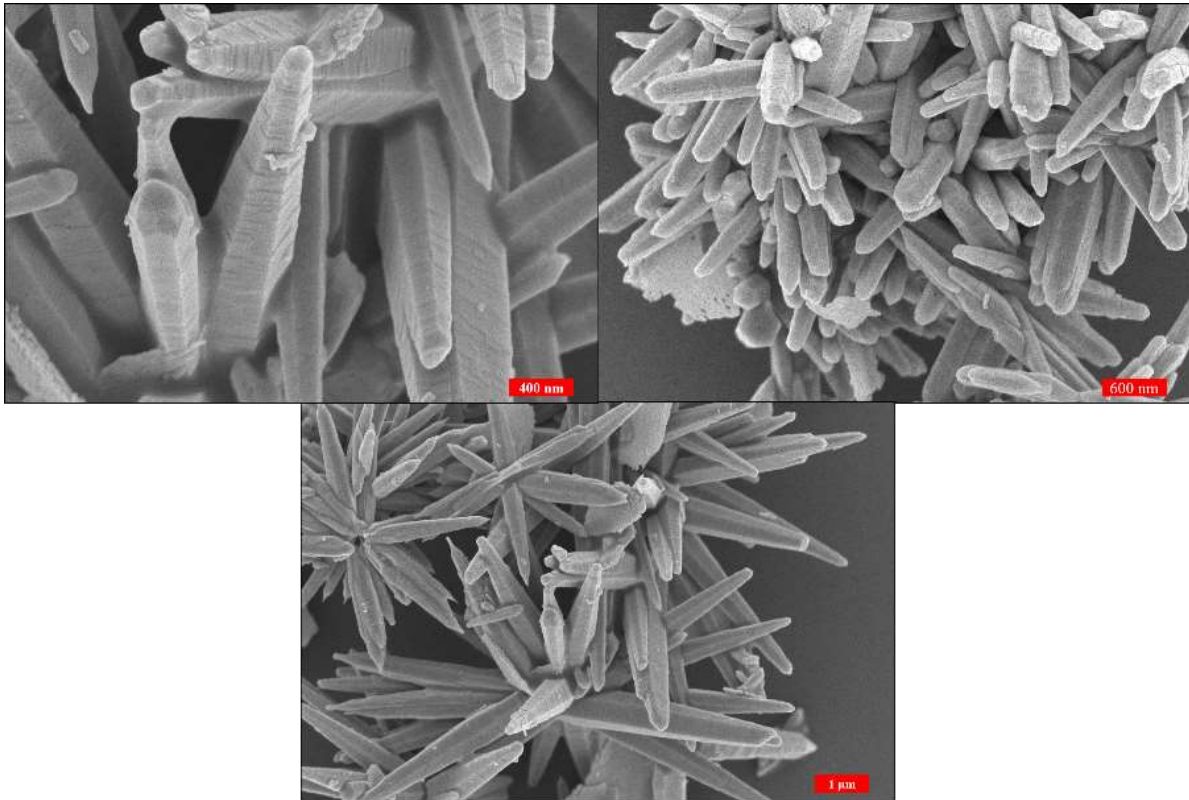


Figure 2. SEM images of ZnO nanowires

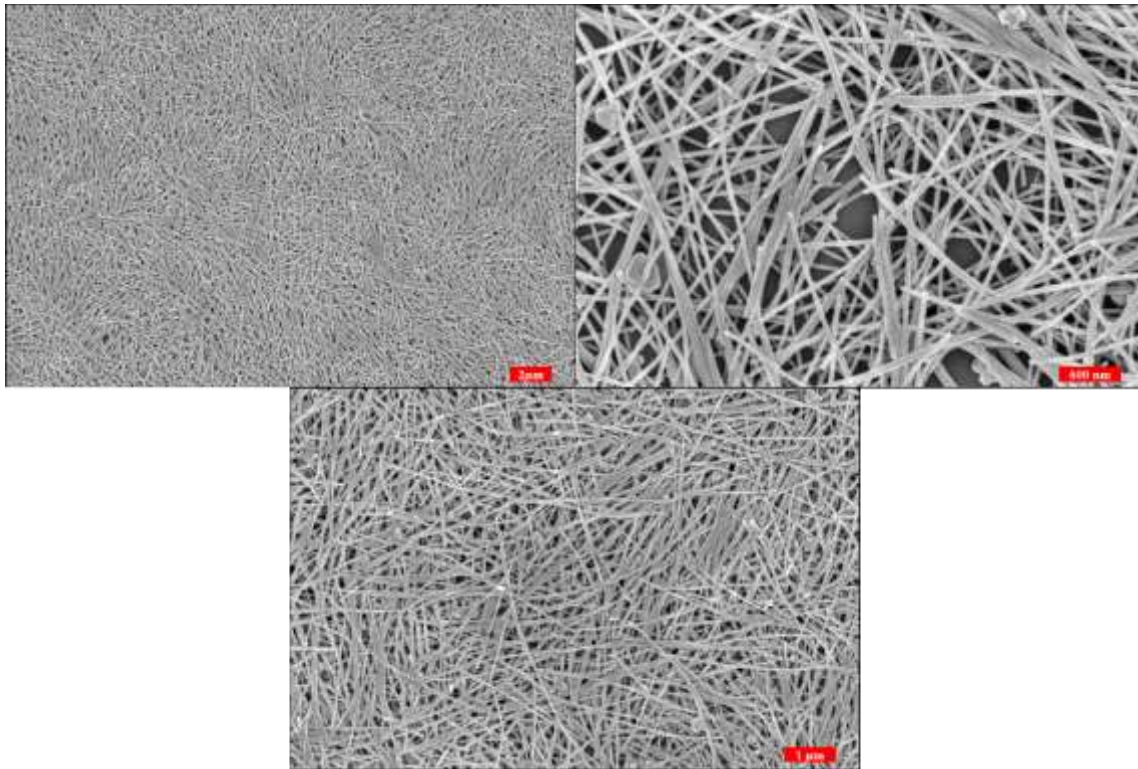


Figure 3. SEM images of AgNWs

3.2. Electromechanical Characterization

Piezoelectric energy conversion of all samples were monitored with an oscilloscope. Every bending movement represented a peak in time-voltage graphs. Maximum signals were determined by V_{p-p} values. V-t graphs of nanogenerators were given in Figure 4. As a result of the voltage measurements, it was observed that the voltage signals increased with increasing ZnO amount. The 9% ZnO doped nanogenerator showed lower piezoelectric output voltage than the 7% ZnO doped nanogenerator. On the other hand, the signal intensity increased up to the addition of 7% ZnO (Figure 4a-IV). The short-circuit current output signals were given in Figure 4b. All nanogenerators showed similar output current characteristics. However, a periodic signal (such as voltage graphs) could not be observed because the current produced was very low and not stable.

As a result of power calculations and P-t graphs, 7% ZnO doped nanogenerator showed the highest output power with 10.88 mW and the most intense signal output (Figure 4c-IV). Maximum output voltage, current and power values are also given in Figure 5. Maximum voltage and power values were obtained from 7% ZnO doped nanogenerator 1.12 V and 10.88 mW. The voltage and power values were increased with ZnO amount [33]. until 7% doping. It can be said that falling at 9% ZnO doping can be caused by increase on ZnO/conductive filler ratio with increasing ZnO amount. In other words, optimum ZnO/conductive ratio was 14 (7% ZnO doping, 0.25% graphene and 0.25% AgNW doping) for nanocomposite-based piezoelectric nanogenerators. The maximum output current as 72 mA was obtained from the 5% ZnO doped nanogenerator.

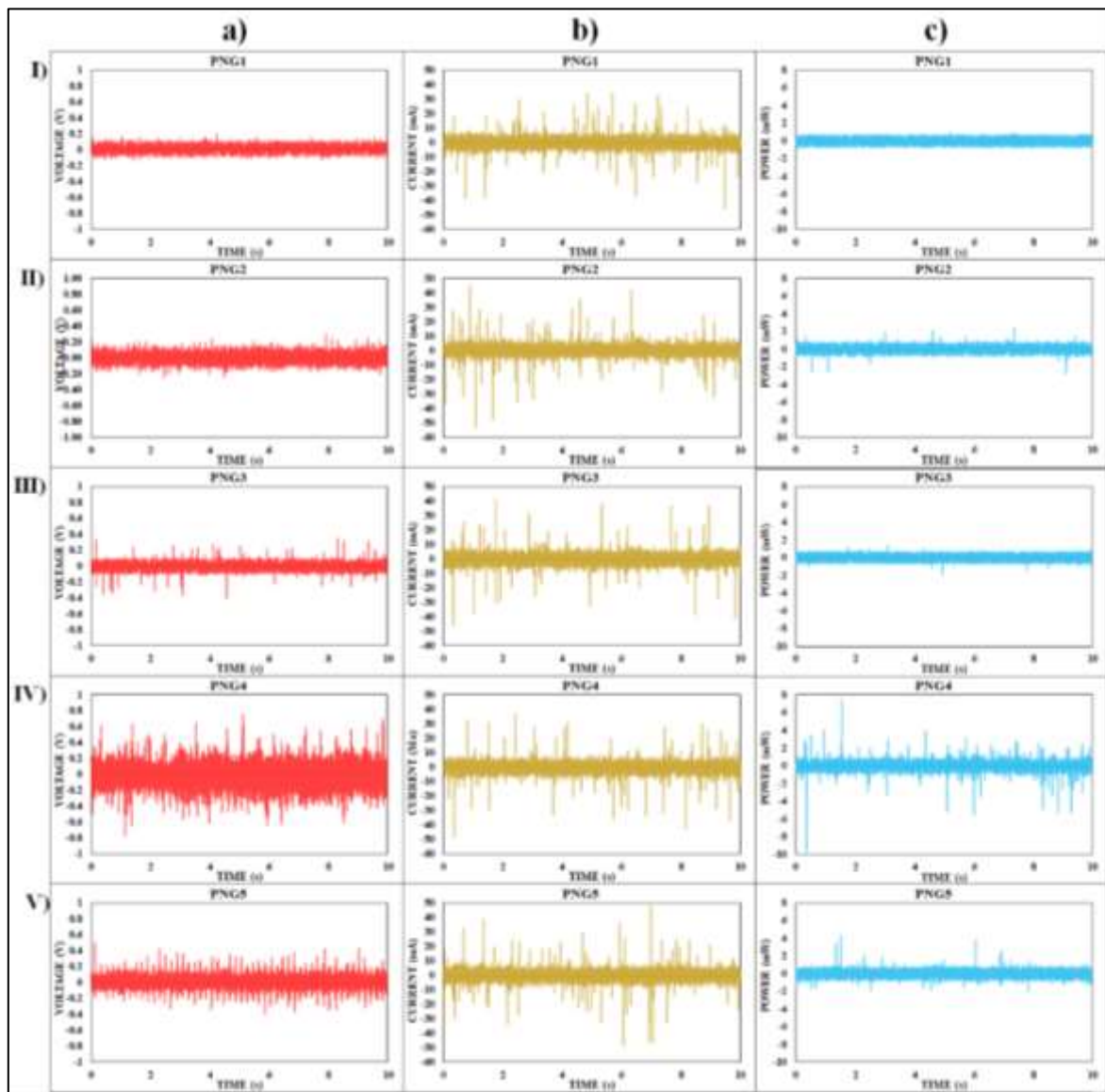


Figure 4. a) Voltage-time, b) current-time, and c) power-time graphs of piezoelectric nanogenerators

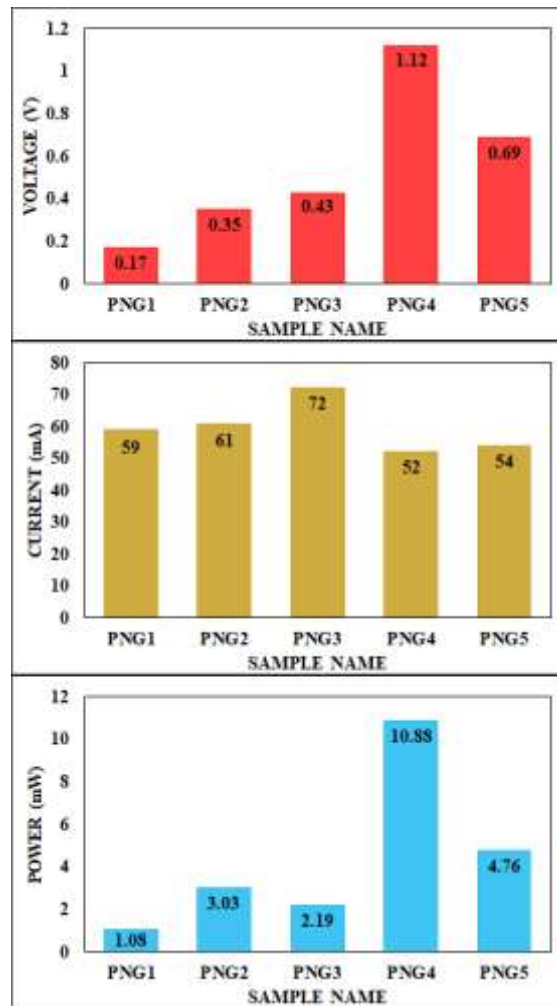


Figure 5. Maximum voltage, current and power output of nanogenerators

4. CONCLUSION

It has been observed that the amount of ZnO used in the produced nanogenerators generally increases in direct proportion to the energy conversion efficiency. According to the electromechanical results, it was observed that the PNG4 sample produced 1.12 V voltage and 52 mA current (the nanogenerator produced a total of 10 mW power). The energy conversion efficiency exhibited by the rGO/ZnO/AgNW doped samples showed that nanogenerators could be used by developing them with these materials. In addition, this study revealed the importance of the "piezoelectric material/conducting material" ratio for nanocomposite-based nanogenerators. It can be clearly seen that increasing the piezoelectric/conductor ratio improves the output signals up to a piezoelectric/conductor ratio of 14. However, above 14 output voltage and current signals started to decrease. Thanks to the sustainable features of nanogenerators, which are cleaner, renewable and environmentally friendly devices, it is predicted that they will take more place in human life in the future.

ACKNOWLEDGEMENTS

This project was supported under the project application number 1139B411900326 within the scope of TUBITAK 2209-B Industry Oriented Undergraduate Research Projects Support Program.

CONFLICT OF INTEREST

The authors stated that there are no conflicts of interest regarding the publication of this article.

REFERENCES

- [1] Commitment O U R, Strategy O U R, E. Use and E Management. *Energy and Renewable Energy*. 2014.
- [2] Johansson T B, Kelly H, Reddy A K N, and Williams R H. *Renewable energy: Sources for fuels and electricity*. 1993
- [3] Silva-Leon J, Cioncolini A, Nabawy M R A, Revell A, and Kennaugh A. Simultaneous wind and solar energy harvesting with inverted flags. *Applied Energy*, 239(February):2019; 846–858
- [4] Bedeloğlu A, Ünsal Ö F, and Bedeloğlu A Ç. İletken Polimer Esaslı Nanojeneratörler. *Afyon Kocatepe University Journal of Science and Engineering*, 2018;18: 640–647
- [5] Indira SS, Vaithilingam C A, Oruganti K S P, Mohd F, and Rahman S. *Nanogenerators as a sustainable power source: state of art, applications, and challenges 2019*
- [6] Xue H, Yang Q, Wang D, Luo W, Wang W, Lin M, Liang D, and Luo Q. A wearable pyroelectric nanogenerator and self-powered breathing sensor. *Nano Energy*, 2017; 38(May): 147–154
- [7] Wang Y, Yang Y, and Wang Z L. Triboelectric nanogenerators as flexible power sources. *Npj Flexible Electronics*, 2017; 1(1): 1–9
- [8] Fan F R, Lin L, Zhu G, Wu W, Zhang R, and Wang Z L. Transparent triboelectric nanogenerators and self-powered pressure sensors based on micropatterned plastic films. *Nano Letters*, 2012; 12(6): 3109–3114
- [9] Wang Z L and Song J. Piezoelectric nanogenerators based on zinc oxide nanowire arrays. *Science*, 2006; 312(5771): 242–246
- [10] Zhou K, Zhao Y, Sun X, Yuan Z, Zheng G, Dai K, Mi L, Pan C, Liu C, and Shen C. Ultra-stretchable triboelectric nanogenerator as high-sensitive and self-powered electronic skins for energy harvesting and tactile sensing. *Nano Energy*, 2020; 70(January): 104546
- [11] Wang L and Daoud W A. Hybrid conductive hydrogels for washable human motion energy harvester and self-powered temperature-stress dual sensor. *Nano Energy*, 2019; 66(July): 104080
- [12] Lu L, Ding W, Liu J, and Yang B. Flexible PVDF based piezoelectric nanogenerators. *Nano Energy*, 2020; 78(July): 105251
- [13] Liu Z, Zhang S, Jin Y M, Ouyang H, Zou Y, Wang X X, Xie L X, and Li Z. Flexible Piezoelectric

- Nanogenerator for Wearable Self-powered Respiration Active Sensor and Healthcare Monitoring. *Materials Research Express*, 2019; 0–12
- [14] He X, Zi Y, Yu H, Zhang S L, Wang J, Ding W, Zou H, Zhang W, Lu C, and Wang Z L. An ultrathin paper-based self-powered system for portable electronics and wireless human-machine interaction. *Nano Energy*, 2017; 39(April): 328–336
- [15] Feng X, Zhang Y, Kang L, Wang L, Duan C, Yin K, Pang J, and Wang K. Integrated energy storage system based on triboelectric nanogenerator in electronic devices. *Frontiers of Chemical Science and Engineering*, 2021; 15(2): 238–250
- [16] Dong K, Peng X, and Wang Z L. Fiber/Fabric-Based Piezoelectric and Triboelectric Nanogenerators for Flexible/Stretchable and Wearable Electronics and Artificial Intelligence. *Advanced Materials*, 2020;32(5): 1–43
- [17] Shin D M, Tsege E L, Kang S H, Seung W, Kim S W, Kim H K, Hong S W, and Hwang Y H. Freestanding ZnO nanorod/graphene/ZnO nanorod epitaxial double heterostructure for improved piezoelectric nanogenerators. *Nano Energy*, 2015; 12: 268–277
- [18] Lin L, Hu Y, Xu C, Zhang Y, Zhang R, Wen X, and Lin Wang Z. Transparent flexible nanogenerator as self-powered sensor for transportation monitoring. *Nano Energy*, 2013; 2(1): 75–81
- [19] Cherumannil Karumuthil S, Rajeev S P, and Varghese S. Piezo-tribo nanoenergy harvester using hybrid polydimethyl siloxane based nanocomposite. *Nano Energy*, 2017; 40(August): 487–494
- [20] Li X, Chen Y, Kumar A, Mahmoud A, Nychka J A, and Chung H J. Sponge-Templated Macroporous Graphene Network for Piezoelectric ZnO Nanogenerator. *ACS Applied Materials and Interfaces*, 2015; 7(37): 20753–20760
- [21] Yilmaz Y and P. Mazumder P. A drift-tolerant read/write scheme for multilevel memristor memory. *IEEE Transactions on Nanotechnology* 2017; 16(6): 1016–1027
- [22] Kandpal M, Palaparthi V, Tiwary N, and Rao V R. Low Cost, Large Area, Flexible Graphene Nanocomposite Films for Energy Harvesting Applications. *IEEE Transactions on Nanotechnology*, 2017; 16(2): 259–264
- [23] Aatur Rahman M, Lee B C, Phan D T, and Chung G S. Fabrication and characterization of highly efficient flexible energy harvesters using PVDF-graphene nanocomposites. *Smart Materials and Structures*, 2013; 22(8):
- [24] Abolhasani MM, Shirvanimoghaddam K, and Naebe M. PVDF/graphene composite nanofibers with enhanced piezoelectric performance for development of robust nanogenerators. *Composites Science and Technology*, 2017; 138: 49–56
- [25] Marcano D C, Kosynkin D V, Berlin J M, Sinitskii A, Sun Z, Slesarev A, Alemany L B, Lu W, and Tour J M. Improved synthesis of graphene oxide. *ACS Nano*, 2010; 4(8): 4806–4814
- [26] Hemmati S, Harris M T, and Barkey D P. Polyol Silver Nanowire Synthesis and the Outlook for a Green Process. *Journal of Nanomaterials*, 2020; 2020: 6–10

- [27] Sağlam G, Borazan I, Hoşgün H L, Demir A, and Bedeloğlu A Ç. Effect of molar ratio of PVP/AgNO₃ and molecular weight of PVP on the synthesis of silver nanowires. *Nonlinear Optics Quantum Optics*, 2017; 48(2): 123–132
- [28] McPeak K M, Le T P, Britton N G, Nickolov Z S, Elabd Y A, and Baxter J B. Chemical bath deposition of ZnO nanowires at near-neutral pH conditions without hexamethylenetetramine (HMTA): Understanding the role of HMTA in ZnO nanowire growth. *Langmuir*, 2011; 27(7): 3672–3677
- [29] Li M, Huang X, Wu C, Xu H, Jiang P, and Tanaka T. Fabrication of two-dimensional hybrid sheets by decorating insulating PANI on reduced graphene oxide for polymer nanocomposites with low dielectric loss and high dielectric constant. *Journal of Materials Chemistry*, 2012; 22(44): 23477–23484
- [30] Ünsal Ö F, Altın Y, and Çelik Bedeloğlu A. Poly(vinylidene fluoride) nanofiber-based piezoelectric nanogenerators using reduced graphene oxide/polyaniline. *Journal of Applied Polymer Science*, 2020; 137(13): 1–14
- [31] Choi S, Cho S, Yun Y, Jang S, Choi J H, Ra Y, La M, Park S J, and Choi D. Development of a High-Performance Handheld Triboelectric Nanogenerator with a Lightweight Power Transmission Unit. *Advanced Materials Technologies*, 2020, 5(4): 1–8
- [32] Shi R, Yang P, Wang J, Zhang A, Zhu Y, Cao Y, and Ma Q. Growth of flower-like ZnO via surfactant-free hydrothermal synthesis on ITO substrate at low temperature. *Cryst Eng Comm*, 2012, 14(18): 5996–6003
- [33] Gu L, Liu J, Cui N, Xu Q, Du T, Zhang L, Wang Z, Long C, and Qin Y. Enhancing the current density of a piezoelectric nanogenerator using a three-dimensional intercalation electrode. *Nature Communications*, 2020, 11(1): 1–9



DEVELOPMENT AND CHARACTERIZATION OF VITAMIN B₉ - ELECTROSPRAYED NON-WOVEN SURFACES FOR WOUND HEALING APPLICATIONS

Fatma Nur PARIN^{1,*} , Kenan YILDIRIM¹ , Gökçe TANER² , Elife KILDALI² 

¹Department of Polymer Materials Engineering, Faculty of Engineering and Natural Sciences, Bursa Technical University, Bursa, Turkey

²Department of Bioengineering, Faculty of Engineering and Natural Sciences, Bursa Technical University, Bursa, Turkey

ABSTRACT

In this study, novel wound dressing materials based on non-woven (NW) surfaces were developed using the electrospaying (e-spraying) process. Polyester spun-bond (PET SPB), polypropylene spun-bond (PP SPB), and polypropylene melt-blown (PP MB) surfaces used as matrix, and folic acid (FA), vitamin B₉ were sprayed on these surfaces. The resulting NW fabrics with the same FA content were investigated in terms of physical, morphological, thermal, wettability properties. Scanning Electron Microscopy and (SEM) and Fourier Transform Infrared (FT-IR) spectroscopy results showed the formation of physical interaction between NWs and FA. Notably, FA was successfully deposited onto NWs with average fiber diameters from 2.6 µm to 23.11 µm. According to the thermogravimetric analysis (TGA), FA loaded-PP SPB has enhanced thermal stability compared to pure one (PP SPB). The FA-loaded surfaces have a hydrophobic property with contact angles values more than >90°. The *in-vitro* release was carried out by UV-Vis within the 8 hour-period phosphate buffer saline (pH 7.2). The results indicated that FA-loaded surfaces have a fast release behaviour. The total FA release amounts of the FA-loaded PET SPB, PP SPB and PP MB NWs were found as 22.8, 17.1, and 17.5 ppm. Moreover, the biocompatibility of all resulting NW surfaces was assessed by 3-(4,5-dimethylthiazol-2-yl)-2,5-diphenyltetrazolium bromide (MTT) and neutral red uptake (NRU) cytotoxicity tests in L929 cell lines. The obtained NWs are biocompatible and non-toxic material, except PET SPB-sFA. The study indicated that FA-loaded NWs can be potential candidates for wound healing applications.

Keywords: Non-woven surfaces, Wound healing, Folic acid, Contact angle, Thermal analysis

1. INTRODUCTION

Cell proliferation, migration, reepithelization, and tissue remodelling are all part of the wound healing process that is assisted by complex interactions between growth factors, extracellular matrix, bioactive agents, and cells [1, 2]. B-vitamins are regenerative agents, which are playing an essential role in many bodily functions as cofactors for enzymes. Especially, due to the epigenetic role of folic acid (C₁₉H₁₉N₇O₆) in many human metabolic activity, it is an important member of B-complex vitamins, which is known as B₉ vitamin, plays a crucial role in the maintenance of many metabolic functional processes in the body, such as cell growth, and development, synthesis of nucleic acids and metabolism of many amino acids [3, 4]. Folic acid (FA) is being studied due to its role in the synthesis of both building-block molecules and their effects on differentiation. It is one of the most important factors in tissue regeneration and repair [2].

There have previously been reported in various studies that folic acid can promote cell growth when added to polymer forms (in cream, fiber, microcapsule, micro/hydrogel, and even neat powder, etc.). In this context, Duman et al. (2018) reported that folic acid enhances wound healing in rats. Fischer et al. investigated the effects of topical folic acid and creatine-containing formulations on skin firmness on collagen gene expression [5]. Moreover, in endothelial cell line proliferation experiments, the effect of folic acid on cell proliferation at different concentrations was investigated by *in vitro* proliferation experiments [2]. In the study that wound healing process simulated by software

*Corresponding Author: nur.parin@btu.edu.tr

Received: 16.08.2021 Published: 30.11.2021

analysis increased cell proliferation was reported compared to the control group by almost 40% at the end of 48 h. In our previous study, cytocompatibility assays results showed folic acid-loaded hydrophilic fibers have no toxicity and neat folic acid improved cell generation by nearly 177 % [6]. It is contrary to the restriction of the utilization of folic acid in pure form, Pagano et al. (2019) synthesized folic acid-based emulgels and MTT tests have indicated cell viability over 100 % [7]. Furthermore, Zhao et al. (2018) indicated folic acid can accelerate collagen formation in diabetic wounds [8]. In a similar study, Khan et al. asserted folic acid could be a potential candidate for the oral mucosal wound healing process [9].

Camacho et al. (2019) created copper-alginate hydrogels containing folic acid. The slow folic acid release observed only at $\text{pH} > 5$, particularly in simulated intestinal conditions, and these organometallic hydrogels performed as a gastro-resistant material ($\text{pH} 8.2$). Furthermore, with a zero-order k , the successful compounds showed greater release in alkaline medium (> 80 ppm) compared to acidic media ($\text{pH} 5.4$) (~ 8 ppm) [10].

Mallakpour and Hatami (2020) prepared chitosan nanocomposite films containing folic acid for use as bone and tooth additives in tissue engineering [11]. Contact angle measurements showed that the produced films had improved wettability and were more hydrophilic. Furthermore, the bioactivity of these NC films by soaking them in simulated body fluid (SBF, $\text{pH} 7.4$), and the pH changes for this solution were observed for 1 month. In a similar study, Acevedo-Fani et al. (2018) developed folic acid/polysaccharide-based nanolaminate films [12]. With the addition of folic acid, the structure of the nanolaminates improved, resulting in homogeneous and smooth layers. At $\text{pH} 3$, only 22% of the FA was released from the films after 7 hours, while at $\text{pH} 7$, over 100% of the FA was released. This is due to folic acid becoming entrapped in nanolaminates due to its poor performance.

Fonseca et al. (2020) did a study on improving folic acid bioavailability. The release behavior of nanofibers containing various amounts of FA (5, 10, and 15 %) were obtained using starch as a matrix. Although the diameters of nanofibers produced below 100 nm did not vary much, some beads in FA-loaded fibers was detected [13].

A study on PVP/dextran octadecyl amine/montmorillonite/ VB_9 conjugate nanofibers have been fabricated by Şimşek et al. (2016). The nanofibers' cytotoxicity tests indicated that VB_9 had no negative effects on Vero cells (liver cells), suggesting that these fibers might be a game-changer in cancer research and tissue engineering applications [14].

Electrospraying (e-spraying), one of the electrohydrodynamic atomization (EHDA) methods, in which low-viscosity liquids through electrical forces are coated with a carrier material to form regular structures in sub-micron or nanoscale sizes by an electric field [15,16]. It is more advantageous than other methods such as spray drying, coacervation, and emulsion with the formation of non-agglomerated capsule structures with high active ingredient content with better size distribution without high temperature, pressure or toxic solvent. Hydrophobic and hydrophilic bioactive molecules, or therapeutics can be encapsulated into polymer matrices with almost 100% efficiency by this method [17].

The current study is focused on the development of FA-loaded fibrous structures via the electrospraying method. As distinct from the previous studies, there is no report on the electrospraying of FA onto melt-blown and spun-bond surfaces. Therefore, the optimum amount of FA was studied to investigate electrospraying capacity, in vitro release in PBS media, and cell viability, and the availability of the wound applications was evaluated. Moreover, a detailed characterization study of the resulting surfaces was carried out by performing Scanning Electron Microscopy and (SEM) Fourier Transform Infrared (FT-IR) spectroscopy, thermogravimetric analysis (TGA), and contact

angle test. TGA curves indicated that FA inhibits the degradation of the FA-loaded PP SPB and acts as an antioxidant at high temperatures. Overall, it has been suggested that the obtained surfaces can be used for wound healing applications.

2. EXPERIMENTAL

2.1. Material

In this study, PET spun-bond (SPB), PP spun-bond (SPB) and PP melt blown (MB) non-woven (NW) fabrics (Mogul Textile Company, Gaziantep/Turkey) were used. Folic acid ($C_{19}H_{19}N_7O_6$) for Biochemistry (98-102 % purity) was supplied from ChemSolute Company (Germany). The ethanol (99 % purity) was purchased from Sigma-Aldrich Chemical Company (USA). Phosphate buffer saline (PBS) tablets (pH 7.2) were used for each *in-vitro* release study. The chemicals used in the MTT and NRU assay tests were purchased from the following suppliers; RPMI (Roswell Park Memorial Institute) 1640 medium, fetal bovine serum (FBS), penicillin-streptomycin, neutral red (NR) (3-amino-7-dimethyl-amino-2-methylphenazine hydrochloride), 3-(4,5-dimethylthiazol-2-yl)-2,5-diphenyltetrazolium bromide (MTT), trypan blue, ethanol from Sigma; dimethyl sulfoxide (DMSO) from Merck; Triton X-100, trypsin-EDTA, Dulbecco's phosphate-buffered saline (DPBS) from Gibco. In all experiments, distilled water was used.

2.2. Method

2.2.1. Electro spraying of FA onto Non-woven Fabrics

10 mL folic acid (22 mg) solution is prepared by mass with a mixture of 2/1 ethyl alcohol-water solvents. The folic acid solution is sonicated in an ultrasonic homogenizer by applying 60% power for 30 min. It was then sprayed onto the surfaces of polyester spun-bond, PP spun-bond, and PP melt-blown non-woven fabrics with 23 kV electrical power, 100 mm distance (drum-to tip) and 150 rpm drum speed at a flow rate ranging from 1-1.5 mL/h (Figure 1).

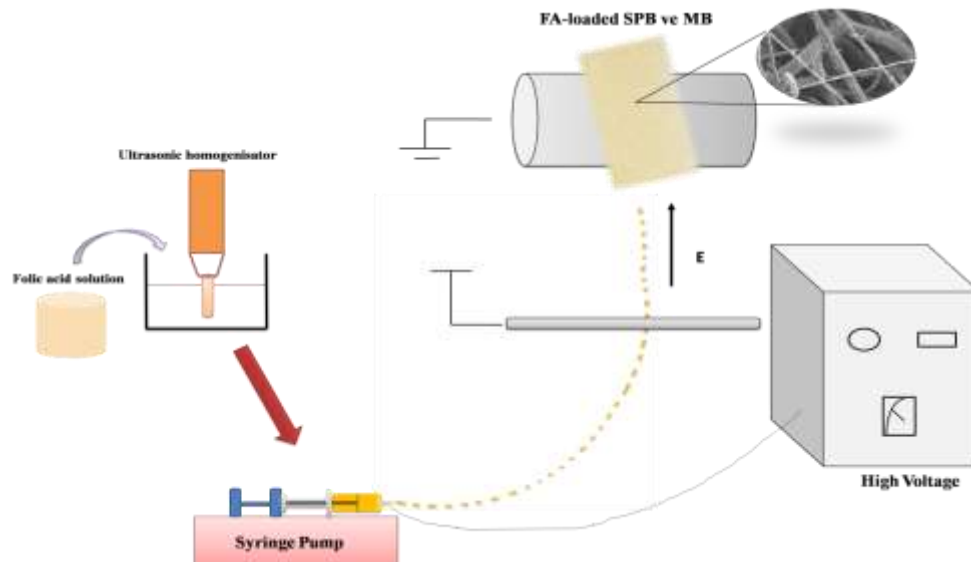


Figure 1. Schematic illustration of electro spraying method.

2.3. Characterization

The **microstructural analysis** of all NWs was observed with Carl Zeiss/Gemini 300 Scanning Electron Microscope (SEM) (ZEISS Ltd., Germany). All samples were coated with gold before analysis. The fiber diameters were measured by using Image J (version 1.520 software) by randomly selecting the diameters of 60 individual fibers for each sample. Average fiber diameters and fiber diameter histogram data were performed with Origin Pro 2018 software.

The **physical analysis** of all samples was analyzed by FT-IR Thermo Nicolet iS50 FT-IR (USA) spectrometer with an ATR adapter (Attenuated Total Reflectance) (Smart Orbit Diamond, USA).

The **contact angles** of the samples were measured with an automatic dispenser system Attension Theta Lite model optical tensiometer (Biolin Scientific, Gothenburg, Sweden). Contact angle measurements were made by dropping 4 μL distilled water to 2.5 cm x 2.5 cm samples. To calculate the average θ value, this analysis was repeated three times.

The **thermogravimetric analysis (TGA)** was realized under nitrogen atmosphere with $20^\circ\text{C min}^{-1}$ heating rate, 30-600 $^\circ\text{C}$ temperature range and then applied oxygen atmosphere with the same heating rate at 600-900 $^\circ\text{C}$ temperature.

The pycnometer (Micromeritics-AccuPycII 1340) was used to measure the fiber volume using helium gas. Therefore, the **porosities** of non-wovens were measured by using the following equation:

$$\text{Porosity} = \frac{\text{Volume (Vf) of NWs by Pycnometer}}{\text{Total Volume (Length x Width x Thickness)}} \quad (1)$$

The **in-vitro release tests** were applied to determine the FA release behaviour of NWs. The FA-release behavior of FA sprayed resulting non-wovens were studied in phosphate buffer solutions (PBS) at pH 7.2 by the total immersion method [18,19]. 20 cm² of the samples were put into sealed glass tubes with each containing 100 mL of PBS, separately. Afterwards, the samples were placed in a shaking incubator at 37 $^\circ\text{C}$ with stirring 120 rpm to apply the release behaviour of the FA. About 3.5 mL of the samples were removed at the specified time intervals with the PBS and the corresponding absorbance value was determined with UV spectrophotometer (Scinco/NEOYSY 2000) at $\lambda_{\text{max}} = 282 \text{ nm}$, which was the characteristic peak of FA. The FA concentration was obtained from the calibration curve of the model vitamin prepared with a FA solution of known concentrations in PBS (pH 7.2). The calibration curve was found to be $Y = 0.0639X + (0.0276)$ ($R^2 = 0.99997$), where X is the concentration of FA (mg/L) and Y is the solution absorbance at 282 nm (linear range of 2.5–25 mg/L) (Figure 2).

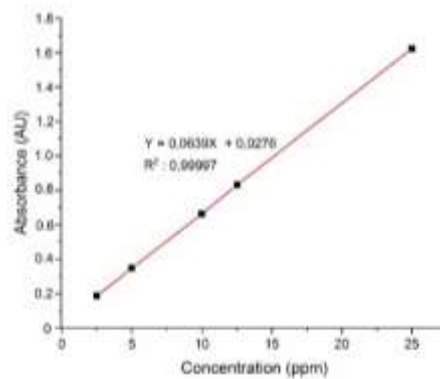


Figure 2. The calibration curve for FA in PBS.

Two *cytocompatibility tests*, MTT and NRU have been carried out on all resulting NW surfaces by using L929 cell lines according to the ISO 10993-5.

3. RESULTS AND DISCUSSION

3.1. Microstructural Analysis

Figure 3-Figure 5 indicates the average fiber diameter distribution with SEM images of pure and FA-sprayed NW surfaces. It is visible that pure NWs exhibit fibrillated smooth surface morphology, while FA particles are deposited on the surface of FA-sprayed NWs. The average fiber diameters of PET SPB and PET SPB-sFA were calculated as $16.91 \pm 3.28 \mu\text{m}$ and $17.55 \pm 2.61 \mu\text{m}$, respectively. PP MBs have more irregular fiber diameters than, and average fiber diameters are also quite low ($2.59 \pm 1.14 \mu\text{m}$). Similarly, Ekabutret al. (2019) found that a 5% (w/v) amount of mangosteen extracts were coated on PP MB and some increase in fiber diameters were observed [20]. Jung et al. (2013) also produced an antibacterial filter and sophora extract (*Sophora flavescens*) was loaded on polyurethane filters having 10-20 mm via electrospaying method [21].

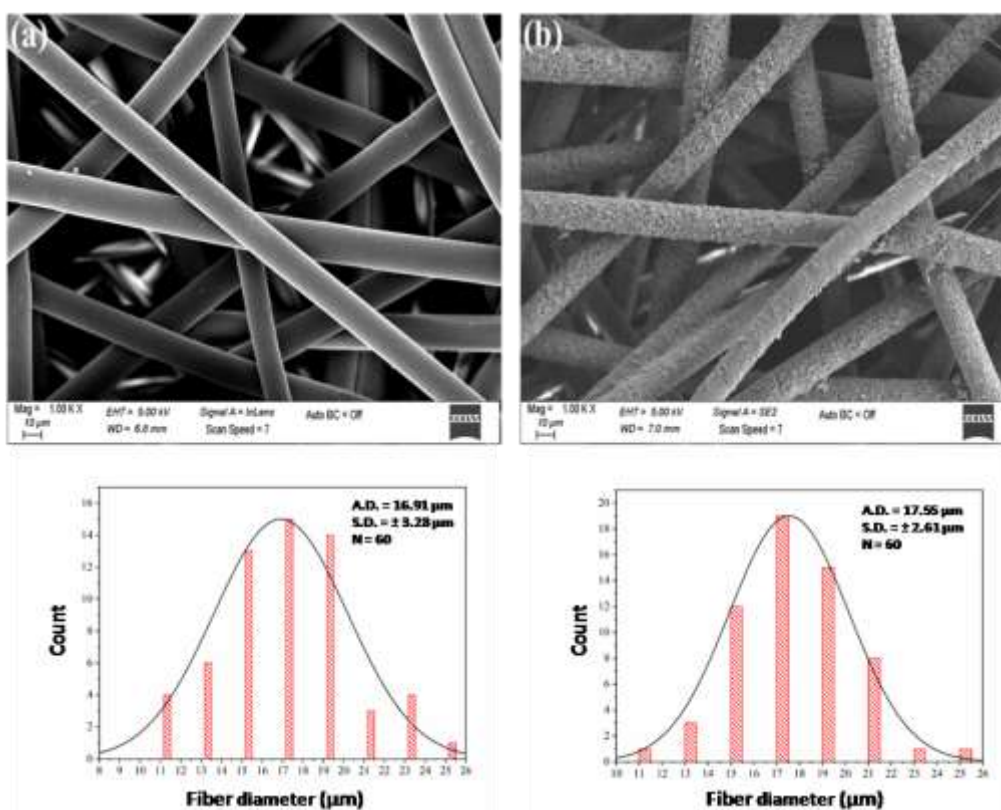


Figure 3. SEM images of non-wovens (a) PET SPB (b) PET SPB-sFA (Magnification 1.00 kX, scale bar : 10 μm).

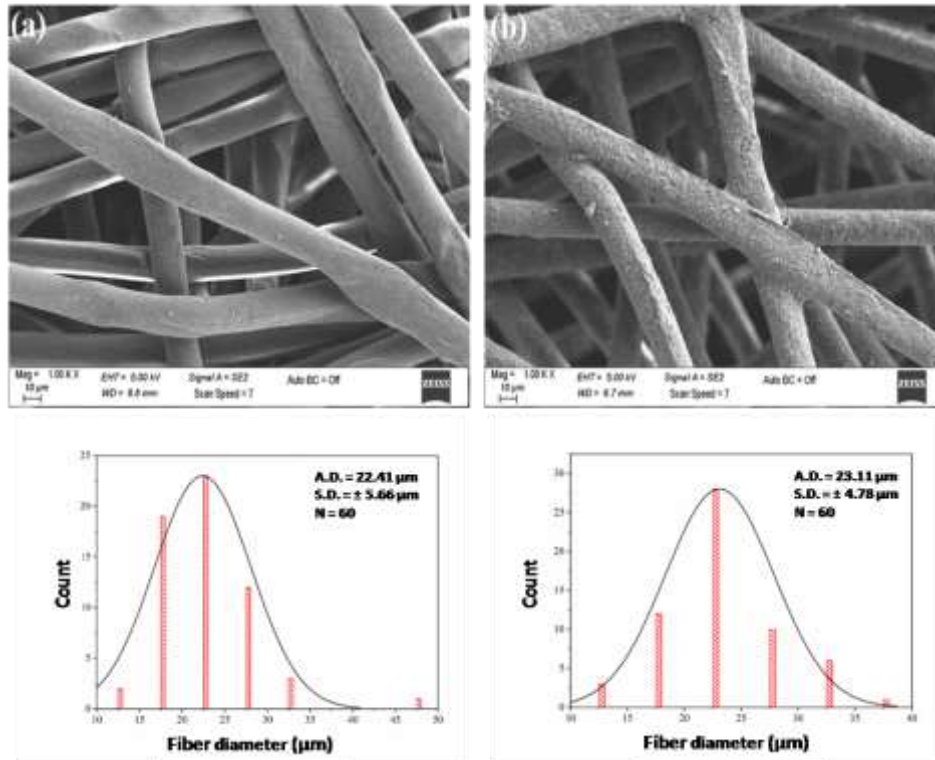


Figure 4. SEM images of non-wovens (a) PP SPB (b) PP SPB-sFA (Magnification 1.00 kX, scale bar : 10 μm).

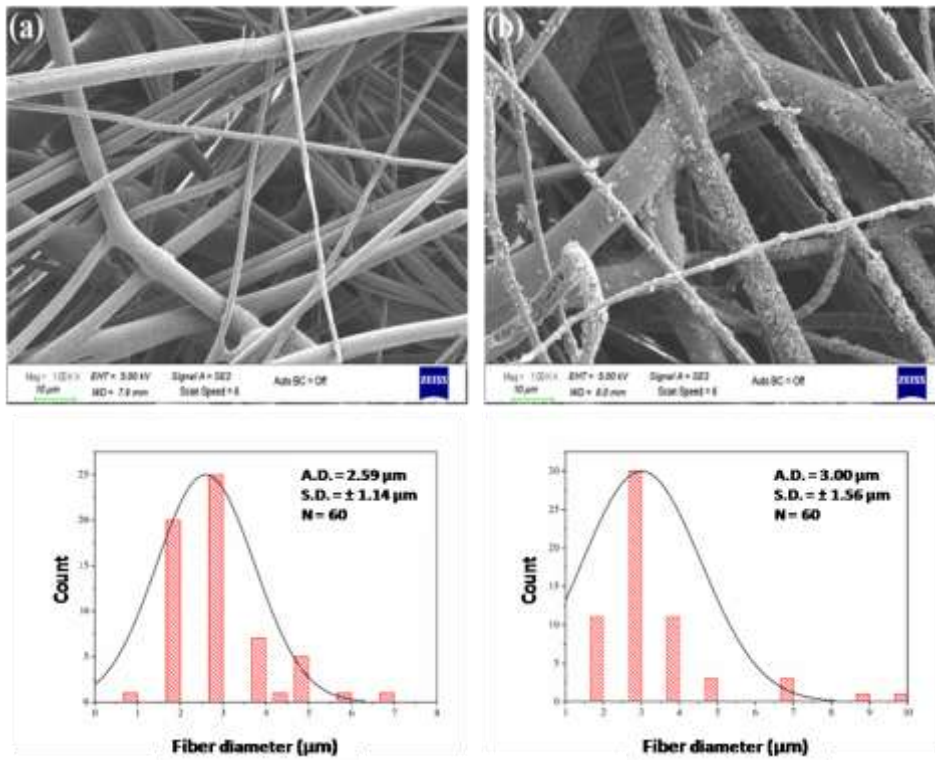


Figure 5. SEM images of non-wovens (a) PP MB (b) PP MB-sFA (Magnification 1.00 kX, scale bar : 10 μm).

3.2. Physical Structural Analysis

FT-IR spectra of the pure non-woven surfaces and resulting FA-loaded nonwovens produced as a result of the electrospaying process are shown in Figure 6. The characteristic peaks of PET SPB show at 1712 cm^{-1} (-C=O) and benzene ring at 1615 cm^{-1} [22]. The deformation vibration of the (-CH_2) group is 1340 cm^{-1} [23]. Another absorption peak at 1240 cm^{-1} is due to the (-C-O-C) stretching vibration. Characteristic IR absorption peaks of FA are confirmed in $3500\text{-}3100\text{ cm}^{-1}$. PP-based SPB non-woven surfaces indicate asymmetric and symmetric stretching vibration peaks at 2948 , 2916 and 2836 cm^{-1} (-CH), respectively. The other peaks appear at 1455 , 1376 cm^{-1} , and 840 cm^{-1} belong to (-CH_2) bending.

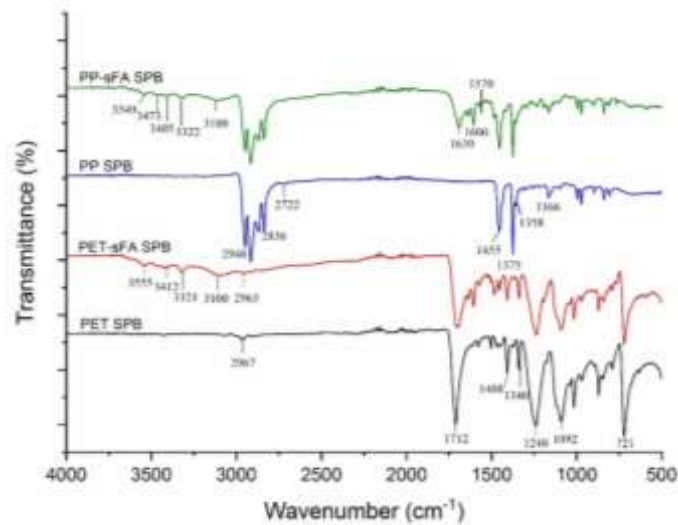


Figure 6. FT-IR spectra of non-woven surfaces.

3.3. Contact Angle Analysis

Wettability is related to the surface's hydrophobicity/hydrophilicity properties that acts an essential role to specify the wound healing management due to adhesion and cell proliferation between matrix/material and cells. Previous studies have suggested that the hydrophilicity of biomaterials is necessary for the cell healing process. However, these hydrophilic-based wound dressings can damage the wound and lead to secondary bleeding. Moreover, many studies have been reported hydrophobic surfaces inhibit bacterial adhesion [24].

The results of the contact angle measurements for water are given in Figure 8. According to the results, all NW surfaces have hydrophobic structure due to contact angle $> 90^\circ$. For all FA-sprayed surfaces, loading of FA with hydrophilic structured on NWs reduced contact angle values. The measurements for water on PET SPB-sFA and PP MB-sFA were slightly similar, which were $102.6 \pm 4.1^\circ$ and $102.5 \pm 4^\circ$ respectively.

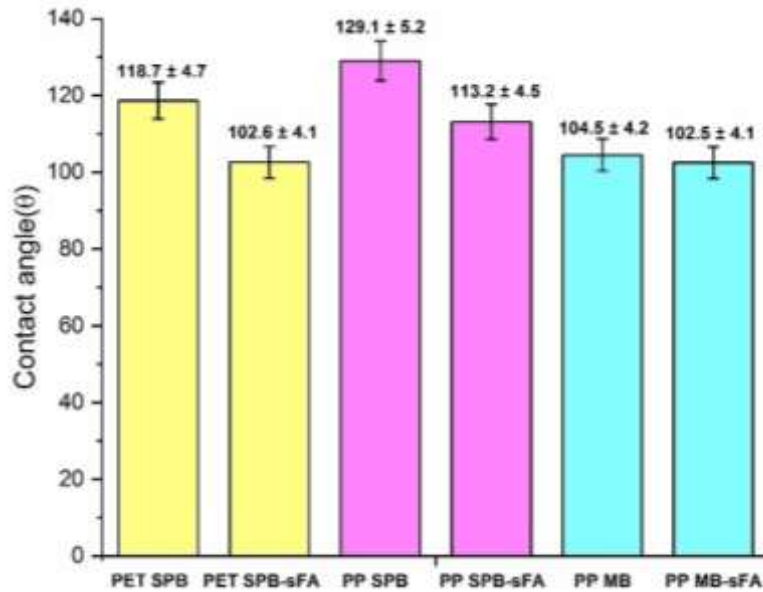


Figure 7. Contact angle values of non-woven surfaces.

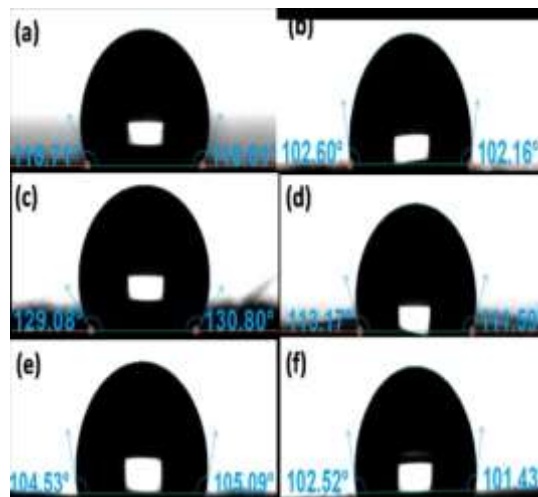


Figure 8. Contact angle images of water droplets on the surface of non-woven surfaces (a) PET SPB, (b) PET SPB-sFA, (c) PP SPB, (d) PP SPB-sFA, (e) PP MB, (f) PP MB-sFA.

3.4. Thermal Analysis

Figure 9 shows TGA thermograms for pure and FA-loaded PET and PP nonwoven (NW) surfaces. All samples showed weight loss in the range of 30-100 °C associated with moisture out of NWs. The first degradation step of pure PET SPB fabrics with two degradation steps has begun at about 380 °C. In this step, the chain scissions of the ester bonds in the structure and the vinyl ester and carboxylic acid groups began to form and ended at 525 °C [25]. The second step is dominated by low molecular weight volatile components due to the complete breakage of the ester bonds with weight loss of 17.1 % about 590 °C to 630 °C.

PET SPB-sFA showed weight loss up to 100°C related to moisture out of sample. After, the first degradation step, which started around 370 °C, was completed at around 560 °C. This step takes

longer than a pure sample to confirm the degradation of the FA. The second (last) step (590-640 °C) was related to the burning of the pyrolysis product which was formed during analysis in the N₂ atmosphere.

For both PP SPB and PP SPB-sFA NWs, single-step degradation has been observed at 350-460 °C and 350-470 °C, respectively.

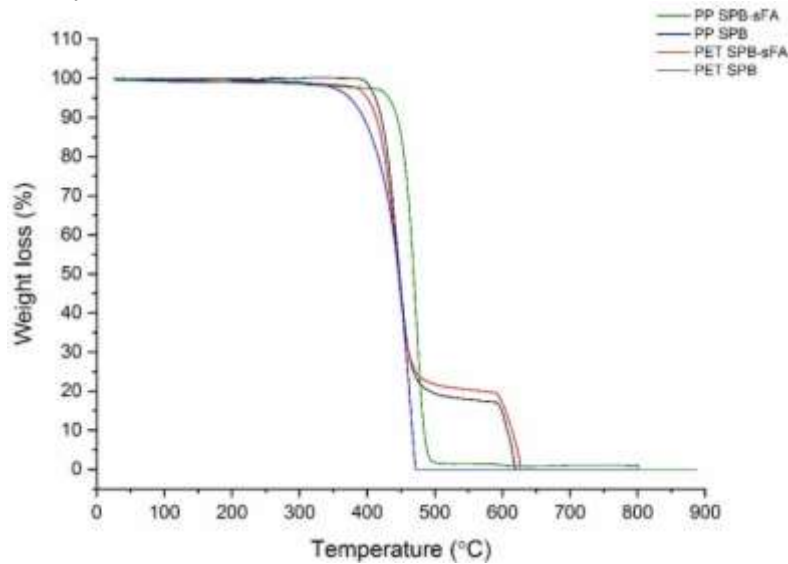


Figure 9. TGA thermograms of non-woven surfaces.

3.5. Porosity Measurements

High and low bulky non-woven fabrics have porosity values in the range of 90–99 % and 45–80 %, respectively [26, 27]. Table 1 shows the results of porosity by both the conventional method and pycnometer.

Table 1. Porosity results by pycnometer and conventional measurement.

Sample ID	Porosity by pycnometer ($1-V_t/V$)*100, (%)	Porosity by conventional measurement (%)
PET SPB	80.92	78.57
PET SPB-sFA	80.52	78.15
PP SPB	75.17	71.55
PP SPB-sFA	77.04	76.73
PP MB	81.58	81.69
PP MB-sFA	80.32	80.33

The porosity of the non-woven surfaces is depends significantly on fiber orientation [28]. The random fiber orientation is clearly observed in SEM images. Generally, FA-loaded NW surfaces have almost the same porosity as pure NWs. This is due to the fact that FA desposited onto fiber structures, and this case does not directly effect the pore structure of the NWs. Further, the porosity phenomenon parallels to the fiber thicknesses. As FA was loaded onto NWs, fiber thicknesses increased slightly. In this study, the porosity values above 71% can be sufficient to increase cell migration in wound healing compared to our previous study [6].

3.6. In-vitro Release Tests

The release study of all FA-loaded NW surfaces was carried out over a period of 8 hours in PBS media (pH 7.2) at 37 °C (Figure 10).

The release profiles show that the amount of cumulative FA releases are 22.8, 17.1, and 17.5 ppm for PET SPB-sFA, PP SPB-sFA and PP MB-sFA, respectively after 8 hours. PET SPB-sFA exhibited an initial burst release profile in the first 4 minutes of analysis while PP SPB-sFA and PP MB-sFA showed burst release in the first 20 minutes. After burst release, there was an increase in the amount of release for PET SPBs. The reason for this is that surface peeling occurs in PET SPBs in a pH 7.2 environment and can be explained by the dissolution of FA in this environment.

After sudden release, PP-based SPBs and MBs showed FA release reached a satisfaction point.

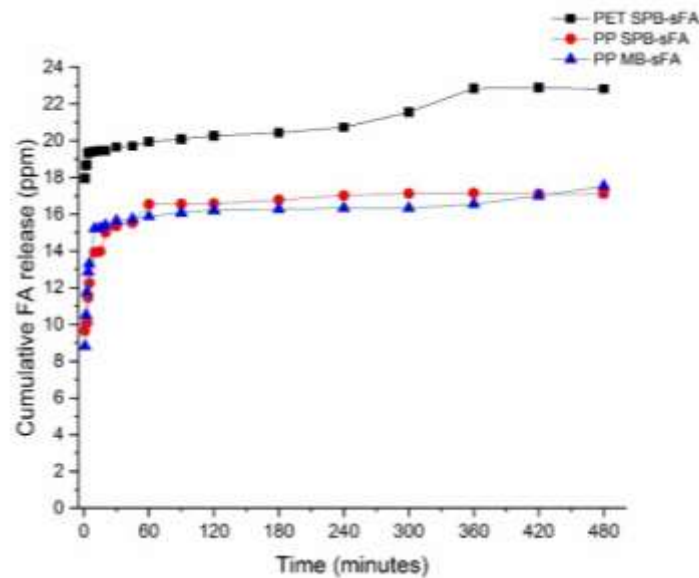


Figure 10. FA *in vitro* release profiles of NWs.

3.7. Cytotoxic Effects of NWs by MTT and NRU Assay

In this study, ISO 10993-12: 2009 standard was used for sample preparation of both references and novel NW materials. Both sides of samples arranged according to standards (3 cm² /mL) were sterilized in a laminar flow cabinet for 1 hour under a UV lamp. 30 cm² (6 cm x 5 cm) sterile samples were put in a 10 mL culture medium (RPMI 1640 containing 1 % Penicillin-Streptomycin, 10 % serum) and kept at 37 °C for 72 hours to obtain extract solutions. At the end of the extraction period, samples were removed, and extract solutions were kept at 37 °C by the time cytotoxicity tests. The cytotoxic effect of the extract solutions of NWs was evaluated by both MTT and NRU assays in L929 cells. To determine the cytotoxicity, the effects of the 100 % concentration of the original extract solutions of all reference and new NW samples on treated cells were compared with the negative control group without any chemicals. The average absorbance values and standard deviation values of living cells were calculated by averaging all the data obtained. In addition, cell viability in the control group was considered as 100 %, and living cell percentages were determined for all sample groups compared to the control. Results of the MTT and NRU tests are summarized in Figure 11. According to the results of cytotoxicity tests applied after 24 h of treatment in L929 cells, all reference and novel

NWs accept PET SPB-sFA are cytocompatible since viability did not fall below 70 %. In this study, 50 % diluted concentrations of all samples (data was not given in the figure) were also tested but there is a clear decrease in viability of cells treated with the original 100 % extract concentration of PET SPB-sFA and cell death is concentration depended.

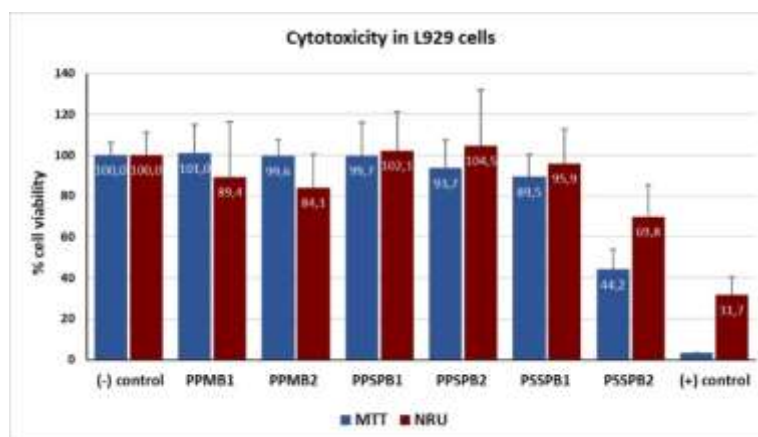


Figure 11. Effects of NW surfaces on cell viability of L929 cells by MTT and NRU assays.

It is important to evaluate the cytotoxic activity of novel biomaterials as a part of ISO 10993 protocols in terms of biocompatibility. In recent years, many methods have been developed to investigate cell viability and proliferation in cell culture. The most widely used of these are cytotoxicity assessments in 96-well plates which many samples can be analyzed quickly and easily in terms of cell viability [29]. In this study, cytocompatibility was determined with 3-(4,5-dimethylthiazol-2-yl)-2,5-diphenyl tetrazolium bromide (MTT) and neutral red uptake (NRU) cytotoxicity tests. MTT and NRU cytotoxicity assays are suitable biomarkers for evaluating live/death cell counts and the proliferation of cells based on mitochondrial and lysosomal functions [30]. In the general reduction of cell viability by more than 30 % is considered as a cytotoxic effect. In this study by using two different cytotoxicity assays effects of the tested materials both on mitochondrial and lysosomal functions were evaluated.

In our previous study, we tested the cytotoxic effects of FA alone with MTT and NRU assays in L929 cells and showed that this antioxidant did not cause any cytotoxic effects [6]. Moreover, we showed FA treatment caused increases in cell proliferation compared to the negative control. Our results also demonstrate that FA plays a critical role in cell growth and development, the synthesis of nucleic acids that promote wound healing.

In recent years, many wound dressings containing different additives have been produced and tested for cytotoxicity similar to our study. Arslan et al. (2014) fabricated fibrous mats via electrospinning from solutions of polyethylene terephthalate (PET), PET/chitosan, and PET/honey at different concentrations. They evaluated the cytotoxicity of fibers by MTT and reported no cytotoxic activity. In this study after exposure to the various dilutions of extract (25, 50, and 100 %), the proliferation of L929 cells was measured and cell death and morphological damage were not observed throughout the incubation period [31]. In another study, Abouzekry et al. (2020) developed nanofibrous wound dressing by electrospinning using bee venom and pomegranate peel extract in combination with polyvinyl alcohol. According to the cytotoxicity testes on L929 cells, manufactured fibrous dressing has no cytotoxic effects [32]. Charernsriwilaiwat et al. (2012) also developed fibrous mats by electrospinning of a mixture of chitosan-ethylene diamine tetraacetic acid (CS-EDTA) (30/70 w/w), polyvinyl alcohol (PVA) solution (10 wt %), and lysozyme for wound healing. Results of the cytotoxicity tests, CS-EDTA/PVA nanofibers with or without lysozyme were nontoxic at 1–10 mg /

mL concentrations [33]. Kalalinia et al. (2021) produced vancomycin (VCM)-loaded hybrid chitosan/polyethylene oxide (CH/PEO) nanofibers via blend-electrospinning. According to the results of the Alamar Blue cytotoxicity testes on HDFs, there were no cytotoxic effects of any groups [34]. Bayat et al. (2019) developed nanofibers that were Bromelain-loaded chitosan for burn wounds repair. Cytotoxic activity of Ch-2 % and 4 % w/v Br were tested with Alamar Blue assay. Although there are no cytotoxic effects of chitosan, Ch-2 % w/v Br, and bromelain nanofibers, crosslinked Ch-4 % w/v Br had a cytotoxic effect when compared to the control group [35]. Merrell et al. (2009) fabricated curcumin-loaded poly(caprolactone) (PCL) nanofibers by electrospinning. They directly loaded Human foreskin fibroblast cells (HFF-1) on curcumin-loaded PCL nanofibers and reported that more than 70 % of cells were viable on nanofibers [36].

4. CONCLUSIONS

In this study, FA was successfully electrospayed onto non-wovens surfaces. In the FT-IR analysis of the resulting materials, characteristic peaks of FA have been observed. The surface roughness of the NWs was investigated by SEM. Further, the wettability studies demonstrated electrospaying process reduces hydrophobicity. In-vitro release test showed a fast release profile of FA from the surfaces. According to NRU test results, PP SPB-sFA surfaces indicated the best cell viability value. Our findings showed FA-loaded NWs can be good candidates for wound care applications.

ACKNOWLEDGEMENTS

This study was supported by Bursa Technical University Scientific Research Projects Coordination Unit (SRP Project No. 190D003).

The authors would like to thank Mogul Textile Company or their kind donation of spun-bond and melt-blown non-woven fabrics and Bursa Technical University Central Research Laboratory (Bursa, Turkey) for the SEM and TGA analysis. The authors would like to thank Cantekin Kaykılarlı, and Metallurgical and Materials Engineering Department for pycnometer test.

CONFLICT OF INTEREST

The authors stated that there are no conflicts of interest regarding the publication of this article.

REFERENCES

- [1] Hu MS, Maan ZN, Wu JC, Rennert RC, Hong WX. Tissue Engineering and Regenerative Repair in Wound Healing, *Annals of Biomedical Engineering*, 2014; 42: 1494-1507.
- [2] Pakdemirli A, Toksöz F, Karadağ A, Mısırlıoğlu HK, Başbınar Y, Ellidokuz H, Açıkgöz O. Role of Mesenchymal Stem Cell-Derived Soluble Factors and Folic Acid in Wound Healing. *Turk J Med Sci*, 2019; 49: 914-921.
- [3] Ammar HO, Ghorab MM, Mostafa DM, Ibrahim ES. Folic Acid Loaded Lipid Nanocarriers with Promoted Skin Antiaging and Antioxidant Efficacy, *Journal of Drug Delivery Science and Technology*, 2016; 31: 72-82.
- [4] Jiao Z, Wang X, Yin Y, Xia J, Mei Y. Preparation and Evaluation of a Chitosan-Coated Antioxidant Liposome Containing Vitamin C and Folic Acid. *Journal of Microencapsulation*, 2018; 35(3): 272-280.

- [5] Duman N, Duman R, Tosun M, Akıncı M, Göksel E, Gökçe B, Alagöz O. Topical Folic Acid Enhances Wound Healing in Rat Model *Advances in Medical Sciences*, 2018; 63(2): 347-352.
- [6] Parın FN, Aydemir İnci Ç, Taner G, Yıldırım K. Co-Electrospun-Electrosprayed PVA/Folic Acid Nanofibers for Transdermal Drug Delivery: Preparation, Characterization, and in vitro Cytocompatibility. *Journal of Industrial Textiles*, 2021; Doi: 10.1177/1528083721997185.
- [7] Pagano C, Perioli L, Latterini L, Nocchetti M, Ceccarini MR, Marani M, Ramella D, Ricci M. Folic Acid-Layered Double Hydroxides Hybrids in Skin Formulations: Technological, Photochemical and in vitro Cytotoxicity on Human Keratinocytes and Fibroblasts. *Applied Clay Science*, 2019; 168: 382-395.
- [8] Zhao M, Zhou J, Chen Y, Yuan L, Yuan M, Zhang X, Hu Y, Yu H. Folic Acid Promotes Wound Healing in Diabetic Mice by Suppression of Oxidative Stress, *J Nutr Sci Vitamin*, 2018; 64(1): 26-33.
- [9] Khan S, Rahman SZ, Ahad A. Local Drug Delivery of Folic Acid Promotes Oral Mucosal Wound Healing. *Journal of Dental Sciences*, 2021; 16(1): 532-533.
- [10] Camacho DH, Uy SJY, Cabrera MJF, Lobregas MOS, Fajardo TJMC. Encapsulation of Folic Acid in Copper-Alginate Hydrogels and It's Slow in vitro Release in Physiological pH Condition. *Food Research International*, 2019; 119: 15-22.
- [11] Mallakpour S, Hatami M. Highly Capable and Cost-Effective Chitosan Nanocomposite Films Containing Folic Acid-Functionalized Layered Double Hydroxide and Their in Vitro Bioactivity Performance. *Materials Chemistry and Physics* 2020; 250: 123044.
- [12] Acevedo-Fani A, Soliva-Fortuny R, Martín-Belloso O. Photo-protection and Controlled Release of Folic Acid using Edible Alginate/Chitosan Nanolaminates. *Journal of Food Engineering*, 2018; 229: 72-82
- [13] Fonseca LM, Crizela RL, Silvaa FT, VazFontesa MR, Zavarezea ER, Guerra Dias AR. Starch Nanofibers as Vehicles for Folic Acid Supplementation: Thermal Treatment, UVA Irradiation, and in vitro Simulation of Digestion, *Journal of the Science of Food and Agriculture*, 2020; <https://doi.org/10.1002/jsfa.10809>.
- [14] Şimşek M, Rzayev ZMO, Bunyatova U, Khalilova S, Türk M. Multifunctional Electrospun Biocompatible Nanofiber Composites from Water Dispersion Blends of Folic Acid Conjugated PVP/Dextran/ODA-MMT Nanocomposites and Their Responses to Vero cells. *Hacettepe Journal of Biology and Chemistry*, 2016; 44(4): 441-450.
- [15] Bock N, Dargaville TR, Woodruff MA. Electrospaying of Polymers with Therapeutic Molecules: State of The Art, *Progress in Polymer Science*, 2012; 37: 1510-1551.

- [16] He L, Zhao Y, Tian L, Ramakrishna S. Nanobiomaterials: Classification, Fabrication and Biomedical Applications. I, Wang, M. Ramalingam, X. Kong, L. Zhao (Eds.), Electrospinning and Electrospinning for Nanobiomaterial Fabrication, 2017; (1st ed., Vol. 6, pp.143-163). New York : Wiley-VCH.
- [17] Alehosseini A, Ghorani B, Sarabi-Jamab M, Tucker N. Principles of electrospaying: A New Approach in Protection of Bioactive Compounds in Foods. *Critical Reviews in Food Science and Nutrition*, 2017; 58(14): 2346-2363.
- [18] Madhaiyan K, Sridhar R, Sundarrajan S, Venugopal JR, Ramakrishna S. Vitamin B12 Loaded Polycaprolactone Nanofibers: A Novel Transdermal Route for The Water Soluble Energy Supplement Delivery. *International Journal of Pharmaceutics*, 2013; 444(1-2): 70-76.
- [19] Parın FN, Yıldırım K. Preparation and Characterization of Vitamin Loaded Electrospun Nanofibers as Promising Transdermal Patches. *Fibres & Textiles in Eastern Europe*, 2021; 1(145): 17-25.
- [20] Ekabutr P, Chuysinuan P, Suksamrarn S, Sukhumsirichart W, Hongmanee P, Supaphol P. Development of Antituberculosis Melt-blown Polypropylene Filters Coated with Mangosteen Extracts for Medical Face Mask Applications. *Polymer Bulletin*, 2019; 76: 1985-2004.
- [21] Jung JH, Lee JE, Bae G. Use of Electrospayed Sophora Flavescens Natural-Product Nanoparticles for Antimicrobial air Filtration. *Journal of Aerosol Science*, 2013; 57: 185-193.
- [22] Xiao X, Chen F, Wei Q, Wu N. Surface Modification of Polyester Nonwoven Fabrics by Al₂O₃ Sol-gel Coating, *Journal of Coatings Technology and Research*, 2009; 6(4): 537-541.
- [23] Alma MH, Yazıcı M, Yıldırım B, Salan, T, Tiyek İ. Spunbond Dokusuz Tekstil Yüzeyi Üzerine Elektro Çekim Yöntemi ile Nano Boyutta Grafen Kaplanması ve Karakterizasyonu. *Tekstil ve Mühendis*, 2017; 24(108): 243-253.
- [24] Delaviz Y, Santerre JP, Cvitkovitch DG. Infection Resistant Biomaterials, *Biomaterials and Medical Device-Associated Infections*, 2015; 11: 223-254.
- [25] Berendjchi A, Ali R, Yousefi A, Yazdanshenas ME. Surface Characteristics of Coated Polyester Fabric with Reduced Graphene Oxide and Polypyrrole, *Applied Surface Science*, 2016; 367: 36-42.
- [26] Ma ZW, Kotaki M, Yong T, He W, Ramakrishna S. Surface Engineering of Electrospun Polyethylene Terephthalate (PET) Nanofibers Towards Development of a New Material For Blood Vessel Engineering. *Biomaterials*, 2005; 26: 2527-2536.

- [27] Sreedhara SS, Tata NR. A Novel Method for Measurement of Porosity in Nanofiber Mat using Pycnometer in Filtration. *Journal of Engineered Fibers and Fabrics*, 2013; 8(4).
- [28] Gültekin E, Çelik Hİ, Nohut, S, Elma SK. Predicting Air Permeability and Porosity of Nonwovens with Image Processing and Artificial Intelligence Methods. *The Journal of the Textile Institute*, 2020; 111(11): 1641-1651.
- [29] Weyermann J, Lochmann, D, Zimmer A. A Practical note on The use of Cytotoxicity Assays. *International Journal of Pharmaceutics*, 2005; 288 (2): 369-376.
- [30] Melo PS, de Medeiros Cavalcante HM, Barbosa-Filho JM, de Fátima Formiga Melo Diniz M, de Medeiros IA, Haun M. Warifteine and Milonine, Alkaloids Isolated from *Cissamppe Lossympodialis Eichl*: Cytotoxicity on Rat hepatocyte Culture and in V79 Cells. *Toxicology Letters*, 2003; 142 (1-2):143-151.
- [31] Arslan A, Şimşek M, Aldemir SD, Kazaroğlu NM, Gümüşderelioğlu, M. Honey-Based PET or PET/Chitosan Fibrous Wound Dressings: Effect of Honey on Electrospinning Process. *Journal of Biomaterials Science, Polymer Edition*, 2014; 25(10): 999-1012.
- [32] Abouzekry S, Abdellatif A, Azzazy Hassan. Fabrication of Pomegranate/Honey Nanofibers for use As Antibacterial Wound Dressings. *Wound Medicine*, 2020; 28: 100181.
- [33] Charernsriwilaiwat N, Opanasopit P, Rojanarata T, Ngawhirunpat T. Lysozyme-Loaded, Electrospun Chitosan-Based Nanofiber Mats for Wound Healing. *International Journal of Pharmaceutics*, 2012; 427(2): 379–384.
- [34] Kalalinia F, Taherzadeh Z, Jirofti N, Amiri N, Foroghinia N, Beheshti M, Fazly B, Bibi S, Hashemi M, Shahroudi A, Pishavar E, Tabassi S, Movaffagh J. Evaluation of Wound Healing Efficiency of Vancomycin-Loaded Electrospun Chitosan/Poly Ethylene Oxide Nanofibers in Full Thickness Wound Model of Rat. *International Journal of Biological Macromolecules*, 2021; 177. 10.1016/j.ijbiomac.2021.01.209.
- [35] Bayat S, Amiri N, Pishavar E, Kalalinia F, Movaffagh J, Hahsemi M. Bromelain-Loaded Chitosan Nanofibers Prepared by Electrospinning Method for Burn Wound Healing in Animal Models. *Life Sciences*, 2019; 229. 10.1016/j.lfs.2019.05.028.
- [36] Merrell JG, McLaughlin SW, Tie L, Laurencin CT, Chen AF, Nair LS. Curcumin-loaded poly(epsilon-caprolactone) nanofibres: diabetic wound dressing with antioxidant and anti-inflammatory properties. *Clinical and experimental pharmacology & Physiology*, 2009; 36(12): 1149–1156.



INVESTIGATION OF 3D CULTURE OF HUMAN ADIPOSE TISSUE-DERIVED MESENCHYMAL STEM CELLS IN A MICROFLUIDIC PLATFORM

Ceren ÖZEL^{1,3} , Yücel KOÇ^{2,3} , Ahmet Emin TOPAL³ , Aliakbar EBRAHIMI^{3,7} 
Tayfun ŞENGEL^{1,6} , Hamed GHORBANPOOR^{3,4} , Fatma DOĞAN GÜZEL⁵ ,
Onur UYSAL^{1,3} , Ayla EKER SARIBOYACI^{1,3} , Hüseyin AVCI^{1,3,7,8*} 

¹ Department of Stem Cell, Institute of Health Sciences, Eskişehir Osmangazi University, Eskişehir, Turkey

² Department of Chemical Engineering, Eskişehir Osmangazi University, Eskişehir, Turkey

³ Cellular Therapy and Stem Cell Production Application and Research Center (ESTEM), Eskişehir Osmangazi University, Eskişehir, Turkey

⁴ Department of Biomedical Engineering, Eskişehir Osmangazi University, Eskişehir, Turkey

⁵ Department of Biomedical Engineering, Ankara Yıldırım Beyazıt University, Ankara, Turkey

⁶ Central Research Laboratory Research and Application Center (ARUM), Eskişehir Osmangazi University, Eskişehir, Turkey

⁷ Department of Metallurgical and Materials Engineering, Eskişehir Osmangazi University Eskişehir, Turkey.

⁸ Translational Medicine Research and Clinical Center (TATUM), Eskişehir Osmangazi University, Eskişehir, Turkey

ABSTRACT

Mesenchymal stem cells (MSCs) are multipotent stem cells that can support various tissues including bone marrow, adipose tissue, and synovial fluids, from which they can be readily isolated. The objective of this study is to harness the advantages of microfluidic systems for controlling and enhancing the maintenance and viability, and regenerative properties of MSCs by providing a 3D culture microenvironment with gelatin methacrylate (GelMA) hydrogel and exposing the cells to a slow fluid flow and low shear stress conditions. GelMA has methacryloyl groups and can be crosslinked by a photocuring process using biocompatible photoinitiators. The most common used photoinitiator for cellular encapsulation within hydrogels is the ultraviolet (UV) initiator 2-hydroxy-4'-(2-hydroxyethoxy)-2-methylpropiophenone (Irgacure 2959 or I2959), but due to its low water solubility and the necessity of using a shorter wavelength light (365 nm), it can lead to cellular phototoxic and genotoxic effects. To overcome these limitations, lithium phenyl-2,4,6-trimethylbenzoylphosphinate (LAP) have recently been used with GelMA as an alternative photoinitiator. Because LAP is highly water soluble and has a 10 times faster polymerization rate, and it requires a visible light ($\lambda = 405$ nm) which makes it much safer for the cells, we use 10% GelMA together with 0.05% LAP photoinitiator for bioprinting human adipose tissue derived MSCs (hAT-MSCs) onto a membrane that has a 40 μ m mesh size. To demonstrate a microfluidic culture advancement for improving the biological activities and regenerative capacity of the cells including cell adhesion, growth, viability and proliferation capacity as ultimate goals of this study, the membrane carrying the bioprinted construct was placed in a PDMS microchannel and exposed to the fluid to obtain dynamic microenvironments found in the human body. As a result, the cells were successfully maintained in the microfluidic 3D cell culture for two days, with a high cell viability of 99%.

Keywords: MSCs, Organ on a chip, GelMA, 3D cell culture, Cell adhesion

1. INTRODUCTION

Organ-on-a-chip (also called organ chip or OoC) is a miniaturized bioreactor technology in a microfluidic cell culture device which reconstitutes the physiology and architecture of a notable functional unit of a specific organ of interest [1-6]. Organ chip technology is a cost-effective approach for the study of disease and treatment and has a potential for predicting drug-induced organ-specific responses and reducing the use of animal experimentation. Organoids are three-dimensional cell culture models composed of either natural extracellular matrix (ECM) molecules or biomaterials interacting with organ-specific cells that self-organize into their peculiar physiology and anatomy and mimic an

*Corresponding Author: havci@ogu.edu.tr

Received: 18.08.2021 Published: 30.11.2021

associated organ *in vivo* [2,7-9]. Organoids typically contain stem cells, though not necessarily, as they can be comprised of some primary cells or differentiated cells. Biomimetic platforms of many organs including the lung, liver, small intestine, kidney, and some other tissues like bone marrow and blood-brain barrier can be designed and studied as organ chips [1]. Studies of drug development and disease, and cosmetic pipelines will likely involve organ-on-a-chip technology soon.

Mesenchymal stem cells, or also called mesenchymal stromal cells (MSCs) are multipotent stem cells that can be isolated from many tissues/organs including bone marrow, adipose tissue, dental pulp, and amniotic or synovial fluids [10]. MSCs are unique cells for regenerative medicine that can support functions of many tissues and organs by releasing soluble factors such as growth factors, anti-apoptotic and anti-inflammation factors, and they can synthesize extracellular matrix (ECM) mainly composed of collagen fibrils, a key component of tissues [11]. Stem cell differentiation is known to be governed by a variety of soluble factors including growth factors, hormones and cytokines whereas numerous studies performed in recent decades point out that in addition to chemical factors, mechanical cues can also have remarkable roles on cellular differentiation, proliferation, biomechanical properties and tissue development. Likewise, MSCs have been shown to be highly responsive to extracellular mechanical cues [12-15], including responses to different magnitudes of shear stresses [16,17]. For instance, Riddle *et al.* uses parallel plate flow chambers to test the effects of high shear stress on human MSCs and report that oscillatory fluid flow-induced shear stress with high flow rates (*i.e.* 1-50 ml/min flow rates) resulted with increased cell proliferation due to a high shear stress-induced increase in intracellular calcium concentration [18]. On the contrary, high magnitude shears stresses above 10 mPa levels can exert damage on rat MSCs and lead to cell detachments and reduced proliferation [19]. Slow fluid flow and low shear stresses at flow rates ranging from few microliters up to hundreds of microliters per min upregulate osteogenic differentiation and proliferation of MSCs in microfluidic devices [20-22]. As such, shear stresses and interstitial fluid flow can influence and regulate the cellular behavior of MSCs. Furthermore, by using microfluidic devices, how interstitial fluid flow influences the MSC viability and differentiation in the presence of 3D cultures can be investigated in microchannels as well.

Photo-crosslinking is a chemical crosslinking method performed by photoinitiation followed by photocuring in bioprinting, and photocurable biomaterials such as gelatin-methacrylate (GelMA) are frequently used as bio-ink material in a bioprinting process. To induce chemical cross-linking of bio-ink right after the printing process, the construct is exposed to light (UV or visible light) in a way that stiffens enough but does not cause any major damage on the cells [23]. 2-hydroxy-4'-(2-hydroxyethoxy)-2-methylpropiophenone (Irgacure 2959), as a most common UV photoinitiator used for cellular encapsulation within hydrogels, has low water solubility, and needs a shorter wavelength of UV light (365 nm) that can cause cellular phototoxic and genotoxic effects in cells. However, recent studies show that lithium phenyl-2,4,6-trimethylbenzoylphosphinate (LAP), as an alternative photoinitiator, can be used to overcome Irgacure limitations. LAP has high water solubility and a 10 times faster polymerization rate than Irgacure. Also, in comparison with Irgacure, LAP needs a higher wavelength of visible light ($\lambda = 405$ nm) for photoinitiation, that is much safer for cells [24-26]. GelMA has been used together with MSCs in recent bioprinting studies whereby tissue regeneration ended up with providing enhanced regenerative properties such as high cell viability, and improved cell adhesion and proliferation [27]. In a recent report, human bone marrow-derived MSC-laden GelMA constructs ended up having larger MSC spreading area and a high cell viability of 90% [28]. In the literature, only a few studies like Miri *et al.* investigate GelMA encapsulated MSCs as a bio-ink in microfluidic culture setups and organ chip studies [29]. As such, MSCs seeded in a 3D matrix of GelMA have not been thoroughly investigated in microchannels under, for instance, fluid flow with low shear stress conditions.

In this study, human adipose tissue-derived mesenchymal stem cells (hAT-MSCs) encapsulated with photo-cross-linkable GelMA hydrogel were used as bio-ink to fabricate a construct for performing 3D

cell culture in a PDMS-based microfluidic channel. The GelMA/hAT-MSCs construct was bioprinted on a membrane which was later cut into a small piece with an appropriate size before transferring from Petri dish to the microfluidic device. The cells were cultured under low shear stress conditions for two days and the viability of the cells was determined by live/dead assay.

2. EXPERIMENTAL

2.1. Production of the Microfluidic Chip

The microfluidic (MF) chip template was prepared using a 3D printer. SLA/DLP 3D printing technology (micraft 100) was used to fabricate of mold with resolution 30-35 micron and velocity 30 sec per layer. OOkuma FP60 resin was applied to prepare the mold. The mold inside area was 39×46×5 mm. Then, PDMS (Sylgard 184 silicon elastomer base and Sylgard 184 silicon elastomer curing agent, Dow Corning, USA) layer was prepared using the soft lithography method [30]. In this study we used the low molecular weight Sylgard™ 184 PDMS polymer (Component A: $M_n = 5.8 \times 10^3$ Da; Component B: $M_n = 7.5 \times 10^3$ Da) [31]. For this, 5.85 g (1.00 mmol) of PDMS (component A) and 0.65 g (0.087 mmol) of crosslinker (Component B) was used for preparation of upper and bottom PDMS microchannels. The mixture of PDMS and crosslinker (9:1) was prepared by stirring for up to 3 min and added to molds and vacuumed in the desiccator for 20 min [32,33]. It was then left to stand at 50 °C overnight, and then the microfluidic chip was prepared by peeling off the PDMS layer. On a PDMS layer, there is a microchannel and the input with output of the channel (top layer). The length of the channels is 15 cm, the width is 1000 μm and the height of the channel is 1000 μm . The other PDMS layer consists of a flat surface without a microchannel (bottom layer). A porous polyethylene terephthalate (PET) membrane with 40 μm pore size (pluriStrainer® pluriSelect, Leipzig, Germany) was used as a membrane. Cells were bioprinted onto the membrane which was later placed between two PDMS layers. Finally, the chip was sandwiched between poly (methyl methacrylate) (PMMA) frames and fastened by screws. Figure 1 shows a schematic view and a final version image of the microfluidic device.

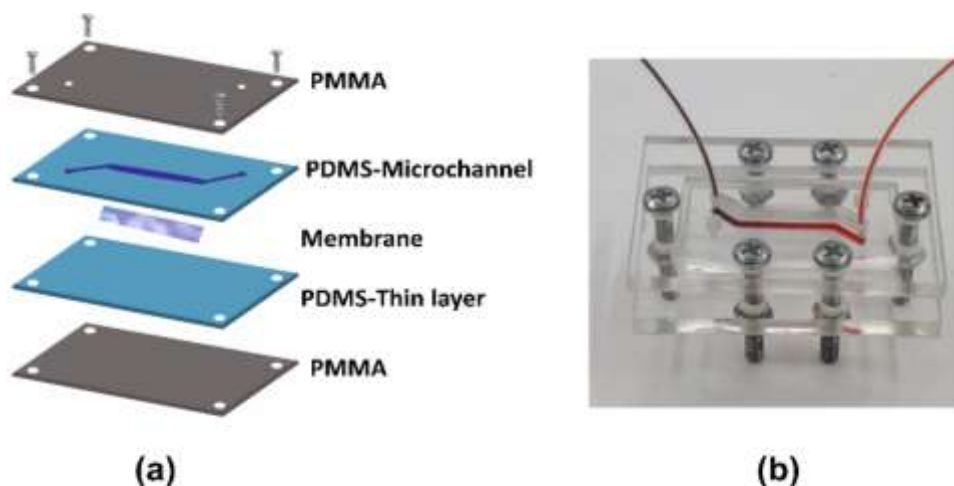


Figure 1. (a) Schematic view and (b) final version image of microfluidic cell culture device.

2.2. Isolation, Culture, and Characterization of MSCs

Human adipose tissue-derived mesenchymal stem cells (hAT-MSCs) were isolated by surgical removal from healthy donors undergoing surgical operation. Tissue samples were harvested from the informed/consented healthy patients under Eskişehir Osmangazi University Clinical Research Ethics Committee permission (Decision number: 23/Date 30.05.2019). Tissue samples were washed several times with Hanks' balanced salt solution (HBSS) with 5% penicillin-streptomycin and without calcium and magnesium. After the washing process, tissues were minced into small blocks and a single cell suspension of adipose tissue cells was obtained by using enzymatic digestion (0.075% type I collagenase, Sigma), and mechanically with shaker water bath 37 °C for approximately 60 min. The cell suspensions were filtered using a 70 µm cell strainer to separate individual cells from debris and undigested adipose tissue fragments. hAT-MSCs were cultured and characterized as in previously described protocols depending *in vitro* differentiation experiments and immunophenotyping by flow cytometry [34].

2.3. On-chip Experiments

MSCs were mixed with 10% (w/v) gelatin methacrylate (GelMA) and 0.05% (w/v) lithium phenyl-2,4,6-trimethylbenzoylphosphinate (LAP) photoinitiator (CELLINK, Sweden). This pre-polymer/MSCs blend was bioprinted by micropipette extrusion on the membrane before the chip was assembled. Due to its biocompatibility, GelMA was selected as hydrogel biomaterial to be used in the microfluidic chip [35]. The cells encapsulated within GelMA bioprinted on the membrane and then statically cultured in a 6-well polystyrene plate for 2 days in a cell culture incubator (Panasonic). After cell proliferation was observed on GelMA at the end of day 2, the membrane coated with GelMA/MSCs was integrated into the microfluidic chip as shown in Figure 1a and 2f, and the cells were grown in another incubator (Esco Lifesciences Group) for 2 days under the dynamic culture conditions. Syringe pump (NE-4000, New Era Pump Systems Inc., NY) was used with a flow rate of 0.5 µl/min to inject the culture medium through Tygon tubing into the microchip placed in the incubator. Waste culture medium was collected from the outlet of microchip in a 15 ml falcon tube inside the incubator. 37 °C with 5% CO₂ gas supply and humid incubator conditions were used for all the experiments. Figure 2 shows the steps applied for on-chip experiments.

Shear stress is the stress created when a tangential force is acting on hAT-MSCs by laminar flow of culture media over area of cell contact with the surface of PDMS microchannel. Shear rate and shear stress can be determined by equations 1 and 2 [36].

$$\text{Shear Rate } (\gamma) = \frac{Q}{W h^2 10^4} \quad (1)$$

$$\text{Shear Stress } (\tau) = \text{Shear Rate } (\gamma) \times \text{Viscosity } (\mu) \quad (2)$$

where W is the width and h the height of the channel, μ is viscosity of culture media, and Q is the volumetric flow rate used in the microfluidic culture setup.

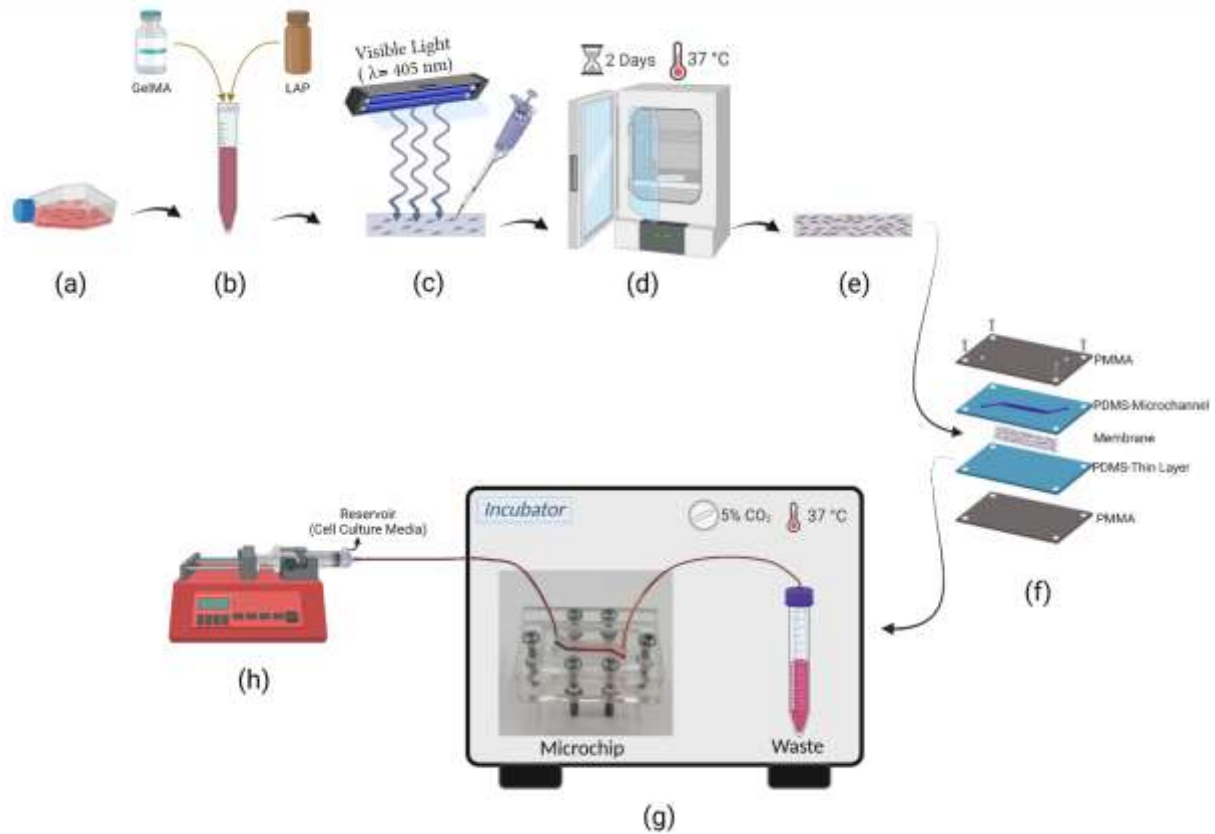


Figure 2. Schematic view of microfluidic cell culture experiment that includes (a) trypsinization, (b) mixing 10% (w/v) GelMA with MSCs, (c) GelMA/MSCs seeding on the membrane followed by photocuring (405 nm), (d) incubation of the coated membrane in a Petri dish for 2 days at 37 °C with 5% CO₂, (e) observation of cell growth, (f) schematic representative of the microfluidic culture device, (g) image of the final version microfluidic culture device shown inside the incubator and (h) a syringe attached on a syringe pump placed outside the incubator.

2.4. Live/Dead Assay

Cells were imaged with a live/dead assay to verify cell viability. To assess the viability of cultured MSCs cells within the microfluidic chip, the cells were incubated in Live/Dead (AAT Bioquest®) solution for 30 min in dark and imaged using Carl ZEISS AXIO OBSERVER D1 fluorescence microscope. The percentage of cell viability was calculated by dividing the number of live cells (green) by the total number of cells, as shown in the equation below:

$$\text{Percentage of Live Cells} = (\text{Live Cells} / \text{Total Cell Number}) \times 100 \quad (3)$$

3. RESULTS AND DISCUSSION

Stem cells are unique cells known for their self-renewal properties that ensure the preservation of the stem cell pool, while they can divide and differentiate into several cell type of tissues within the body according to their differentiation potential. This phenomenon refers to the potency (*i.e.* stem cells can be totipotent, pluripotent, multipotent, oligopotent or unipotent) [37]. MSCs are multi-potent cells that can differentiate into multiple types of cells present in specific organs. In stem cell research, it is important to maintain stem cells in undifferentiated state or controlled differentiation. The main reason for that is because stem cells are highly responsive to microenvironment alterations such as mechanical stimuli and biochemical signals that can change stem cell fate, and eventually leading to loss of potency

and stem cell identity [38]. Microfluidic technology has important potential for stem cell research. By utilizing a sophisticated microfluidic environment design, manipulation of stem cells can be controlled better than in conventional cell culture techniques. To direct the stem cell differentiation, it is crucial to know the role of various biochemical cues (*e.g.*, soluble factors including trophic factors like growth factors and hormones, and also glucose, oxygen concentrations, etc.) in the decision-making process. Microfluidic devices have been used to study microenvironment mainly by focusing on the following two aspects: screening a wide range of conditions in a high-throughput fashion and reconstructing the physiological environment like heterogeneous, complex and 3D growth conditions. By utilizing the advantages of nanotechnology like micro- and nanofabrication tools and using various biomaterials that are biocompatible and bear hydrogel properties and/nanofibrous structures and assemblies which cells like to attach and live with, many different works have been performed using stem cells in microfluidic devices containing different polymeric materials with well-defined geometries and patterns [22].

In this study, we aim to provide *in vivo* like 3D and microfluidic culture conditions for the maintenance human adipose derived-mesenchymal stem cell *in vitro*. MSCs were obtained from liposuction materials of healthy donors and cultured conventional method before using in a microfluidic bioreactor device. Afterwards, the cells were subjected separately to both 3D microfluidic culture and static control which had the same 3D culture conditions used in for encapsulation of MSCs with GelMA hydrogel and culture on a membrane. In this regard, the isolated cells from human adipose tissue adhered on the culture flasks and were successfully cultured, and as a result, most cells displayed a spindle-shaped and fibroblast-like morphology, as shown in Figure 3. The cultured cells reached a monolayer confluency in the primary culture 7 days after the first passage and were expanded until they reached passage 3 (P3). Morphology of the cells indicate that the isolated cells can attach and expand on the surface of polystyrene cell culture flasks and proliferate over subcultures.

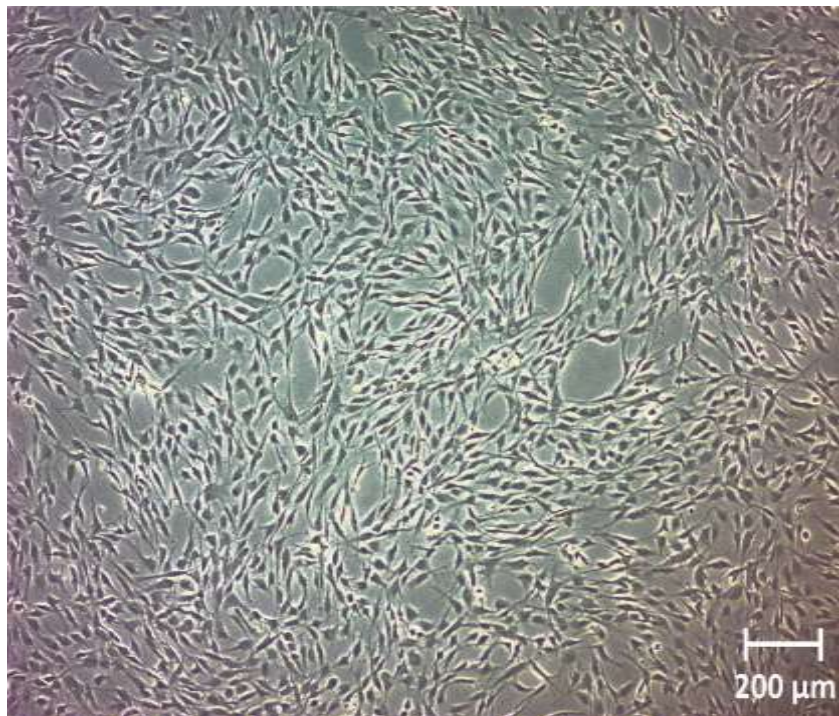


Figure 3. Phase contrast microscopy image of hAT-MSCs in a polystyrene culture dish showing the MSC morphology of the expanded cells (scale bar 200 μm).

The cells isolated from human adipose tissue adhered to polystyrene flasks (Figure 3), and flow cytometry was used to show that they were phenotypically positive for CD90, CD73, CD29, and CD105 markers but negative for CD34, CD45, MHC class II (HLA-DR) and hematopoietic lineage markers as shown in Figure 4. These results suggest that the isolated cells can be identified as MSCs, as previously described [39]. Moreover, previous works by our group showed that these cells could differentiate into chondrocytes, adipocytes, and osteoblasts [34, 40, 41].

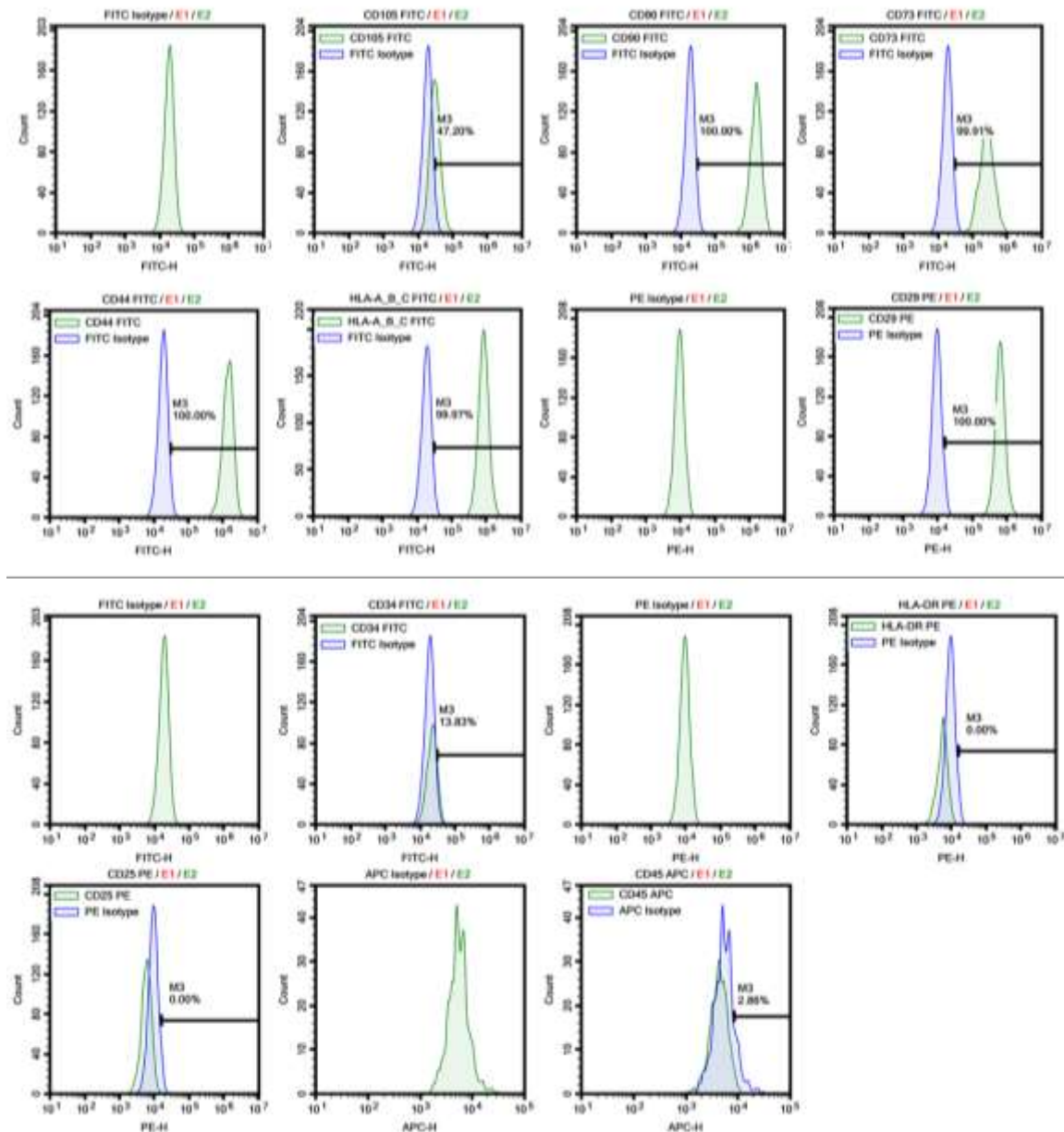


Figure 4. The immunophenotypic characterization of MSCs isolated from human adipose tissue by flow cytometry. Flow cytometry analysis of MSCs were performed at P3 (P: passage number).

MSCs were stained with calcein AM (green) within the microfluidic chip for live cells and with propidium iodide (red) for dead cells, which was followed by observing at an inverted fluorescence microscope (Zeiss Axio Observer D1), as shown in Figure 5. The microfluidic chip culture system

containing the hAT-MSCs could be maintained successfully for 2 days with approximately 99% of cell viability within 10% (w/v) GelMA. Fibroblast-like and spindle-shaped morphologies of MSCs were observed on microfluidic chip culture (Fig. 3 and 5b). On the other hand, the morphology and cytoskeletal structure of the MSCs in static culture conditions were slightly more filamentous. Cell adhesion is key to formation of morphological characteristics of cells. Thus, ECM components such as collagen and its derivatives including gelatin-based hydrogels such as GelMA can regulate cytoskeletal rearrangements, cell traction forces and shape [42,43]. Here, the GelMA/hAT-MSCs construct was bioprinted on a PET membrane with 40 μm pore size of which we considered a membrane for allowing the cells and GelMA to attach on it, and this approach could be used in future organ-on-a-chip studies. As a future experiment, cell adhesion molecules can be immunostained, cell-cell contact interactions and cell-ECM interactions between hAT-MSCs and GelMA can also be analyzed in detail. However, imaging of the MSCs directly inside the microfluidic device comes with difficulty of resolving the details of cytoskeletal structures of the cells, especially when using a typical inverted fluorescence microscope.

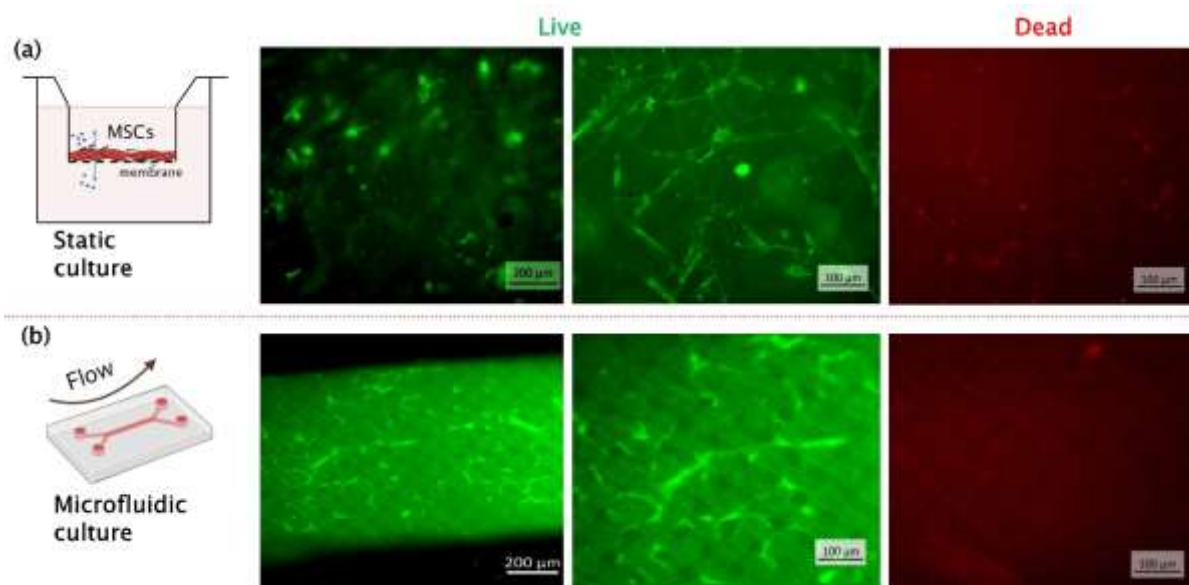


Figure 5. Live/dead assay images of static culture of MSCs on membrane under fluorescence microscope captured at the end of day 2 (a). Live/dead assay images of microfluidic chip culture MSCs on membrane under fluorescence microscope captured at the end of day 2 (b). The green mesh-like background view shows the membrane, and also microfluidic channel area of the chip on b. Scale bar of the images on the left is 200 μm , and scale bars of the images at the middle and on the right are 100 μm .

In an organism, stem cells reside in a specific anatomical location, that is called a stem cell niche, that consists of biochemical cues (*e.g.*, cytokines, proteins, growth factors, glucose, oxygen, or inorganic components like calcium, etc.), stromal and other tissue-related cells (in some cases immune cells), extracellular matrix (ECM) of which GelMA was used for mimicking in this study. Blood vessels have a regulatory role in stem cell niche, and MSCs can be found surrounding capillaries to differentiate or control other cells in response to injury or tissue homeostasis. In order to mimic vascular environment, we used a microfluidic channel and cell culture medium (DMEM) instead of blood flow.

GelMA is known to support cell attachment and viability and promote cellular differentiation of many cell types including MSCs [29,44]. Moreover, GelMA has also been reported to form well-defined bioprinted constructs that contain MSCs in addition to allowing cell viability and maintenance [29]. Here, we use a GelMA/hAT-MSCs construct bioprinted on a membrane via micropipette extrusion method followed by photocuring and then tested it in a PDMS microfluidic channel. An important aspect

of our study is that GelMA provides a physiological relevance as it consists of gelatin, that is, a baked mixture of collagenous proteins and also provides a mesh structure as an extracellular cue that the cells can respond to and like to attach. As a result of this study, the viability of the cells on GelMA in a 3D cell culture system was preserved under a fluid flow with low shear stress conditions. Moving from a static culture of GelMA-entrapped MSCs on the membrane (40 μm) to its corresponding dynamic culture setup in a microchannel under slow fluid flow (*i.e.*, with a flow rate of 0.5 $\mu\text{l}/\text{min}$) does not reduce the viability of the cells and also does not cause a dramatic change in the morphology and appearance of the cells. This result may suggest that the GelMA-entrapped hAT-MSCs under slow fluid flow and hence exposed to low shear stress can be a representative of *in vivo* conditions, and the 3D microenvironment provided to the cells here can be used to imitate a stem cell niche present in human body. Stem cells have the ability to self-renew and can stay in a quiescent state in the body and can also become active and start differentiating upon receiving a bioactive signal or a significant change in the environment. Mechanical cues can play significant roles on mesenchymal stem cell decisions to proliferate or differentiate, for example, stem cells residing on a soft matrix at subkiloPascal levels can become rounder and stay quiescent whereas an increase in the stiffness of the matrix or substrate they attach towards kiloPascal levels or more can influence the stem cell fate as human MSCs have been reported to have a tendency to choose a stiffer substrate/matrix rather than a compliant one [45].

Here we calculate the shear stress value acting on hAT-MSCs used in this study as follows: by assuming that the viscosity μ of the culture medium is 0.89 mPa·s (DMEM) as previously reported for water at room temperature and the properties have been shown to be almost identical to those for water [46]. We calculate the shear rate as 0.05 s^{-1} by using equation 1, and the magnitude of shear stress acting on hAT-MSCs as 0.0445 mPa from equation 2, as also presented in Table 1.

Table 1. The flow rate and shear stress profiles to achieve the desired shear rate and shear stress within the microchannel.

Shear Rate ($\dot{\gamma}$)	Shear Stress (τ)	Volumetric Flow Rate (Q)	Viscosity (μ)
0.05 s^{-1}	0.0445 mPa	0.5 $\mu\text{l}/\text{min}$	0.89 mPa·s

Flow-induced shear stresses that MSCs can respond to by proliferation and osteogenesis were previously reported as 10^{-4} Pa and 10^{-5} Pa, respectively, where bone-marrow derived human MSCs and PET matrices were used [16-17]. As the shear stress acting on hAT-MSCs we report in this study is between those two values, our results imply that hAT-MSCs used in this study are expected to show proliferative properties, as supported by the viability result obtained in the microfluidic culture experiments shown in Figure 5. In addition, BrdU staining, or another similar assay should be done in order to further investigate and show that they can also have such good proliferative profiles in this microfluidic setup. High shear stresses, such as flow induced-deviatoric shear stresses, it is reasonable to say that very high stresses acting on cells under fast fluid flows at ml per min levels or greater can be detrimental on MSCs and cause cell detachments due to convection [17], however, values converging to 0.01-0.1 Pa interval as to play remarkably important roles in developmental biology such as mesenchymal condensation and tissue morphogenesis [47-50].

3. CONCLUSIONS

In conclusion, we showed that the hAT-MSCs could be successfully cultured with a high viability by using our microfluidic chip design under fluid flow conditions with low shear stress. Therefore, this microfluidic bioreactor culture has the potential for maintaining hAT-MSCs and improving their stem cell characteristics for further studies including self-renewal, differentiation potential and senescence phenotype. Furthermore, this setup can be tested as a candidate setup to be used in organ-on-a-chip studies inasmuch as GelMA is considered a biocompatible material which mimics the extracellular microenvironment of MSCs inside human body. Microfluidic devices are powerful tools for the

reconstruction of stem cell microenvironment and recapitulation of important physiological functions for both high-throughput detection of biological processes and controlling the stem cell fate within a 3D microenvironment resembling the physiological conditions. As a future study, biomarker expressions of MSCs can be determined via immunocytochemistry at the end of microfluidic chip culture. The cells can be evaluated with their senescence phenotype and the expression of MSC-specific genes related with self-renewal and differentiation.

ACKNOWLEDGMENTS

This study was carried out as a part of thesis of Ceren ÖZEL within the scope of 100/2000 The Council of Higher Education (CoHE) Doctoral Scholarship program-spring term of the 2017-2018 academic year in the field of biomaterials and tissue engineering. This study was also supported by Turkish Scientific and Technological Council (TÜBİTAK 1004-Regenerative and Restorative Medicine Research and Applications) under the grant numbers of 20AG003 and 20AG031.

CONFLICT OF INTEREST

The authors stated that there are no conflicts of interest regarding the publication of this article.

REFERENCES

- [1] Ingber DE. Developmentally Inspired Human ‘Organs on Chips’. *Development*, 2018; 145(16):dev156125.
- [2] Bhatia SN, Ingber DE. Microfluidic Organs-on-Chips. *Nat Biotechnol*, 2014; 32(8):760-72.
- [3] Avci H, Güzel FD, Erol S, Akpek A. Recent Advances in Organ-on-A-Chip Technologies and future Challenges: A Review. *Turkish Journal of Chemistry*, 2017; 42(3):587-610.
- [4] Zhang YS, Aleman J, Shin SR. et al. Multisensor-Integrated Organs-on-Chips Platform for Automated and Continual in Situ Monitoring of Organoid Behaviors. *Proceedings of the National Academy of Sciences*, 2017; 114(12):E2293-E2302.
- [5] Shin SR, Zhang YS, Kim D-J. et al. Aptamer-Based Microfluidic Electrochemical Biosensor for monitoring Cell-Secreted Trace Cardiac Biomarkers. *Analytical Chemistry*, 2016; 88(20):10019-10027.
- [6] Shin SR, Kilic T, Zhang YS. et al. Label- Free and Regenerative Electrochemical Microfluidic Biosensors for Continual Monitoring of Cell Secretomes. *Advanced Science*, 2017; 4(5):1600522.
- [7] Mancio-Silva L, Fleming HE, Miller AB. et al. Improving Drug Discovery by Nucleic Acid Delivery in Engineered Human Microlivers. *Cell Metabolism*, 2019; 29(3):727-735. e3.
- [8] de Souza N. Organoids. *Nature Methods*, 2018; 15(1):23-23.
- [9] Garbioglu DB, Demir N, Ozel C, Avci H, Dincer M. Determination of Therapeutic Agents Efficiencies of Microsatellite Instability High Colon Cancer Cells in Post- Metastatic Liver Biochip Modeling. *The FASEB Journal*, 2021; 35(9):e21834.










- [10] Uccelli A, Moretta L, Pistoia V. Mesenchymal Stem Cells in Health and Disease. *Nature Reviews Immunology*, 2008; 8(9):726-736.
- [11] Pers YM, Ruiz M, Noël D, Jorgensen C. Mesenchymal Stem Cells for the Management of Inflammation in Osteoarthritis: State of The Art and Perspectives. *Osteoarthritis and Cartilage*, 2015; 23(11):2027-2035.
- [12] Topal AE. Mesenchymal Stem Cell Mechanics on Osteoinductive Peptide Nanofibers. PhD, Bilkent University, Ankara, Turkey, 2017.
- [13] Topal AE, Tansik G, Ozkan AD, Guler MO, Dana A, Tekinay AB. Nanomechanical Characterization of Osteogenic Differentiation of Mesenchymal Stem Cells on Bioactive Peptide Nanofiber Hydrogels. *Advanced Materials Interfaces*, 2017; 4(20):1700090.
- [14] Engler AJ, Sen S, Sweeney HL, Discher DE. Matrix Elasticity Directs Stem Cell Lineage Specification. *Cell*, 2006; 126(4):677-689.
- [15] Mousavi SJ, Hamdy Doweidar M. Role of Mechanical Cues in cell Differentiation and Proliferation: a 3D Numerical Model. *PloS one*, 2015; 10(5):e0124529.
- [16] Zhao F, Chella R, Ma T. Effects of Shear Stress on 3- D human Mesenchymal Stem Cell Construct Development in a Perfusion Bioreactor System: Experiments and Hydrodynamic Modeling. *Biotechnology and Bioengineering*, 2007; 96(3):584-595.
- [17] Higuera GA, van Boxtel A, van Blitterswijk CA, Moroni L. The Physics of Tissue Formation with Mesenchymal Stem Cells. *Trends in Biotechnology*, 2012; 30(11):583-590.
- [18] Riddle RC, Taylor AF, Genetos DC, Donahue HJ. MAP Kinase and Calcium Signaling Mediate Fluid Flow-Induced Human Mesenchymal Stem Cell Proliferation. *American Journal of Physiology-Cell Physiology*, 2006; 290(3):C776-C784.
- [19] Dash SK, Sharma V, Verma RS, Das SK. Low Intermittent Flow Promotes Rat Mesenchymal Stem Cell Differentiation in Logarithmic Fluid Shear Device. *Biomicrofluidics* 2020; 14(5):054107.
- [20] Kim KM, Choi YJ, Hwang J-H. et al. Shear Stress Induced by An Interstitial Level of Slow Flow Increases the Osteogenic Differentiation of Mesenchymal Stem Cells Through TAZ Activation. *PloS one*, 2014; 9(3):e92427.
- [21] Bissoyi A, Bit A, Singh BK, Singh AK, Patra PK. Enhanced Cryopreservation of MSCs in Microfluidic Bioreactor by Regulated Shear Flow. *Scientific Reports*, 2016; 6(1):1-13.
- [22] Zhang J, Wei X, Zeng R, Xu F, Li X. Stem Cell Culture and Differentiation in Microfluidic Devices Toward Organ-on-A-Chip. *Future Science OA*, 2017; 3(2):FSO187.
- [23] Costa- Almeida R, Domingues RM, Fallahi A. et al. Cell- Laden Composite Suture Threads for Repairing Damaged Tendons. *Journal of Tissue Engineering and Regenerative Medicine*, 2018; 12(4):1039-1048.

- [24] Lim KS, Galarraga JH, Cui X, Lindberg GC, Burdick JA, Woodfield TB. Fundamentals and Applications of Photo-Cross-Linking In Bioprinting. *Chemical Reviews*, 2020; 120(19):10662-10694.
- [25] Wong DY, Ranganath T, Kasko AM. Low-Dose, Long-Wave UV Light Does Not Affect Gene Expression of Human Mesenchymal Stem Cells. *PloS one*, 2015; 10(9):e0139307.
- [26] Lawrence KP, Douki T, Sarkany RP, Acker S, Herzog B, Young AR. The UV/Visible Radiation Boundary Region (385–405 nm) Damages Skin Cells and Induces “dark” Cyclobutane Pyrimidine Dimers in Human Skin in vivo. *Scientific Reports*, 2018; 8(1):1-12.
- [27] Rajabi N, Rezaei A, Kharaziha M. et al. Recent advances on bioprinted gelatin methacrylate-based hydrogels for tissue repair. *Tissue Engineering Part A*. 2021; 27(11-12):679-702.
- [28] Yin J, Yan M, Wang Y, Fu J, Suo H. 3D Bioprinting of low-Concentration Cell-Laden Gelatin Methacrylate (GelMA) Bioinks with A Two-Step Cross-Linking Strategy. *ACS Applied Materials & Interfaces*, 2018; 10(8):6849-6857.
- [29] Miri AK, Nieto D, Iglesias L. et al. Microfluidics- Enabled Multimaterial Maskless Stereolithographic Bioprinting. *Advanced Materials*, 2018; 30(27):1800242.
- [30] Didarian R, Ebrahimi A, Ghorbanpoor H, Dizaji AN, Hashempour H, Guzel FD, Avci H. Investigation of Polar and Nonpolar Cyclotides Separation from Violet Extract Through Microfluidic Chip. 8. *International Fiber and Polymer Research Symposium*; 18-19 June 2021, Eskişehir Osmangazi University, Eskişehir, Turkey.
- [31] Gupta NS, Lee K-S, Labouriau AJP. Tuning Thermal and Mechanical Properties of Polydimethylsiloxane with Carbon Fibers. *Polymers*, 2021; 13(7):1141.
- [32] Dizaji AN, Ozturk Y, Ghorbanpoor H. et al. Investigation of the Effect of Channel Structure and Flow Rate on On-Chip Bacterial Lysis. *IEEE Trans Nanobioscience*, 2021; 20(1):86-91.
- [33] Kaur J, Ghorbanpoor H, Öztürk Y. et al. On- Chip Label- Free Impedance- Based Detection of Antibiotic Permeation. *IET Nanobiotechnology*, 2021; 15(1):100-106.
- [34] Ozdemir AT, Ozgul Ozdemir RB, Kirmaz C. et al. The Paracrine Immunomodulatory Interactions Between the Human Dental Pulp Derived Mesenchymal Stem Cells and CD4 T Cell Subsets. *Cell Immunol*, 2016; 310:108-115.
- [35] Gao G, Schilling AF, Hubbell K. et al. Improved Properties of Bone and Cartilage Tissue from 3D Inkjet-Bioprinted Human Mesenchymal Stem Cells by Simultaneous Deposition and Photocrosslinking in PEG-GelMA. *Biotechnology Letters*, 2015; 37(11):2349-2355.
- [36] Dupuy A, Ju LA, Passam FH. Straight Channel Microfluidic Chips for the Study of Platelet Adhesion under Flow. *Bio-protocol*, 2019; 9(6):e3195.
- [37] Zakrzewski W, Dobrzyński M, Szymonowicz M, Rybak Z. Stem Cells: Past, Present, and Future. *Stem Cell Research & Therapy*, 2019; 10(1):1-22.

- [38] Park D, Lim J, Park JY, Lee S-H. Concise Review: Stem Cell Microenvironment on A Chip: Current Technologies for Tissue Engineering and Stem Cell Biology. *Stem Cells Translational Medicine*, 2015; 4(11):1352-1368.
- [39] Dominici M, Le Blanc K, Mueller I. et al. Minimal Criteria for Defining Multipotent Mesenchymal Stromal Cells. *The International Society for Cellular Therapy Position Statement Cytotherapy*, 2006; 8(4):315-7.
- [40] Karaöz E, Demircan PÇ, Erman G, Güngörürler E, Sarıboyacı AE. Comparative Analyses of Immunosuppressive Characteristics of Bone-Marrow, Wharton's Jelly, and Adipose Tissue-Derived Human Mesenchymal Stem Cells. *Turkish Journal of Hematology*, 2017; 34(3):213.
- [41] Özdemir RBÖ, Özdemir AT, Sarıboyacı AE, Uysal O, Tuğlu Mİ, Kırmaz C. The Investigation of Immunomodulatory Effects of Adipose Tissue Mesenchymal Stem Cell Educated Macrophages on The CD4 T Cells. *Immunobiology*, 2019; 224(4):585-594.
- [42] Wade RJ, Burdick JA. Engineering ECM Signals into Biomaterials. *Materials Today*, 2012; 15(10):454-459.
- [43] Choi CK, Breckenridge MT, Chen CS. Engineered Materials and The Cellular Microenvironment: A Strengthening Interface Between Cell Biology and Bioengineering. *Trends in Cell Biology*, 2010; 20(12):705-714.
- [44] Xiao S, Zhao T, Wang J et al. Gelatin methacrylate (GelMA)-Based Hydrogels for Cell Transplantation: An Effective Strategy for Tissue Engineering. *Stem Cell Reviews and Reports*, 2019; 15(5):664-679.
- [45] Winer JP, Janmey PA, McCormick ME, Funaki M. Bone Marrow-Derived Human Mesenchymal Stem Cells Become Quiescent on Soft Substrates But Remain Responsive to Chemical or Mechanical Stimuli. *Tissue Engineering Part A*, 2009; 15(1):147-154.
- [46] Dhall A, Lab C. Simulating Fluid Flow Through a Culture Chip for Cell Migration Studies in Microgravity. *COMSOL Conference*; 2016, Boston, USA.
- [47] Song MJ, Brady-Kalnay SM, McBride SH, Phillips-Mason P, Dean D, Knothe Tate ML. Mapping The Mechanome of Live Stem Cells using A Novel Method to Measure Local Strain Fields in Situ at the Fluid-Cell Interface. *PLoS One*, 2012; 7(9):e43601.
- [48] Song MJ, Dean D, Knothe Tate ML. In Situ Spatiotemporal Mapping of Flow Fields Around Seeded Stem Cells at The Subcellular Length Scale. *PLoS one*, 2010; 5(9):e12796.
- [49] McBride SH, Falls T, Knothe Tate ML. Modulation of stem cell shape and fate B: Mechanical Modulation of Cell Shape and Gene Expression. *Tissue Engineering Part A*, 2008; 14(9):1573-1580.
- [50] Tate MLK, Falls TD, McBride SH, Atit R, Knothe UR. Mechanical Modulation of Osteochondroprogenitor Cell Fate. *The International Journal of Biochemistry & Cell Biology*, 2008; 40(12):2720-2738.



DESIGN OF ALGINATE BASED BLENDS FOR LIVING COMPOSITE FIBERS TO PROMOTE WOUND HEALING

Ceren OZEL^{1,6} , Tayfun SENDEL^{1,7} , Aliakbar EBRAHIMI^{2,6} , Elif APAYDIN^{3,6} ,
Hamed GHORBANPOOR^{4,6} , Ayla EKER SARIBOYACI^{1,6} , Onur UYSAL^{1,6} ,
Mete OZKURT⁵ , Huseyin AVCI^{2,6,8} *

¹ Department of Stem Cell, Institute of Health Sciences, Eskişehir Osmangazi University, Eskişehir, Turkey

² Department of Metallurgical and Materials Engineering, Eskişehir Osmangazi University Eskişehir, Turkey

³ Department of biochemistry, Institute of Health Sciences, Anadolu University, Eskişehir, Turkey

⁴ Department of Biomedical Engineering, Eskişehir Osmangazi University, Eskişehir, Turkey

⁵ Department of Physiology, Faculty of Medicine, Eskişehir Osmangazi University, Eskişehir, Turkey

⁶ Cellular Therapy and Stem Cell Production Application and Research Center (ESTEM), Eskişehir Osmangazi University, Eskişehir, Turkey

⁷ Central Research Laboratory Research and Application Center (ARUM), Eskişehir Osmangazi University, Eskişehir, Turkey

⁸ Translational Medicine Research and Clinical Center (TATUM), Eskişehir Osmangazi University, Eskişehir, Turkey

ABSTRACT

The currently used approaches in the treatment of wounds and burns have been studied for many years to eliminate problems related with mechanical strength, elasticity, biocompatibility and cost. Nowadays, fabrication of composite fibers by a fiber as core and hydrogels as shell, which can be seeded by cells is rapidly increasing. In this study, it is aimed to produce a natural polymer-based dressing that can provide controlled antibiotic release to accelerate wound healing with low cost and high efficiency. The composites have been achieved by using surgical suture as a core and alginate in the shell part, which modified with starch and gelatin. Evaluating low-cost hydrogel material such as alginate, starch and gelatin in the shell layer of composite fibers by different concentrations were investigated in addition to study their swelling and drug release behaviors. The parameters for the model of an antibiotic release that can prevent common infections can be manipulated by using a biotextile-based approach to quantify the amount of antibiotics and its release to satisfy clinical requirements. Toluidine blue and Penicillin/Streptomycin were chosen as antibiotic models for drug release experiments. Moreover, human adipose tissue-derived mesenchymal stem cells (hAT-MSCs) were applied to evaluate cell viability experiments. Results demonstrated that alginate modified starch and gelatin can be used as low-cost and promising materials for use in biomedical applications.

Keywords: Wound dressing, Composite fibers, Hydrogel, Core-shell, bio Textile

1. INTRODUCTION

The skin, known as the largest organ of the human body, is exposed to many external factors. Skin injury can be occurred by trauma, UV exposure, burns, and in some cases, wounds healing may take a long time and can lead to chronic wounds [1]. Since the recovery of the skin after injuries is a complex phenomenon that brings together many stages such as homeostasis, inflammation and re-epithelialization [2]. In particular, various genetic disorders and chronic diseases such as type I diabetes or aging leads to chronic wounds, and that can make wound healing processes difficult [3]. The patients are generally suffering from leg and foot ulcers; their management requires the use of the wound dressings. Further, poor circulation also makes systemic administration of antibiotics ineffective and using high antibiotic doses leads to adverse effects in these patients. Only small local

*Corresponding Author: havci@ogu.edu.tr

Received: 20.08.2021 Published: 30.11.2021

doses above the minimum inhibitory concentration are sufficient at the infected wound area. Finally, wound dressings that can provide recovery with systemic approaches in a short time are more advantageous than the expenses required for long-term wound care.

Developing fiber-based composite material for wound healing using hydrogels is a promising platform in tissue engineering [4-7]. Hydrogels have a significant place among the biomaterials due to their high-water absorption capacity. In addition, hydrogels can reach deep wound tissues with minimal surgical intervention, and can also take the shape of the damaged area. Thus, they can create lower risk of scarring, inflammation, and infection in the tissues [8, 9]. For the last 30 years, alginate fibers play an important role in the wound care industry and known to have a positive impact. This is because it has specific properties that facilitate wound healing, high moisture absorption and ion exchange ability, excellent biocompatibility of material in fiber form and it is an easily obtainable natural material. Alginate fibers are one of the useful raw material, especially for highly absorbent wound dressings [10].

Sodium alginate is a member of compounds Generally Recognized as Safe (GRAS) compounds [11]. Sodium alginate is an inexpensive, biodegradable biomaterial with low antimicrobial properties, and extracted from seaweed. Its structure enables absorbing edema in the wound. Alginate based composite has great potential such providing microbial protection and stimulation of wound healing processes [12, 13]. Alginate is known to form gel structures by covalent crosslinking with polycationic water-soluble polymers such as poly-L-lysine, chitosan, DEAE-dextran, amino-poly (oxyethylene) or proteins. Alginate shows a stable structure when cross-linked with Ca^{+2} as a multivalent cation. The viscosity of the alginate increases, as the pH decreases. For instance, the viscosity is maximized by forming hydrogen bonds at pH 3-3.5 due to the alginate skeleton becomes protonated. This is generally undesirable situation because during the mixing and injection stages of cell encapsulation, tensile stress from high viscosity can occur, which can damage cells or protein structures [13-15]. Alginate dressing maintains a physiologically moist micro-environment, minimizes bacterial infection in the wound area and treats the wound. These gels also ensure that the newly formed granulation tissue is not disrupted and the skin surrounding the wound is not damaged. Moreover, they act as an effective hemostatic agent in bleeding wounds. Alginates can absorb liquid up to 15-20 times their weight and make them an ideal dressing material for wounds with high exudate [10, 11]. In this way, they can stay on the wound for several days, thus minimizing the need for dressing changes. In comparative studies with hydrocolloid bandages, alginate dressings have been shown to be better in terms of fluid control, gel blocking, pain control and healing properties [16].

Alginate gels are promising for cell transplantation in tissue engineering. In this approach, hydrogels deliver cells to the desired site, provide space for new tissue formation, and control the structure and function of the treated tissue. As another property, alginate can release drug molecules from small chemical drugs up to macromolecular proteins, which is possible depending on the type and method of the cross-linking. In addition to the superior properties of the alginate, various additives can be added to the alginate such as starch and gelatin in order to control the desired drug release, strength and degradation processes [17].

Starch is a material composed from amylose and amylopectin. When the starch is heated in the presence of water, it undergoes a process known as gelatinisation, in which the granules swell, leach amylopectin and lose birefringence [18]. Studies have shown that it is a suitable material for different applications due to its biodegradability, easy availability and economic advantages. Starch stands out as risk-free and low-cost alternative material, which plays role in increasing cellular activity, differentiation and tissue remodeling among the materials used in scaffold fabrication [4, 19, 20]. Also, starch offers excellent potential for crosslinking due to the presence of abundant hydroxyl (-OH) groups and has proven to be a good precursor material for the preparation of hydrogels [21, 22].

However, its highly hydrophilic nature and poor mechanical properties have hindered its usage in tissue engineering compared to some expensive, commercial polymers [23]. In addition, gelatin is a biocompatible protein, which is used to prepare composite films for biomedical applications due to its low cost, excellent functional and filmogenic properties. Gelatin is obtained by treating collagen-containing tissues with acid and/or alkali and then heat-treating in the presence of water to irreversibly break the collagen fibrillary structure. Gelatin is a material with a distinctive odor, colorless or slightly yellow, suitable for use found in the form of strips, powders or granules. Gelatin derivatives are one of the most efficient materials used in wound healing, which is a natural component of human skin [24, 25]. In addition, gelatin derivatives have advantages in absorbing excess exudates due to its excellent ability to absorb water 5-10 times more than its own weight [26]. So, they are quite suitable for use as a composite material due to their distinct properties of being natural hydrogel.

A composite material is a combination of two or more specialized materials to do a specific function with different physical and chemical properties, without dissolving or blending them into each other [27]. Investigations for development of cell-laden composite fiber have gained momentum in recent years. The reason behind this is that these composite fibers possess compositional and structural multifunctionality. Cell-laden composite fibers have core-shell structure in which the core part is biologically relevant in terms of mechanical properties and/or consisting of biodegradable polymer fibrils, and the shell part comprised of living cells and hydrogels which contains other bioactive agents such as growth factors or antibiotics [28-30]. This core/shell architecture provides a mechanically weak scaffold especially considering the shell part, while it also prevents the risk of fracture of fibers by benefitting from the strength of the fibers [30]. Loading of cells on the shell part is particularly important for the replacement of the lost tissues and for their regeneration with secreted bioactive molecules [28, 30]. Furthermore, the core/shell structure allows the formation of hydrogel which brings many advantages: Hydrogels are the hydrophilic, biodegradable and biocompatible, can bear bioactive components and encapsulate the cells, can be modified easily and be used as delivery vehicle.

In the design of this study, various combinations of alginate, gelatin and starch were used to determine the optimum structural combination for the most appropriate drug release profile. The swelling rates and drug release profiles of these hydrogels and viability of hAT--MSCs in hydrogels coated to surgical sutures as core/shell composites were studied and structure of core/shell composites were imaged by SEM techniques.

2. MATERIAL AND METHODS

2.1. Preparation of Alginate and Mixtures

Alginate (low viscosity sodium alginate derived from brown algae, Sigma), starch (Cottnal KS) and gelatin (Gelatin from bovine skin, Sigma) used in our study were prepared using double distilled water at different concentrations (w/w). Alginate was prepared as different variety concentrations between 1-5% (w/v). Alginate blends were prepared with gelatin and starch by adding to the pre-polymer alginate solutions at a ratio between 1-3%. While preparing alginate and gelatin, the preparation was made by mixing at 50°C for 2 hours at a speed of 750-1000 rpm. The obtained mixtures were cross-linked using 0.2 M CaCl₂ prepared in double distilled water.

2.2. Performing Swelling Experiments

The prepared mixtures were first polymerized to produce hydrogels for swelling experiments. After the polymerization process, the excess water on the obtained hydrogels was removed by means of

blotting paper, and the hydrogels were weighted. The liquid loss of the hydrogels was achieved by keeping them in an incubator at 37°C for 24 hours. After 24 hours, dry weights (M_{dry}) of the hydrogels were recorded. Then, each hydrogel was taken into 100 mL of double distilled water and allowed to swell at 37°C for 24 hours. At the end of 24 hours, the excess water of the hydrogels were removed with blotting paper. The wet weight of hydrogels (M_{wet}) were obtained and recorded. Swelling calculations were made by using the obtained weights in the following equation:

$$Swelling\ Ratio = \frac{M_{wet} - M_{dry}}{M_{dry}} \times 100$$

2.3. Scanning Electron Microscopic Imaging

The prepared alginate hydrogel was pulled around the 3-0 surgical suture to form core/shell layers (core: surgical suture, shell: hydrogel). A commercial absorbable Poly(glycolide/L-Lactide) surgical suture (MITSU™ POLYGLACTIN 910) which is composed of a copolymer made 90% Glycolide and 10% L-Lactide, with a size of 3-0, was used as a core part of core/shell form. The surgical suture is coated with hydrogel by passing through in-house with a custom-built needles/tips having a flow rate of 2 ml/min. The composite was then kept in 0.2 M CaCl₂ solution for 15 minutes for crosslinking process and after that washed 3 times with PBS. After this stage, the sample was left to dry in a graduated ethanol series (30 – 50 – 70 – 90 – 100) under hood. After the sample was fixed on the stub using carbon tape, they were coated with 4 nm gold/palladium (Leica EM CPD300). Then the sample was analyzed by scanning electron microscope device (SEM, Hitachi Regulus 8230) at 1kV voltage.

2.4. Toluidine Blue and Antibiotic Release from Alginate Hydrogels

The release of Toluidine blue (sigma) and Penicillin/streptomycin (Gibco) from the alginate and alginate doped gelation or starch hydrogels were investigated. For this aim, different ratio of aqueous mixtures of alginate, and different mixtures of alginate with gelatin or starch were prepared. 1 gr Toluidine blue was added to 10 ml of each mixture or 1 ml of Penicillin/streptomycin (10,000 units/mL penicillin/10,000 µg/mL streptomycin) was added to 9 ml of each mixture and mixed at 500 rpm in a dark environment for 2 hours at 40°C. After mixing process, the samples were cross-linked in 0.2 M CaCl₂ solution for 15 minutes and then allowed to release for 24 hours at room temperature. Then, the samples were analyzed by UV-Vis spectrophotometer (A&ELAB).

2.5. Demonstration of Cellular Encapsulation on the Composite Fibers

A red PKH26 (Sigma) fluorescent dye were used to stain hAT-MSCs according to the manufacturer's protocol before encapsulation with hydrogels. Mesenchymal stem cells (500×10^5 cells/ml) stained with PKH26 (Sigma) fluorescent dye were added to alginate pre-polymer hydrogel mixture and homogenized, which was followed by coating of the surgical sutures with the same method described “living core-shell fiber preparation” Afterwards, the formation of cell-laden hydrogel shell layer was obtained.

2.6. Cell Viability/Cytotoxicity Test

In order to examine cell viability within composite living fibers, isolated and characterized human adipose tissue-derived mesenchymal stem cells (hAT-MSCs) were used from our previous studies which had been isolated and cryopreserved from informed/consented lipoaspirates of healthy donors undergoing elective liposuction, under Eskişehir Osmangazi University Clinical Research Ethics Committee permission (no: 80558721/231, 09/06/2017-12). hAT-MSCs were cultured and

characterized as in previously described protocols depending *in vitro* differentiation experiments and immunophenotyping by flow cytometry[30-32]. hAT- MSCs were thawed and cultured in 75 cm²dishes, at 37 °C and 5% CO₂ conditions for their expansion. For this aim, hAT-MSCs were collected after centrifugation and plated in complete DMEM-F12 MSC culture medium containing 10% FBS and 1% penicillin-streptomycin and 1% (mL/mL) stable L- Glutamine (Glutamax, Sigma), 15mM HEPES and Dulbecco's Modified Eagle Medium (DMEM-F12, Sigma), and the cells incubated at 37°C in 5% CO₂ and 99% relatively humidified incubator.

Fluorescent live/dead staining (Live/Dead (AAT Bioquest®) was used to determine the viability of hAT-MSCs within composite living fibers after 24 hours in hAT-MSC culture medium at 37°C in 5% CO₂. For this purpose, after washing the samples 3 times with PBS, they were incubated in the dark for 1 hour with 1 μM Calcein-AM and 2 μM Propidium Iodide. Live (green) and dead (red) cells were visualized under a fluorescent microscope. Calcein-AM green was stimulated in the FITC channel, and Propidium iodide red in the Texas Red channel.

3. RESULTS AND DISCUSSION

In our study, different concentrations of alginate mixtures (alginate alone or alginate + starch or gelatin) were prepared and after crosslinking process (hydrogel formation), swelling, release and cellular survival results of them were investigated. In this study, it was aimed to control the swelling profile of hydrogels with different density of alginate and also by adding starch or gelatin. Swelling rates obtained for 1%, 3% and 5% of alginate were respectively 2634.78; 2488.89 and 5460 (Table 1).

Alginate is composed of mannuronic and guluronic acid units [32]. Guluronic acid densed alginate has a high viscosity and will swell less because it will bind to more calcium units [33]. When alginate gels are placed in saline, Na⁺ ions in the swelling medium enter inside hydrogel and undergo ion exchange with Ca⁺⁺ ions bound to the –COO– groups of 1,4-linked β-D-mannuronic (M) blocks. This, along with increased swelling, causes the M chains to relax. The external Na⁺ ions then enter the 'egg-box' spaces and replace the existing Ca⁺⁺ ions. This also results in facial swelling. The fully hydrated structure begins to lose its structural integrity due to disruption of the 'egg box' cavities and the alginate chains begin to break down and dissolve [34]. The observed increases in swelling rate for 5% alginate hydrogel may be due to the anionic nature of alginate, increase in density of alginate will cause increased repulsion between the molecular chains, resulting in an increase in swelling rate [35].

Table 1. Swelling data of surgical sutures covered with alginate and various additives.

Mixture	Dry Weight (g)	Swelling Weight (g)	Swelling Rate
1%Alginate	0.23	6.29	2634.78
1%Alginate + 1%Gelatin	0.085	0.132	55.29
1%Alginate +1%Starch	0.33	1.09	230.30
2% Alginate +2% Gelatin	0.029	0.103	255.17
2% Alginate + 2% Starch	0.53	2.75	418.87
3% Alginate	0.27	6.99	2488.89
3% Alginate + 2% Gelatin	0.091	0,871	857.14
3% Alginate + 2% Starch	0.067	1.28	1810.45
5% Alginate	0.125	6.95	5460
5% Alginate + 1% Gelatin	0.156	8.15	5124.36

According to data obtained for alginate-gelatin hydrogels, the addition of gelatin to the alginate provides a significant control of the swelling rates depending on the percentage of gelatin in the mixture. When 1% gelatin was added to 1% alginate solution, the swelling ratio of the obtained hydrogel was 55.29. This rate is approximately 2% of the swelling rate of 1% alginate. Also, for 3% alginate, 2% gelatin mixture hydrogel swelling rate is 34% of the swelling rate of 3% alginate. As another group in this study, the swelling ratio of the hydrogel obtained by adding 1% gelatin to 5% alginate solution was 5124.36. This swelling rate is 94% of the swelling rate of 5% Alginate hydrogel. Yao et al. (2012) that obtained microspheres from mixtures of alginate and gelatin at different concentrations in their study, revealed that alginate was the main gelation factor for the obtained spheres and suggested that less stable and lower strength spheres were formed [36]. Here, 2 profiles were detected for alginate-gelatin hydrogels. The first one is the increase in swelling rate with increase in total density of polymers (total polymers density: 2%, 5%, 6%, swelling rate: $55.29 < 857.14 < 5124.36$). This result is the same as the result obtained for alginate hydrogels. The second one is decreasing in swelling rate by adding gelatin to alginate. In a study conducted by Pulat in 2018, it was shown that the swelling rate decreases as the gelatin concentration increases [37].

When the ratio of alginate and gelatin is the same (1% alginate + 1% gelatin), sharply decrease in swelling rate in compare with alginate (1%) was detected (from 2634.78 to 55.29), and by increasing of the ratio of alginate to gelatin in hydrogel composition, the swelling ratio in compare with alginate hydrogels was increased ($2% < 34% < 94%$). These results show that when the ratio of alginate is dominant to gelatin (5%:1%) the swelling rate of the hydrogel on a large scale controlled by alginate (94% of the swelling rate of 5% alginate).

When 1% starch is added to the 1% alginate solution, the swelling rate of the prepared hydrogel was found to be approximately 9% of the 1% alginate hydrogel. The same as gelatin doped alginate hydrogels, adding of starch with the same ratio of alginate to hydrogel composition (1% alginate: 1% starch) cause to a sharp decrease in swelling ratio in compare with 1% alginate hydrogel. By increasing the ratio of the alginate in hydrogels composition, increase in swelling ratio of hydrogels were detected (alginate/gelatin ratio: 1, 1.5, swelling rate: $230.30 < 1810.45$). These results show that adding starch to alginate has the same profile detected for adding of gelatin. Increasing in the ratio of starch in hydrogel composition cause to decrease in swelling rate.

Swelling behaviors of a hydrogel depend on composition, monomer ratio, ionic charge content, and polymerization route, type and density of crosslinker [38]. By increasing the degree of crosslinking, alginate will significantly reduce its swelling in the presence of solvent, resulting in reduced permeability of different solutes. As a result, the release of encapsulated drugs in alginate matrices will be delayed by increase of the degree of crosslinking and as a result it is suitable for use in controlled drug release applications [39]. Also, according to swelling results for hydrogels prepared by mixing different ratios of alginate with starch or gelatin, it has been shown that it is possible to control the swelling properties of the alginate based hydrogels (Figure 1). The data obtained from the experiments showed that gelatin caused a greater decrease in swelling data compared to starch.

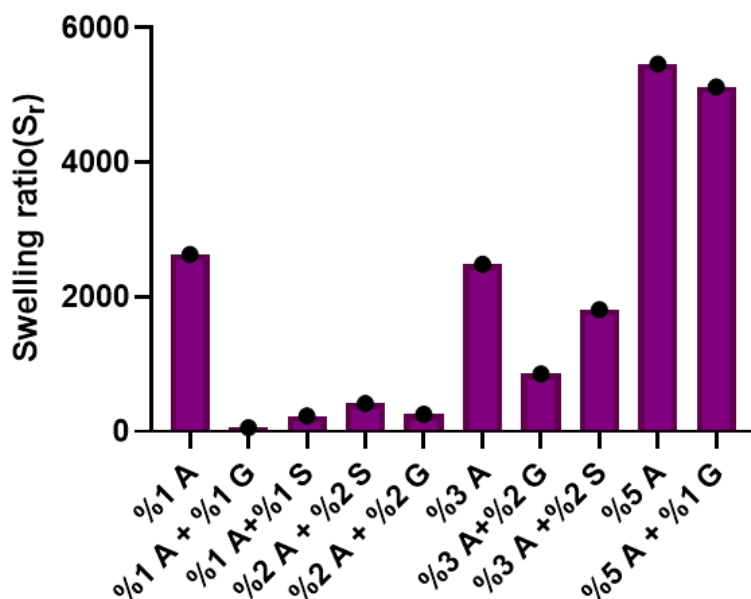


Figure 1. Swelling ratio of surgical sutures coated with alginate hydrogels or hydrogels composed of different mixtures of alginate with starch or gelatin. A: Alginate, G: Gelatin, S: Starch.

Although starch is thought to increase hydrophilic property of the hydrogel due to its hydrophilic nature, the complex macromolecular chain sequence obtained as a result of mixing can delay the penetration of water molecules into the hydrogel and therefore reduce the swelling rate. In hydrogels consisting of the mixture of starch and alginate, a high degree of cross-linking between molecules result in reduced swelling rates [35].

Structural analyzes of surgical sutures coated with alginate were made by SEM imaging. Analysis with 3-0 suture samples coated with antibiotic-loaded alginate hydrogel show the formation of hydrogel layer around the sutures. Analyzes performed using Image J (version 1.53k), showed that the diameter of the surgical sutures before then coating was 340 μm and the thickness after hydrogel coating was 390 μm (Figure 2). The thickness of the coating layer was considered to be 25 μm .

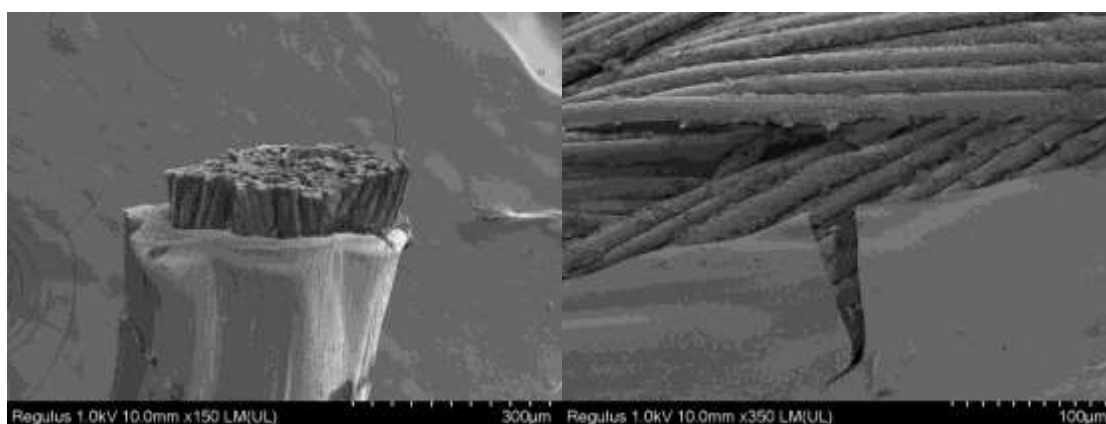


Figure 2. Structural analysis of core/shell composite (suture/hydrogel) fibers with SEM.

The polymeric structures and properties of hydrogels were evaluated. Drug release studies were carried out in order to examine the potential biomedical applicability of these alginate-based hydrogels. Toluidine Blue was used as first model drug for release studies. According to the obtained results, it was found that the releases of toluidine blue showed changes with increasing the alginate ratio. It is seen that the toluidine blue release capacity decreases with the increase in the density of the alginate. There was not any positive effect on toluidine blue release by adding gelatin to the alginate. Only hydrogel formed with 5% alginate + 1% gelatin mixture showed approximately 10% increase in the drug release (Table 2). Although different ratio of starch had different effects, it generally had a negative effect on toluidine blue release.

Table 2. Release profile for hydrogels (alginate and its mixtures with starch or gelatin) of toluidine blue (TB) and Penicillin/Streptomycin (Pen_Strep).

HYDROGEL	TB	PEN/STREP
1% Alginate	3.00	2.71
1%Alginate + 1%Gelatin	2.10	1.10
1%Alginate + 1% Starch	3.12	3.01
2%Alginate + 2% Gelatin	2.02	1.98
2%Alginate + 2% Starch	2.61	2.01
3%Alginate	2.17	1.22
3%Alginate + 2% Gelatin	1.66	1.44
3%Alginate + 2% Starch	1.53	1.53
5%Alginate	1.05	1.02
5%Alginate + 1% Gelatin	1.15	1.01

In the case of penicillin streptomycin, it is observed that the release of the drug from alginate-gelatin hydrogels is lower than the alginate hydrogel when the ratio of alginate is 1 or 2% (gelatin ratio is the same as alginate 1%:1% or 2%:2%). But with increase the ratio of alginate to 3 or 5% the drug release amount increases by increasing the gelatin ratio to 2%.

In different studies, swelling tests of alginate: gelatin mixtures at different doses were performed. The common opinion of the studies has been shown that the swelling levels increase with the addition of gelatin[40-42]. The reason of the converse results for lower ratio of alginate (1 and 2%) in our study is thought to be the used CaCl₂ concentration and the difference in chemical crosslinker.

There is no correlation in the toluidine blue release profile in the hydrogels obtained by adding starch. However, in penicillin streptomycin release amounts, high levels of release were observed by adding starch in compare with hydrogel composed only from alginate. This result is thought to be due to the fact that starch is a water-insoluble material, and that molecules are trapped in the voids during polymerization, creating a higher surface area.

Surgical sutures coated with MSC loaded alginate were labeled with PKH26 (red). Fluorescent microscope imaging of these sutures shows the presence of MSCs in shell part of the fibers. Surgical sutures are coated with alginate in order to cover them with a cell-loaded hydrogel layer in the form of a core-shell. For crosslinking process of the alginate, the coated fibril (surgical suture + MSC-alginate) was kept in CaCl₂ solution for about 2 minutes and then imaged under the fluorescent microscope (Figure 3). As seen in Figure 3, hAT-MSCs showed a homogeneous distribution. In core/shell composite fibers, it has been shown that the shell of alginate-based blend hydrogel polymers can encapsulate mesenchymal stem cells with high viability rate.

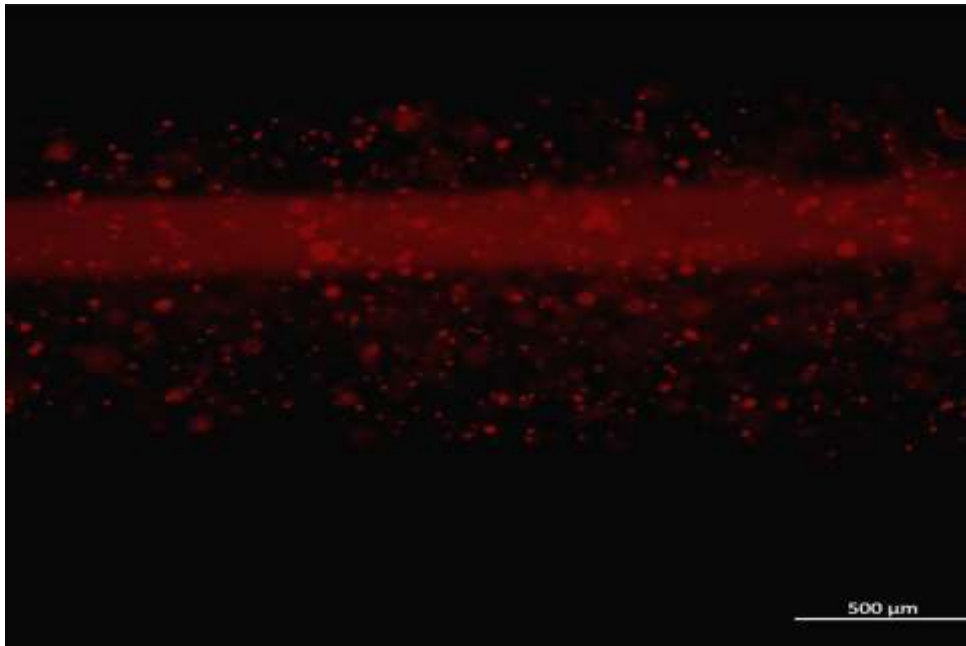


Figure 3. Fluorescent microscope image of live composite suture coated with Mesenchymal Stem Cell loaded %3Alginate:%2Gelatin labeled with PKH26 (red) in a core-shell structure.

The data we obtained in this study showed that not only the swelling and drug release profile of alginate and starch or gelatin added alginate hydrogels can be controlled, but also, it has been shown that living cells can adhere to the alginate hydrogel and maintain their vitality within hydrogel. Due to these properties, alginate and starch or gelatin doped alginate hydrogels appear as low-cost polymers that can be used in biomedical applications. Nowadays, biomedical studies are mostly focused on biomaterials such as hyaluronic acid, cellulose and its derivatives, and chitosan. This study showed that alginate and alginate-based materials to be used directly, it should be both low cost and highly effective. It is thought that alginate and its mixtures, which have been shown to be effective both in cost and in the data of our study, can be developed further with future studies to produce medically usable living products.

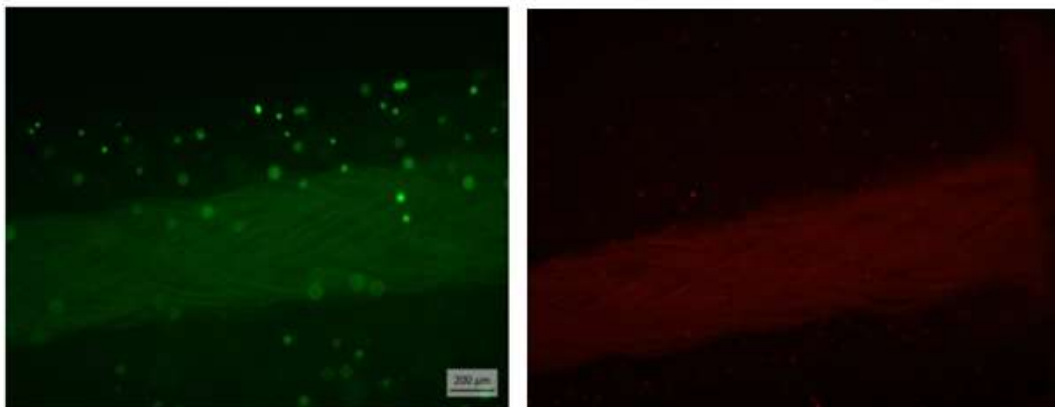


Figure 4. Biocompatibility assessment of the core-shell fiber construction process with live/dead cell viability assay. Fluorescence images of human adipose tissue-derived mesenchymal stem cells (hAT-MSCs) encapsulated within composite fibers. 3D core-shell was generated from surgical sutures coated with

%3Alg:%2Gel hydrogel blend were imaged post-24 hours cell culture. Scale bars, (a) and (b) 200 μm . (a), Live cells are green (calcein acetoxymethyl) and (b) dead cells are red (propidium iodide).

In this study, biocompatibility of core-shell fiber preparation process with alginate: gelatin blends has been demonstrated by live dead staining. Cell viability of composite fibers was evaluated by using hAT-MSCs in shell part of composite fibers. The high cellular viability after 24 hours of culture indicates that living core-shell fiber preparation process did not cause any significant cytotoxic effect to the cells. This result indicated that encapsulated cells remained alive after 24 hours (Figure 4a, 4b). In a reported study regarding composite fibers, more than 50 % cells was found dead after 7 days culture from encapsulation with hydrogel layer was composed of alginate [43]. Alginate may not be suitable for long-term culture, but it is a suitable biomaterial for encapsulating cells. Since, it can be used with cell-friendly biomaterials (*i.e.* gelatin, collagen, fibronectin etc.) as blend formulations, while enabling shape fidelity. Alginate and gelatin can be used as primary coating materials as composite form due to favorable rheological properties [44]. Although alginate is a biocompatible material and adjustable properties with greater mechanical stiffness and strength among the other biomaterials, it is inert material for cellular attachment due to the lack of essential amino acid sequences (RGD). Thus, it is not appropriate to use alginate alone as ECM in tissue engineering approaches [45]. For maintaining biological activities such as cell adhesion, proliferation, migration, growth, peptide containing-hydrogels have been studied for decades [46]. Gelatin can be suggested as bi-functional coating material as biocompatible and biodegradable, since it possesses RDG motifs naturally for cellular adhesion, and it can be easily degraded by cells with particularly MMP enzymes that is released from cells [47]. However, when gelatin is exposed to heat, its loss of shape fidelity. Using gelatin with alginate at the appropriate concentration prevents this mechanical stability issue. According to a recent study by Wang et al. (2018), the viability of human adipose-derived stem cells within the alginate/gelatin mixture was evaluated, it has shown that alginate/gelatin mixture did not have any cytotoxic effect on cells and is suitable for cell proliferation [48].

In another study conducted with gelatin derivatives: alginate containing composite fibers in 2019, it was shown that the encapsulated cells remained viable for up to 21 days [4]. Cell survival and proliferation has positive correlation with gelatin concentration, whereas negative correlation with alginate concentration. On the other hand lower alginate percentage shape fidelity and stability of material during coating process with a suitable viscosity [48]. Therefore, based on these results in our study, 3 % alginate: 2 % gelatin ratio was used for fabrication composite living fibers.

4. CONCLUSIONS

The results of this study showed that the swelling and drug release profiles of alginate and starch or gelatin doped hydrogels can be controlled. Also, it has been shown that cell survival can be maintained in the alginate hydrogel with high viability. Due to these properties, alginate and doped alginate hydrogels appear as low-cost polymers that can be used in biomedical applications. Recent biomedical studies are mostly focused on biomaterials such as hyaluronic acid, chitosan, cellulose and its derivatives. This study showed that it would be advantageous to use alginate-based materials in the living composite fibers for biomedical studies, in terms of low cost and high efficacy. It is thought that alginate and its mixtures, which have been shown to be effective in our study, can be developed further with future studies to produce medically usable products.

ACKNOWLEDGMENTS

This study is supported by Turkish Scientific and Technological Council (TÜBİTAK-1002) under the grant number of 219S647.

CONFLICT OF INTEREST

The authors stated that there are no conflicts of interest regarding the publication of this article.

REFERENCES

- [1] Martin P. Wound Healing--Aiming for Perfect Skin Regeneration. *Science*, 1997; 276: 75-81.
- [2] Gonzalez ACDO, Costa TF, Andrade ZDA & Medrado, ARAP. Wound Healing-A Literature Review. *Anais Brasileiros de Dermatologia* 2016; 91:614-620.
- [3] Tatara AM, Kontoyiannis DP, Mikos AG. Drug Delivery and Tissue Engineering to Promote Wound Healing in the Immunocompromised Host: Current Challenges and Future Directions. *Advanced Drug Delivery Reviews*, 2018; 129: 319-329.
- [4] Costa- Almeida R, Domingues RM, Fallahi A, Avci H, Yazdi IK, Akbari M, et al. Cell- Laden Composite Suture Threads for Repairing Damaged Tendons. *Journal of tissue Engineering and Regenerative Medicine*, 2018; 12:1039-1048.
- [5] Fallahi A, Yazdi IK, Serex L, Lesha E, Faramarzi N, Tarlan F, et al. Customizable Composite Fibers for Engineering Skeletal Muscle Models. *ACS Biomaterials Science & Engineering* 2019; 6:1112-1123.
- [6] Tamayol A, Yazdi I, Fallahi A, Nabavinia M, Avci H, Costa-Almeida R, et al. Textile Tissue Engineering: a Path Towards Organ Weaving. in *Front. Bioeng. Biotechnol. Conference Abstract: 10th World Biomaterials Congress FBIOE*, 2016 doi: 10.3389/conf..
- [7] Costa-Almeida R, Tamayol A, Yazdi I, Avci H, Fallahi A, Annabi N. et al. A Textile Platform using Mechanically Reinforced Hydrogel Fibres Towards Engineering Tendon Niche, *European Cells and Materials*, 2016; 31: 1473-2262.
- [8] Adeli H, Khorasani MT and Parvazinia MJI. Wound Dressing Based on Electrospun PVA/Chitosan/Starch Nanofibrous Mats: Fabrication, Antibacterial and Cytocompatibility Evaluation and in vitro Healing Assay. *International Journal of Biological Macromolecules*, 2019; 122: 238-254.
- [9] Baghaie S, Khorasani MT, Zarrabi A and Moshtaghian JJJ. Wound Healing Properties of PVA/Starch/Chitosan Hydrogel Membranes with Nano Zinc Oxide as antibacterial Wound Dressing Material. *Polymer Edition*, 2017; 28:2220-2241.
- [10] Zhang M & Zhao X. Alginate Hydrogel Dressings for Advanced Wound Management. *International Journal of Biological Macromolecules*, 2020; 162: 1414-1428
- [11] Mayet N, Choonara YE, Kumar P, Tomar LK, Tyagi C, Toit L. C. Du, et al. A comprehensive review of advanced biopolymeric wound healing systems. *Journal of Pharmaceutical Sciences* 2014; 103: 2211-2230.
- [12] Lee KY, Mooney DJ. Alginate: Properties and Biomedical Applications. *Progress in Polymer Science*, 2012;37: 106-126.

- [13] Gaspar-Pintilieşcu A, Stanciu AM and Craciunescu O. Natural Composite Dressings Based on Collagen, Gelatin and Plant Bioactive Compounds for Wound Healing: A Review. *International Journal of Biological Macromolecules*, 2019;138: 854-865.
- [14] Hasnain MS, Nayak AK. *Alginates: Versatile Polymers in Biomedical Applications and Therapeutics*. CRC Press, 2019.
- [15] Sudha PN. *Industrial Applications Of Marine Biopolymers*. CRC Press, 2017.
- [16] Mir M, Ali MN, Barakullah A, Gulzar A, Arshad M, Fatima S, et al. Synthetic Polymeric Biomaterials for Wound Healing: A Review. *Progress in Biomaterials*, 2018; 7:1-21.
- [17] Christensen BE. *Alginates as Biomaterials in Tissue Engineering. Carbohydrate Chemistry: Chemical and Biological Approaches*, 2011; 37:227-258.
- [18] Torres FG, Commeaux S & Troncoso OP. Starch- Based Biomaterials for Wound- Dressing Applications. *Starch- Stärke*, 2013; 65: 543-551.
- [19] Naseri-Nosar M, Ziora ZM. Wound Dressings from Naturally-Occurring Polymers: A Review On Homopolysaccharide-Based Composites. *Carbohydrate Polymers*, 2018; 189:379-398.
- [20] Campbell FC. *Structural Composite Materials*. ASM international, 2010.
- [21] Malafaya PB, Silva GA & Reis RL. Natural–Origin Polymers as Carriers and Scaffolds for Biomolecules and Cell Delivery in Tissue Engineering Applications. *Advanced Drug Delivery Reviews*, 2007; 59: 207-233.
- [22] Pourjavadi A, Ebrahimi AA & Barzegar, S. Preparation and Evaluation of Bioactive and Compatible Starch Based Superabsorbent for Oral Drug Delivery Systems. *Journal of Drug Delivery Science and Technology*, 2013; 23:511-517.
- [23] Zhang LM, Yang C & Yan L. Perspectives on: Strategies to Fabricate Starch-Based Hydrogels with Potential Biomedical Applications. *Journal of Bioactive and Compatible Polymers*, 2005; 20: 297-314.
- [24] Afewerki S, Sheikhi A, Kannan S, Ahadian S & Khademhosseini A. Gelatin- Polysaccharide Composite Scaffolds for 3D Cell Culture and Tissue Engineering: Towards Natural Therapeutics. *Bioengineering & Translational Medicine*, 2019; 4: 96-115.
- [25] Choi YS, Hong S R, Lee YM, Song KW, Park MH & Nam YS. Study on Gelatin-Containing Artificial Skin: I. Preparation and Characteristics of Novel Gelatin-Alginate Sponge. *Biomaterials*, 1999; 20: 409-417.
- [26] Princely S, Saleem Basha N, Nandhakumar S and Dhanaraju MJSRL. Design and Evaluation of Controlled Release Gentamycin Incorporated Gelatine Alginate Matrices for Wound Management. *Scholars Research Library*, 2015; 7:145-153.
- [27] Abdullah MF, Nuge T, Andriyana A, Ang BC and Muhamad, F. Core–Shell Fibers: Design, Roles, and Controllable Release Strategies in Tissue Engineering and Drug Delivery. *Polymers*, 2019; 11:2008

- [28] Avci H, Ghorbanpoor H and Nurbas M. Preparation of Origanum Minutiflorum Oil-Loaded Core–Shell Structured Chitosan Nanofibers with Tunable Properties. *Polymer Bulletin*, 2018; 75:4129-4144.
- [29] Karaöz E, Demircan PÇ, Erman G, Güngörürler E and Sarıboyacı AE. Comparative Analyses of Immunosuppressive Characteristics of Bone-Marrow, Wharton’s Jelly, and Adipose Tissue-Derived Human Mesenchymal Stem Cells. *Turkish Journal of Hematology*, 2017; 34:213.
- [30] Özdemir AT, Özdemir RBÖ, Kırmaz C, Sarıboyacı AE, Halbutoğlları ZSÜ, Özel C, et al. The Paracrine Immunomodulatory Interactions Between The Human Dental Pulp Derived Mesenchymal Stem Cells and CD4 T Cell Subsets. *Cellular Immunology*, 2016; 310:108-115.
- [31] Özdemir RBÖ, Özdemir AT, Sarıboyacı AE, Uysal O, Tuğlu Mİ and Kırmaz C. The Investigation of Immunomodulatory Effects of Adipose Tissue Mesenchymal Stem Cell Educated Macrophages on The CD4 T Cells. *Immunobiology*, 2019; 224:585-594.
- [32] Zhuang Y, Yu F, Chen H, Zheng J, Ma J and Chen J. Alginate/Graphene Double-Network Nanocomposite Hydrogel Beads with Low-Swelling, Enhanced Mechanical Properties and Enhanced Adsorption Capacity. *Journal of Materials Chemistry A*, 2016; 4:10885-10892.
- [33] Matyash M, Despong F, Ikonomidou C and Gelinsky M. Swelling and Mechanical Properties of Alginate hydrogels with Respect to Promotion of Neural Growth. *Tissue Engineering Part C: Methods* 2014; 20:401-411.
- [34] Bajpai S and Kirar N. Swelling and Drug Release Behavior of Calcium Alginate/Poly (Sodium Acrylate) Hydrogel Beads. *Designed Monomers and Polymers*, 2016; 19:89-98.
- [35] Roy A, Bajpai J and Bajpai A. Dynamics of Controlled Release of Chlorpyrifos from Swelling and Eroding Biopolymeric Microspheres of Calcium Alginate and Starch. *Carbohydrate Polymers*, 2009; 76:222-231.
- [36] Yao R, Zhang R, Luan J and Lin F. Alginate and Alginate/Gelatin Microspheres for Human Adipose-Derived Stem Cell Encapsulation and Differentiation. *Biofabrication*, 2012; 4:025007.
- [37] Pulat M. The Preparation of Gelatin Coated Sodium Alginate Hydrogels. *The Eurasia Proceedings of Science Technology Engineering and Mathematics*, 2018; 4:149-155
- [38] El-Sherbiny I, Lins R, Abdel-Bary E and Harding D. Preparation, Characterization, Swelling and in vitro Drug Release Behaviour of Poly [N-acryloylglycine-Chitosan] Interpolymeric pH and Thermally-Responsive Hydrogels. *European Polymer Journal*, 2005; 41:2584-2591.
- [39] Wang Q, Hu X, Du Y and Kennedy JF. Alginate/Starch Blend Fibers and Their Properties for Drug Controlled Release. *Carbohydrate Polymers*, 2010; 82:842-847.
- [40] Dong Z, Wang Q and Du Y. Alginate/Gelatin Blend Films and Their Properties for Drug Controlled Release. *Journal of Membrane Science*, 2006; 280:37-44.
- [41] Fan L, Du Y, Huang R, Wang Q, Wang X and Zhang L. Preparation and Characterization of Alginate/Gelatin Blend Fibers. *Journal of Applied Polymer Science*, 2005; 96:1625-1629.

- [42] Rosellini E, Cristallini C, Barbani N, Vozzi G and Giusti P. Preparation and Characterization of Alginate/Gelatin Blend Films for Cardiac Tissue Engineering. *Journal of Biomedical Materials Research Part A: An Official Journal of The Society for Biomaterials, The Japanese Society for Biomaterials and The Australian Society for Biomaterials and the Korean Society for Biomaterials*, 2009; 91:447-453.
- [43] Akbari M, Tamayol A, Laforte V, Annabi N, Najafabadi AH, Khademhosseini A. et al. Composite Living Fibers for Creating Tissue Constructs using Textile Techniques. *Advanced Functional Materials*, 2014; 24:4060-4067
- [44] He Y, Yang F, Zhao H, Gao Q, Xia B and Fu J. Research on The Printability of Hydrogels in 3D bioprinting. *Scientific Reports*, 2016; 6:1-13.
- [45] Axpe E and Oyen ML. Applications of Alginate-Based Bioinks in 3D Bioprinting. *International Journal of Molecular Sciences*, 2016; 17:1976
- [46] Wells RG. The Role of Matrix Stiffness in Regulating Cell Behavior. *Hepatology*, 2008; 47:1394-1400.
- [47] Kalia S. *Polymeric Hydrogels As Smart Biomaterials*. Springer, 2016; Berlin, Germany.
- [48] Wang XF, Lu PJ, Song Y, Sun YC, Wang YG and Wang Y. Nano Hydroxyapatite Particles Promote Osteogenesis in A Three-Dimensional Bio-Printing Construct Consisting of Alginate/Gelatin/hASCs. *RSC Advances*, 2016; 6:6832-6842.



INVESTIGATION OF MECHANICAL AND PHYSICAL PROPERTIES OF GRAPHENE WITH EPOXY MATRIX

Mahide Betül ÖZTÜRKMEN^{1,2} , Merve ÖZKUTLU DEMİREL^{1,3} , Yahya ÖZ¹ *

¹ Advanced Composite Materials Technology Center, R&D Directorate, Turkish Aerospace, Ankara, Turkey

² Department of Chemical Engineering, Graduate School Of Natural And Applied Sciences, Gazi University, Ankara, Turkey

³ Department of Chemical Engineering, Graduate School Of Natural And Applied Sciences, Middle East Technical University, Ankara, Turkey

ABSTRACT

Composite materials have become a highly preferred technology nowadays in the industry with their advantages such as superior mechanical performance and weight loss for aerospace applications, especially due to the combination of different components and the formation of new products. In addition, with nanocomposites, this technology skips a step further and allows more effective products to be produced. Nanocomposites are produced using carbon allotropes such as graphene and carbon nanotubes, which have the title of being one of the strongest materials that have been the subject of academic studies in recent years.

Keywords: Graphene, Epoxy Resin, Nanocomposites

1. INTRODUCTION

The world of nanoscience, nanotechnology and nanocomposites has developed in recent years and the importance of this subject has increased with the diversity of automotive, aerospace, electronics, biotechnology, flexible sensors and many other applications. In this context, an important gain has been made with nanocomposites to innovations based on graphene materials.

Graphene, which is the main building block of graphite, nanotube and C60, which makes sp^2 hybridization in the honeycomb crystal structure, was synthesized and characterized only in 2004. The term "graphene", which is derived from the words "Graphite" and "ene" in English, has found its equivalent in Turkish as graphene. The 2010 Nobel Prize in Physics was awarded to Andre Geim and Konstantin Novoselov "for their groundbreaking experiments on the two-dimensional graphene material".

Graphene is the basic structural unit of carbon materials such as carbon nanotubes, graphite, fullerene and the like [1, 2]. Due to its excellent physical and chemical properties, it has become the research point of materials science and coacervation physics in physics research and practical applications since it was discovered in 2004 [3].

Graphene has a high surface area as well as high adsorption and surface reactions, electron mobility, thermal conductivity and mechanical strength. As the thinnest known material, graphene has high thermal conductivity, quantum hall effect, high Young's modulus (1 TPa), high optical transmittance and high electronic transport, barrier and flame retardant properties.

With its high surface area compared to any nanomaterial, it increases the interaction between the layers and the polymer material in nanocomposites. It has applications in a variety of fields, including electronics and biomedicine. Graphene-based composite materials attract the attention of materials scientists today. Because structural fabrication is possible, it is expected to lead to new applications. Extensive research and development work has been carried out on graphene-reinforced polymer composites in the last two decades. The addition of graphene as a reinforcing agent in a polymer matrix has resulted in improving the overall performance and properties of such composites. The unique mechanical, thermal, electrical and physicochemical properties of graphene are among the most important reasons why graphene is the subject of much research. In addition to these, it has also been the focus of attention, especially with its structural thinness. Due to these properties, extensive studies have been initiated for the promising graphene technology to be applied in many sectors and fields.

Graphene can be obtained by many different production methods [4]. The main ones of these methods can be listed as micromechanical separation of graphite layers (Exfoliation) [1], chemical vapor deposition method [5], reduction of graphene oxide [4] and epitaxial growth [6].

Potential applications of graphene and its derivatives are mainly focused on specific properties, with the phased production of different graphene materials (graphene oxide (GO), reduced graphene oxide (rGO), functionalized graphene oxide (fGO), functionalized reduced graphene oxide (frGO) and modified graphene (mG)). is directed.

If we talk about the direction that graphene and its derivatives give to the sector in aviation in the world, very light batteries for airplanes at NASA's Langley Research Center (source: Mackey, Paul J. "Graphene Based Ultra-Light Batteries for Aircraft", NASA, <https://nari.arc.nasa.gov/node/301>), a new solution-free graphene synthesis technique called Holey Graphene (source: Vitug, Eric; (2017), "NASA Langley's Technology Further Enhances Graphene Functions", NASA, <https://www.nasa.gov/langley/business/feature/nasa-langley-s-technology-further-enhances-graphene-functions>), high-power capacitors for electric vehicles (source: Kovo, Yael; (2015), "Technology Opportunity: Graphene Composite Materials for Supercapacitor Electrodes", NASA, <https://www.nasa.gov/ames/partnerships/technology/technology-opportunity-graphene-composite-materials-for-supercapacitor-electrodes>.) and protective material development for spacecraft.

In this study, a nanomaterial was reinforced into a thermosetting resin curing at 180 °C and conforming to aerospace standards. Mechanical/thermal properties and microstructure were analyzed outside the process.

2. METHODS

2.1. Materials

HexFlow RTM6 (resin transfer molding), an aerospace grade epoxy resin purchased from Hexcel, was used as the matrix material in the experiments. Graphene nanoplatelets with an average thickness of 6-8 nm and an average lateral size of 25 µm were used. Graphene nanoplatelets (GNP) powder used as reinforcement was provided by Nanografi Co. Inc. and used as received. Three different types of nanomaterial were used. The difference is in the surface area (150, 500 and 800 m²/g). LOCTITE brand 700-NC was used as a mold release agent.

2.1. Procedure

GNP reinforcement content was mixed in epoxy resin with the dispersion process, which is one of the nanocomposite production methods, which has been recently studied in the literature (Figure 1). In this method, three roll mill system is used. By making use of centrifugal force, the rollers rotate clockwise and counterclockwise, passing the resin through 3 cylinders and making it homogeneous. During the experimental studies, wt% 0.25, 0.50, 1, 2 and 4 GNP nanomaterials were added to the resin and subjected to the three roll mill process.

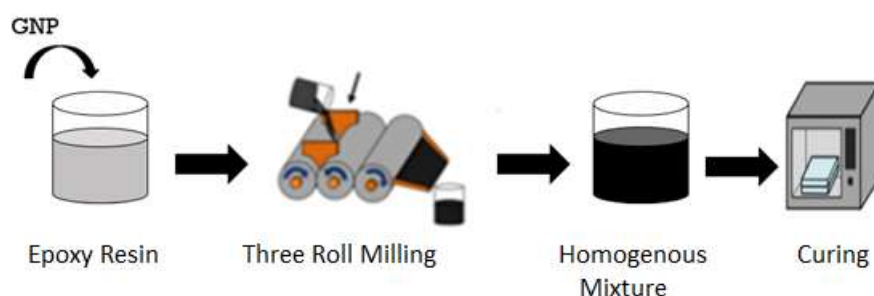


Figure 1. Process flow chart

After the dispersion process is completed, the resin mixture is placed in a vacuum at 80 °C for 30 minutes for degassing. It is then cured at 180 °C for 2 hours.

The morphologies of the obtained samples were examined with a Quanta 400 F Field Emission scanning electron microscope. Before analysis, the surfaces of the samples were coated with gold/palladium.

Three-point bending (3PB) tests were carried out to determine the mechanical properties of the samples. The three-point bending test was performed using the Shimadzu Universal Tester according to the ISO 178 standard.

Thermal gravimetric analyzes were carried out to determine the thermal properties of the composites. Thermal degradation behavior was investigated with TA Instruments Thermal Gravimetric Analyzer with a heating rate of 10 C^o/min under nitrogen atmosphere. Decomposition temperatures at maximum weight loss were determined from the first derivative of the weight loss - temperature curves.

3. RESULTS & DISCUSSION

Scanning electron microscopy (SEM), thermogravimetric analysis (TGA), and three point bending tests were performed on the samples obtained as a result of experimental studies.

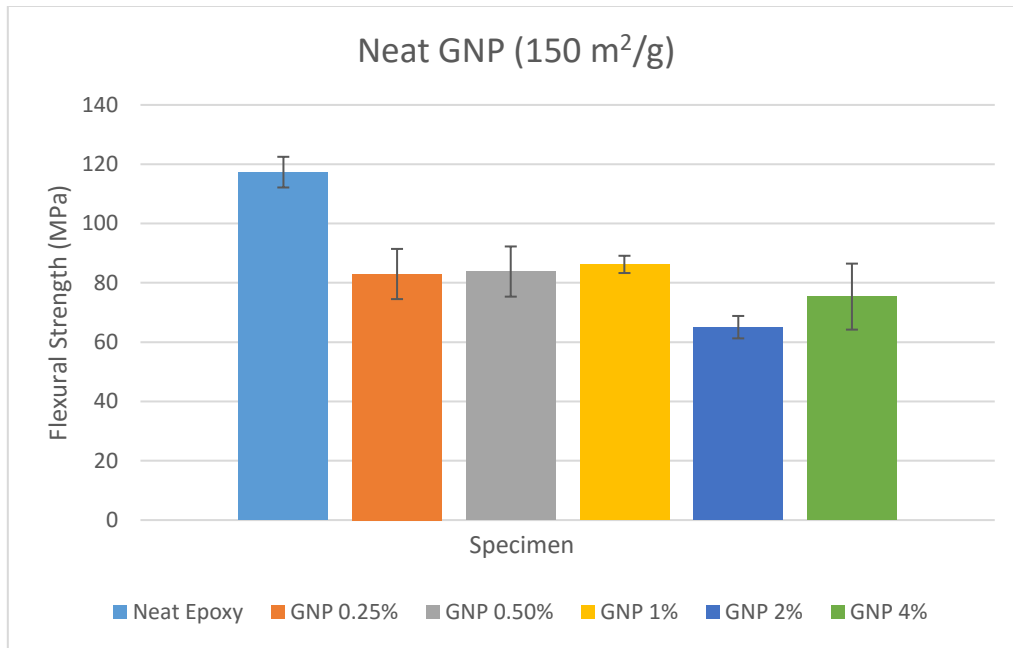
The temperatures at 5% weight loss in TGA analysis, the temperatures at maximum weight loss obtained from the first derivative of the weight loss versus temperature curve curves, and the amount of ash remaining after complete degradation of the material, including residual carbon at 900 °C, of epoxy-graphene based composites are given in Table 1.

Table 1. Temperatures at 5% weight loss, temperatures at maximum weight loss and char yield of epoxy-graphene composites.

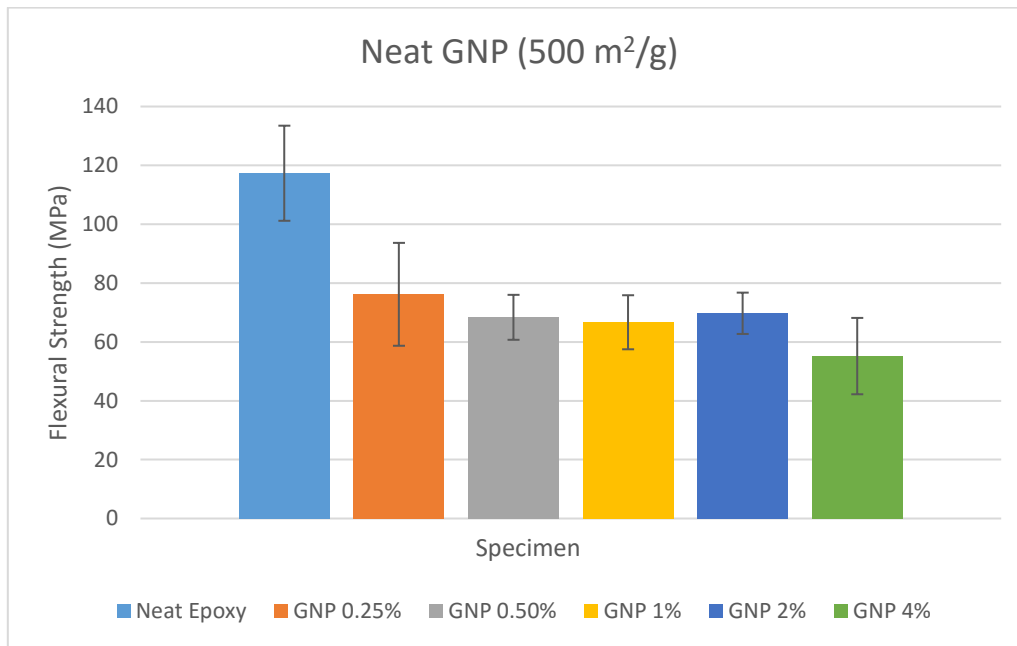
Nanomaterials	Td%5 [°C]	Tdmax [°C]	Char [%]
Epoxy	351	404	10.79
%0.25-G150	343	400	12.83
%0.5-G150	341	388	13.77
%1-G150	340	390	10.42
%2-G150	341	390	14.32
%4-G150	338	393	12.72
%0.25-G500	337	395	12.16
%0.5-G500	338	397	11.18
%1-G500	343	399	12.23
%2-G500	339	397	15.78
%4-G500	350	397	15.09
%0.25-G800	338	389	11.32
%0.5-G800	340	397	11.15
%1-G800	341	388	12.51
%2-G800	340	397	13.02
%4-G800	340	394	15.03

According to Table 1, the addition of graphene in epoxy matrix decreased the temperature at 5 wt. % loss of the epoxy. This can be due to the high thermal conductivity of graphene particles than the epoxy matrix which may act as heat dissipating source during the earlier steps of the thermal degradation. The temperature at maximum weight loss of the epoxy-graphene composites is also lower than the neat epoxy. Addition of a carbon based material in the matrix may accelerate the thermal degradation of the epoxy composites. Wang et al. and Song et al. also found lowered thermal stability with the addition of graphene into epoxy matrix and explained this with the presence of thermally unstable chemicals, which on decomposition, lowered T_d as compared to monolithic epoxy [7,8]. The char yield values of the epoxy graphene based composites were higher than the neat epoxy. Generally, higher percent addition of nanocomposites increased the char yield of the epoxy. This can be due to the high surface area of the graphene nanocomposites which enhanced the catalytic effects of the charring reaction. In general, this trend is observed regardless of the surface area of the nanomaterial.

The bending strength of the samples was measured with a three point bending test according to ASTM D790 and ISO 178 tests for each doping ratio. Considering the results, the flexural strength of the pure epoxy resin (0% GNP by volume) was measured at an average of 117 mPa. It was also observed that the mechanical properties were related to the surface area of the GNPs according to their volume percent doping ratio. As the surface area increased, a decrease in flexural strength was observed at the same doping ratio in the sample. This jump in flexural strength is indicated in Figure 2. The reason for this interaction is the increased surface area and the possibility of agglomeration, which negatively affects the mechanical properties.



(a)



(b)

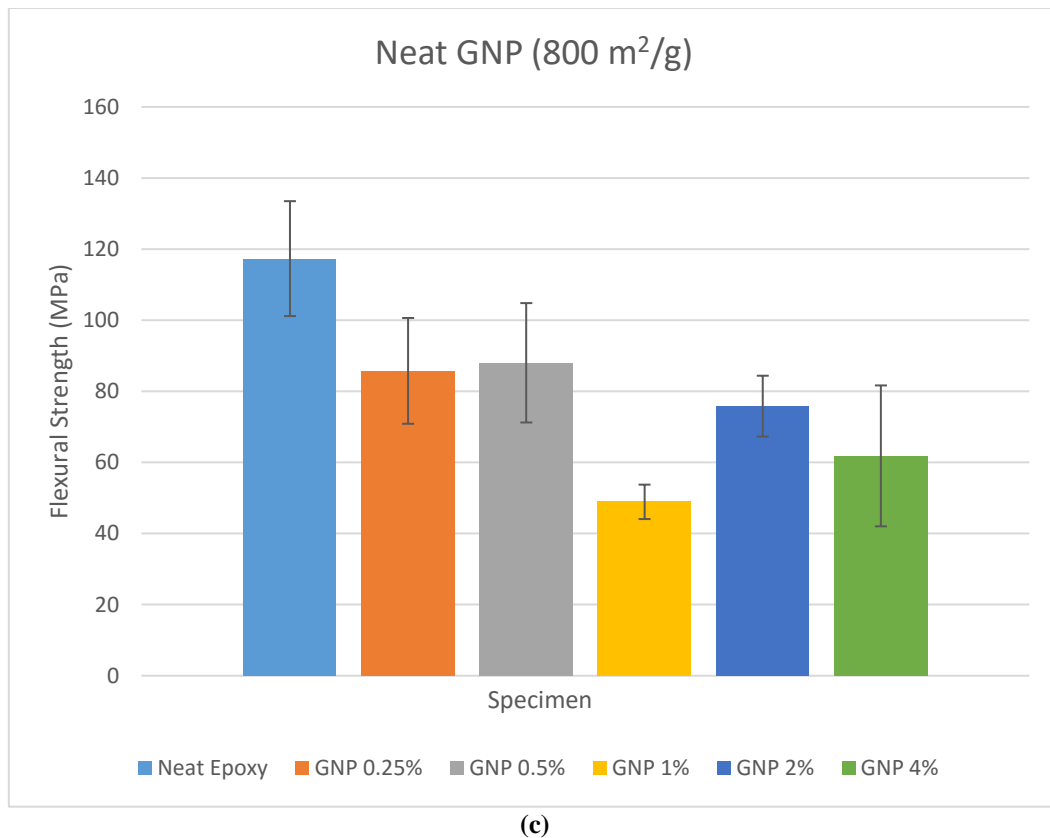
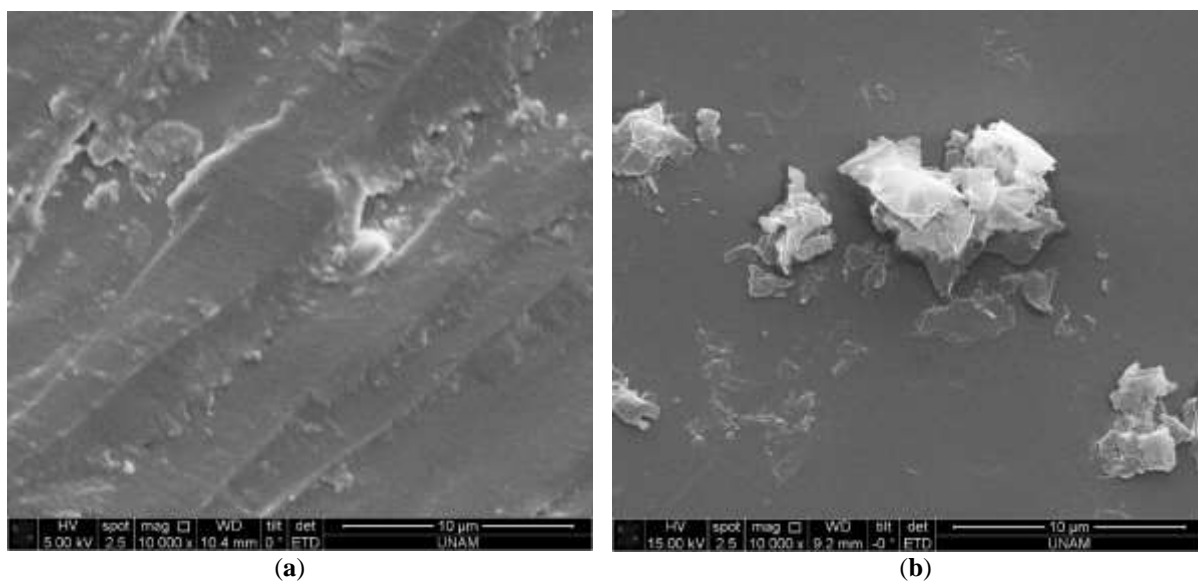


Figure 2. Mechanical test results and standard deviation

The dispersion of GNPs in epoxy after grinding was used SEM for nanocomposite suspension. Distribution is the most important factor to consider. When replacing a polymer matrix, the agglomeration of the nanofill can affect the stress concentration. SEM images of the surfaces of epoxy nanocomposites as taken are shown (Figure 3).



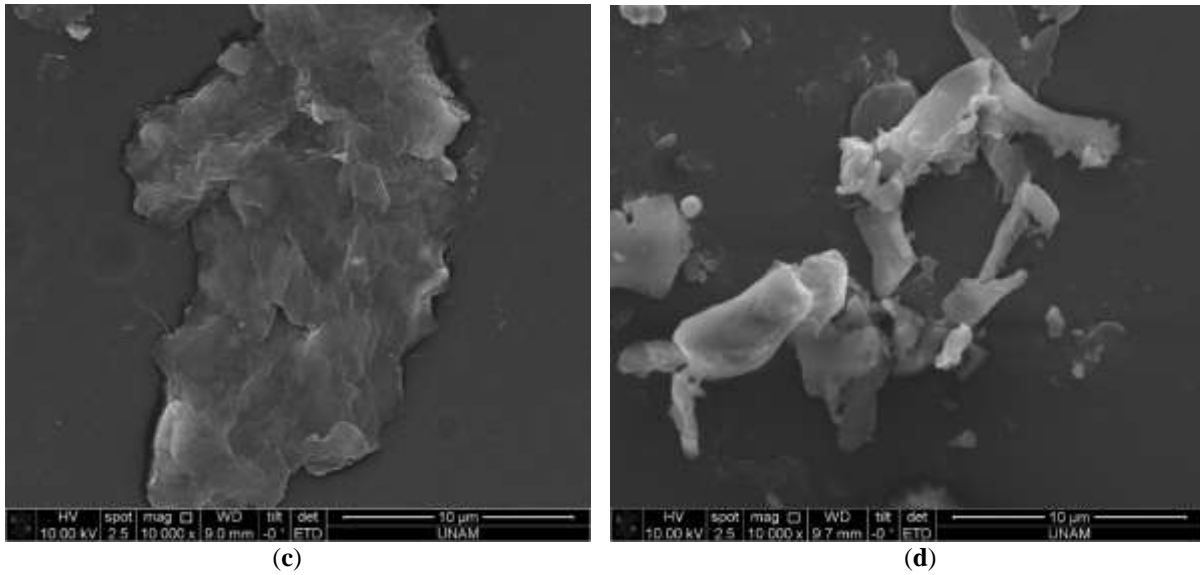


Figure 3. (a) Neat epoxy and, respectively, agglomerations in epoxy resin doped with 1% pure GNP (b) 150, (c) 500 and (d) 800.

Moreover, SEM analysis found that the nanoparticles were homogeneously dispersed in the epoxy resin and in a small fraction of the wrinkled GNPs, as seen in Figure 3. These findings show that it is possible to detect agglomerations formed at a given doping rate. It has been observed that the agglomeration problem has decreased significantly, especially at 1% and below.

4. CONCLUSION

The aim of this study is to improve the physical and mechanical properties of polymers with nanomaterial reinforcement. In the experimental studies, various combinations of GNP and Epoxy resin systems were studied at different doping rates. Approximately 20 samples were produced to reach the optimum result. It was observed that the yields of the samples with low doping ratio were higher. At the same time, their mechanical performance and thermomechanical results are quite good compared to polymers with high doping ratios. Considering the results obtained from the study, it is aimed that the structural parts will be nanodoped composite, that is, nanocomposite, by combining the resin and GNP mixture fiber, which will give the most optimum result in the future, in accordance with aviation standards.

ACKNOWLEDGMENTS

The authors accept financial support within the scope of TUBITAK projects 5189901 and 20AG001. We also thank Bilkent-UNAM and Middle East Technical University for providing the necessary infrastructure. We would also like to thank Nanografi Co. Inc. whose infrastructure we used during the experimental studies and for valuable discussions.

CONFLICT OF INTEREST

The authors stated that there are no conflicts of interest regarding the publication of this article.

REFERENCES

- [1] Novoselov KS, Geim AK, Morozov SV. Electric field in atomically thin carbon films. *Sci* 2004; 306 (5696): 666–669.
- [2] Hirata M, Gotou T, Horiuchi S, Fujiwara M and Ohba M. Thin-film particles of graphite oxide 1: high-yield synthesis and flexibility of the particles. *Carbon* 2004; 42(14): 2929–2937.
- [3] Yang QH, Lu W, Yang YG and Wang MZ. Free two dimensional carbon crystal-single-layer graphene. *New Carbon Mater* 2008; 23(2): 97–103.
- [4] Park S & Ruoff RS. Chemical methods for the production of graphenes. *Nat Nanotech* 2009; 4(4): 217-224.
- [5] Reina A, Jia XT, Ho J, Nezich D, Son HB, Bulovic V, Kong J. Large Area, FewLayer Graphene Films on Arbitrary Substrates by Chemical Vapor Deposition. *Nano Lett* 2009; (1): 30- 35.
- [6] Kosynkin DV, Higginbotham AL, Sinitskii A, Lomeda JR, Dimiev A, Price BK & Tour JM. Longitudinal unzipping of carbon nanotubes to form graphene nanoribbons. *Nature* 2009; 458(7240): 872-875.
- [7] Wang Z, Wei P, Qian Y and Liu J. The synthesis of a novel graphene-based inorganic–organic hybrid flame retardant and its application in epoxy resin. *Compos Part B* 2014; 60: 341–349.
- [8] Song L, Wang X, Pornwannchai W, Hu Y and Kandola B. The effect of graphene presence in flame retarded epoxy resin matrix on the mechanical and flammability properties of glass fiber-reinforced composites. *Compos Part A* 2013; 53: 88–96.



SiO₂ PARTICLE EMBEDDED SILICA AEROGELS: ENVIRONMENTAL AND ENERGY APPLICATIONS

Sultan BUTUN SENDEL ¹, Seyda SOMAKLI ², Vural BUTUN ³

¹ Department of Biomedical Engineering, Faculty of Engineering and Architecture, Eskisehir Osmangazi University, Eskisehir, Turkey

² Polymer Science and Technology, Eskisehir Osmangazi University, Eskisehir, Turkey

³ Department of Chemistry, Faculty of Science and Letters, Eskisehir Osmangazi University, Eskisehir, Turkey

ABSTRACT

The purpose of the study is the preparation of silica aerogels by using the hydro(solvo)thermal synthesis assisted sol-gel method, the preparation of SiO₂ particle-added silica aerogels, and the investigation of their potential use in the environment and energy fields. It has been observed that the prepared silica aerogels can be used removal applications as an adsorbent for 4-nitrophenol, methylene blue, Victoria blue, bromophenol blue organic contaminants. The aerogel was modified nanoparticle as SiO₂ and –NH₂ group increasing adsorption capacity minimum 3 fold. The energy application, silica aerogel was used as a catalyst. It has been observed that silica aerogels progressed rapidly in the reaction of NaBH₄ with methanol. Again silica aerogel was modified increase catalytic activity and prolonging self-life. SiO₂ particles embedded silica aerogel was used same reaction. Self methanolysis reaction was completed about 20 minute at 25 °C. By using protonated silica aerogel, the reaction was completed about 4 minutes at same temperature.

Keywords: Silica aerogels, Hydro(solvo)thermal synthesis, Catalyst, Methanolysis, Adsorption

1. INTRODUCTION

Silica aerogels are highly porous, open-cell, low-density materials. Since its microstructure consists of nano-sized pores and associated primary particles, it has unique properties such as low thermal conductivity, good sound absorption and refractive index, sound velocity and dielectric constant [1]. Silica aerogels are used in various sectors thanks to their properties.

Silica aerogels are generally synthesized by the sol-gel method. Hydro(solvo)thermal method is considered as synthesis by chemical reactions of substances in a closed and heated aqueous solution or organic solvent at suitable temperature (100-1000 °C) and pressure (1-100 MPa). By using this method, many compounds or materials with special structures and properties that cannot be prepared from solid state synthesis can be obtained by hydrothermal and solvothermal reactions [2].

The components used during the synthesis of silica aerogel affect the properties of the product. The most frequently used Si precursors are alkoxides such as tetramethoxysilane, tetraethoxysilane (TEOS), polyethoxysilane, methyltriethoxysilane etc. can be used as silica source, as well as water-glass (sodium silicate) solution can be used in the current commercial synthesis of silica aerogels [3].

Mahani et al. used MTMS-based, APD-dried silica aerogels to investigate the effects of sol-gel parameters on the removal of contamination from crude oil in seawater. To investigate the effects of sol-gel parameters, they prepared aerogels under pH values (4 and 8) and various EtOH/MTMS molar ratios, and the adsorption capacity of the prepared aerogels was evaluated for heavy and light

*Corresponding Author: sultanbutun.sengel@ogu.edu.tr

Received: 20.08.2021 Published:30.11.2021

commercial crude oil under multiple adsorption-desorption cycles. In optimum condition, silica aerogels have reached the conclusion that it can take heavy and light crude oil at 16.7 and 13.7 degrees, respectively [4].

Gu et al. prepared super hydrophobic silica nanoparticles with a short reaction time using a two-step synthesis route using TEOS as a silicon source, NH_4OH as a catalyst and HDTMS as hydrophobic component [5].

Sheng et al. studied the nitrobenzene adsorption of hydrophobic silica aerogels in wastewater and investigated the effects of adsorption density on pH value, adsorption temperature, adsorption time and amount of silica aerogels. They concluded that SiO_2 aerogel adsorption density of nitrobenzene in wastewater can reach 68.76%, the adsorption properties are related to the hydrophobicity of aerogels, the surface area of the organic solution, and the structure of the aerogels [6].

Hrubesh et al. used hydrophobic aerogel in their solvent removal studies and compared their results with standard granular activated carbon adsorption capacities. Using hydrophobic silica aerogel, they compared their adsorption isotherms for % (toluene, ethanol, trichloroethylene, chlorobenzene) in water mixtures with comparable granular activated carbon (GAC) on gram per gram for all solvents tested. The improved performance of the adsorption capacity by aerogel over GAC ranged from factors 30-fold for low molecular weight, highly soluble solvents to 130-fold for non-miscible solvents. They concluded that these significant improvement factors significantly reduced the cost factors that would greatly aid in the use of GAC for VOC capture and solvent cleaning applications [7].

Silica aerogels can be modified with various modification agents to increase their use efficiency. In order to increase the performance of the gels in applications, NH_2 groups have been added with APTES modification then protonated. The addition of new functional groups to the structure increases the application potential of silica aerogel. It allows for new modifications. Sometimes nano/microparticles can be added directly to the medium instead of adding new groups with agents. If the dispersion is well provided, such structures provide an advantage for obtaining tailored materials for specific applications.

In this study, hydro(solvo)thermal assisted synthesis was carried out in a shorter time and in a controlled manner compared to the currently used methods. It was aimed to increase the surface area and increase the application performance by adding SiO_2 particles to the silica aerogels. The application potential of the produced aerogels and their doped forms in the field of environment and energy has been investigated.

2. MATERIALS AND METHOD

2.1. Materials

Tetraethylortosilicate (TEOS, 98%, Sigma-Aldrich), ethanol (99.9%, Merck), ammonium hydroxide (NH_4OH , 26%, Sigma-Aldrich), hydrochloric acid (HCl, 37%, Honeywell), sodium borohydride (NaBH_4 , 98%, Merck), methanol (99.8%, Sigma-Aldrich), 4-nitro phenol (4-NP, 99%, ABCR), methylene blue (MB, Sigma-Aldrich), bromophenol blue (BFB, AFC), Victorian blue (VB, Acròs). Double distilled water was used throughout the experiment.

2.2. Method

Silica aerogels were prepared in two different combinations which are (1) bare silica aerogels, and (2) SiO_2 nanoparticle embedded silica aerogels. Synthesis stages are shown in Figure1.

2.2.1. Bare silica aerogels, SA

Alcohol/water/TEOS mixture acid-catalyzed hydrolysis and base-catalyzed condensation reactions were carried out at 10-60 minutes time intervals. Afterwards, the mixture was transferred to the autoclave and kept in an oven at 180-200 °C for 2-72 hours for gelation. The reaction time and temperature parameters were studied systematically to find optimum conditions. Particle doped aerogels were prepared under these specified conditions. The gel was first washed with ethanol and then with an ethanol/water mixture and the impurities were removed by solvent exchange. Afterwards, it was dried by the supercritical carbon dioxide drying method (Figure 1).

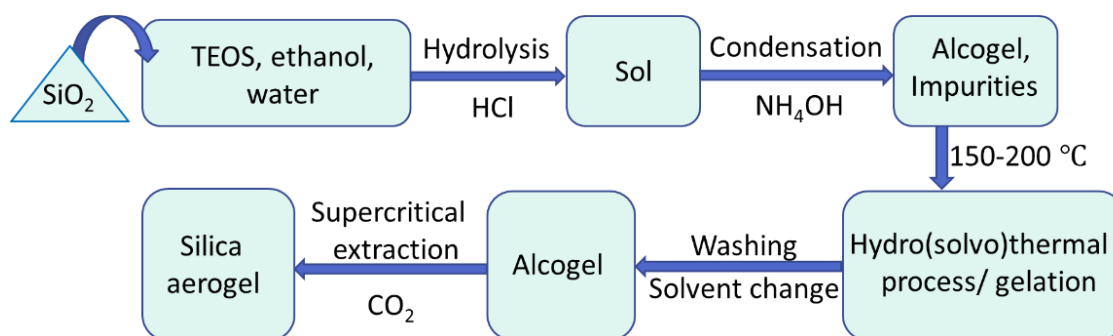


Figure 1. Schematic representation of hydro(solvo)thermal assisted silica aerogel synthesis.

2.2.2. SiO₂ nanoparticle embedded silica aerogels, SiO₂-SA

SiO₂ nanoparticles were added into the silica aerogel and then the above mentioned processes were applied exactly. The SiO₂ nanoparticles were synthesized as monodisperse in different sizes by the Stöber method [8, 9]. The sonicator was used to prevent the nanoparticles added to the medium from collapsing and clumping. SiO₂ particles have -OH groups and their nano-size will play a role in catalytic applications due to their high surface area. It can be modified outside as well as allowing new groups to be added by post modification after the template is placed. Sometimes the particles is used to produce pore/hole by reaction of HF or NaOH.

2.2.3. APTES modification

In order to increase the performance of the gels in applications, amino groups were added with APTES modification and then APTES modified form was protonated. The reaction schematic is shown in Figure 2.

For the APTES modification, 0.5 g of empty aerogel/SiO₂ embedded silica aerogel was taken and mixed with 50 mL of ethanol at 600 rpm for 18 hours. 2.5 mL of APTES and 2.5 mL of water were mixed by vortexing and then added dropwise to the mixture at regular intervals. Stirring was continued for 18 hours. Afterwards, the aerogels washed three times with ethanol, water (1/1, v/v). Then the gels were dried by using freeze dryer.

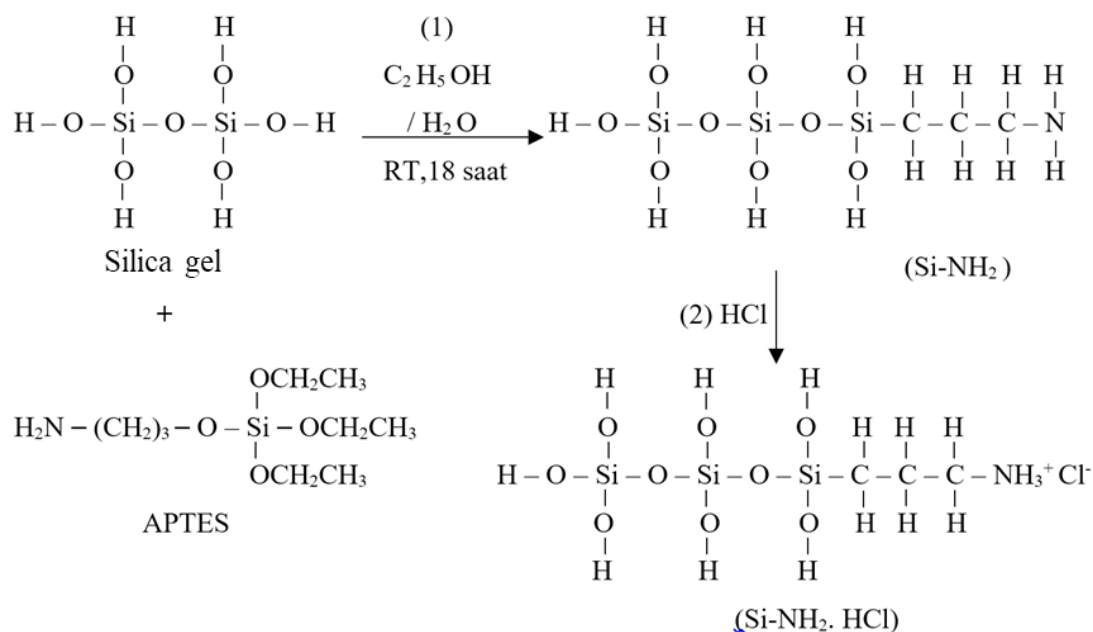


Figure 2. APTES modification to silica gel.

2.2.4. Application studies

In order to increase the performance of the gels in applications, new groups have been added with the modification. The application potential of the prepared silica aerogels in environmental applications as an adsorbent for organic pollutants such as 4-nitrophenol and some textile dyes investigated. To environmental study, removal of contaminant from aqueous media is important. Adsorbent properties important to use real applications. Properties such as high adsorption capacity, easy desorption, reusability, regenerable, having long self-life, handable, easily take after application, being cheap and easily available are some important desired properties. Silica aerogel is stable and different additive could be adding before gelation by dispersing homogeneously. The additive may be chose to increase performance and designed focusing the application. Organic contaminant removal study, knowing adsorbent's surface charge is important to understand interaction of contaminant. When it is necessary to change the charge of the adsorbent, we want to add new functional group to gain opposite charge with contaminant. Another way is directly use polymeric, metallic, or composite particles embedding in the adsorbent.

By using the prepared silica aerogels directly as a catalyst in the reaction of NaBH_4 with methanol, its application potential in the field of energy was also investigated. The methanolysis reaction is known acid catalysis, and increased acidity is resulted in high catalytic activity. Silica aerogel was modified APTES adding active $-\text{NH}_2$ group to the structure by reacting with hydroxyl group on the silica aerogel. The $-\text{NH}_2$ group can be protonated with increasing acidity.

3. RESULT AND DISCUSSION

3.1. Synthesis and Characterization

3.1.1. Bare silica aerogel synthesis and characterization

In order to determine the optimum conditions for silica aerogel production, the effects of factors such as component amounts, pH, mixing time, holding time and temperature on the gelation process were investigated. As a result of the studies, there were cases where polymerization was not observed as well as in particulate and gel structures. In the studies, TEOS was used as the source of silanation, HCl and NH₄OH were used as acid and base catalyst. The optimum condition was reached with a temperature of 180 °C and a holding time of 18 hours, but formation of the gel was observed within 4 hours in the autoclave. The gels after hydro(solvo)thermal synthesis were washed ethanol. Digital camera images of the wet and dried form of the bare silica aerogel and SEM image are shown in Figure 3. As shown the figure, bare wet gel is transparent (Figure 3a). One piece of wet gel was taken and dried by supercritical carbon dioxide drying. After drying so light, transparent silica aerogel was obtained as shown Figure 3(b). Surface morphology of the prepared aerogels was evaluated by SEM. The SEM images of the aerogel can be seen in Figure 3(c) with the porous nature.

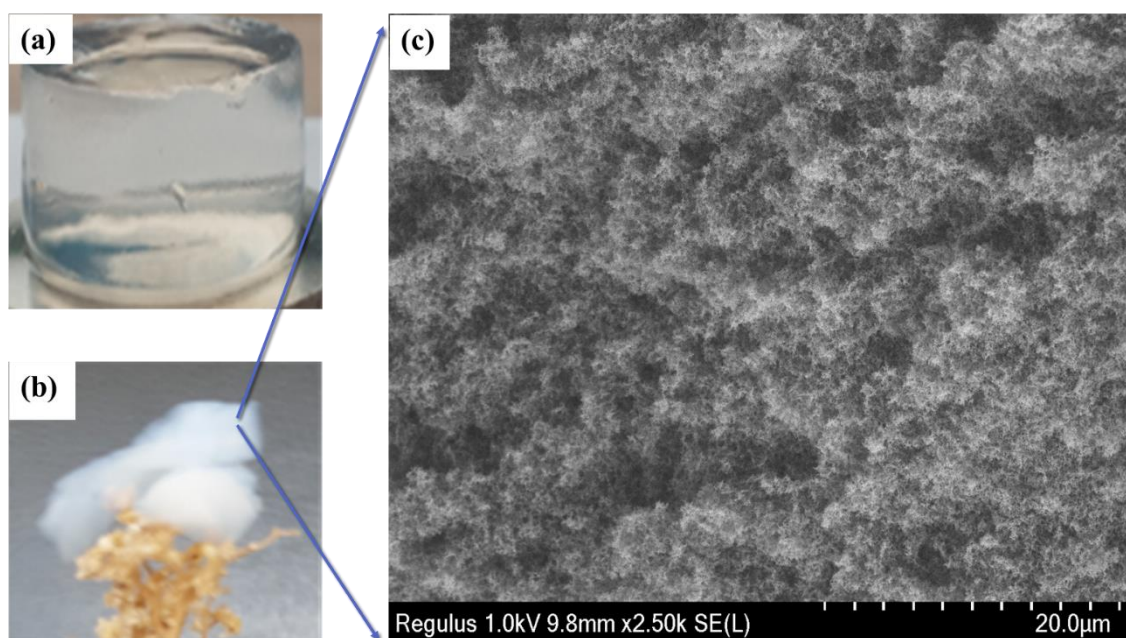


Figure 3. Bare silica aerogel (a) wet state of silica gel digital camera image (b) aerogel dried by supercritical drying, (c) SEM image of bare silica aerogel.

3.1.2. SiO₂ particle embedded silica aerogel synthesis and characterization

To prepare SiO₂ particle embedded silica aerogel, first of all, SiO₂ particles were synthesized by using Stöber method. SEM and DLS methods were used in the characterization of these particles. Results are shown in Figure 4. As shown SEM image, the particles have spherical shape and uniform size. This result supported by DLS measurement resulting 183 nm radius and 0.11 polydispersity index value. SiO₂ particles were synthesized successfully Stöber method. The particle was used to prepare SiO₂ embedded silica aerogel preparation by using same way for the bare silica aerogel.

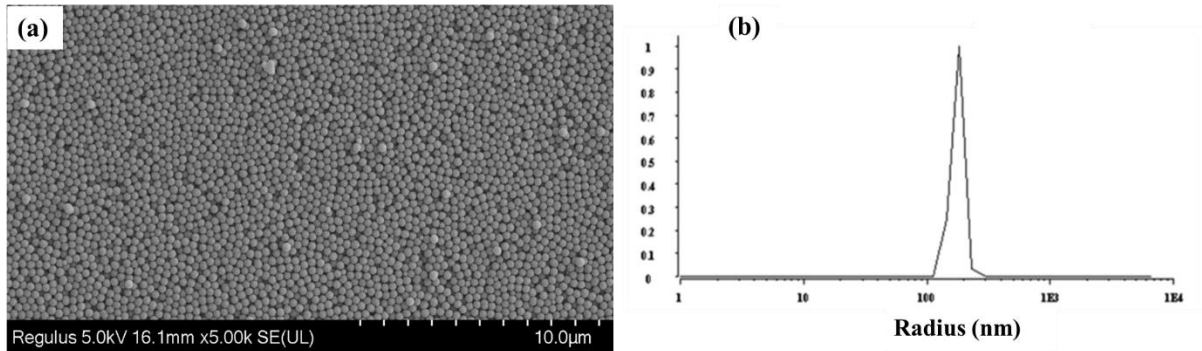


Figure 4. SEM image and DLS result of SiO₂ particle synthesized by Stöber method.

Digital camera images of the wet and dried form of the SiO₂ particles containing silica aerogel and SEM image are shown in Figure 5. As shown Figure 5, SiO₂-silica aerogel' wet form is white. A piece of wet gel was taken and dried by supercritical carbon dioxide drying. After drying so light, whiter than bare one silica aerogel was obtained as shown Figure 5(b). To evaluate surface morphology of the prepared aerogels and to see SiO₂ particles in it was used SEM analyze. The SEM images of the aerogel can be seen in Figure 5(c) with the porous nature and SiO₂ particles.

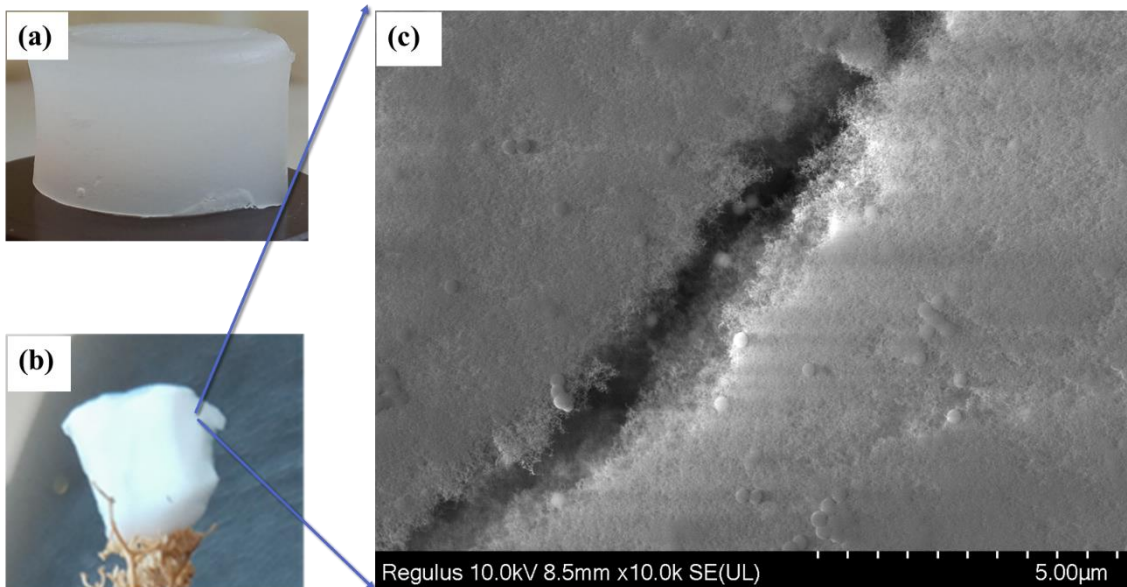


Figure 5. SiO₂ embedded silica aerogel (a) wet state of silica gel digital camera image (b) aerogel dried by supercritical drying, (c) SEM image of SiO₂ embedded silica aerogel.

3.2. Environmental and Energy Applications

3.2.1. Environmental applications

As an environmental application, the aerogels used as a adsorbent for the adsorption/removal of organic contaminant as 4-nitrophenol and textile dyes as methylene blue, bromophenol blue, victorian blue in water has been studied. As shown Table 1, the synthesized aerogels have different adsorption capacity. The aerogel can be modified by adding different functional groups to enhance adsorption capacity.

Table 1. Organic contaminant and dye adsorption on silica aerogels.

Adsorban	4-Nitrophenol (mg/g)	Methylene blue, (mg/g)	Victoria blue, (mg/g)	Bromophenol blue, (mg/g)
SA	41.05	14.09	91.66	5,93
SiO ₂ -SA	51.76	6.70	84.09	3.39
SA-APTES	137.34	60.14	137.82	10.34
SiO ₂ -SA-APTES	140.89	44.09	138.26	17.10

The results given in Table 1 obviously say that after APTES modification, the aerogels adsorption capacity increased from 41.05 mg/g to 140.89 mg/g for 4-nitrophenol, from 14.09 mg/g to 44.09 mg/g for methylene blue, 91.66 mg/g to 138.26 mg/g for victoria blue, 5.93 mg/g to 17.10 mg/g for bromophenol blue.

3.2.2. Energy application

For the energy application, silica aerogels directly used as catalyst in the reaction of NaBH₄ with methanol to produce H₂. The methanolysis reaction with 50 mM NaBH₄ at 25 °C, 1000 rpm without using a catalyst was named as a reference.

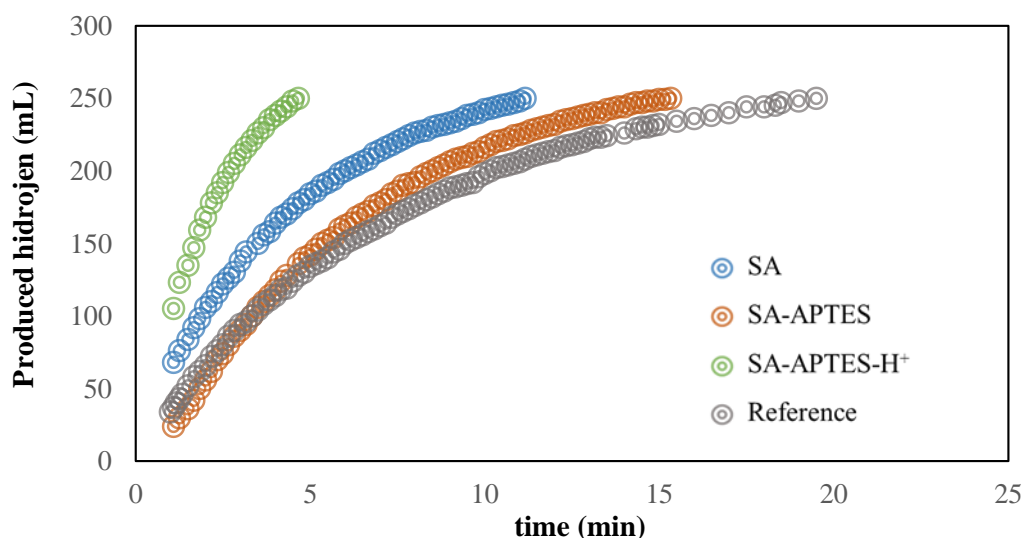


Figure 6. The use of bare silica aerogel and modified forms as a catalyst in the production of H₂ from the reaction of NaBH₄ with methanol [50 mg catalyst, 50 mM NaBH₄, 25 °C 1000 rpm].

The products obtained by modification and protonation of the synthesized empty silica aerogel with APTES were compared with the reference. It was observed that they played an active role in increasing the reaction rate compared with self methanolysis. The catalytic activities of synthesized silica aerogels were tested using the same catalyst amounts in the methanolysis reaction. When the reaction rates were

compared, it was shown that modified and protonated form of bare silica aerogel had higher catalytic activity as in Figure 6.

Reference reaction was performed absence of catalyst and hydrogen production rate calculated as 24 ml/min at 25 °C. Using SA as catalyst, hydrogen production rate calculated as 39 ml/min at same temperature. APTES modified SA produced 32 ml/min hydrogen, and protonated SA-APTES performed maximum hydrogen production rate as 83 ml/min.

Same result observed for the SiO₂ particles embedded silica aerogel and its modified forms catalytic activity (Figure 7). Using SiO₂-SA as catalyst, hydrogen production rate calculated as 40 ml/min at same temperature. APTES modified SiO₂-SA produced 36 ml/min hydrogen, and protonated SiO₂-SA-APTES performed maximum hydrogen production rate as 50 ml/min.

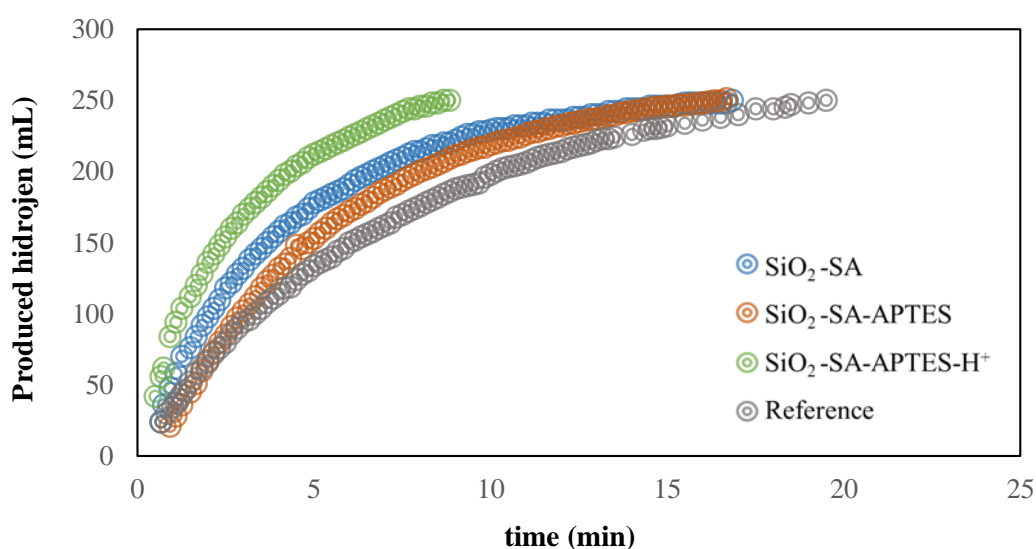


Figure 7. The use of APTES-modified forms of SiO₂-silica aerogel as a catalyst in the production of H₂ from the reaction of NaBH₄ with methanol [50 mg catalyst, 50 mM NaBH₄, 25 °C, 1000 rpm].

Protonated form of SiO₂ embedded silica aerogel has higher catalytic activity as in Figure 7. The reaction of NaBH₄ with methanol is acid catalyzed as supported literature [10-12].

4. CONCLUSION

As a result of the optimization studies, combination ratio of the mixture, pH of the mixture, hydrolysis and condensation time, thermal reaction time, reaction temperature, drying process and time were determined. It has been observed that prepared silica aerogels can be used as an adsorbent for organic contaminant with the increasing capacity 3-fold. An increase in the adsorption capacity of the silica aerogels was observed after modification with APTES. It has been observed that silica aerogels progressed rapidly in the reaction of NaBH₄ with methanol as using catalyst silica aerogel and its modified forms. Hydrogen production rate increased from 24 ml/min to 50 ml/min and 83 ml/min by using protonated SiO₂-SA-APTES and SA-APTES, respectively. These prepared silica gels are promising materials for the environmental and energy applications.

ACKNOWLEDGEMENTS

Eskişehir Osmangazi University (ESOGU) is thanked for financial support. This work was supported by the commission of scientific research projects of ESOGU as thesis project 2021/15A104.

CONFLICT OF INTEREST

The authors stated that there are no conflicts of interest regarding the publication of this article.

REFERENCES

- [1] Tang Q, Wang T. Preparation of silica aerogel from rice hull ash by supercritical carbon dioxide drying. *J Supercrit Fluids*, 2005; 35:91-94.
- [2] Feng SH, Li GH. Hydrothermal and solvothermal syntheses. In: Xu R, Xu Y, eds. *Modern Inorganic Synthetic Chemistry*, Elsevier; 2017:73-104.
- [3] Dorcheh A, Abbasi M. Silica aerogel; synthesis, properties and characterization. *J Mater Process Technol*, 2008; 199:10-26.
- [4] Mahani A, Motahari S, Mohebbi A. Sol-gel derived flexible silica aerogel as selective adsorbent for water decontamination from crude oil. *Mar Pollut Bull*, 2018; 129:438-447.
- [5] Gu H, Zhang Q, Gu J, Li N, Xiong J. Facile preparation of super hydrophobic silica nanoparticles by hydrothermal-assisted sol-gel process and effects of hydrothermal time on surface modification. *J Sol-Gel Sci Technol*, 2018; 87:478-485.
- [6] Sheng C, Liu X, Liu Y, Shen X, Lin B, Han G, Wu Z. Adsorption properties of nitrobenzene in wastewater with silica aerogels. *Sci China Technol Sci*, 2010; 53:2367-2371.
- [7] Hrubesh L, Coronado P, Jr J. Solvent removal from water with hydrophobic aerogels. *J Non-Cryst Solids*, 2001; 285:328-332.
- [8] Sato-Berrú R, Saniger JM, Flores-Flores J, Sanchez-Espíndola M. Simple method for the controlled growth of SiO₂ spheres. *J Mater Sci Eng A*, 2013; 3:237.
- [9] Qi D, Lin C, Zhao H, Liu H, Lü T. Size regulation and prediction of the SiO₂ nanoparticles prepared via Stöber process. *J Dispersion Sci Technol*, 2017; 38:70-74.
- [10] Sahiner N, Sengel SB. Quaternized polymeric microgels as metal free catalyst for H₂ production from the methanolysis of sodium borohydride. *J Power Sources*, 2016; 336:27-34.
- [11] Sahiner N, Sengel SB. Environmentally benign halloysite clay nanotubes as alternative catalyst to metal nanoparticles in H₂ production from methanolysis of sodium borohydride. *Fuel Process Technol*, 2017; 158:1-8.
- [12] Sahiner N, Sengel SB. Various amine functionalized halloysite nanotube as efficient metal free catalysts for H₂ generation from sodium borohydride methanolysis. *Appl Clay Sci*, 2017; 146:517-525.



SYNTHESIS AND CHARACTERIZATION OF POLY[(2-DIMETHYLAMINO)ETHYL METHACRYLATE]-PAN/TiO₂ COMPOSITE CRYOGELS AND THEIR USE IN SEPARATION STUDY

Sultan BUTUN SENDEL ¹, Kutalmis GOKKUS ², Kubra KEYIK ³, Vural BUTUN ³

¹ Department of Biomedical Engineering, Faculty of Engineering and Architecture, Eskisehir Osmangazi University, Eskisehir, Turkey

² Department of Environmental Engineering, Faculty of Architecture and Engineering, Kastamonu University, Kastamonu, Turkey

³ Department of Chemistry, Faculty of Science and Letters, Eskisehir Osmangazi University, Eskisehir, Turkey

ABSTRACT

The aim of this study was to prepare high surface area nano-sized polyacrylonitrile (PAN) particles and their nanocomposite with TiO₂ (PAN/TiO₂) by using electro-spraying method and to use it in super porous composite cryogel preparation using pH responsive monomer, 2-(dimethylamino)ethyl methacrylate. The cryogel composite was synthesized via cryogelation method by including the PAN/TiO₂ nanoparticle within polymeric matrices before cryogelation. The cryogel system was preferred for the polymeric system because of its features such as its super-porous structure, shape retention, reusability, and its fast response to the application. In this way, an increase in performance is expected in separation and purification studies by creating synergy by processing nanoparticles into the macro system.

Keywords: Electro-spraying, PAN/TiO₂ Nanocomposite, PDMA cryogel, Separation, Purification

1. INTRODUCTION

Electro-spraying or electrodynamic spraying is a simple technology with scalability, reproducibility. This technology formulates a technique based on liquid atomization used for the production of micro- and nanoparticles. Electro-spraying conditions generally need to be optimized for each polymer system. Electro-spraying by using electro-spinning technic/device is affected by a number of variables such as applied voltage, tip diameter, flow rate, tip-to-collector distance, and environmental influences. In this way, the morphology of the materials obtained by electrodynamic spraying is closely related to the properties of the polymer solution or dispersion used and directly affects the micro-nanoparticle forming performance. The solvent is critical and its volatility is an important factor.

Electro-spraying has many advantages compared with the traditional mechanical spraying systems as (1) narrow droplet size distribution with low standard deviation, (2) droplet size can be smaller than 1 µm, (3) droplets are electrically charged, (4) movement of the charged droplets can be easily controlled. The process of electro-spraying was reviewed by plenty of researchers because of its many advantages [1-4].

TiO₂ nanoparticle is non-toxic, stable, biocompatible and readily available. It has three main crystal phases; brookite, anatase and rutile. Among them, rutile is thermodynamically stable. Anatase and brookite are semi-stable. These nanoparticles are also an effective photocatalyst and have been the subject of many studies [5]. TiO₂ has found application in many areas such as ceramic industry, paint industry, inorganic membranes, sunscreen, sensors and biological implants [6].

*Corresponding Author: sultanbutun.sengel@ogu.edu.tr

Received:20.08.2021 Published: 30.11.2021

Cryogels can be defined as a class of hydrogels where controlled polymerization of gel-forming polymers and monomers occurs at sub-zero temperatures and yields macropores surrounded by an elastic network of interconnected ones [7]. Cryogels are naturally interconnected macroporous characteristic structure, allowing water to flow freely in sponge like structure and out of the cryogel, so that the shape of the cryogel can be fixed by squeezing it out of the free water and quickly return to its original shape by absorbing the water. The interesting properties of cryogels such as higher elasticity, flexibility and high mechanical stability, sponge-like porous interconnected microstructures and high porosity make them favorite. Cryogels are widely used as chromatographic materials, tissue engineering scaffolds and high performance materials [8]. In some applications, such as the separation of biomolecules, it can be performed very efficiently due to the large, adjustable and interconnected pore sizes. For effective separation study, cryogel can be modified adding new functional group to the structure. Alternatively, TiO₂, SiO₂, clays, polymeric nano- and microparticles, magnetic particles with different active substances can be embedded to the structure of cryogel. Thus, the interaction between the targeted molecules and the cryogel will increase, thanks to having both very high surface area and the active groups of the embedded substances [9-11].

In the literature, there are several study using polymeric materials such as nano-microgel [12, 13], hydrogel [14-17], cryogel [11, 18-22] and their composite forms [13, 23] in separation and purification studies for dye removal, biomolecules, ion and so.

Here, we revealed in this study that the species embedded in the cryogel allows controlled study by adjusting the interaction with the target substance in separation and purification [24, 25]. The super-porous cryogel prepared from pH sensitive 2-(dimethylamino)ethyl methacrylate (DMA) monomer and PDMA-PAN/TiO₂ composites formed with PAN/TiO₂ nanoparticles can be used in many applications in the environment and health fields due to their synergistic effects and non-hazardous structures.

2. EXPERIMENTAL

2.1. Material

Materials used in particle synthesis by electrospray technique are polyacrylonitrile (PAN, Carbosynth Mw:150000 g/mol), dimethylformamide (DMF, 99.8%, Sigma-Aldrich), titanium (IV) oxide (TiO₂, mixture of rutile and anatase, < 100 nm particle size, Sigma-Aldrich). Cryogels were prepared using (2-dimethylamino)ethyl methacrylate (DMA, ≥ 99.0%, Sigma-Aldrich) as a monomer, N,N'-methylenebisacrylamide (MBA, 99%, Acros) as a cross-linker, N,N,N',N'-tetramethylethylenediamine (TEMED, 99%, Across) as accelerator, potassium persulfate (KPS, 99%, Sigma-Aldrich) as redox initiator. Methylene blue (MB, Sigma-Aldrich), 4-nitrophenol (4-NP, 99%, ABCR), congo red (CR, Sigma-Aldrich), eosin yellowish (EY, Merck), gentian violet (GV, Merck) were used application study. Ultrapure water was used throughout the experiment.

2.2. Method

2.2.1. PAN nanoparticle synthesis

The particle was synthesized via electrospraying method using Inovenso NE200 electrospinning device. First, 2% (w/v) polyacrylonitrile solution was prepared in DMF. This solution was sprayed with the Inovenso NE200 electrospinning device with 15.5 kV electrical power, the distance between the collector plate and the tip was 10 cm, using a 30 G needle. The solution flow rate was adjusted to 0.75 ml/h. A total of 5.0 mL of solution was sprayed on the same surface.

2.2.2. PAN/TiO₂ nanocomposite synthesis

TiO₂ nanoparticles were added into a 2% (w/v) polyacrylonitrile solution in DMF and mixed with the aid of a sonication for a long time. The TiO₂ concentration of the mixture was adjusted to 4 mg/mL. The mixture containing titanium oxide was sprayed to the plate in the same way as the PAN nanoparticle at the same flow rate, electrical power and distance.

2.2.3. PDMA cryogel synthesis

For the preparation of PDMA cryogel, 0.50 mL of DMA monomer was dissolved in 7.0 mL of water. Next, 15% of the molar amount of monomer MBA cross-linker was added to this mixture to dissolve for about 2 hours at room temperature and then cooled in an ice bath. Then, 0.05 mL TEMED was added into the mixture. Finally, 1.5% KPS by mole of monomer was added to the medium as an initiator (dissolved in 1.0 mL of water) and vortexed and the mixture was filled into the injectors and the injector tip was closed. The injector was immersed in liquid nitrogen to freeze quickly. The mixture was then placed in the freezer at -20 °C for about 48 hours for cryogelation. After cryogel formation, the cryogel was removed from the injector, cut into cylinders of 3-5 mm in length and cleaned with water for 3-5 hours, and the wash water changed frequently.

2.2.4. PDMA-PAN/TiO₂ composite cryogel synthesis

It was prepared in the same way as PDMA, and PAN/TiO₂ nanocomposite was added to the DMA/MBA/water medium before the addition of accelerator/initiator and dispersed via sonication. Shock freezing is provided with the help of liquid nitrogen to prevent any collapse/clumping. The reaction was continued at -20 °C for 12-48 hours. At the end of the period, the ice was expected to dissolve at ambient temperature, and the species that did not react with plenty of water were washed away.

2.2.5. Application of composite cryogel

The potential use of synthesized PAN/TiO₂ embedded composite cryogels in separation and purification studies was investigated. Cryogel has been used as column filler and used to quickly and effectively separate pesticides, organic pollutants and textile dyes from aqueous solutions with the effect of embedded nanocomposite.

3. RESULTS AND DISCUSSIONS

In this study, electrospraying technique was used for the preparation of all nano- and microparticles. First, PAN particle was synthesized the size smaller than 1 µm diameter. SEM images of the PAN particles is shown in Figure 1. Firstly, it was observed that PAN particles seem to polydisperse size distribution ranging from 400 nm to 850 nm. Secondly, PAN/TiO₂ nanocomposite was synthesized under the same conditions by adding TiO₂ nanoparticles in PAN-DMF solution. The sizes of used TiO₂ nanoparticles were smaller than 100 nm and it contains two phases as rutile and anatase. Measured specific surface area, pore size and pore volume parameters for TiO₂ is found as 74.29 m²/g, 16.27 nm and 5.44 cm³/g, respectively. The particle can be classified as mesoporous material. SEM image of the PAN and PAN/TiO₂ composite was given in Figure 1(a, b).

The difference between blank and TiO₂-containing PAN particles was very clear. Both particles were spherical, but some sphere composite particles collapsed (inset Figure 1b). TiO₂ nanoparticles also may be the reason for this collapsed view in the PAN spheres after spraying.

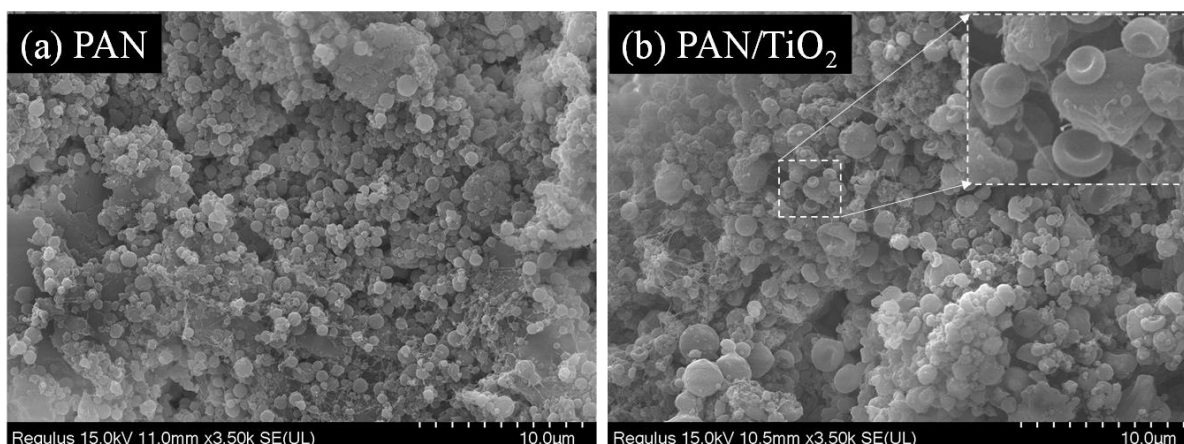


Figure 1. SEM images of PAN nanoparticle (a), and PAN/TiO₂ composite nanoparticles (b) prepared by electrospaying.

PAN and PAN/TiO₂ particles were used for PDMA-PAN/TiO₂ composite cryogel synthesis. Firstly, bare cryogel was prepared by using DMA monomer in cryogenic condition to obtain PDMA cryogel. Both scheme for the pathway of cryogel preparation and digital camera images of PAN/TiO₂ embedded cryogel (PDMA-PAN/TiO₂) were depicted in Figure 2. While PDMA cryogel was transparent, PDMA-PAN/TiO₂ composite cryogel was bright white because of PAN and TiO₂.

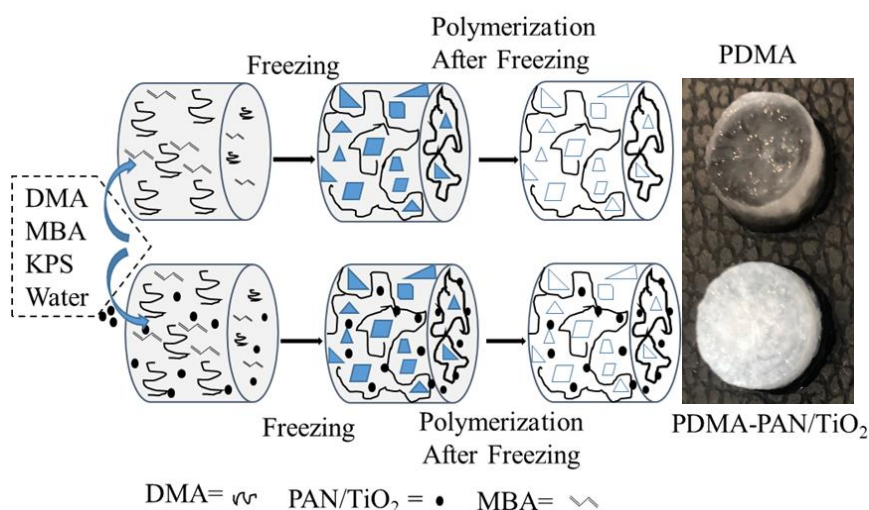


Figure 2. Schematic illustration of the preparation of PDMA cryogel, PDMA-PAN/TiO₂ cryogel composite and digital camera images.

It has been observed that gels were soft, compressible, can take their former shape again, and have a structure that absorbs water very quickly. The SEM images of cryogels were illustrated in Figure 3 (a-d) with different magnifications. SEM images indicated macro pores. The pores of the composite cryogel were slightly closed/smaller than the bare one because of filling PAN/TiO₂ particles (Figure 3b).

In the Figure 3, as shown at high magnification (inset Figure 1a), PDMA cryogel had a smooth pore surface and super porous structure. Unlike PDMA cryogel, composite cryogel had no flat surfaces on

its surface in high magnification images (Figure 3c, d), and these cryogels were prepared using 15% cross-linker (according to used monomer mole ratio) and 10% PAN/TiO₂ by used monomer weight.

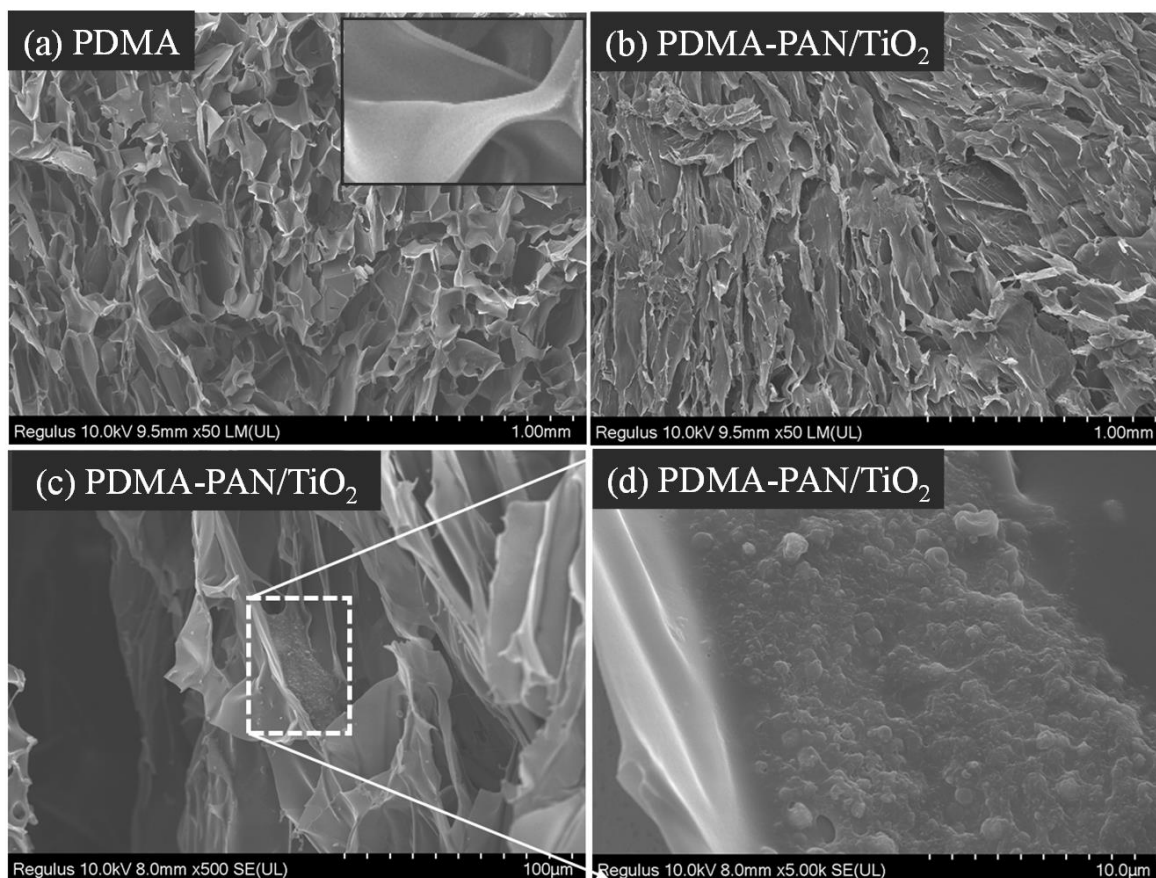


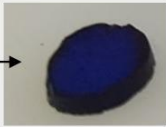

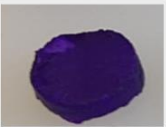

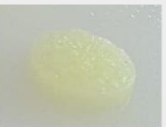
Figure 3. SEM images of PDMA cryogel (a), PDMA-PAN/TiO₂ composite cryogel with different magnifications (b, c, d).

PDMA-PAN/TiO₂ super-porous composites cryogel can be used in different fields to separation and purification applications. In this study, composite cryogels were polymerized in an injector cryogenic condition. After cryogelation, the gels removed from the injectors as a whole were transferred to the larger injector. In this way, the cleaning/washing process was carried out and the gel swelled up to the diameter of the injector and its pores were further opened because of absorbing more water. Therefore, it was aimed to show that PAN/TiO₂ doped PDMA composite cryogels could be used in separation and purification studies.

In parallel with the increasing population and industrialization, water pollution is gradually increasing. It is a common situation that textile dyes/organic pollutants discharged to the clean water sources for various reasons. These pollutants must be removed from the environment in order to increase the quality of life and sustain the life of aquatic organisms. Therefore, textile dyes such as MB, EY, GV, CR and organic pollutant as 4-NP were studied to remove them effectively to obtain sustainable environment. For this purpose, firstly, composite cryogel was used as adsorbent for MB, EY, GV, CR, 4-NP organic contaminants. 100 mg/L initial solution concentration was used in all studies. Approximately 50 mg composite cryogel was filled in the injector/column. Then 5 mL dye solution was passed through column. The interaction of the composite particle doped cryogel with MB, CR, 4-NP solutions was examined separately and visualized. Then their mixture as MB, EY and MB, GV, 4-NP were prepared and passed through PDMA-PAN/TiO₂ containing column. After adsorption study, adsorbed amount of

contaminant was determined by using UV-vis spectrophotometer. Adsorption capacity of the composite cryogel was given in Table 1 as the amount of mg contaminant adsorbed per g composite cryogel. Adsorption capacity was calculated as 67.22 mg/g, 11.53 mg/g, 53.66 mg/g, 2.03 mg/g and 43.78 mg/g for MB, EY, GV, CR and 4-NP, respectively.

Table 1. Maximum adsorption capacity of composite cryogels and their digital camera images after adsorption

Contaminants	MB	EY	GV	CR	4-NP
Composite cryogel after adsorption					
Maximum adsorption capacity	67.22 mg/g	11.53 mg/g	53.66 mg/g	2.03 mg/g	43.78 mg/g

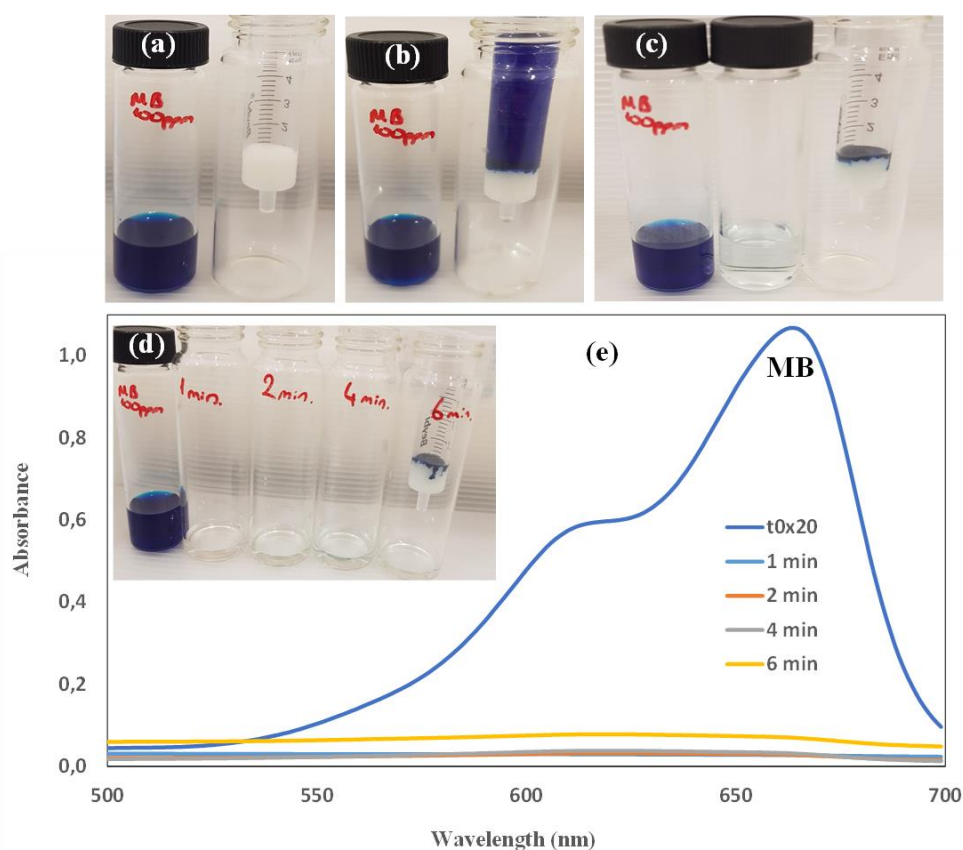


Figure 4. Digital camera images of MB dye and PDMA-PAN/TiO₂ composite filled column (a), dye transferred column (b), MB removal from aqueous solution passing through columns recording to retention time (c, d), UV-Vis spectra of MB solution before (x20 dilution) and after passing through columns (directly) time to time (e) [5 mL 100 ppm MB aqueous solution, 50 mg composite cryogel].

Separation process of MB by using PDMA-PAN/TiO₂ composite cryogel evaluated by UV-Vis spectra of MB eluted solution were illustrated in Figure 4(a-e). As can be clearly seen from Figure 4c composite cryogel adsorb/remove MB dye because of their negatively charged PAN/TiO₂ and opposite to MB dye.

Figure 4d shows the differences of eluents collected 1 min to 6 min. The UV-Vis absorption spectra of eluted MB solution were demonstrated in Figure 4e. Because initial concentration was out of calibration curve, the solution was diluted 20-fold. Then absorbance value were recorded 500-700 nm because of the maximum absorption wavelength at about 664 nm of MB. As seen Figure 4e, initial MB absorbance value at 664 nm was over 1.0, although 20-fold dilution. In same figure, eluent absorbance was recorded directly passing dye solution after 1 min, 2 min, 4 min, and 6 min. The MB concentration of the eluent was a little increased with the increasing retention time. In total, column color was mostly white, only upper site was blue. Considering the separation performance, it can be implied that much more MB solution may be pass through over adsorption capacity.

Figure 5 depicted the separation of CR (a-d) and 4-NP (e-h) apart from by using PDMA-PAN/TiO₂ composite filled column. The retention time of the dye solutions in the column and the concentration of the resulting solution depended on the interaction between the column material and mobile phase (CR, 4-NP). As can be seen from the digital camera images in Figure 5 (c, g), the interaction with the cryogel was not high with CR and 4-NP. The amount of dye adsorbed was determined by measuring the solution after adsorption with UV-vis. The result was different from MB separation because of different charge. For CR, Figure 5c showed before and after passing CR solution through column. 5 mL CR solution passed in 4 min and absorbance recorded by UV-vis spectrophotometer 350-650 nm because of the maximum absorption wavelength at about 498 nm of CR for 1 min, 2 min, and 4 min (eluent diluted 2-fold same as initial sample). When the color of the solution was checked (Figure 5c, after 4min), it was easy to understand change in concentration is little.

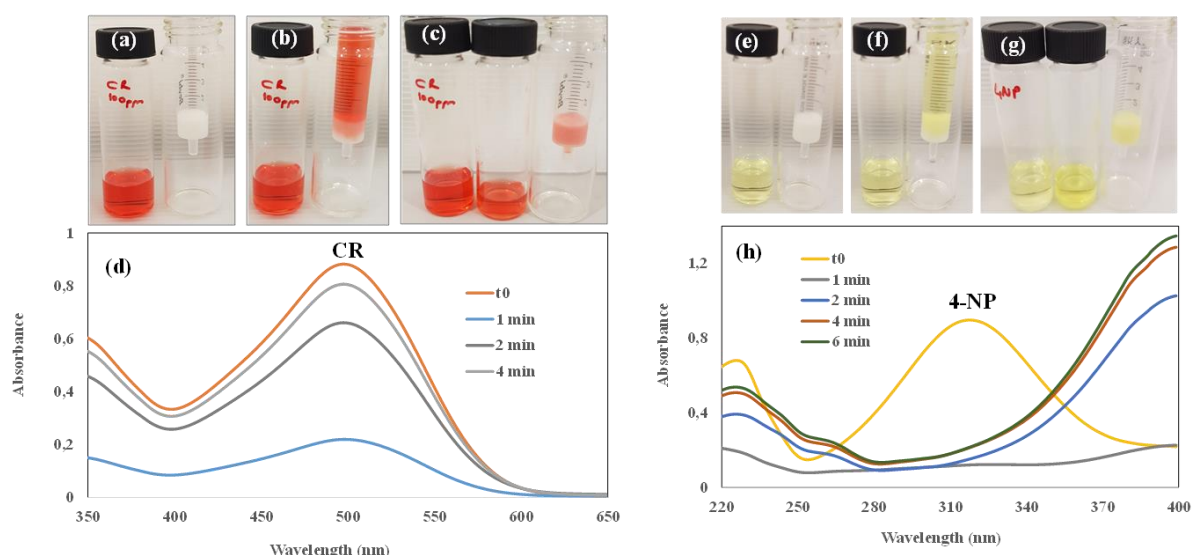


Figure 5. Digital camera images of CR dye and 4-NP organic contaminant PDMA-PAN/TiO₂ composite filled column (a, e), dye transferred column (b, f), CR and 4-NP removal from aqueous solution passing through columns recording to retention time (c, g), UV-Vis spectra of CR (x2 fold dilution) and 4-NP (x6.66 fold dilution) solution before and after passing through columns (d, h) [5 mL 100 mg/mL CR dye and 4-NP aqueous solution, 50 mg composite cryogel].

Separation process of 4-NP by using PDMA-PAN/TiO₂ composite cryogel evaluated by UV-Vis spectra of 4-NP eluted solution were illustrated in Figure 5(e-h). As can be clearly seen from Figure 5g composite cryogel adsorbed/removed 4-NP. Figure 5h showed the differences of eluents collected 1-6 min. The UV-Vis absorption spectra of eluted 4-NP solution were demonstrated in Figure 5h. All the solution was diluted 10-fold including initial one. Then absorbance value were recorded 220-400 nm

because of the maximum absorption wavelength at about 317 nm for 4-NP. As seen Figure 5h, initial 4-NP absorbance max value was 317 nm but after passing through the column the eluent absorbance max was shifted as 400 nm. This means that 4-NP was deprotonated by amino group of DMA, that is, PDMA was protonated.

In this model study, as well as separating dye solutions, dye mixtures were prepared and separation studies were carried out. Figure 6 showed the digital camera images taken from time to time after the transfer of the dye mixtures to the column. From this, it was clearly seen that the dyes interacted differently with the filler in the injector and have different retention time.

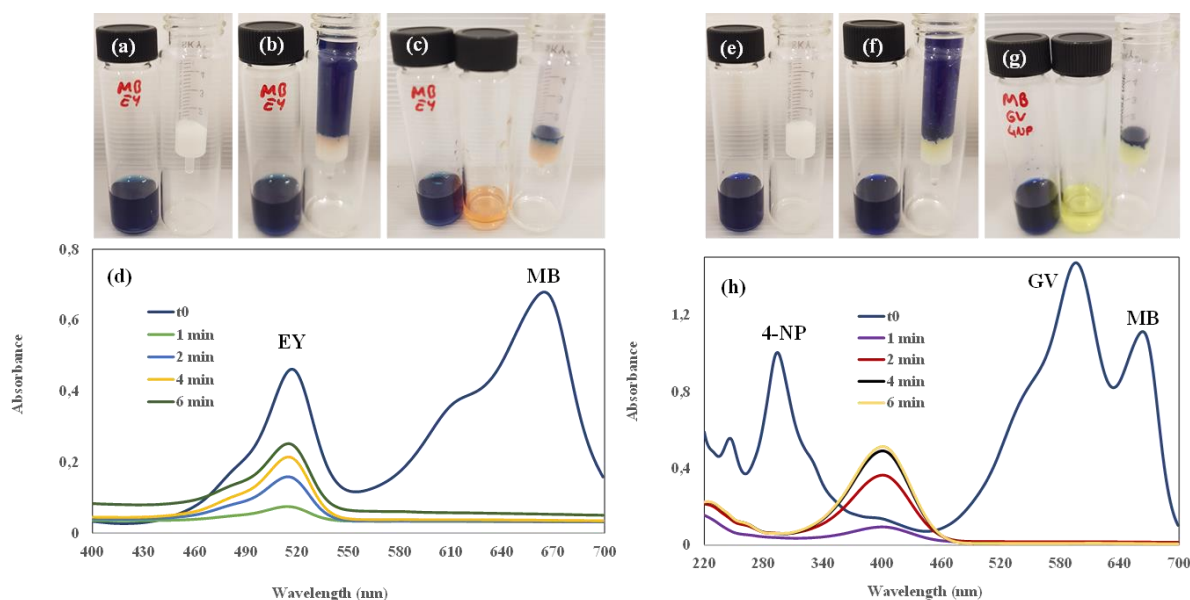


Figure 6. Digital camera images of MB-EY mix and MB-GV-4-NP mix contaminant PDMA-PAN/TiO₂ composite filled column (a,e), dye transferred column (b,f), MB-EY mix and MB-GV-4-NP mix removal from aqueous solution passing through columns recording to retention time (c, g), UV-Vis spectra of MB-EY mix (x10 fold dilution) and MB-GV-4-NP mix (x6 fold dilution) solution before and after passing through columns (d, h) [5 mL 50 mg/mL MB-EY and 33 mg/mL MB-GV-4-NP aqueous solution, 50 mg composite cryogel].

Figure 6 (a-h) showed the mixture of MB, EY and MB, GV, 4-NP separation process. The digital camera images in Figure 6a-c revealed the process step by step, digital camera images of MB-EY mix and PDMA-PAN/TiO₂ composite filled column (a), dye transferred column (b), MB-EY mix removal from aqueous solution passing through column (c). When glancing to the Figure 6c, blue color (MB) was at top of the column and orange color was at the bottom of the column. When checked the eluent absorbance by UV-vis (Figure 6d, x10 dilution), there was no MB in the excite solution checking wavelength at 664 nm. EY passed the column as CR. The cryogel colored with the weak interactions. The mixture of MB, GV, and 4-NP separation process given in the Figure 6(e-h). Figure 6c, the blue color (MB, GV) was at the top of the column and yellow color was at the bottom. Measured absorbance by UV-vis (Figure 6h, x6 dilution), there was no MB and GV in the excite solution checking wavelength at 664 nm for MB and 590 nm for GV. Maximum absorption wavelength at about 317 nm for initial 4-NP solution. After passing column the mixture 4-NP absorbance maximum was shifted as 400 nm because of deprotonation as shown Figure 5(e-h). As a result of the studies, it was predicted that this noncomposite embedded cryogel could be used both as a column filler material and successfully in the separation and purification of different materials.

4. CONCLUSIONS

In this work, PAN particles and TiO₂ doped PAN composite particles were successfully synthesized by electro spraying technique adjusting the polymer concentration via electro spinning device, used needle tips, applied force/power and distance of between tip and the collector. Besides, super-porous cryogels were synthesized via cryogelation of pH responsive DMA monomer. The cryogel composite including the PAN/TiO₂ nanoparticle within polymeric matrices before cryogelation was prepared. New functional material was prepared by embedding the materials prepared with electro spray in cryogel. By combining the physical-chemical properties/application potential of the synthesized nanoparticles with the property/application potential of the super-porous cryogel, much more functional and positive composite structures have been formed. Both embedded particles in cryogel and cryogel have modifiable nature/structure, therefore both one will be tailored to special application. This prepared composite cryogels might have potential usages in separation and purification studies.

CONFLICT OF INTEREST

The authors stated that there are no conflicts of interest regarding the publication of this article.

REFERENCES

- [1] Jaworek A. Micro-and nanoparticle production by electro spraying. *Powder Technol*, 2007; 176:18-35.
- [2] Li J, Pan K, Tian H, Yin L. The potential of electro spinning/electro spraying technology in the rational design of hydrogel structures. *Macromol Mater Eng*, 2020; 305:2000285.
- [3] Alehosseini A, Ghorani B, Sarabi-Jamab M, Tucker N. Principles of electro spraying: a new approach in protection of bioactive compounds in foods. *Crit Rev Food Sci Nutr*, 2018; 58:2346-2363.
- [4] Sosnik A. Production of drug-loaded polymeric nanoparticles by electro spraying technology. *J Biomed Nanotech*, 2014; 10:2200-2217.
- [5] Ari B, Sengel SB, Sahiner N. The use of titanium dioxide particles embedded in anionic hydrogel composite for photocatalytic degradation of methylene blue. *SPE Polymers*, 2021; 2: 97-109.
- [6] Daghrrir R, Drogui P, Robert D. Modified TiO₂ for environmental photocatalytic applications: a review. *Ind Eng Chem Res*, 2013; 52:3581-3599.
- [7] Zhao X, Guo B, Wu H, Liang Y, Ma, PX. Injectable antibacterial conductive nanocomposite cryogels with rapid shape recovery for noncompressible hemorrhage and wound healing. *Nat Commun*, 2018; 9:1-17.
- [8] Okay O. Ed. *Polymeric Cryogels: Macroporous Gels with Remarkable Properties*. Springer:2014.
- [9] Sengel SB, Sahiner M, Aktas N, Sahiner N. Halloysite-carboxymethyl cellulose cryogel composite from natural sources. *Appl Clay Sci*, 2017; 140:66-74.
- [10] Demirci S, Suner SS, Sahiner M, Sahiner N. Superporous hyaluronic acid cryogel composites embedding synthetic polyethyleneimine microgels and halloysite nanotubes as natural clay. *Eur Polym J*, 2017; 93:775-784.

- [11] Sahiner N, Yildiz S, Sagbas, S. Graphene oxide embedded p(4-VP) cryogel composites for fast dye removal/separations. *Polym Compos*, 2018; 39:1694-1703.
- [12] Sengel SB, Sahiner N. Poly (vinyl phosphonic acid) nanogels with tailored properties and their use for biomedical and environmental applications. *Eur Polym J*, 2016; 75:264-275.
- [13] Berger S, Singh R, Sudha JD, Adler HJ, Pich A. Microgel/clay nanohybrids as responsive scavenger systems. *Polymer*, 2010; 51:3829-3835.
- [14] Li S, Liu X, Huang W, Li W, Xia X, Yan S & Yu J. Magnetically assisted removal and separation of cationic dyes from aqueous solution by magnetic nanocomposite hydrogels. *Polym Adv Technol*, 2011; 22:2439-2447.
- [15] Mandal B, Ray SK. Synthesis of interpenetrating network hydrogel from poly (acrylic acid-co-hydroxyethyl methacrylate) and sodium alginate: Modeling and kinetics study for removal of synthetic dyes from water. *Carbohydr Polym*, 2013; 98:257-269.
- [16] Panic VV, Velickovic SJ. Removal of model cationic dye by adsorption onto poly (methacrylic acid)/zeolite hydrogel composites: kinetics, equilibrium study and image analysis. *Sep Purif Technol*, 2014; 122:384-394.
- [17] Thomas PC, Cipriano BH, Raghavan SR. Nanoparticle-crosslinked hydrogels as a class of efficient materials for separation and ion exchange. *Soft Matter*, 2011; 7:8192-8197.
- [18] Sahiner N, Demirci S. Poly ionic liquid cryogel of polyethyleneimine: Synthesis, characterization, and testing in absorption studies. *J Appl Polym Sci*, 2016; 133:43478.
- [19] Ihlenburg RB, Lehnen AC, Koetz J, Taubert A. Sulfobetaine cryogels for preferential adsorption of methyl orange from mixed dye solutions. *Polymers*, 2021; 13:208.
- [20] Ertürk G, Mattiasson B. Cryogels-versatile tools in bioseparation. *J Chromatogr A*, 2014; 1357:24-35.
- [21] Dobritoiu R, Patachia S. A study of dyes sorption on biobased cryogels. *Appl Surf Sci*, 2013; 285:56-64.
- [22] Sahiner N. Super macroporous poly (N-isopropyl acrylamide) cryogel for separation purpose. *Polym Adv Technol*, 2018; 29:2184-2191.
- [23] Kong Y, Zhuang Y, Han Z, Yu J, Shi B, Han K, Hao H. Dye removal by eco-friendly physically cross-linked double network polymer hydrogel beads and their functionalized composites. *J Environ Sci*, 2019; 78:81-91.
- [24] Ertürk G, Mattiasson B. Cryogels-versatile tools in bioseparation. *J Chromatogr A*, 2014; 1357:24-35.
- [25] Busquets R, Ivanov AE, Mbundi L, Hörberg S, Kozynchenko OP, Cragg PJ, Cundy AB. Carbon-cryogel hierarchical composites as effective and scalable filters for removal of trace organic pollutants from water. *J Environ Manage*, 2016; 182:141-148.